Sayab, Mohammad (2005)

N-S shortening during orogenesis in the Mt Isa Inlier: the preservation of W-E structures and their tectonic and metamorphic significance.

PhD thesis, James Cook University.

N-S shortening during orogenesis in the Mt Isa Inlier: the preservation of W-E structures and their tectonic and metamorphic significance

Volume I

Thesis submitted by

Mohammad Sayab M. Phil (University of Peshawar, 2001)

in March 2005

for the degree of Doctor of Philosophy

in the School of Earth Sciences

James Cook University of North Queensland

Australia

STATEMENT OF SOURCES

Declaration

I declare that this thesis is my own work and has not been submitted in any form for another degree or diploma at any university or other institution of tertiary education. Information derived from the published or unpublished work of others has been acknowledged in the text and a list of references given.

Mohammad Sayab

March, 2005

STATEMENT OF ACCESS

I, the undersigned, the author of this thesis, understand that James Cook University will make it available for use within the University Library and, by microfilm or other means, allow access to other users in other approved libraries.

All users consulting this thesis will have to sign the following statement:

> *In consulting this thesis, I agree not to copy closely or paraphrase it in whole or in part without the written consent of the author; and to make proper public written acknowledgement for any assistance, which I have obtained from it.*

Beyond this, I do not wish to place any restriction on access to this thesis.

Mohammad Sayab
March, 2005

Acknowledgements

During three years of my Ph. D. project I was sponsored by International Post-graduate Research Scholarship (IPRS), James Cook University Post-graduate Award and *pmd**CRC top-up scholarship.

I would like to express extreme gratitude and thanks to my mum, dad, brother (Mani) and sisters (Sonia Rani and Sana Rani) in the Pakistan whom I have missed dearly during my stay here in Australia. They have always supported and encouraged me in every endeavor I have undertaken.

My supervisors Mike Rubenach and Tim Bell were always a source of encouragement and enthusiasm. I would like to acknowledge Mike for initiating this project and Tim for reviewing thesis drafts.

I am indebted to all of the people who have passed through SAMRI and EGRU during my tenure for fruitful discussions, especially Peter Welch, Tom Evans, Mustafa Cihan, Kris Butera, Damien Foster, Leonardo Filtrin, Nick Lisowiec, Mark E & R, David Gillen and James Austin.

The Petrographic lab at James Cook University provided a superb facility for thin section preparation. A special thanks to Dr. Kevin Blake for all of his support with microprobe analysis. I would also like to thank Mr. Elvy Grigolato for XRF analysis.

CONTENTS OF VOLUME I

(Text and references)

CONTENTS OF VOLUME II

(Figures, tables and appendices)

THESIS FORMAT

This thesis consists of four independent sections (A to D), which have been prepared as individual papers for international journals. Section A, which contains confidential geophysical dataset of pmd*CRC, will be submitted in January 2005 after disclosure release. Sections B to D have been submitted. Details of the submission process are given in the first page of each section. Each section contains its own set of references and figures, which results in some of the figures being repeated. The thesis is presented as two volumes. Volume I contains text and reference lists for each section. Volume II contains figures, tables and appendices.

Appendices are arranged according to each section (A – D). Appendix – E contains sample catalogue with reference to Australian Map Grid (AMG) coordinates, zone 54. The catalogue also contains information regarding thin sections used in this study, polished sections, rocks used for major element XRF analysis and rock chips and blocks.

THESIS ABSTRACT

Mesoproterozoic Mt Isa inlier of NW Queensland exhibits complex tectonometamorphic history that is generally considered to result from low-pressure/high-temperature (LP/HT) metamorphism with an anticlockwise pressure-temperature-deformation path. Yet studies regarding the nature of the P-T history and tectonic regime that led to such a LP/HT signature have been quite limited. A detailed FIA (**F**oliation **I**ntersection/**I**nflection **A**xes preserved in the porphyroblast**s**) analysis combined with textural relationships and P-T pseudosections, using key localities across the Eastern Fold Belt of the Mt Isa Inlier, has resolved the cause of the LP/HT signature. Measurement of FIAs in the Eastern Fold Belt has revealed phases of deformation and metamorphism that could not previously be distinguished from one another. Both the 'asymmetry switch' and 'FitPitch' FIA measurement techniques have been applied to key localities of polymetamorphosed and multiply deformed Eastern Fold Belt, and they yielded the same result. These independent techniques have revealed (1) W-E trending structures that formed during N-S bulk shortening (O_1) and N-S oriented structures that formed during W-E bulk shortening (O_2) in the Eastern Fold Belt, (2) the presence of separate periods of metamorphism associated with each direction of bulk shortening, and (3) the crustal scale tectonic processes associated with polymetamorphism. The structural overprinting relationships do not support previously suggested non-coaxial west vergent, nappe-style folding in the region. A progressive succession of overprinted FIA trends reveals a clockwise rotation of the principal direction of bulk shortening with time. This requires a radical shift of relative plate movement from N-S to W-E during development of the

north Australian craton in the Mesoproterozoic (*ca* 1.60 and 1.50Ga). Significantly, O_1 porphyroblasts preserving W-E FIAs exhibit mineral textures of Barrovian style, whereas O_2 formed porphyroblasts preserving N-S FIAs are Buchan in style. This supports the emplacement of the Williams/Naraku Batholiths after O_1 around the onset of O_2. Higher-pressure garnet cores, modeled in MnNCKFMASH P-T pseudosections preserved early W-E FIAs and formed during O_1. This was followed by decompression and then low pressure – high temperature (LP/HT) metamorphism when N-S FIAs were preserved within porphyroblasts. This is further supported by the presences of at least two distinctive generations of staurolite and kyanite that grew both before and after andalusite/cordierite. Middle to upper amphibolite facies metamorphic conditions occurred during O_1 with crustal thickening followed by fast erosion and near-isothermal decompression leading to LP/HT conditions. This was followed by O_2 and a second period of middle- to upper- amphibolite facies metamorphism that obliterated and/or obscured the tectonometamorphic signature of primitive O_1 in the matrix of most rocks. This history appears to correlate better with that observed in the southwest United States, which may have been located against the NE of the Australia at this period in time.

THESIS INTRODUCTION

The Mesoproterozoic Mount Isa Inlier of NW Queensland, Australia, is a multiply deformed terrain and a world-class epigenetic base- and noble-metal province. Three dominant north-south striking belts have been recognized based on the tectonostratigraphic setting. From east to west, these are the Eastern Fold Belt, Kalkadoon-Leichhardt Belt and Western Fold Belt. The structural framework of the Eastern Fold Belt consists of an intensely developed north-south striking, subvertical D_2 fabric and associated folds that has obscured and obliterated early D_1 structures. The latter structures are only locally preserved in low strain zones of D_2. The recognition and geometric interpretation of earlier D_1 structures is very much dependent on the intensity of D_2 strain zones. These W-E trending D_1 structures have been recognized in some regions, but their interpretations have been the subject of considerable controversy. The purpose of this study is to understand the geometric characterization of D_1 structures through detailed macro- to microstructural analysis. Section A presents structural mapping and a tectonic mechanism for the development of S_2 foliation during D_2. Sections B to D describe microstructures and related deformation processes and metamorphism with emphasis on the geometry of D_1 structures.

The content of each section is briefly described below, and individual ABSTRACTS are provided in each section.

Section A

Two different tectonic models exist in the literature for the structural evolution of the Eastern Fold Belt of the Mt Isa Inlier. The first model is based on the Mount Isa deep seismic section with some field examples and suggests initial west directed D_2 thin-skinned or nappe-style folding followed by thick-skinned deformation and upright folding and faulting. In this model, D_2 foliation (S_2) is interpreted to be initiated as predominantly shallow dipping. The second model suggests that the terrain experienced a far more complex deformation history during the Isan Orogeny, which caused the overprinting of successive near-orthogonal foliations. In the latter model, D_2 is characterized by regional W-E shortening that produced a pervasive steep north-south striking regional S_2 foliation. Whether S_2 was initially developed as predominantly a shallow fabric or a steep one is the subject of this paper. A detailed structural analysis of foliations from a micro- to macroscopic scale has been undertaken in a key area of the Eastern Fold Belt, the southern Selwyn Range. Comparisons have also been made with a newly developed 3D multiscale edge detection analysis using wavelet techniques (Worms).

Section B

This paper compares two independent quantitative microstructural techniques for measuring foliations preserved in porphyroblasts using the same set of oriented thin sections. It shows that the combination of both 'asymmetry switch' and 'FitPitch' techniques for determining FIA (**F**oliation **I**ntersection/**I**nflexion **A**xes preserved in porphyroblast**s**) provide a robust method for determining the deformation history and for assessing all aspects of 3D geometry of inclusions trails. These techniques are used to geometrically characterize the W-E trending D_1 structures of the Isan Orogeney, which can no longer be recognized in the N-S striking penetrative foliation.

Section C

This section provides evidence of extensively developed W-E trending microstructures preserved in porphyroblasts across the Eastern Fold Belt. A succession of distinct FIA sets have been obtained in the Eastern Fold Belt that formed contemporaneously with pre-D_2 relic macrostructures. In addition, the succession of FIA sets reveal more deformation events and associated phases of metamorphism than previously recognized. The FIA data across the orogen shows remarkably consistent trends and the significance of this data has been discussed in detail with respect to Mesoproterozoic regional tectonics and apparent polar wander paths of northern Australia.

Section D

In this paper, FIAs were used to distinguish porphyroblasts of different generations across the Eastern Fold Belt of the Mt Isa Inlier. P-T estimates, consistent with textural relationships and field observations, have been obtained from rocks preserving different FIA sets. P-T pseudosections were calculated in the chemical system MnNCKFMASH using THERMOCALC-3.21. The combination of new thermodynamic modeling and textural data reported here with re-interpretations of previously published and unpublished data allows a new tectonothermal model to be presented that dramatically extends the deformation history and associated thermal regimes for the Eastern Fold Belt. The model may provide a general explanation for LP/HT terrains characterized by similar tectonometamorphic settings elsewhere.

SECTION A

3D successions of folds in the Mt Isa Inlier

3D successions of near-orthogonal progressive bulk inhomogeneous shortening resulting in multiple generations of folds in the Mount Isa Inlier

Abstract

Integrated macro, meso and microstructural analyses of the Sandy Creek, Anitra Prospect and Jasper Ridge/Camel Dam domains (southern Eastern Fold Belt, Mount Isa Inlier) have revealed that the structural evolution of these rocks involved four dominant fabric-generating events. D_1 is preserved in low strain zones as local outcrop scale north and south verging tight to isoclinal recumbent folds (S_0/S_1) with approximately W-E trending fold axes. D_2 is characterized by close, tight to isoclinal, upright to overturned N-S to SSW-NNE trending folds with a pervasive steeply dipping axial plane foliation (S_2), subparallel to S_0/S_1. Strain during D_3 was very heterogeneously developed in the region and appears to be controlled by rheological contrast among the structural domains. Where pelites dominate in Sandy Creek and parts of the Anitra Prospect domain, D_3 is prevalent and occurs as a shallow-dipping, spaced foliation (S_3) and associated west and east verging F_3 folds with a pronounced north and NNE plunging L^2_3 intersection lineation. Mesoscopic scale S_3 crenulations are locally developed in the Jasper Ridge/Camel Dam domain, where dense quartzitic and psammitic units dominate. These observations do not support previously suggested non-coaxial west vergent, nappe-style folding in the region. Shallow S_3 formed as a result of subvertical shortening of S_2. Deformation during D_4 was intense in the Jasper Ridge/Camel Dam domain. It involved recycling of pre-existing foliations with S_3 reactivated and S_2 reused by D_4 shear. In the Anitra Prospect and Sandy Creek domains, D_4 can be observed as small scale tight to isoclinal, upright N-S trending F_4 folds overprinting either S_2 or S_3 with north and NNE plunging L^2_3 and L^2_4 intersection lineations, respectively. Detailed matrix and porphyroblast-matrix microstructural relationships agree with meso- and macroscale D_2 to D_4 structures in the area and accord with NNE trending **F**oliation **I**ntersection **A**xes preserved in porphyroblast**s** (FIA**s**) from the Jasper Ridge/Camel Dam domain. These relationships are consistent with 'worms' derived from a newly acquired and processed 3D geophysical gravity/magnetic data set. The geometry of these 'worms' indicates a steep crustal signature in the Jasper Ridge/Camel Dam domain, but ranging from steep to shallow in the Sandy Creek domain. D_2 metamorphism in the area is characterized by high temperatures and low pressures with andalusite replaced by sillimanite. The latter mineral aligned along the L^2_2 mineral lineation.

1. Introduction

The subhorizontal or flat-lying foliations in many medium- to high-grade metamorphic belts are thought to be the product of thrusting, nappe-style tectonics or extensional detachments. Examples include the Appalachians (e.g., Rosenfeld, 1968; Thompson et al., 1968; Spear et al., 1990; Robinson et al., 1991; Armstrong et al., 1992;

Florence et al., 1993), the Variscan belt and the European Alps (e.g., Matte and Burg, 1981; Meissner et al., 1981; Thompson and Bard, 1982; Selverstone, 1985; Matte and Mattauer, 1987; Matte, 1986; 1991; Demange, 1994; Mattauer et al., 1996; Martínez Catalán et al., 1997 and many others). These models adequately explain P-T histories or metamorphic cycles involving compression (crustal thickening) followed by decompression (exhumation). However, they do not explain the tectonic origin of meso- to microscopic scale steep fabrics in low strain zones of predominantly subhorizontal foliation (e.g., Bell and Johnson, 1989; Hayward, 1990, 1992; Aerden, 1994, 1998; Stallard, 1998; Rey et al., 2001). Recently, detailed macro- to microstructural studies across these regions have resolved the tectonic origin and significance of this steep fabric, which is preserved in low strain zones of flat-lying foliations, for example, the Variscan Belt (e.g., Aerden, 1994, 1995, 1998; Aerden and Malavieille, 1999) and the Appalachians (e.g., Bell et al., 1998; Stallard, 1998; Hickey and Bell, 1999, 2001; Bell and Welch, 2002; Ham and Bell, 2004). These authors proposed multiple successions of subhorizontal and subvertical shortening events that generated the steep and shallow dipping structures, respectively. They addressed the significance and importance of gravity driven tectonic processes and the associated fabric development, after crustal over thickening during orogenesis.

The Mt Isa Inlier of northwest Queensland, Australia, is a Mesoproterozoic multiply deformed and polymetamorphosed terrain of significant economic value (e.g., Oliver et al., 1998). The inlier has been divided into three N-S trending tectono stratigraphic belts; the Western Fold Belt, the Kalkadoon-Leichhardt belt and the Eastern Fold Belt (Fig. 1; Blake, 1987; Blake and Stewart, 1992). The long-lived Isan orogenic event (*ca.* 1610 to 1520Ma; Page and Bell, 1986; Hand and Rubatto, 2002) produced multiple deformation and associated foliations. The tectonic interpretations of these fabric generating events have been the subject of considerable controversy (e.g., Bell, 1983; Passchier and Williams, 1989; Holcombe et al., 1991; Bell et al., 1992; Connors and Lister, 1995; Betts et al., 2000). Two different tectonic models exist in the literature for the structural evolution of the Eastern Fold Belt. The first model is based on the Mount Isa deep seismic section with some field examples and suggests initial west directed D_2 thin-skinned or nappe-style folding followed by thick-skinned deformation and upright folding and faulting (e.g., O'Dea et al., 1997ab; Giles et al., 1998; Goleby et al., 1998; MacCready et al., 1998; Betts, et al., 2000). The second model suggests that the terrain experienced a far more complex deformation history during the Isan Orogeny, which caused the overprinting of successive near-orthogonal foliations (Reinhardt, 1992; Adshead-Bell, 1998, 2000; Bell and Hickey, 1998; Mares, 1998; Rubenach and Lewthwaite, 2002). In the latter model D_2 is characterized by regional W-E compression that produced a pervasive or continuous (terminology after Powell, 1979; Borradaile et al., 1982) steep north-south striking regional S_2 foliation, whereas, D_3 produced a subhorizontal S_3 fabric, possibly as a result of gravity collapse. Whether S_2 was initially developed as predominantly a shallow fabric (e.g., MacCready et al., 1998; Betts et al., 2000) or a steep one (e.g., Adshead-Bell., 1998) is the subject of this study. To test which orogenic process was responsible for the west-east bulk shortening (D_2) and sequential fabric development during the Isan Orogeny, a detailed structural analysis of foliations from a micro- to macroscopic scale has been undertaken in a key area of the Eastern Fold Belt, the southern Selwyn Range (Fig. 1). This area is characterized by superposed folding sequences (Giles et al., 1998) and ideal for developing an understanding of the tectonic significance of overprinting deformation events during and immediately after the Isan Orogeny. Detailed geological mapping was carried out at 1:20,000 scale using the 1: 100,000 Bureau of Mineral Resources (BMR, 1984) 7054 index as base a map. Forty oriented rock samples were collected for detailed microstructural analysis and a series of horizontally and vertically oriented thin sections were prepared. Comparisons have been made with a newly developed 3D multiscale edge detection analysis using wavelet techniques (Worms). The area is prospective as it lies between giant Ag-Zn-Pb and Cu-Au mines, that is, Cannington in the west, Osborne in the south and Selwyn-Starra in the north (Fig. 1). Three domains, defined by variations in the lithology, structural intensity and style and metamorphic zone were recognized. From west to east, these are the Jasper Ridge/Camel Dam, Anitra Prospect and Sandy Creek (Fig. 2; A0 map in appendix-A).

2. Regional geology and background

The Mount Isa Inlier experienced two major tectonic events, the Barramundi and Isan orogenies. The Barramundi Orogeny represents the earliest phase of tectonism *ca.* 1840-1890Ma, whereas the Isan Orogeny occurred between 1610 to 1510Ma (e.g., Etheridge et al., 1987; Page and Bell, 1986, Page and MacCready, 1997; Page and Sun, 1998). Supracrustal sequences were deposited during episodic extensional and basin forming ‘rift-phase’ and ‘sag phase’ periods between *ca.* 1800 and *ca.* 1620Ma (Beardsmore et al., 1988; Page and MacCready, 1997; Page and Sun, 1998). Bimodal volcanics and various generations of granitic plutons were emplaced during and immediately after the Isan Orogeny and there has been several periods of regional metasomatic alteration (e.g., Pollard and McNaughton, 1997; Page and Sun, 1998; Oliver et al., 1998; Wyborn, 1998; Mark et al., 2004). The Inlier is divided into three north-south trending fold belts, the Western Fold Belt, the Kalkadoon-Leichhardt Belt and the Eastern Fold Belt separated by regional reverse and/or strike-slip faults (e.g., Blake, 1987; O'Dea et al., 1997ab; MacCready et al., 1998). The evidence for Barramundi tectonism in the terrain is preserved in basement gneisses of the Kalkadoon-Leichhardt Belt (Fig. 1). The Eastern and Western fold belts consist dominantly of supracrustal metasediments deformed and metamorphosed during the Isan Orogeny at *ca.* 1620-1510 (e.g., Bell, 1983; Bell et al., 1992; Reinhardt, 1992; Rubenach, 1992, Rubenach and Barker, 1998; Rubenach and Lewthwaite, 2002). The present day structural framework of the Eastern and Western fold belts consist of N-S trending, tight to isoclinal, upright and overturned antiforms and synforms with a pervasive steep S_2 foliation. However, in the Tommy Creek Block and to the north of Snake Creek Anticline, W-E trending folds are common.

High-temperature/low-pressure (HT/LP) metamorphism with anticlockwise pressure (P), temperature (T) and deformation (*d*) paths have been proposed for the Isan Orogeny across the Mount Isa Inlier with a syn- to late D_2 (*ca*. 1545Ma) peak metamorphic event (Rubenach, 1992; Reinhardt, 1992; Oliver et al., 1991; Rubenach and Baker, 1998). However, Rubenach and Lewthwaite (2002), based on detailed microstructural relationships, proposed that the metamorphic peak was late to post-D_3 in the Snake Creek Anticline of the Eastern Fold Belt (Fig. 1). Giles and Nutman (2002) argued that the amphibolite facies peak metamorphism in the Eastern Fold Belt occurred *ca*. 50Ma before that in the Western Fold Belt, based on SHRIMP U-Pb monazite dating of fabrics (*ca.*1585±5Ma) from Cannington and the Maronan homestead at the eastern margin of the Eastern Fold Belt (Fig. 1). However, recent monazite dates across the region from Hazeldene area of the Western Fold Belt, Rosebud Syncline and Tommy Creek Block of the Eastern Fold Belt yield consistent ages of around *ca.*1575±10Ma as the metamorphic peak (Hand and Rubatto, 2002). This suggests that it occurred early-D_2 (1585-1575Ma) and was consistent over the whole Mount Isa terrain, rather than bipartite from east to west as suggested by Giles and Nutman (2002).

3. The study area

3.1. Lithological units

Metasedimentary units are dominated by pelites, psammopelites, psammites and quartzities, respectively from east to west. The rocks show paucity of both younging indicators and usable stratigraphic marker horizons. Granite/pegmatite bodies are abundant in the Anitra Prospect and Sandy Creek domains. Amphibolites dominate in the Jasper Ridge/Camel Dam domain.

3.2. Sandy Creek domain

The Sandy Creek domain is distinguished by the occurrence of a substantial pelitic component with subordinate psammites. In terms of the relative abundance (based on the thickness of each unit) the average pelite versus psammite ratio in the Sandy Creek domain is ~6 : 4. Thickness of individual layer ranges from 0.05 to 1.5 meters. The pelitic rocks are medium- to coarse-grained Ms-Bt schists (symbols after Kretz, 1983). Sillimanite was not observed in hand specimens. However, in thin sections it occurs as masses of fibrolite (see sections 6 and 7 of this manuscript).

Primary sedimentary structures are not well preserved in the rocks. However, millimeter to centimeter scale bedding laminae can locally be observed in psammites. Unfortunately, a stratigraphic polarity could not be established in the Sandy Creek domain. At location 46 (Fig. 2), where D_1 folds were observed in psammite, the grain size of bedding laminae increases from core to limb (fining upward), possibly indicating a younging direction (Fig. 4e,f).

3.3. Anitra Prospect domain

In the Anitra Prospect domain, the average relative abundance of pelite *vs.* psammite *vs.* quartzite ratio is approximately 3.6 : 4.4 : 2. The thickness of individual layers is between 0.1 to a maximum of 1.6 meters. To the south of the Anitra Prospect, north-south trending fibrolite aligned with the L^2_2 mineral lineation (Fig. 4g), and sillimanite nodules (~1.5cm × 0.8cm) that have replaced K-feldspar, are not uncommon (Fig. 4h) in coarse-grained quartzites or psammites. No prominent sedimentary structures were observed in the rocks except for thin bedding laminae in the quartzitic and psammitic bands. Possible younging directions could not be determined due to the overprinting of pervasive foliations plus the weathering and alteration of the rocks.

3.4. Jasper Ridge/Camel Dam domain

The area is characterized by relatively high relief outcrops and contains interbedded psammites, quartzities, psammopelites and carbonaceous pelites. The average relative abundance of interbedded psammites *vs.* quartzites *vs.* psammopelites *vs.* carbonaceous pelite ratio is ~2 : 3 : 2 : 3. S_0/S_1 has largely been obliterated due to intensely developed S_2 and later events. Younging directions were difficult to interpret except at few locations (e.g., 444, 458 and 450, Figs. 2 and 4a,b). Andalusite porphyroblasts, which have been replaced by coarse-grained muscovite, are common. Garnet is weathered or occurs as relics. Staurolite is fresh and was only observed to the north of the Camel Dam subdomian.

3.5. Pegmatite

Pegmatites with and without a tectonic fabric are relatively abundant in the east compared to the west (Fig. 2). Pegmatites with a tectonic fabric occur from centimeter scale segregations to approximately hundreds of meter tabular sheets and preserve pervasive to semi-pervasive or spaced N-S striking S_2. The intensity of the tectonic fabric generally increases towards the pegmatite margins and they have sharp to transitional contacts with the host rocks. The density of pegmatites without a tectonic fabric is relatively high. These pegmatites form prominent small ridges, especially in the Anitra Prospect domain (Fig. 2) occurring as irregular bodies of various dimensions (~20×20m to 50×50m) the crosscut the foliation.

3.6. Amphibolite

Metabasic rocks constitute a small proportion of the total area but are relatively abundant in the Camel Dam subdomain and in the western part of the Anitra Prospect domain. They are generally concordant with the lithological units, occur as tabular sheets, and consist of hornblende + plagioclase ± biotite with a pervasive tectonic fabric.

3.7. Stratigraphic correlation

In the Selwyn Range, north of the study area (Fig. 1), Beardsmore et al. (1988) reassigned the Staveley Formation and Answer Slate to the Mary Kathleen Group in the west and the Kuridala has re-interpreted as the Soldiers Cap Group in east. The stratigraphic order within the Soldiers Cap Group in the Selwyn Range, from east to west, is described as Llewellyn Creek Formation, Mount Norma Quartzite and Toole Creek Volcanics (Beardsmore et al., 1988). In this study, direct correlation has not been attempted because of the lack of characteristics of typical Soldiers Cap Group rocks (e.g., Derrick et al., 1976). The package of rocks may represent a part of the Soldiers Cap Group, but not the whole succession. This study tentatively supports the stratigraphic interpretations of Beardsmore et al. (1988) in the Selwyn Range (Fig. 1).

4. Deformation history

4.1. D_1 structures

The earliest deformation is characterized by mesoscopic north and south verging F_1 folds that are parallel to near-similar shape in profile (Fig. 4a,c,e). They were found only in the competent units such as psammite or quartzite and have approximately west-east trending subhorizontal fold axes. They were not recognized by previous workers (Giles et al., 1998; Williams and Phillips, 1991). The interlimb angle is generally close to tight ($\leq 50^{o}$)' rarely isoclinal, with an almost horizontal axial plane cleavage (S_1). Such folds are classified as tight recumbent folds (terminology after Fleuty, 1964). Some, such as those shown in figure 4c and 4e, are preserved in the hinge region of D_2 folds. S_1 lies subparallel to the bedding or at high angle near the hinge region, is faintly visible as a north-south alignment of fine-grained muscovite. The fold axes of these primitive folds lies at right angles to the subsequent macro and mesoscopic D_2, D_3 and D_4 folds.

4.2. D_2 structures

4.2.1. Jasper Ridge/Camel Dam domain

In the Jasper Ridge/Camel Dam domain, S_2 is defined by a steep, pervasive, SSW-NNE striking axial plane foliation (Fig 3a) and lies subparallel to S_0/S_1. The intersection lineation, $L^{0/1}{}_2$, (terminology after Bell and Duncan, 1978) is scantily exposed in this particular domain, having been destroyed and obscured by later deformational phases. Moreover, F_2 fold closures could not be directly observed due to their steep, upright isoclinal nature, erosion of hinges and the presence of pervasive S_2. Since, original bedding is not well preserved, the only criteria used to define antiform/synform pairs were S_0/S_1 – S_2 asymmetry switches and apparent opposite dip directions. Some possible antiform/synform pairs were considered but discarded because of a lack of internal consistency of right-side-up or up-side-down beds and the pervasive and subparallel nature of S_2 to S_0/S_1. Moreover, the discrimination of S_2 foliation from S_4 in this particular domain remained an enigma as they have similar orientations, except in low strain D_4 zones, where S_2 is locally rotated by D_3 and overprinted by D_4 (see below).

4.2.2. Anitra Prospect and Sandy Creek domains

D_2 in the Anitra Prospect domain is characterized by macro- to mesoscopic scale N-S and SSW-NNE trending close, tight to isoclinal F_2 folds (Figs. 3a,b and 5a,b). Generally, the F_2 folds are parallel in profile but similar shaped folds have also been observed. In the central and eastern part of the Anitra Prospect domain, D_2 folds are upright, tight to isoclinal and uncommonly overturned counterclockwise to moderate or shallow orientations (Fig. 6a,b). In the western part of the domain, east verging folds with a clockwise asymmetry are common. Rotation of the steep $S_0/S_1/S_2$ fabric to shallow dips is attributed to the effects of the later D_3 event (Fig. 6c,d). The F_2 fold axes in the Anitra Prospect domain are shallowly plunging to the north or NNE (see $L^{0/1}{}_2$ and $L^2{}_2$ stereoplots; Fig. 3b). In the Sandy Creek domain, the effect of D_3 is predominant with uncommon upright F_2 folds, and S_2 preserved in the hinges of subhorizontal S_3 cleavage (Fig. 6e,f) or rotated from a steep to shallow orientation (*cf.* Figs. 7 and 12).

4.3. D_3 structures

Deformation during D_3 appears to be more heterogeneously developed than D_2, rotating the previously developed S_2 and D_2 structures to low angles and generating shallow dipping S_3 differentiated crenulation cleavages and F_3 folds. The $L^2{}_3$ intersection lineation is gently to moderately plunging to the north and NNE in the region (Fig. 3b). Steeply to moderately inclined S_2 is preserved in the hinges or microlithons of S_3 crenulations (*cf.* Figs. 6c and 12).

D_3 in the Jasper Ridge/Camel Dam domain is characterized by subhorizontal, locally differentiated west-east striking crenulations with S_3 axial plane (Fig. 8a,b,c,d). Generally, the mesoscale S_3 fabric is scarce in the Jasper Ridge/Camel Dam domain due to the inherited competency of the units plus the effects of later steep and intense D_4. In the Anitra Prospect domain, shallow dipping D_3 differentiated crenulations and S_3 cleavage seams have rotated macro- and mesoscopic D_2 structures and S_2 fabric into shallow orientations during the development of F_3 folds (Fig. 6c,d). The rotation of S_2 to shallow dips and the production of S_3/F_3 involved stretching of the limbs of the F_2 folds to form boudins (Fig. 6a,b), flexural slip to maintain the original thickness of the beds, coaxial shortening to produce shallowly dipping F_3 folds (Fig. 6c,d), and the development of non-coaxial subhorizontal S_3 differentiated crenulations (e.g., Fig. 6e).

In the Sandy Creek domain macro- to mesoscale asymmetric east and west verging F_3 folds are common with a prominent shallowly dipping axial planar S_3 cleavage (Fig. 3, 7a,d). These folds are tight to locally isoclinal and have typical Class 2 similar profile. The fold axes plunge shallowly to the north. Both counterclockwise and clockwise asymmetries are present indicating bulk coaxial deformation during D_3.

However, evidence locally exists for non-coaxial deformation with a top-to-the-west shear sense (Fig. 7f,g).

4.4. D_4 structures

Several small-scale N-S and SSW-NNE trending upright F_4 folds with steep S_4 axial plane, and millimeter scale steep differentiated crenulation cleavages, can locally be observed on vertical, north- or south-facing outcrop surfaces. D_4 overprinted S_2 and S_3 in the Anitra Prospect and Sandy Creek domains forming shallowly plunging L^2_4 or L^3_4 intersection lineations, respectively (e.g., Figs. 6c,d and 9a,c). In the Jasper Ridge/Camel Dam domain, S_2 and S_4 are very similar in orientation and difficult to separate, unless rotation of S_2 by D_3 has occurred in the outcrop. Rotation of S_2 to a moderate orientation in regions of higher D_3 strain allowed the development of steep S_4 (Fig. 9e). The main effect of D_4 in the Jasper Ridge/Camel Dam domain was the development of several mesoscale tight to isoclinal F_4 folds and an intense vertical foliation, which essentially reactivated and decrenulated the pre-existing S_3, reused S_2 and formed a composite $S_{2/3/4}$ foliation. Reactivation, as defined by Bell (1986) and Bell et al. (2003), occurs when progressive synthetic shearing parallel to the axial plane of folds switches to zones of progressive antithetic shearing along the fold limb. The process causes decrenulation of newly forming axial plane crenulations (Fig. 9e,f). Reuse, defined by Davis and Forde (1994), occurs when the progressive shearing component in a subsequent deformation operates in a synthetic sense along pre-existing foliations in subsequent events. More examples are shown in the microstructural section of this paper.

4.5. D_5 structures

The last deformation phase present at a mesoscale in the area was observed in only a few places in the Camel Dam subdomain (3b). It is characterized by shallow dipping, broad crenulations with S_5 as axial plane (Fig. 8a,b,e,f). The asymmetry of S_5 on $S_{2/4}$ is dominantly top-to-the-west. This geometric relationship produced a south plunging $L^{2/4}{}_5$ intersection lineation. S_3 can be discriminated from S_5 by its more intense development and opposite dip direction to S_5 (Figs. 3b and 8c,d).

5. Multiscale edge detection analysis (Worms)

Multiscale edge detection analysis using wavelets (Worms) have recently been developed in a collaborative project between the CSIRO Division of Exploration and Mining and Fractal Graphics Ltd. The edge detection of geological entities forms the basis of the approach, such as discrete interfaces between geological units of contrasting density (gravity) or magnetic susceptibility (magnetics). For example, stratigraphic contacts, intrusions, unconformities, metamorphic isograds, faults or separate rocks with different densities/magnetic susceptibilities. It provides a powerful tool for 3D terrain scale analysis of potential gravity and magnetic data (e.g., Archibald et al., 1999; Holden et al., 2000). Further information on the theory and processing of the wavelet techniques can be found at,

http://www.agcrc.csiro.au/projects/3054CO
www.fractalgraphics.com.au

Figure 10 shows the use of the multiscale edge or worm technique on the 1:100 000 BMR Selwyn Range index map 7054 (*pmd**CRC internal dataset). The overall worming pattern is steep. There are no subhorizontal worm signatures, except for local anomalies such as the Sandy Creek area. The worms clearly discriminate 1) the contact between the Squirrel Hill's granite and the Soldiers Cap Group metasediments, 2) the steep crustal signature of the Cloncurry Fault (Fig. 1), and 3) the steep signatures of the Selwyn-Starra high strain zones. The most intriguing features of the worms regarding the area are, 1) the SSW-NNE striking and steeply dipping signatures of the Jasper Ridge/Camel Dam domain, 2) the shallowly to moderately dipping signatures in the Anitra Prospect domain, and 3) the subhorizontal signatures in the Sandy Creek domain. These signatures agree with the surface geology described above.

6. Microstructures

Six fabric-generating events have been recognized within a series of spatially oriented thin sections. Figure 11a shows the scheme adopted for the preparation of thin sections. About 120 vertical (P-section, cut parallel to L^2_2 mineral lineation and N-section, cut perpendicular to the L^2_2 lineation, terminology after Bell and Rubenach, 1983) and horizontal (H-section, cut parallel to L^2_2 but perpendicular to S_0/S_1-S_2) thin sections were prepared in this study.

6.1. Matrix microstructures

6.1.1. D_1 microstructures

Microstructural evidence for D_1 is poorly preserved in N or P-sections largely due to the effect of later deformation events reorienting and transposing S_1, especially during D_2. In H-sections, relic bedding laminae are subparallel to S_2 or $S_{2/4}$ (Fig. 11b).

6.1.2. D_2 microstructures

The S_2 matrix foliation is a pervasive, intensely developed, moderately to steeply dipping fabric. In the Sandy Creek and Anitra Prospect domains, S_2 consists of medium- to coarse-grained quartz and phyllosilicates. It dips moderately to shallowly in hinge zones of D_3 (Fig. 12). In the Jasper Ridge/Camel Dam domain, S_2 is locally preserved as it has been reused or recycled (terminology after Ham and Bell, 2004) during D_4 shearing. The recycled fabric can also be distinguished due to its intensity and grain size variation. However, it can be observed as a steeply oriented fabric in low strain zones of D_3 and D_4, or as steeply pitching inclusion trails in porphyroblasts (see below).

6.1.3. D_3 microstructures

The effect of D_3 is more distinct in thin section and is defined by the rotation of steep S_2 (and S_0/S_1) into shallow orientations with the development of a pervasive or semi-pervasive axial plane S_3 (*cf.* Figs. 12 and 13a,b). In the Sandy Creek and parts of Anitra Prospect domain, S_2 is rotated to moderate or shallow dips by the overprinting of D_3 and in most of the vertical N-sections, both clockwise (top-to-the-east) and counterclockwise (top-the-the-west) rotation of S_2 have been observed, potentially indicating overall coaxial deformation during D_3 (Fig. 12a). However, predominant clockwise shear (Fig. 12b) to counterclockwise shear (Fig. 12c) are also common across the axial planes of F_3 folds where opposite shear senses are preserved on opposing limbs of folds (e.g., Fig. 7a,b). In the Jasper Ridge/Camel Dam domain, S_3 in the matrix is only preserved in areas of low D_4 strain (Fig. 13c,d) and in the strain shadows of porphyroblasts (Fig. 16)

6.1.4. D_4 microstructures

In the Jasper Ridge/Camel Dam domain, D_4 is generally characterized by steep S_4 at stage 4 to 5 and locally 6 of crenulation cleavage development (Fig. 14; Bell and Rubenach, 1983). The asymmetry of S_4 on $S_{2\pm3}$ is dominantly counterclockwise and locally clockwise (*cf.* Figs. 13c,d and 14a,b), indicating dominantly non-coaxial deformation and local coaxial deformation in hinges, respectively. D_4 initially produced a steep S_4 fabric, and during the deformation reused the pre-existing S_2 and reactivated S_3 (Figs. 14b and 15). S_4 in the Sandy Creek and Anitra Prospect area is similar in orientation to the Jasper Ridge/Camel Dam domain. However, the intensity of D_4 is relativity low (Figs. 12b and 13a,b).

6.1.5. D_5 and D_6 microstructures

Weak, almost west-east striking and shallowly dipping broad crenulations that deform $S_{2/4}$ fabric have been interpreted as S_5, and have been observed in few thin sections from the Jasper Ridge/Camel Dam domain (Fig. 13c,d). D_6 is a local, weakly developed event that is steeply oriented and rotates the S_5 and $S_{2/4}$ with an anticlockwise shear sense. This deformation appears to be the last event in the structural history of the Jasper Ridge/Camel Dam domain.

6.2. Description of foliations in porphyroblasts

6.2.1. Staurolite

Staurolite contains inclusion trails of elongate quartz, graphite and ilmenite (Fig. 16). The most common inclusion trail geometry consists of a foliation defined by inclusion poor (Fig. 16a,b,c) to inclusion rich cores (Fig. 16d,e,f), slightly curving in the median region and becoming straight. At the rim, the inclusion trails are generally continuous with the matrix foliation and locally truncated (terminology after Bell and Johnson, 1989; Adshead-Bell and Bell, 1999). The inclusion trails form typical staircase geometries with a near-orthogonal pattern. This staircase geometry of inclusion trail pattern is due the opposing shear senses on S_3 and S_4 (Fig.16; e.g., Bell et al., 2003) and cannot be readily explained by porphyroblast rotation models (see section 8 of this manuscript).

S_0/S_1 trails were not observed in staurolite porphyroblasts, suggesting that this phase (staurolite) grew late in the deformation history. Near orthogonal S_2, S_3 and S_4 are preserved, suggesting at least two stages of porphyroblast growth (Fig. 16). The foliations can be correlated with matrix S_2, S_3 and S_4, respectively. S_2 is defined by steeply oriented, relatively fine-grained quartz and ilmenite inclusions, preserved in the core of staurolite porphyroblasts (Fig. 16). In the median region, S_2 curves into shallow dipping S_3 forming slight sigmoidal geometries. S_3 is consistently subhorizontal in all thin sections observed. From median to rim, S_3 inclusion trails are generally continuous and rarely truncated against S_4.

6.2.2. Andalusite

Andalusite is commonly replaced by coarse-grained muscovite and the degree of replacement varies from minor to total replacement (Fig. 17a,d). Two generations of muscovite are observed. The first generation of coarse muscovite is aligned parallel to the subhorizontal S_3 foliation (Fig. 17d), whereas the second generation is subvertical, parallel to S_4 and elongate at the margins of the porphyroblast. The inclusion trails are straight, staircase or slightly sigmoidal in shape and generally continuous with the matrix.

Near orthogonal S_2 , S_3 and S_4 are preserved and can be correlated with matrix S_2, S_3 and S_4, respectively (Fig. 17). The inclined orientation of S_2 in porphyroblasts is largely due to the effect of D_3 rotating S_2 to moderate dips prior to porphyroblast growth and this relationship can be recognized by the angular geometry of steep S_4 matrix foliation with moderately dipping S_2 inclusion trails (Fig. 17a,b). S_3 is consistently subhorizontal and continuous with S_4 inclusion trails at the rim of the porphyroblasts. Where S_3 is not preserved, S_2 is continuous with the matrix S_4.

6.2.3 Garnet

The garnet porphyroblasts are highly weathered/altered and were recognized based on their octahedral shape. They were only found in the Jasper Ridge/Camel Dam domain and occur as relics in the matrix (Fig. 11b) or within pseudomorphed andalusite (Fig. 18a). Relic garnet with reaction rims of biotite or chlorite has been found in pelitic schists, north of the study area (Adshead-Bell, 2000).

6.2.4. Sillimanite

In the Anitra Prospect and Sandy Creek domains, fibrolite is parallel to the S_2 foliation and locally folded and aligned with shallow dipping S_3 (Fig. 18b). In P-sections, fibrolite is subparallel to the L^2_2 mineral lineation and plunges moderately to shallowly to the north. It locally replaces biotite. However, in the Jasper Ridge subdomain, fibrolite lies parallel to the S_4 matrix foliation (Fig. 17a,c) and locally replaces andalusite and Ms.

6.3. FIA measurements

Methods for measuring **F**oliation **I**ntersection/**I**nflexion **A**xes in porphyroblast**s** (FIAs) were described by Hayward (1990) and Bell et al. (1995, 1998). The method uses multiple vertical oriented thin sections cut in a radial pattern through a sample. The asymmetry switch of inclusion trails from clockwise to counterclockwise or vice versa is determined (Fig. 19). A set of eight vertical thin sections are required to measure a FIA trend within a 10° range, with one cut every 30° around the compass and two cut 10° apart where the asymmetry of the inclusion trails switch. Thus, a FIA is recorded for a sample or for group of porphyroblasts in a sample, rather than for an individual porphyroblast.

FIAs have been measured from two samples containing andalusite or staurolite with S_2, S_3 and S_4 inclusion trails. A consistent asymmetry switch of S_2 to S_3 and S_3 to S_4 between 010^o and 030^o has been measured (Fig. 19). Only limited FIA measurements were possible because the porphyroblasts were either weathered (garnets) or partially pseudomorphed by coarse muscovite (andalusite), plus there was only a low density of porphyroblasts in many rocks. The NNE trending FIA measurements appear to be consistent with the NNE plunging mesoscopic $L^2{}_3$ and $L^3{}_4$ intersection lineations measured in the field.

7. Metamorphic zones

Mineral assemblages in the pelitic rocks indicate that the metamorphic grade increases from west to east and two metamorphic zones are evident,

1. The andalusite plus sillimanite zone, comprising the Jasper Ridge/Camel Dam domain,
2. The sillimanite zone comprising the Anitra Prospect and Sandy Creek domains

7.1. Andalusite plus sillimanite zone

Andalusite with or without relic garnet has been found in the Jasper Ridge/Camel Dam domain, whereas staurolite and pseudomorphed andalusite has been observed in few pelitic bands north of the Camel Dam subdomain. Partial to total replacement of andalusite by coarse muscovite is common. The latter phase is locally replaced by sillimanite. In the Jasper Ridge subdomain, fibrolite is aligned parallel to the matrix S_4 foliation (Fig. 17a,b,c) and locally replaces coarse muscovite at the margin of the andalusite. In the latter case, andalusite porphyroblasts preserve S_2 or S_3 trails and the sillimanite is aligned parallel to the matrix S_4 foliation. This relationship suggests that the sillimanite in the Jasper Ridge subdomain locally grew during or late D_4. D_4 sillimanite growth has also been described from rocks in the high strain zones of the Selwyn Range, north of the study area (Fig. 1; Adshead-Bell, 2000).

7.2. Sillimanite (K-feldspar) zone comprising Anitra Prospect and Sandy Creek domains

In this zone, it appears that andalusite has been pseudomorphed by aggregates of fibrolitic sillimanite that define S_2 and L^2_2. The co-existence of sillimanite (that has replaced K-feldspar nodules) with abundant syn-D_2 foliated pegmatite/granite partial melts indicates at least upper amphibolites facies conditions. The occurrence of a second generation of undeformed pegmatite in the same zone suggests that a later thermal pulse occurred. These second-generation pegmatites cross cut the D_2, D_3 and even D_4 fabric in the Anitra Prospect and Sandy Creek domains. The presence of unstrained sillimanite along S_4 in the adjacent zone 1 also indicates local high temperature conditions during or immediately after D_4. Therefore, it is suggested that the intensity of D_4 in zone 2 was not high in terms of pervasive fabric development, but temperature conditions may have been high enough to produce second generation partial melts in the form of coarse-grained pegmatite. This suggests that peak metamorphism in the Eastern Fold Belt was of a dual nature and may resolve the prolonged controversy over D_2 to D_4 peak metamorphic periods elsewhere in the Eastern Fold Belt (*cf.* Rubenach, 1992; Rubenach and Barker, 1998; Hand and Rubatto, 2002; Rubenach and Lewthwaite, 2002).

7.3. KFMASH P-T pseudosection

A P-T pseudosection has been calculated to constrain the P-T conditions of the formation of mineral phases using the reactions that limit their stability fields for a representative rock sample (e.g., Spear and Cheney, 1989; Powell et al., 1998). The sample (SR8.1) consists of an And (replaced by coarse-grained muscovite) St-Bt-Ms schist, north of the Camel Dam subdomain (Fig. 20). Since CaO and MnO occur in insignificant amounts, a 6-component system phase diagram KFMASH (K_2O-FeO-MgO-Al_2O_3-SiO_2-H_2O) has been prepared using the software THERMOCALC 3.2 (Powell et al., 1998) to examine mineral appearance and disappearance with respect to univariant reaction lines. The software uses the thermodynamic dataset of Holland and Powell (1998) and Powell et al. (1998).

7.4. Metamorphic conditions

Based on the appearance and disappearance of mineral phases and textural relationships, the following path is suggested. Andalusite in the sample is partially pseudomorphed by muscovite. Therefore, the timing of mineral growth is uncertain. However, andalusite with S_1 inclusion trails has been found from the Selwyn-Starra region (Adshead-Bell, 2000), ~2km north of the studied sample, and also from the Houdini Prospect area, lying ~4km west of the Jasper Ridge subdomain. This suggests that andalusite grew first in deformation history and during the D_2 event preserving S_1. This is consistent with the first appearance of andalusite in the P-T pseudosection (Fig. 20). Staurolite growth would have commenced after andalusite during D_3, preserving S_2 inclusion trails. This is obvious from the staurolite-in reaction line for the St-Bt-And field. Staurolite porphyroblasts contain steep S_2, shallow S_3 and steep S_4 inclusions (Fig. 16). N-S trending FIAs have been obtained for And and St. Therefore the P-T path constructed is for the W-E shortening D_2 event plus subsequent events. The path for D_1 metamorphism cannot be constrained, as no W-E trending FIAs have been obtained. However, relic garnet porphyroblasts with reaction rims have been observed within andalusite from the Jasper Ridge subdomian and may have formed earlier during higher-pressure D_1 metamorphism (Fig. 18a). The relic nature of garnet porphyroblasts with reaction rims indicates a low-pressure overprint (e.g., García-Casco and Torres-Roldán, 1996, 1999). This appears to be in agreement with locations where relic garnets have been observed in the cores of andalusite porphyroblasts. The pseudomorphed nature of andalusite could be due to a relatively higher-pressure W-E shortening overprint of St along the P-T path (e.g., Pattison et al., 1999, 2002). Alternatively, Ms acted in a catalytic capacity during prograde metamorphism (Carmichael, 1969; Rubenach and Bell, 1988).

The metamorphic field gradient has been shown on Fig. 20 for the Jasper Ridge/Camel Dam domain in the west (Andalusite+sillimanite zone) to Anitra Prospect and Sandy Creek domains in the east (sillimanite+K-feldspar zone). The second sillimanite isograde reaction line (Ms+Qtx =Al_2O_3+K-feldspar+H_2O) is also shown to define the metamorphic conditions of the Anitra Prospect and Sandy creek domains.

8. Discussion and conclusions

8.1. Development of foliations / lineations and their regional correlation

W-E trending D_1 folds have formed a weak S_1, which has been overprinted by near-orthogonal D_2 folds with pervasive S_2. These D_1 folds are best preserved in low strain portions of D_2 structures and were observed locally in the Sandy Creek, Anitra Prospect and Jasper Ridge/Camel Dam domains, signifying their regional distribution. This further suggests mechanical anisotropy during D_1 or that D_2 more extensively transposed D_1 structures in the pelites due to their lowest competency compared with the quartzite or psammite.

Similar structures at the meso and microscale have been observed across the Eastern Fold Belt, such as in the Selwyn Range (De Jong, 1995; Adshead-Bell, 1998, 2000), Fairmile/Partridge (Mares, 1998), Hampden Synform (Betts, et al., 2000), Rosebud Syncline (Reinhardt, 1992), Snake Creek Anticline (Rubenach and Lewthwaite, 2002) and even in the Western Fold Belt (Bell, 1983). These authors interpreted that these D_1 structures were related either to the initial north-south shortening phase of the Isan Orogeny or folds predating the D_2 event. Based on their regional distribution, it is suggested that these relic D_1 folds can be correlated across the Eastern Fold Belt and resulted from the early N-S shortening phase of the Isan Orogeny.

D_2 produced pervasive, steep N-S striking S_2 foliation and a pronounced L^2_2 mineral lineation. The N-S orientation of S_2 suggests D_2 formed as a result of west-east shortening and refolded S_0/S_1. Many workers have observed macro- to microscale tight to isoclinal, upright and overturned north-south trending folds in the Eastern and Western Fold belts, now interpreted as the main structural grain of the Mount Isa Inlier (e.g., Bell et al., 1992; Reinhardt, 1992; Mares, 1998; Betts et al., 2000).

The intensity and effect of D_3 was variable, due to rheological and strain heterogeneity across the region. In the Sandy Creek domain, where pelites and psammopelites dominate, shallow dipping D_3 structures are prevalent. They consist of S_3 and asymmetric macro to mesoscopic scale F_3 folds (Fig. 21a). In the Anitra Prospect domain, where competent and incompetent units are present, D_3 strain is heterogeneously developed and has rotated S_2 into moderate dips, either with the development of subhorizontal crenulation cleavages or by stretching of F_2 fold limbs. In the Jasper Ridge/Camel Dam domain where rheological contrast is minimal in terms of competency, the development of S_3 is very localized. This suggests that D_3 was a phase of subvertical shortening and the gravitational potential energy, which developed due to thickening of the orogen in D_2, was released by gravitational collapse to form S_3 (Fig. 21a). The importance of meso and macroscale shallow dipping structures was described by Whitelock (1989) in the White Blow Formation, Mary Kathleen Fold Belt and Bell and Hickey (1998) within the Mount Isa and Hilton mine regions. Bell and Hickey (1998) named those structures $D_{2.5}$ to retain the previous nomenclature as D_1, D_2 and D_3 in the Mount Isa region. Subsequently, numerous macro- to microscale shallow dipping structures were identified in the Snake Creek Anticline (Rubenach and Baker, 1998; Rubenach and Lewthwaite, 2002), Fairmile (Mares, 1998), Tommy Creek Block (Lally, 1997) and Selwyn Range (Adshead-Bell, 1998, 2000) of the Eastern Fold Belt. Betts et al. (2000) recognized shallow crenulation cleavages in the Hampden Synform, but did not interpret the tectonic origin and significance of these foliations. Thus, from D_1 to D_3, a 3D succession of folds were produced during the Isan Orogeny as a result of N-S D_1 shortening, followed by D_2 W-E shortening and then D_3 subvertical shortening.

$S_{4,}$ which formed as a result of west-east shortening during D_4, is defined by a steep fabric overprinting both S_2 and S_3 in the region and is more intense in the Jasper Ridge/Camel Dam domain. Elsewhere in the Eastern and Western fold belts, evidence exists for a second-generation steep deformation event. For example, in the Selwyn Range (Adshead-Bell, 1998, 2000), Snake Creek Anticline (e.g., Rubenach and Lewthwaite, 2002) and in the Mount Isa (Bell and Hickey, 1998). Based on their similar geometry and style, the D_4 of this study appears to be equivalent to these structures.

8.2. Nature of D_2 versus effects of D_3

In a group of recent publications (Giles and MacCready, 1997; Giles et al., 1998; Goleby et al., 1998; MacCready et al., 1998; Betts, et al., 2000) it has been argued that the geometry of D_2 in the Eastern Fold Belt initially evolved through west directed thin-skinned deformation and nappe-style folding, followed by thick-skinned deformation and upright folding and faulting producing N-S striking steep structures (Fig. 21b). This argument is based on the Mt Isa deep seismic section (Fig. 1) plus some field examples. Giles et al. (1998) recognized two major deformation episodes in the study area and supported the west-vergent low angle thin-skinned to think-skinned tectonic model. However, based on detailed macrostructural surface analysis, this study shows that S_2 was initially formed as steep pervasive fabric during D_2, which was subsequently rotated to shallow angles due to the effect of subvertical shortening D_3 or subhorizontal stretching (Sayab, 2004). This observation is further strengthened by microstructures that are consistent with the field observations from all three domains with near-orthogonal steep and shallow S_2 and S_3 foliations, respectively. The 3D geophysical data supports a steep crustal signature rather than shallow structures.

8.3. Near-orthogonal multiple fabric generating folding events

Sets of intersection lineations, that is, $L^2{}_3$, $L^2{}_4$, $L^3{}_4$ and $L^2{}_5$ and their respective S_2, S_3, S_4 and S_5 planar fabrics show multiple near-orthogonal deformation events, rather than nappe-style deformation (e.g., Giles et al., 1998; MacCready et al., 1998). The multiple overprinting of fabric development is consistent from field to matrix microstructures to within porphyroblasts. The intersection lineation data suggests that there are at least five outcrop scale-folding events. In addition, there is no evidence of east or west trending $L^2{}_2$ or $L^3{}_3$ mineral stretching lineation, which could have resulted from west vergent nappe-style folding. Instead, $L^2{}_2$ is shallowly to moderately plunging to the north.

8.4. Porphyroblast rotation versus non-rotation models

Structural geologists who supported rotational models for porphyroblasts behavior during ductile deformation (e.g., Williams and Schoneveld, 1981; Passchier et al., 1992; Williams and Jiang, 1999; Jiang and Williams, 2004) argued for the development of sigmoidal or spiral inclusion trails in a single non-coaxial deformation, but partially accepted the validity of porphyroblast non-rotation in some conditions (e.g., Passchier and Speck, 1994; Passchier and Trouw, 1998). Those using the non-rotational model explain the development of sigmoidal/staircase inclusion trails as the result of sequential porphyroblast growth over steep or shallow fabric producing events (e.g., Bell and Johnson, 1989; Steinhardt, 1989; Aerden, 1995, 1998; Williams, 1994; Cihan, 2004). Bell et al. (2003) showed that staircase inclusion trails geometries can only be formed via non-rotational porphyroblast models acting differently on either limb of a preexisting regional fold. They envisage incremental near-orthogonal fabric development as being responsible for staircase (with opposite asymmetry from steep to flat or vice versa) or spiral (with same asymmetry from steep to flat or vice versa) geometries within porphyroblasts. They argued that these multiple fabrics preserved in porphyroblasts can even be dated (Bell and Welch, 2002).

Only porphyroblasts with staircase inclusion trails have been observed in the Jasper Ridge/Camel Dam domain. Rotational models do not adequately explain the development of staircase inclusion patterns (Williams and Jiang, 1999). Only inclusion trail patterns resulting from opposing differentiation asymmetries within the porphyroblasts, from steep to flat and then flat to steep (e.g., S_2 to S_3 and S_3 to S_4 in this study), can explain the formation of staircase patterns. This also accords well with matrix and outcrop scale structures.

References

Adshead-Bell, N. S., 1998. Evolution of the Starra and Selwyn high-strain zones, Eastern Fold Belt, Mount Isa Inlier: implications for Au-Cu mineralization. Economic Geology 93, 1450-1462.

Adshead-Bell, N. S., 2000. Structural constraints of the ironstone hosted Au-Cu Starra deposit and Selwyn Range Region, Eastern Fold Belt, Mt Isa Inlier. Unpublished Ph. D thesis, James Cook University, Townsville, Queensland, D1-D55.

Adshead-Bell, N. S., Bell, T. H., 1999. The progressive development of a macroscopic upright fold pair during five near-orthogonal foliation-producing events: complex microstructures versus a simple macrostructure. Tectonophysics 306, 121-147.

Aerden, D. G. A. M., 1994. Kinematics of orogenic collapse in the Variscan Pyrenees deduced from microstructures in porphyroblastic rocks from Lys-Caillaouas Massif. Tectonophysics 238, 139-160.

Aerden, D. G. A. M., 1995. Porphyroblast non-rotation during crustal extension in the Variscan Pyrenees. Journal of Structural Geology 17, 709-726.

Aerden, D. G. A. M., 1998. Tectonic evolution of the Montagne Noire and a possible orogenic model for syn-collisional exhumation of deep rocks, Hercynian belt, France. Tectonics 17, 62-79.

Aerden, D. G. A. M., Malavieille, J., 1999. Origin of a large-scale fold nappe in the Montagne Noire (Variscan Belt France). Journal of Structural Geology 21, 1321-1333.

Archibald, N., Gow, P., Boschetti, F., 1999. Multiscale edge analysis of potential field data. Exploration Geophysics 30, 38-44.

Armstrong, T. R., Tracy, R. J., Hames, W. E., 1992. Contrasting styles of Taconian, Eastern Acadian and Western Acadian metamorphism, central and western New England. Journal of Metamorphic Geology 10, 415-426.

Beardsmore, T. J., Newbery, S. P., Laing, W. P., 1988. The Maronan Supergroup: an inferred early volcanosedimentary rift sequence in the Mount Isa Inlier, and its implications for ensialic rifting in the middle Proterozoic of northwest Queensland. Precambrian Research 40/41, 487-507.

Bell, T. H., Duncan, A. C., 1978. A rationalized and unified shorthand terminology for lineation and fold axes in tectonites. Tectonophysics 47, T1-T5.

Bell, T. H., 1983. Thrusting and duplex formation at Mount Isa, Queensland, Australia. Nature 304, 493-497.

Bell, T. H., Rubenach, M. J., 1983. Sequential porphyroblast growth and crenulation cleavage development during progressive deformation. Tectonophysics 92, 171-194.

Bell, T. H., 1986. Foliation development and refraction in metamorphic rocks: reactivation of earlier foliation and decrenulation due to shifting pattern of deformation partitioning. Journal of Metamorphic Geology 4, 421-444.

Bell, T. H., Forde, A., Wang, J., 1995. A new indicator of movement direction during orogenesis: measurement technique and application to the Alps. Terra Nova 7, 500-508.

Bell, T. H., Hickey, K. A., 1998. Multiple deformations with successive subvertical and subhorizontal axial planes in the Mount Isa Region: their impact on geometric development and significance for mineralization and exploration. Economic Geology 93, 1369-1389.

Bell, T. H., Hickey, K. A., Upton, J. G., 1998. Distinguishing and correlating multiple phases of metamorphism across a multiply deformed region using the axes of spiral, staircase and sigmoidal inclusion trails in garnet. Journal of Metamorphic Geology 16, 767-794.

Bell, T. H., Johnson, S. E., 1989. Porphyroblast inclusion trails: the key to orogenesis. Journal of Metamorphic Geology 7, 297-310.

Bell, T. H., Reinhardt, J., Hammond, R. L., 1992. Multiple foliation development during thrusting and synchronous formation of vertical shear zones. Journal of Structural Geology 14, 791-805.

Bell, T. H., Welch, P. W., 2002. Prolonged Acadian Orogenesis: revalations from foliation intersection axis (FIA) controlled monazite dating of foliations in porphyroblasts and matrix. American Journal of Science 302, 549-581.

Bell, T. H., Ham, A. P., Hickey, K. A., 2003. Early formed regional antiforms and synforms that fold younger matrix schistosities: their effect on sites of mineral growth. Tectonophysics 367, 253-278.

Betts, P. G., Ailleres, L., Giles, D., Hough, M., 2000. Deformation history of the Hampden Synform in the Eastern Fold Belt of the Mt Isa terrane. Australian Journal of Earth Sciences 47, 1113-1125.

Blake, D. H., 1987. Geology of the Mount Isa Inlier and environs, Queensland and Northern Territory. Bureau of Mineral Resources, Geology and Geophysics Bulletin 225, 1-83.

Blake, D. H., Stewart, A. J., 1992. Stratigraphic and tectonic framework, Mount Isa Inlier. In Stewart, A. J., Blake, D, H., (Eds.): Detailed studies of the Mount Isa Inlier. Bureau of Mineral Resources, Geology and Geophysics Bulletin 243.

Borradaile, G. J., Bayly, M. B., Powell, C. M. A., 1982. Atlas of deformational and metamorphic rock fabrics. Springer, Berlin Heidelberg New York.

Carmichael, D. M., 1969. On the mechanisms of prograde metamorphic reactions in quartz-bearing pelitic rocks. Contribution to Mineralogy and Petrology 20, 244-267.

Carter, E. K., Brooks, J. H., Walker, K. R., 1961. The Precambrian mineral belt of northwestern Queensland. Bureau of Mineral Resources, Geology and Geophysics Bulletin 51, 1-344.

Cihan, M., 2004. The drawbacks of sectioning rocks relative to fabric orientation in the matrix: A case study from the Robertson River Metamorphics (Northern Queensland, Australia. Journal of Structural Geology 26, 2157-2174.

Connors, K. A., Lister, G. S., 1995. Polyphase deformation in the western Mount Isa Inlier, Australia: episodic or continuous deformation? Journal of Structural Geology 17, 305-328.

Davis, B. K. Forde, A., 1994. Regional slaty cleavage formation and fold axis rotation by re-use and reactivation of pre-existing foliations: the Fiery Creek Slate Belt, North Queensland. Tectonophysics 230, 161-179.

De Jong, G., 1995. Post metamorphic alteration and mineralization in a highly deformed Proterozoic terrain: the eastern Selwyn Range, Cloncurry District NW Queesland. Unpublished Ph. D thesis, James Cook University, Townsville, Queensland.

Demange, M., 1994. Antevariscan evolution of the Montagne Noire (France): From a passive margin to a foreland basin. Comptes Rendus de Í Academie des Sciences de Paris 318, 921-933.

Derrick, G. M., Wilson, I. H., Hill, R. M., 1976. Revision of the stratigraphic nomenclature in the Precambrian of northwestern Queensland. V Soldiers Cap Group. Queensland Government Mining Journal 77, 600-604.

Etheridge, M. A., Rutland, R. W. R., Wyborn, L. A. I., 1987. Orogenesis and tectonic process in the Early to Middle Proterozoic of northern Australia. American Geophysical Union, Geodynamics Series 17, 131-147.

Fleuty, M. J., 1964. The description of folds. Proceedings of the Geological Association 75, 461-492.

Florence, F. P., Spear, F. S., Kohn, M. J., 1993. P-T paths from northwestern New Hampshire: metamorphic evidence for stacking in a thrust/nappe complex. American Journal of Science 293, 939-979.

García-Casco, A., Torres-Roldán, R. L., 1996. Disequilibrium induced by fast decompression in St-Bt-Grt-Ky-Sill-And metapelites from the Betic Belt (southern Spain). Journal of Petrology 37, 1207-1239.

García-Casco, A., Torres-Roldán, R. L., 1999. Natural metastable reactions involving garnet, staurolite and cordierite: implications for petrogenetic grids and the extensional collapse of the Betic-Rif Belt. Contributions to Mineralogy Petrology 136, 131-153.

Giles, D., MacCready, T., 1997. The structural and stratigraphic position of the Soldier Cap Group in the Mount Isa Inlier. In: Ailleres, L., Betts, P. (eds.), Structural elements of the Eastern Succession – A field guide illustrating the structural geology of the Eastern Mount Isa Terrane, Australia. Australian Crustal Research Centre, Technical Publication 63, 61-73.

Giles, D., Ailleres, L., Betts, P., Jeffriess, D., 1998. Geologic traverse of the Camel Dam – Pegmont region southeast Mount Isa Inlier. Australian Crustal Research Centre, Technical Publication 66, 1-31.

Giles, D., Nutman, A. P., 2002. SHRIMP U-Pb monazite dating of 1600-1580 Ma amphibolite facies metamorphism in the southeastern Mt Isa Block, Australia. Australian Journal of Earth Sciences 49, 1- 11.

Goleby, B. R., MacCready, T., Drummond, B. J., and Goncharov., 1998. The Mount Isa Geodynamic Transect-Crustal Implications. In: Braun, J., Dooley, J., Goleby, B., Van der Hilst, R., Klootwijik, C., (Eds), Structure and Evolution of the Australian continent, American Geophysical Union, Geodynamic 26, 109-117.

Goscombe, B. D., Passchier, C. W., Hand, M., 2004. Boudinage classification: end-member boudin types and modified boudin structures. Journal of Structural Geology 26, 739-763.

Ham, A. P., Bell, T. H., 2004. Recycling of foliations during folding. Journal of Structural Geology 26, 1989-2009.

Hand, M., Rubatto, D., 2002. The scale of the thermal problem in the Mt Isa Inlier. Geoscience 2002, Expending Horizons. 16th Australian Geological Convention, Geological Society of Australia, Abstract Volume 67, 173.

Hayward, N., 1990. Determination of early fold axis orientation in multiply deformed rocks using porphyroblasts inclusion trails. Tectonophysics 179, 353-369.

Hayward, N., 1992. Microstructural analysis of the classical spiral garnet porphyroblasts of south-east Vermont: Evidence for non-rotation. Journal of Metamorphic Geology 10, 567-587.

Hickey, K. A., Bell, T. H., 1999. Behaviour of rigid objects during deformation and metamorphism: a test using schists from the Bolton syncline, Connecticut, USA. Journal of Metamorphic Geology 17, 211-28.

Hickey, K. A., Bell, T. H., 2001. Resolving complexities associated with the timing of macroscopic folds in multiply deformed terrains The Spring Hill synform, Vormont. Bulletin of the Geological Society of America 113, 1283-1298.

Holcombe, R. J., Pearson, P. J., Oliver, N. H. S., 1991. Geometry of a Middle Proterozoic extensional decollement in northeastern Australia. Tectonophysics 191, 255-274.
Holdaway, M. J., 1971. Stability of andalusite and the aluminum silicate phase diagram. American Journal of Science 271, 97-131.

Holden, D. J., Archibald, N. J., Boschetti, F., Jessell, M. W., 2000. Inferring geological structures using wavelet-based multiscale edge analysis and forward models. Exploration Geophysics 31, 67-71.

Holland, T. J. B., Powell, R., 1998. An internally consistent thermodynamic data set of petrological interest. Journal of Metamorphic Geology 16, 309-343.

Jiang, D., Williams, P. F., 2004. Reference frame, angular momentum, and porphyroblast rotation. Journal of Structural Geology 26, 2211-2224.

Kretz, R., 1983. Symbols for rock-forming minerals. American Mineralogist 68, 277-279.

Lally, J. H., 1997. The structural history of the central Eastern Fold Belt, Mount Isa Inlier, northwest Queensland, Australia. Unpublished Ph. D thesis, James Cook University, Townsville, Queensland, 1- 245.

MacCready, T., Goleby, B. R., Goncharov, A., Drummod, B. J., Lister, G. S., 1998. A framework of overprinting orogens based on interpretation of the Mount Isa deep seismic transect. Economic Geology 93, 1422-1434.

Mares, V. M., 1998. Structural development of the Soldiers Cap Group in the Eastern Fold Belt of the Mt Isa Inlier: a successive of horizontal and vertical deformation events and large-scale shearing. Australian Journal of Earth Sciences 45, 373-387.

Mark, G., Foster, D. R. W., Pollard, P. J., Williams, P. J., Tolman, J., Darvall, M., Black, K. L., 2004. Stable isotope evidence for magmatic fluid input during large-scale Na-Ca alteration in the Cloncurry Fe oxide Cu-Au district, NW Queensland, Australia. Terra Nova 16, 54-61.

Marshall, J. L., Oliver, N. H. S., 2001. Mechanical controls on fluid flow and brecciation in the regional host rocks for Eastern Fold Belt ironstone Cu-Au deposits, Mt Isa Block. Geological Society of Australia, Specialist Group in Economic Geology "Mineralisation, alteration and magmatism in the Eastern Fold Belt, Mount Isa Block Australia: Geological Review and Field Guide", Special Publication No 5, 30 -45.

Martínez Catalán, J. R., Arenas, R., Diaz García, F., Abati, J., 1997. Variscan accretionary complex of Northwest Iberia; tarrane correlation and succession of technometamorphic events. Geology 25, 1103-1106.

Mattauer, M., Laurent, P., Matte, Ph., 1996. Plissement Hercynien synschisteus post-nappe et étirement subhorizontal dans le versant sud de la Montagne Noire. Comptes Rendus de l' Academie des Sciences de Paris 322, 309-315.

Matte, Ph., 1986. Tectonics and plate tectonic model for the Variscan belt of Europe. Tectonophysics, 126, 329-374.

Matte, Ph., 1991. Accretionary history and crustal evolution of the Variscan belt in Western Europe. Tectonophysics 196, 309-337.

Matte, Ph., Burg, J. P., 1981. Sutures, thrusts and nappes in the Variscan Arc of western Europe: plate tectonic implications. In: McClay, K. R., Price, N. J. (Eds.), Thrust and Nappe Tectonics. Geological Society Special Publication 9, 353-358.

Matte, Ph., Mattauer, M., 1987. Hercynian orogeny in the Pyrenees was not a rifting event. Nature 325, 739.

Missner, R., Barthelsen, H., Murawski, H., 1981. Thin skinned tectonics in the northern Rhenish Massif, Germany. Nature 290, 399-401.

O'Dea, M, G., Betts, P. G., MacCready, T., Ailleres, L., 1997a. Sequential development of a midcrustal fold-thrust complex in the eastern Mount Isa Inleir, Australia. Australian Crustal Research Centre, Technical Publication 47, 1-28.

O', Dea, M. G., Lister, G. S., MacCready, T., Betts, P. G., Oliver, N. H. S., Pound, K. S., Huang, W., Valenta, R. K., 1997b. Geodynamic evolution of the Proterozoic Mount Isa terrane: In Burg, J. P., Ford, M., (Eds.). Orogeny through time. Geological Society of London Special Publication 121, 99-122.

Oliver, N. H. S., Holcombe, R. J., Hill, E. J., Pearson, P. J., 1991. Tectono-metamorphic evolution of the Mary Kathleen Fold Belt, northwest Queensland: A reflection of mantle plume processes? Australian Journal of Earth Sciences 38, 425-455.

Oliver, N. H. S., Rubenach, M. J., Valenta, R. K., 1998. Precambrian metamorphism, fluid flow, and metallogeny of Australia. AGSO Journal of Australian Geology and Geophysics 17(4), 31-53.

Page and MacCready, 1997. Rocks of Mount Isa Group age in the Eastern Fold Belt. AGSO Research Newsletter 26, 16-17.

Page, R. W., Bell, T. H., 1986. Isotopic and structural responses of granite to successive deformation and metamorphism. Journal of Geology 94, 365-379.

Page, R. W., Sun, S-S., 1998. Aspects of geochronology and crustal evolution in the Eastern Fold Belt, Mt Isa Inlier. Australian Journal of Earth Sciences 45, 343-361.

Passchier, C. W., Williams, P. R., 1989. Proterozoic extensional deformation in the Mount Isa Inlier: Queensland, Australia. Geological Magazine 126, 43-53.

Passchier, C. W., Speck, P. J. H. R., 1994. The kinematic interpretation of obliquely-transected porphyroblasts: an example from the Trois Seigneurs Massif, France. Journal of Structural Geology 16, 971-984.

Passchier, C. W., Trouw, R. A. J., Zwart, H. J., Vissers, L. M., 1992. Porphyroblast rotation: eppur si muove? Journal of Metamorphic Geology 10, 283-294.

Passchier, C. W., Trouw, R. A. J., 1998. Micro-tectonics. Springer, Berlin Heidelbreg New York.

Pattison, D. R. M., Spear, F. S., Cheney, J. T., 1999. Polymetamorphic origin of muscovite+cordierite+staurolite+biotite assemblages: implications for the metapelitic petrogenetic grid and for P-T paths. Journal of metamorphic Geology 17, 685-703.

Pattison, D. R. M., Spear, F. S., Debuhr, C. L., Cheney, J. T., Guidotti, C. V., 2002. Thermodynamic modeling of the reaction muscovite+cordierite = Al_2SiO_5+biotite+quartz+H_2O: constraints from natural assemblages and implications for the metapelitic petrogenetic grid. Journal of Metamorphic Geology 20, 99-118.

Pollard, P. J., McNaughton, N. J., 1997. U/Pb geochronology and Sm/Nm isotope characteristics of Proterozoic intrusive rocks: In the Cloncurry district, Mount Isa Inlier, Australia. In Pollard, P. J., (Eds.), AMIRA P438 Clouncury Base Metals and Gold 1997 Annual Report, 4.1-4.19.

Powell, C. M. A., 1979. A morphological classification of rock cleavage. Tectonophysics 58, 21-34.

Powell, R., Holland, T., Worley, B., 1998. Calculating phase diagrams involving solid solutions via non-linear equation, with examples using THERMOCALC. Journal of Metamorphic Geology 16, 577-588.

Ramsay, J. G., 1967. Folding and fracturing of rocks. New York, McGraw-Hill, 1- 568.

Reinhardt, J., 1992. Low-pressure, high-temperature metamorphism in a compressional tectonic setting: Mary Kathleen Fold Belt, northeastern Australia. Geological Magazine 129, 41-57.

Rey, P., Vanderhaeghe, O., Teyssier, C., 2001. Gravitational collapse of the continental crust: definition, regimes and modes. Tectonophysics 342, 435-449.

Robinson, P., Thompson, P. J., Elbert, D. C., 1991. The nappe theory in the Connecticut Valley region: Thirty-five yeas since Jim Thompson's first proposal. American Mineralogist 76, 689-712.

Rosenfeld, J. L., 1968. Garnet rotation due to the major Paleozoic deformation in southeast Vermont. In: Zen, E-AN, White, W. S., Hadley, J. B., Thompson, J. B., (Eds.), Studies of Appalachian Geology: Northern and Maritime. Interscience publishers, New York, 185-202.

Rubenach, M. J., 1992. Proterozoic low-pressure/high temperature metamorphism and an anticlockwise P-T-t path for the Hazeldene area, Mount Isa Inlier, Queensland, Australia. Journal of Metamorphic Geology 10, 333-346.

Rubenach, M. J., Bell, T. H., 1988. Microstructural controls and the role of graphite in matrix/porphyroblast exchange during synkinematic andalusite growth in a granitiod aureole. Journal of Metamorphic Geology 6, 651-666.

Rubenach, M. J., Barker, A. J., 1998. Metamorphic and metasomatic evolution of the Snake Creek Anticline, Eastern Succession, Mt Isa Inlier. Australian Journal of Earth Sciences 45, 363-372.

Rubenach, M. J., Lewthwaite, K. A., 2002. Metasomatic albitites and related biotite-rich schists from a low-pressure polymetamorphic terrane, Snake Creek Anticline, Mount Isa Inlier, north-eastern Australia: microstructures and P-T-d paths. Journal of Metamorphic Geology 20, 191-202.

Sandiford, M., 1989. Horizontal structures in granulite terrains: A record of mountain building or mountain collapse? Geology 17, 449-452.

Sayab, M., 2004. 3D successions of near-orthogonal progressive bulk inhomogeneous shortening resulting in multiple generations of folds in the Mt Isa Inlier. In McPhie, J., McGoldrick, P. (eds), Dynamic Earth: Past, Present and Future. Abstracts of the 17th Australian Geological Convention, Hobart, Tasmania, Australia 73, 183.

Selverstone, J., 1985. Petrologic constraints on imbrication, metamorphism and uplift in the SW Tauern Window, Eastern Alps. Tectonics, 687-704.

Spear, F. S., Cheney, J. T., 1989. A petrogenetic grid for pelitic schists in the system SiO2-Al2O3-FeO-MgO-K2O-H2O. Contributions to Mineralogy and Petrology 101, 149–164.
Spear, F. S., Hickmott, D. D., Selverstone, J., 1990. The metamorphic consequences of thrust emplacement, Fall Mountain New Hampshire. Geological Society of America Bulletin 102, 1344-1360.

Stallard, A., 1998. Episodic porphyroblast growth in the Fleur de Lys Supergroup, Newfoundland: timing relative to the sequential development of multiple crenulation cleavages. Journal of Metamorphic Geology 16, 711-728.

Steinhardt, C., 1989. Lack of porphyroblast rotation in noncoaxially deformed schists from Petrel Cove, South Australia, and its implications. Tectonophysics 158, 127-140.

Thompson, J. B., Robinson , P., Clifford, T. N., Trask, N. J., 1968. Nappes and gneiss domes in west-central New England. In: Zen, E-AN, White, W. S., Hadley, J. B., Thompson, J. B., (Eds.), Studies of Appalachian Geology: Northern and Maritime. Interscience publishers, New York, 203-218.

Thompson, P. H., Bard, J. P., 1982. Isograds and mineral assemblages in the eastern axial zone, Montagne Noire (France). Implications for temperature gradients and P-T history. Canadian Journal of Earth Sciences 19, 129-143.

Whitelock, J., 1989. Structural analysis of the synclinal Scott Outlier, Cattle Creek Area, SSW of Mary Kathleen, Mt Isa Inlier. Unpublished Honors thesis, James Cook University, Townsville, Queensland, 1-301.

Williams, P. F., Schoneveld. Chr., 1981. Garnet rotation and the development of axial plane crenulation cleavage. Tectonophysics 78, 307-334.

Williams, P. J., Phillips, G. N., 1991. JCU Cloncurry mapping project 1991. Department of Geology and National Key Centre in Economic Geology, James Cook University. Report to sponsors upon completion of fieldwork, 1-22.

Williams, M. L., 1994. Sigmoidal inclusion trails, punctuated fabric development, and interaction between metamorphism and deformation. Journal of Metamorphic Geology 12, 1-12.

Williams, P. J., 1998. Metalliferous economic geology of the Mt. Isa Eastern Succession, northwest Queensland. Australian Journal of Earth Sciences 45, 329-341.

Williams, P. F., Jiang, D., 1999. Rotating garnets. Journal of Metamorphic Geology 17, 367-378.

Wyborn, L., 1998. Younger *ca.* 1500 Ma granites of the Williams and Naraku Batholiths, Cloncurry district, eastern Mt Isa Inlier: geochemistry, origin, metallogenic significance and exploration indicators. Australian Journal of Earth Sciences 45, 397-411.

SECTION B

N-S shortening in the Mt Isa Inlier

Microstructural evidence for N-S shortening in the Mount Isa Inlier: the preservation of early W-E trending foliations in porphyroblasts revealed by independent 3-D measurement techniques

Abstract

3-D microstructural analyses of porphyroblast inclusion trails using both the ‘asymmetry method’ for determining **F**oliation **I**ntersection **A**xes preserved in porphyroblasts (FIAs) and the recently developed ‘FitPitch’ method, reveal W-E and N-S trending FIA sets in the White Blow Formation of the Mt Isa Inlier. Each method reveals two subsets of FIAs centered on each of these major trends. These were distinguished based on the relative timing, trend and orientation of inclusion trail patterns. Thirty-six samples were analyzed using both techniques and produced very similar results. Pitches of the inclusion trails preserved within the porphyroblasts in vertically oriented thin-sections and trends in horizontal sections yield distinct near-orthogonal modal orientations from all the analyzed samples. This indicates that the porphyroblasts host successive fabrics as crenulation foliations and did not rotate with respect to geographical axes. W-E and N-S trending FIAs have been obtained from both garnet and staurolite porphyroblasts hosting differentiated crenulation cleavages. Garnet and staurolite growth during bulk north-south shortening recorded the development of multiple foliations and an associated succession of metamorphic events at middle-amphibolite facies conditions that predates the metamorphic history generally recognized in this terrain. This period of bulk shortening and associated metamorphism formed during a period of orogenesis called (O_1). W-E shortening formed N-S striking foliations that preserve a period of orogenesis (O_2), and another succession of metamorphism involving more phases of porphyroblast growth preserving N-S trending FIAs. Overprinting of successive FIA trends (WSW-ENE, WNW-ESE, NNW-SSE and SSW-NNE) suggests a relative clockwise rotation of the bulk shortening direction through time as it switching from N-S to W-E overall with a major ‘tectonic break’ or decompression between O_1 and O_2. The porphyroblast inclusion trail patterns preserving W-E trending FIAs provide a window into the lengthy period of earlier deformation and metamorphism that is no longer preserved within the matrix foliations.

1. Introduction

A development in tectonics has been the recognition of several distinctly oriented successions of datable foliations preserved in porphyroblasts (Bell and Welch, 2002; Williams and Jercinovic, 2002) that potentially allow the reconstruction of the history of the tectonic evolution of large regions (e.g., Bell et al., 2004). This implies the extensive recycling of matrix foliations with deformation and time, but with their preservation in porphyroblasts, allowing them to be used for kinematic analysis (e.g., Steinhardt, 1989; Hayward, 1990; Davis, 1995; Johnson, 1999; Ilg and Karlstrom, 2000; Bell and Kim, 2004). Recent studies using porphyroblast inclusion trails across orogenic belts have revealed a prolonged and 'step-by-step' tectonic evolution of multiply deformed terrains (e.g., *cf*. Johnson, 1990a; 1990b and Turnbull, 1981; Craw, 1985; Aerden, 1998 and Thompson and Bard, 1982; Bell et al., 1998 and Rosenfeld, 1968; Stallard and Hickey, 2002 and Cawood et al., 1994). Thus, previous studies suggest only very limited information on tectonics can be gained from macro- and/or mseoscopic scale structures alone because of the strong tendency for progressive shearing to be accommodated along the bedding or compositional layering (e.g., Ham and Bell, 2004).

The Mesoproterozoic Mount Isa Inlier of NW Queensland, Australia, is a multiply deformed terrain and a world-class epigenetic base- and noble-metal province (e.g., Oliver et al., 1998). Several structurally controlled, giant mineral deposits are hosted within the inlier. To understand the genesis of these deposits, it is essential that the tectonic processes and overprinting role of multiple deformation phases are well understood as they directly link to prospect analysis and timing and controls on mineralization. Three dominant north-south striking belts have been recognized based on the tectono stratigraphic setting (Carter et al., 1961; Blake, 1987). From east to west, these are the Eastern Fold Belt, Kalkadoon-Leichhardt Belt and Western Fold Belt (Fig. 1). The main structural grain of the inlier involves regional north-south oriented upright D_2 structures that resulted from W-E shortening. The role of D_1 is controversial. Recently, it has been argued that the deformation in the Eastern Fold Belt began with W-E extension during D_1, followed by west-vergent thin-skinned or nappe-style folding during D_2, followed by thick-skinned or upright folding and faulting (e.g., Giles and MacCready, 1997; O'Dea et al., 1997ab; MacCready et al., 1998; Goleby et al., 1998). This argument is based on the W-E oriented Mount Isa Deep Seismic Profile plus some field examples (e.g., Betts et al., 2000). However, Bell (1983), Loosveld (1989) and Bell et al. (1992) have recognized W-E oriented meso- to macroscopic scale structures that resulted from earlier N-S shortening in the western and eastern part of the Mt Isa Inlier. They argued that prior to D_2 there was a period of N-S shortening that formed the D_1 event, rather than extension. The presence and nature of the early W-E striking D_1 structures have been considered controversial in the Eastern Fold Belt of the Mount Isa Inlier due to the intensity of the overprinting D_2 W-E shortening event.

This study geometrically characterizes as earlier period of north-south shortening in the White Blow Formation of the Mt Isa Inlier. The White Blow Formation is located approximately in the middle of the seismic section line (Fig. 1; MacCready et al., 1998). It produced west-east trending structures, which are measured by both the 'asymmetry method' for FIA (**F**oliation **I**ntersection/**I**nflexion **A**xes preserved within porphyroblasts; Hayward, 1990; Bell et al., 1998) and the new 'FitPitch' method (Aerden, 2003). These independent techniques produce similar results, from more than 600 spatially oriented thin sections, even though the procedures involved are quite different. This paper compares these two independent techniques for measuring foliations preserved in porphyroblasts using the same set of oriented thin sections. It shows that the combination of both techniques provides a robust method for determining the deformation history and for assessing all aspects of 3-D geometry of inclusions trails. Significantly, for Isa orogenesis, the early polyphase (e.g., Bell et al., 1992) north-south period of shortening in the Eastern Fold Belt, documented in this study, was accompanied by a significant period of metamorphism that has previously not been distinguished. This causes considerable problems for the above mentioned extensional tectonic model argument that omits the early N-S shortening event (e.g., Giles and MacCready, 1997; MacCready et al., 1998; Betts et al., 2000).

2. Geological setting

The Mt Isa Inlier of northwest Queensland, Australia, contains multiply deformed Mesoproterozoic metasedimentary rocks and extensive intrusive and extrusive igneous complexes. The Isan Orogeny occurred between *ca.* 1620 and *ca.* 1510Ma (Page and Bell, 1986). Supracrustal sequences were deposited during episodic extensional and basin forming periods between *ca.* 1800 and 1620±5Ma (Fig. 1; Beardsmore et al., 1988; Page and MacCready, 1997; Page and Sun, 1998). The present day structural framework of the Mt Isa Inlier consists of north-south striking, intensely deformed and moderately to steeply dipping D_2 structures with late strike-slip or reverse faults. The nature and existence of pre-D_2 or post-D_2 structures and their tectonic implications have been the subjects of considerable controversy (Loosveld, 1989; Passchier and Williams, 1989; Holcombe et al., 1991; Bell et al., 1992; Giles and MacCready, 1997; MacCready et al., 1998; Bell and Hickey, 1998; Betts et al., 2000). Low pressure/high temperature (LP/HT) metamorphism with upper amphibolite facies and an anticlockwise P-T-t paths have been proposed for the Eastern Fold Belt of the Mount Isa Inlier (e.g., Reinhardt, 1992; Rubenach and Lewthwaite 2002). It has been suggested that peak metamorphic conditions were broadly synchronous with west-west D_2 shortening in a number of publications (e.g., Reinhardt, 1992; Rubenach and Barker, 1998; Oliver et al., 1998; Rubenach and Lewthwaite, 2002). Yet the cause of initial LP/HT conditions has not been demonstrated in any of these publications.

The White Blow Formation is located in the Eastern Fold Belt, approximately in the middle of the Mount Isa Inlier and provides a key location for the investigation of the structural history of this world-class mineral province (Fig. 1 and 2). It mainly contains Grt-St-Ms-Bt schist (symbols after Kertz, 1983) and records middle-amphibolite facies conditions (Whitelock, 1989). The White Blow Formation is a part of the Mount Albert Group (Derrick et al., 1977). Its lower contact with the Mary Kathleen Group has been interpreted as high angle thrust fault (Fig. 2; Whitelock, 1989; Looseveld and Schreurs, 1987) so the exact stratigraphic relationship between the Mount Albert Group and the Mary Kathleen Group is uncertain. However, both record the regional D_2 deformation phase of the Isan orogeny (Blake, 1987; Loosveld, 1989).

The White Blow Formation is bound by high-angle reverse faults that separate it from the adjacent Mary Kathleen Group rocks (Whitelock, 1989; Loosveld and Schreurs, 1987). The Bagman Fault (Whitelock, 1989) on the eastern margin is marked by irregular bodies of vein quartz up to 10m thick, dipping steeply to the west with small pockets of Cu-mineralization in a very fine-grained graphitic schist. The eastern contact of the White Blow Formation with the Corella Formation is marked by a thin band of light green fine-grained talc schist derived from the Corella Formation (*pers. comm., M. Rubenach, 2004*). However, to the south, several brecciated zones and irregular lenses of vein quartz associated with high angle reverse faults have been observed (Fig. 2). Therefore, the

White Blow Formation has been placed above the Mary Kathleen Group rocks (Whitelock, 1989; Looseveld and Schreurs, 1987).

3. Structural field data

S_2 in the Mount Isa Inlier is a steep overall N-S striking foliation, as mentioned above. The geometry of D_1 and associated $S_0//S_1$ in the Eastern Fold Belt are poorly understood, but demonstrably vary with D_2 strain. For example, in high strain areas, $S_0//S_1$ is parallel or sub-parallel to N-S striking S_2, whereas $S_0//S_1$ trends W-E in low strain zones of D_2 (e.g., Loosveld and Schreurs, 1987; Reinhardt, 1992; Bell et al., 1992; Mares, 1998; Betts et al., 2000).

Bedding (S_0) and bedding-parallel foliation (S_1) are well preserved in the White Blow Formation and adjacent Mary Kathleen Group units. In D_2 low strain zones, $S_0//S_1$ dips steeply to moderately north or south (Figs. 2c, 3ab). Where relatively competent west-east striking $S_0//S_1$ structures were observed, S_2 is a crosscutting and spaced foliation, indicating a relatively low influence of the D_2 event on these particular horizons (Fig. 3ab). Within the White Blow schist, $S_0//S_1$ is largely obscured or transposed due to the dominant pelitic component and high D_2 strain (Fig. 3c). Consequently, the original geometric configuration of S_0/S_1 is difficult to reconstruct.

The axial planar D_2 foliation in the White Blow schist is a pervasive, steep to vertically dipping S_2 (Fig. 2c, 3c), associated with a conspicuous steeply southwest plunging mineral lineation L^2_2 (Fig. 3d; terminology after Bell and Duncan, 1978). L^2_2 is mainly defined by biotite in schists and/or amphiboles in calc-silicate rocks. The steeply pitching nature of L^2_2 on S_2 reveals a vertical stretch during the inferred horizontal shortening (see also Reinhardt, 1992). The poles to S_2 produce tight clusters mainly on the eastern half of a Schmidt projection, with the mean S_2 plane oriented almost exactly north-south (Fig. 2c). S_2 in the schist is commonly a differentiated foliation with rare relics of $L^{0/1}{}_2$ (intersection of S_0/S_1 with S_2) crenulation hinges (Fig. 2c).

4. Sample description

Sixty-five oriented porphyroblastic samples were collected mainly from the White Blow schist, but including a few from garnet-bearing calc-silicate bands (Fig. 2b). Thirty-seven samples contained inclusion trail patterns of sufficient quality for further microstructural analysis, thirty from the White Blow schist and seven from garnet-bearing calc-silicates. Garnet porphyroblasts are generally small (less than 0.2-0.3cm), whereas staurolite porphyroblasts typically range from 0.5 to 1cm in size (Fig. 3bd).

The metamorphic assemblage visible in thin-section includes garnet, staurolite, biotite and muscovite, with rare andalusite, sillimanite, graphite, ilmenite and very rare rutile. Microstructural data were mainly collected from garnet and staurolite porphyroblasts and matrix foliations. Inclusion trail patterns within the porphyroblasts show different stages of differentiation (Bell and Rubenach, 1983) and range from staircase to slightly to moderately sigmoidal shapes (see below).

5. FIA determination and interpretation

5.1. Asymmetry technique

The technique used to measure the FIAs is described in Hayward (1990), Bell and Hayward (1991) and Bell et al. (1995, 1998, 2004). The method involves observing the switch in the asymmetry of curved inclusion trails, preserved in porphyroblasts, in a series of differently oriented thin sections (Fig. 4a). Initially six vertical thin sections were cut at every 30^o interval from true North. Additional thin sections were cut to constrain the asymmetry switch within 10^o (±5^o, see Fig. 4c). The trend of the FIA is taken as being midway between the two oriented vertical thin sections across which the flip occurs, and can be expressed graphically (Fig. 4cd). Where both asymmetries are observed equally (both 'S' and 'Z'), but the asymmetry in thin sections to the either side switched, the FIA is considered to lie in the plane of that section. The FIA trends are bi-directional so values between 000^o and 180^o were assigned for simplicity. To determine uni-directional FIA measurements, FIA plunges can be measured by observing the asymmetry switch in radially dipping thin sections cut with strike perpendicular to the FIA trend (Bell et al., 1995).

5.2. FIA sets

The discovery of sequentially developed multiple fabrics preserved within porphyroblasts needs the development of a strict nomenclature to separate the foliations of different generations. As described below, two dominant bulk shortening events have been recognized based on FIAs separated by a 'tectonic break'. The foliations are numbered in chronological order with respect to successive W-E trending FIAs as S_a, S_b, S_c….that formed during bulk N-S shortening orogenesis (O_1) and N-S trending FIAs as S_A, S_B, S_C....that formed during bulk W-E shortening orogenesis O_2. The terms O_1 and O_2 are used instead of D_1 and D_2, as both periods of shortening are accompanied by multiple phases of deformation and associated middle-amphibolite facies metamorphism. The two orogenic events are separated by decompression (chapters 3 and 4 of this dissertation).

Altogether, 72 FIA measurements were obtained mainly from garnet and staurolite porphyroblasts (Table-1). Figure 5a shows a rose plot of the total garnet and staurolite FIA trends measured from all samples. Both garnet and staurolite porphyroblasts preserve the dominant W-E and N-S FIA trends, reflecting at least two periods of porphyroblast growth in the first instance. However, four separate FIA trends can be seen oriented WSW-ENE, WNW-ESE, NNW-SSE and SSW-NNE. The last of these, the SSW-NNE FIA trend, parallels the present day structural grain of the White Blow Formation (Fig. 2). FIA sets can be distinguished not only based on the switch of the inclusion trail patterns from clockwise to anticlockwise asymmetries, but also with respect to the change in orientation from subhorizontal to subvertical or vice versa. These relationships are summarized in Fig. 5b. However, the presence of differentiated crenulation cleavage in the porphyroblasts that is not preserved in the matrix reveals that these structures were progressively destroyed by younger events (Figs. 6, 8).

6. Relative timing of FIAs

FIA sets were recognized based on the relative timing of successive foliations whereby, (1) multi FIA analysis, that is FIAs change trend in a consistent manner from porphyroblast cores to rims in some samples, shown graphically (Fig. 4d; Bell et al., 1998, 2004), (2) successions of prograde porphyroblast growth hosting different orientations or generations of inclusion trails, for example garnet inside staurolite, (3) truncation vs. continuous inclusion trail microstructures (e.g., Adshead-Bell and Bell, 1999; Passchier and Trouw, 1998), and (4) FIA trends near-parallel or perpendicular to outcrop foliation.

6.1. FIA set 1

A few multi FIA samples have been recognized from garnet and staurolite porphyroblasts (Table-1). Garnet and/or staurolite porphyroblasts containing the 080°-105° FIA range of trends dominantly contain subhorizontal inclusion trails in the core that curve to subvertical at the median and/or rim with clockwise or anticlockwise asymmetries (Fig. 6). Inflection and/or truncation of the subvertical or steep inclusion trails to subhorizontal at the rims are uncommon in garnet porphyroblasts, but common in the staurolite (Fig. 6). The inclusion trails in porphyroblasts preserving these FIA orientations are at stage 3 to 4 of differentiated crenulation cleavage development (Bell and Rubenach, 1983) and are not continuous with the matrix foliation. The nomenclature of the inclusion trail foliations preserved within the porphyroblasts hosting this FIA population have been allocated based on relative timing of crenulated versus crenulation cleavages. Porphyroblasts preserving subhorizontal foliation S_a were followed by steep axial planar S_b and then subhorizontal S_c (Fig. 6).

To obtain the P-T conditions of garnet core growth, a P-T pseudosection was constructed using THERMOCALC-3.21 after bulk XRF analysis of sample WB161 (Fig. 7; Powell and Holland, 1998). P-T estimates for the garnet core were obtained by intersection of compositional isopleths (X_{Mn}, X_{Fe}, X_{Ca}) technique (Vance and Mahar, 1998). This sample is a garnet-staurolite-biotite-muscovite schist. Garnet porphyroblasts range in size from 1-3mm and staurolite from 4 to 9mm. The garnet core compositional isopleths intersect at 3.7-4.4kb/542-547°C in the Chl-Grt-Bt-Pl field (Fig. 7; Table-2).

6.2. FIA set 2

Garnet and staurolite porphyroblasts preserve 105^{o}- 120^{o} trending FIAs belong to set 2. The inclusion trail geometries are dominated by moderately dipping or subvertical patterns in the core curving to subhorizontal orientations at the rim (Fig. 8). However, at high magnification (~20-30x), subhorizontal crenulations can be observed within the steep inclusions trails. FIA set 2 occurs in garnet and staurolite porphyroblasts hosting subhorizontal S_c, which was the end product of FIA set 1 (see below), followed by steep S_d and then subhorizontal S_e (Figs. 5b, 6, 8). The steep foliation (S_d) preserved within the porphyroblast controls the trend (105^{o}- 120^{o}) of FIA set 2. Figure 8 shows a subidioblastic staurolite porphyroblast hosting a deformation sequence from S_d to S_e and $S_e(S_A)$ to S_B. Differentiation crenulation cleavage within the porphyroblast can be observed at high magnification due to moderately pitching S_d overprinted by sub-horizontal S_e (Fig. 8b). It is noticeable that the inclusion trails within the core of the porphyroblast show partial truncational patterns, that is between S_d and S_e /S_A.

Two samples preserve both the FIA set 1 and FIA set 2 from the core to rim respectively of the porphyroblasts (samples 161, 139). None of these porphyroblasts have inclusion trails continuous with matrix foliation. Thus, several samples preserve a consistent geometric succession from flat to steep to flat about one FIA trend in one set of garnet porphyroblasts (FIA 1), followed by steep to flat for the second FIA trend for the other set (FIA 2; Fig. 5b).

6.3. FIA set 3

Sample 9.1 contains a 135^{o} FIA resulting from a transition from subhorizontal to subvertical inclusion trails at the rim of the porphyroblasts. Therefore, it can be inferred that the rock preserves shallow S_e curving into a moderately steep foliation at the rim S_f

that controls the FIA trend (135°). This FIA trend was only obtained from one rock sample (sample WB9.1), this suggests a weak event or the waning stages of the overall N-S shortening phase of the Isan Orogeny. None of these porphyroblasts belonging to FIA set 1, 2 or the one with 135° have inclusion trails continuous with the matrix foliation, further suggesting that their growth pre-dates the matrix foliation.

6.4. FIA set 4

A fourth set of samples with garnet porphyroblasts containing FIA ranging between 350° to 020° have moderate to subhorizontal inclusion trails in the core and subvertical trails in the rim. Roughly, 60% of these foliations preserved as inclusion trails are continuous with the matrix foliations, especially those where the FIA ranges between 000° to 020° (Fig. 9a). Those with FIA trends ranging between 350° to 000° are mostly truncated (Fig. 9b). This is interpreted to result from a change in the bulk shortening direction from slightly WSW-ENE to slightly WNW-ESE. This fourth FIA set results from W-E shortening (the O_2 event) of subhorizontal S_A in the core or rim (Figs. 8, 9), that curves into and is continuous with the matrix S_B foliation. The subhorizontal S_A of O_2 appears to be equivalent to the subhorizontal S_e of O_1.

7. Matrix microstructures and correlation with field structures

The matrix foliation is a product of extensive recycling of foliations through repeated reactivation and reuse of earlier foliations (e.g., Ham and Bell, 2004). However, in low strain zones or relatively competent portions of the rock, overprinting relationships can be preserved and correlated with the orientation of inclusion trails within the porphyroblasts. For example, several N-S vertically oriented thin-sections from the White

Blow schist contain subvertical S_b and/or S_d foliation overprinted by subhorizontal S_c and/or S_e semi-differentiated crenulations (Fig. 10). This geometric relationship is evident from those porphyroblasts showing FIA 1 and 2 from subhorizontal to subvertical inclusion trail patterns or vice versa. This strengthens the observation that at least two major deformation events occurred during O_1 with an initial steep axial planar west-east oriented S_b or S_d foliation, followed by subvertical shortening that formed gently-dipping S_c or S_e foliation. In the west-east oriented thin sections, both garnet and staurolite preserve shallow $S_e(S_A)$ that is continuous with the matrix S_B foliation (Fig. 9), which is the dominant foliation of the White Blow Formation. Therefore, the north-south striking S_2 in the field is actually the S_B of O_2.

8. 'FitPitch' technique

Measurements of particular planar structures as apparent dips on different sections around the compass should lie in a plane when plotted on a stereographic projection. Therefore, several measurements of one generation of inclusion trail pitches from a radial set of vertical oriented thin sections can be used to estimate and construct the foliation plane defined by those inclusion trails. This approach has been applied using a recently developed computer program called 'FitPitch', which calculates one, two or three best-fit planes based on unimodal, bimodal or trimodal groups of linear structural elements distributed in 3D space with statistical constraints (Aerden, 2003). The intersection of the two best-fit planes from two distinct orientations of pitches should, theoretically define the FIA (Aerden, 2003). 'FitPitch' is especially useful for those inclusion trail patterns showing no asymmetry or close to straight orientations. FIA set(s) can potentially be determined using 'FitPitch' for foliations that show no asymmetric curvature. Such foliations cannot be used to measure FIAs by the asymmetry method. Another advantage of the 'FitPitch' technique is that the program calculates the FIA plunge and trend based on the intersection of two best-fit planes (Aerden, 2003) as discussed below.

8.1. Measuring procedures

Seven oriented thin sections, six of which are vertical at 30^{o} intervals around the compass, and one of which is horizontal were prepared from each sample for 3D microstructural analysis using the 'FitPitch' computer program. Thirty-six samples were analyzed. One sample (no. WB38) was not suitable for recording pitches because of the complex geometry of the inclusion trails. The same vertical oriented sets of thin sections were used for the conventional FIA method. An additional horizontal thin section was prepared for each sample to constrain the strike of the inclusion trails (Aerden, 2003).

Data were divided into two main groups (after Aerden, 2003). A-type microstructures were classified as straight to moderately sigmoidal inclusion trails and B-type microstructures were classified as axial traces of microfolds or different stages of differentiated crenulation cleavages (Fig. 6; Bell and Rubenach, 1983). A total of 3835 pitches were measured both from A- and B-type microstructures preserved within the porphyroblasts and in the matrix and plotted on rose diagrams (Fig. 11). A distinct gently dipping modal peak was obtained for A-type microstructures and a steeply dipping modal peak for B-type microstructures (Fig. 11a). Horizontal thin sections show dominantly W-E and N-S strikes of inclusion trails preserved within the porphyroblasts (Fig. 11b). Data from individual thin sections have been plotted on the rose diagrams and exhibit bimodal or trimodal inclusion trail pitches (see below) Data were not recorded from the low density inclusion trail patterns that locally occur at the rim of the porphyroblasts or from poorly defined or complex inclusion trail patterns.

8.2. Results

Most of the thirty-six analyzed samples yield similar results (Fig. 12a) to that obtained using the conventional FIA method. Table-1 shows a comparison of ‘FitPitch’ with the conventional FIA method. The ‘FitPitch’ method produced two significant advantages. FIA trends were obtained from inclusion trail patterns with no asymmetry. For example, W-E FIA trends were obtained from samples WB48 and WB180 using both the techniques (Table-1). However, ‘FitPitch’ calculates additional N-S FIA from inclusion trails preserved within the porphyroblasts that show no asymmetry and are almost continuous with the matrix foliation (e.g., Fig. 8c; Table-1). These N-S FIA trends are in excellent agreement with those samples that do show inclusion trail asymmetry. Similarly, ‘FitPitch’ calculates an additional W-E FIA trend for samples WB35 and WB148 that were not determined by the asymmetry switch method.

In addition, ‘FitPitch’ calculates the FIA plunge (Fig. 12a). It is noticeable that almost all the FIA plunges lie at less than 40^o, confirming shallow fold axes orientation related to the O_1 and O_2 phases of Isan Orogenesis. Similarly, poles to the best-fit planes are preferentially located at the periphery and near the center of the stereo plot (Fig. 12b), further strengthening the data shown in figure 11 with optimal statistical constraints (Fig. 12c). Figure 13a and 13b are excellent examples of how ‘FitPitch’ calculates FIA based on a two best-fit plane solution with high Rd and Rm values (see below).

8.3. Criteria for choosing ‘FitPitch’ 2- or 3-bestfit planes: textural vs. statistical constraints

The advantage of data acquisition through the conventional FIA method is that it not only constrains the geometry of inclusion trail patterns, but also the relative timing of porphyroblast growth with respect to multiple foliation development. Measuring pitches for 'FitPitch' and correlating microstructures with known and unknown timing with respect to porphyroblast growth and foliation development need strict criteria. Interpretation of this data has a strong influence on best-fit planes and their respective FIAs using the 'FitPitch' program. For example, 'FitPitch' can calculate two closely-spaced steeply dipping best-fit planes with favorable statistical calculations and a FIA trend and plunge. However, it will be shown here that it might be possible that those two closely-spaced steeply oriented best-fit planes are, indeed, one steep plane based on textural relationships, even though statistically this may not be favored. That is, FIA from two steep planes may be just an artifact (see also Aerden, 2003).

Aerden (2003, 2004) proposed that data should be fitted to one, two or three best-fit planes, whichever produces the smallest standard deviation for high Rd and Rm values. Rd is expressed as the degree of the tightness of the best-fit plane solution, whereas Rm is the degree of internal consistency of a data set from radial thin sections. During data collection it was observed that inclusion trails for one generation, or related to one deformation event always have slightly different orientation from porphyroblast to porphyroblast and from thin section to thin section. This occurs because, (1) variation in the amount of rotation of the foliation by synchronous deformation prior to porphyroblasts growth during a single deformation phase (Fig. 14a). (2) Anastomosing cleavages included at different porphyroblasts growth sites (Fig. 14b). (3) a cut effect.

Therefore, data from moderately varying inclusion trails from six different oriented vertical thin sections may statistically fall into two best-fit plane solution rather than one plane. Nevertheless, the two-planes with tight statistical constraints would lie close to each other and actually result from one plane (Fig. 15, see also Aerden, 2003). Similarly, a three plane best-fit solution yields three FIAs, which may be statistically favored, but may not in agreement with textural relationships. The extra FIAs are just an artifact. In this study, most of the samples analyzed by 'FitPitch' are in good agreement both texturally and statistically with respect to two- or three- plane solutions (Figs. 11, 12).

8.4. Samples with three-plane solution

Most of the samples calculated with a three-plane solution show porphyroblasts with an extended microstructural history, e.g., steep S_d in the core followed by gently dipping $S_e(S_A)$ in the median and steep S_B in the rim, which is in most cases continuous with the matrix foliation (e.g., Fig. 8). However, not all the porphyroblasts show an extended microstructural history and few multi-FIAs have been obtained.

W-E or N-S FIAs were obtained using the conventional FIA method except for samples WB33, WB149, WB166, WB179, WB51, WB43 (Table-1). Multi-FIAs were also obtained using 'FitPitch', for samples WB48, WB35, WB180, WB179, WB161, WB148, WB43. Inclusion trails from porphyroblasts showing no asymmetry yield N-S (samples WB48, WB161, WB180) or W-E (samples WB148, WB35) FIAs in a three plane solution. For example, in sample WB43 (Fig. 16), a 105^o FIA was obtained by the conventional FIA method from S_d to S_e, whereas a 000^o FIA was obtained for $S_e(S_A)$ to S_B. Porphyroblasts preserving only S_B and showing no asymmetry also yield N-S FIA. This relationship is consistent with respect to the orientation of pitches of the inclusion trails and, therefore a three-plane solution is in excellent agreement with both statistical constraints and the textural relationships.

9. Discussion and conclusions

9.1. 'Asymmetry switch' technique vs. 'FitPitch'

Both techniques give similar results from the same set of oriented thin sections, even though the procedures are quite different. This strong agreement confirms the validity of both methods for determining the FIA trends preserved within the porphyroblasts. In particular, the early formed W-E oriented structures related to O_1 have been thoroughly documented in spite of the fact that they are no longer preserved within the matrix. 'FitPitch' generates very close (±5^o) FIA trend/plunge results to the Bell, et al. (1995) method, if equally spaced 18 vertical oriented thin section are prepared and analyzed, but this is more expensive and time consuming (*cf*. Fig. 13a). The 'asymmetry switch' method, initiated by Hayward (1990) and established by Bell et al. (e.g., 1995, 1998), is extremely useful in determining the timing of porphyroblast growth with respect to foliation development and determining shear senses across the regional folds or pre-existing folds (e.g., Ham and Bell, 2004). However, this method cannot be used for porphyroblasts with straight inclusion trails with no curvature at the rims and additional differently dipping thin sections striking perpendicular to the FIA trend are needed to characterize the FIA plunge.

The invention of 'FitPitch' provides a method that uses different criteria than the 'asymmetry method' to characterize the orientation of FIAs with statistical constraints.

The program complements the existing asymmetry technique and is useful as an alternative to assess the different generations of FIAs determined by the Hayward (1990) method. An advantage of ‘FitPitch’ is the quantitative analysis or geometric characterization of inclusion trails in the form of planes from a set of oriented thin sections that form FIA intersection axes. ‘FitPitch’ not only calculates FIA trends but also FIA plunges without the need for the extra differently dipping thin sections. However, without reliable textural relationships, this technique is not useful for timing the FIA with respect to foliation development and porphyroblast growth. The combination of both techniques provides a powerful and robust method for determining the deformation history and for assessing all aspects of 3-D geometry of inclusion trails.

The program could potentially be improved as ‘FitPitch’ cannot distinguish textural relationships that statistically favor either two plane or three plane solutions, as discussed above. This can be solved by adding nomenclature, if possible, to the data file to specify microstructures. For example, if nomenclature is assigned to steep differentiated cleavages of one generation preserved in porphyroblasts as, for example, B2-type, then ‘FitPitch’ will not divide the result into two steep planes. This would influence the interpretation of timing of differently oriented planes on a stereo plot.

9.2. Implications of FIA sets for Isan Orogenesis

In a group of recent publications (e.g., MacCready et al., 1998; Goleby et al., 1998; Drummond et al., 1998; Betts, et al., 2000) it has been argued that deformation in the Eastern Fold Belt of the Mount Isa Inlier involved initial D_1 extension followed by D_2 thin-skinned non-coaxial deformation followed by thick-skinned deformation based on the west-east oriented Mt Isa Deep Seismic Profile. An interesting aspect of this seismic study is that most of the structures are interpreted as kilometer scale nappe-folds, whereas the surface geology is characterized by a steep S_2 fabric along the whole transect (e.g., Australian Bureau of Mineral Resources 1:100,000 scale maps and cross sections). Indeed, 3D gravity and magnetic geophysical data in the form of 'geophysical worms – multiscale-edge analysis' indicate steep lithological boundaries and, consequently steep structures deep within the crust consistent with the outcrop-scale geology (*Predictive Mineral Discovery* - *Cooperative Research Center* - internal data). This makes interpretation of the seismic section ambiguous. Moreover, Bell et al. (1992) recognized multiple subvertical and subhorizontal foliations and associated stretching lineations that developed during a N-S shortening event in the Wonga-Duchess Belt and Rosebud Syncline lying adjacent to the study area (Fig. 1). This data is strongly supported by the evidence for multiple generations of foliations that produced the N-S O_1 shortening described herein, which predate the matrix foliation preserved in these rocks.

3D microstructural analysis has revealed the existence of early formed foliations as crenulation cleavages preserved within the porphyroblasts. The first formed shallowly plunging 080^o-105^o oriented FIA set defined by shallow S_a in the core, differentiated steep S_b, and shallow S_c at the rim of the porphyroblasts, indicate a primary phase of N-S shortening. S_b formed as the axial plane foliation to F_1 folds with west-east oriented fold axes during O_1. The second FIA set, which lies between 105^o-120^o, resulted from steep S_d overprinted by shallow S_e and indicates a second period of bulk shortening. The third FIA at 135^o observed only in one rock sample, preserving shallow S_e curving into a moderately steep S_f, suggests a gradual transition from N-S O_1 shortening to W-E O_2 shortening or the waning stages of the overall N-S shortening phase of the Isan Orogeny.

It appears that subhorizontal S_e remained the dominant foliation at the end of O_1 rather than S_f and defines decompression of O_1 orogenesis (chapters 3 and 4 of this dissertation). These periods of N-S shortening and associated deformation and metamorphism, plus at least three phases of porphyroblast growth, are no longer preserved in the matrix and can only be detected by comprehensive 3D microstructure analysis.

O_2, the product of W-E bulk shortening, is preserved throughout the entire Eastern Fold Belt by north-south pervasive fabrics in the matrix that have been previously called S_2 in the field (e.g., Loosveld and Schreurs, 1987; Betts et al., 2000). This phase of orogenesis obliterated and obscured previously formed structures in the inlier. Porphyroblast growth hosting shallow $S_A(S_e)$ with inflection due to S_B at the rim continued during the deformation and metamorphic events that accompanied O_2. Most porphyroblasts hosting shallow S_A in the core and median regions and steep S_B in the rim have FIAs lying between 350^o to 000^o and are generally not continuous with the matrix foliation. On the other hand, FIAs lying between 000^o to 020^o, formed from inclusion trails that are continuous with the matrix, and resulted from last stage of porphyroblast growth. This slight variation from 350^o to 000^o and 000^o to 020^o suggests a slight change in bulk shortening direction. This study complements Mares (1998), who found early W-E followed by N-S trending FIAs in the Fairmile area of the Eastern Fold Belt (Fig. 1).

9.3. Correlating multiple phases of metamorphism based on FIA sets

It is generally assumed that porphyroblast growth is broadly synchronous with syn-metamorphic-tectonic processes in a homogenous matrix (e.g., Spear et al., 1991; Kohn et al. 1992; Florence et al., 1993; Menard and Spear, 1994; Daniel and Spear, 1998). In these studies, most of the aspects of garnet nucleation and growth have been covered, without putting or classifying them into different tectonic modes with respect to foliation development. However, in a group of recent studies, based on a very detailed microstructural work, it has been demonstrated that porphyroblast growth is episodic and heterogeneously developed from sample to sample and from outcrop to outcrop (e.g., Bell and Welch, 2002; Stallard and Hickey, 2002; Kim and Bell, *in press*). Therefore, constructing P-T paths from just a few samples and inferring tectonic processes without absolute or relative timing constraints on porphyroblast growth with respect to multiple foliation development is meaningless. The acquisition of more meaningful pressure-temperature estimates requires detailed microstructural analysis or, more specifically, FIA analysis in the first instance to establish the timing of porphyroblast growth with respect to bulk shortening. For instance, 9-component MnNCKFMASH pseudosections were prepared from garnet bearing schist rock samples (Grt, St, And, Crd, Ms schists) from the Snake Creek Anticline of the Eastern Fold Belt. Garnet in these samples contains N-S and W-E FIAs. Garnet porphyroblasts preserving early W-E FIAs have relatively higher-pressure cores (5-6Kb) than those hosting N-S FIAs (3-4Kb). These results are consistent with early N-S shortening and associated medium pressure conditions followed by decompression (with the production of And/Crd) at the end of O_1. Garnet cores preserving N-S FIAs began to grow during LP/HT conditions with increasing pressure during W-E shortening or 'O_2' in the Mt Isa Inlier (chapter 4 of this dissertation). This study shows the pre-eminence of 3D FIA analysis in not only determining deformation phases with respect to foliation development, but also in revealing early phases of porphyroblast growth and metamorphism that accompanied N-S shortening during O_1. This also explains the earlier phase of metamorphism O_1 followed by decompression (subhorizontal Se at the end of O_1) responsible for LP/HT conditions in the Mt Isa Inlier.

9.4. Implications of FIA for porphyroblast non-rotation versus rotation

Both porphyroblast rotation (e.g., Regnier et al., 2003) and non-rotation models (e.g., Bell et al., 2004) are still used as kinematic indicators to unravel the tectonic evolution and metamorphic histories of the orogenic belts. The rotational model is generally described as involving non-coaxial shear within a shear zone (e.g., Williams and Jiang, 1999), whereas the non-rotational model involves multiple generations of crenulation cleavage development and associated episodic porphyroblast growth irrespective of whether there is shearing (e.g., Bell and Johnson, 1989). Significantly, rotational models have only been applied to porphyroblasts containing spiral trails (e.g., Rosenfeld, 1968; Passchier et al., 1992) or sigmoidal patterns (e.g., Ikeda et al., 2002; Regnier et al., 2003) on one-thin section per rock without comprehensive 3-D analysis of inclusion trails. Non-rotational models provide an explanation for the geometries of inclusion trail patterns from spiral to staircase end members and from differentiated crenulations to reactivated fabric preserved within the porphyroblasts (e.g., Stallard and Hickey, 2002; Bell et al., 2004).

Most of the porphyroblasts, in this study, preserved differentiated crenulations and/or staircase or sigmoidal geometries. No arguments against staircase inclusion patterns or porphyroblast showing differentiated crenulation cleavages have appeared in the literature so far (e.g., figs. 7.4 and 7.5 of Passchier and Trouw, 1998). Pitches of the inclusion trails preserved within the porphyroblasts measured from horizontal and vertical oriented thin sections indicate near-orthogonal patterns, that is, early W-E followed by younger N-S trends in horizontal thin sections and shallow and steep modes in vertical oriented thin sections, respectively. These results are similar to early W-E and younger N-S FIAs. If the porphyroblasts were rotated then the pitches on the rose diagrams should be all over the place. Additionally, FIA analysis with distinct model azimuths with respect to geographical reference axes, using either the ‘asymmetry method’ or the ‘FitPitch’ method, provides considerable data demonstrating that porphyroblasts retain original foliations as crenulation cleavages and can be linked to deformation phases that are no longer preserved in the matrix.

References

Adshead-Bell, N. S., Bell, T. H., 1999. The progressive development of a macroscopic upright fold pair during five near-orthogonal foliation-producing events: complex microstructures versus a simple macrostructure. Tectonophysics 306, 121-147.

Aerden, D. G. A. M., 1998. Tectonic evolution of the Montagne Noire and possible orogenic model for syn-collisional exhumation of deep rocks, Hercynian belt, France. Tectonics 17, 62, 79.

Aerden, D. G. A. M., 2003. Preferred orientation of planar microstructures determined via statisticl best-fit of measured intersection-lines: the 'FitPitch' computer program. Journal of Structural Geology 25, 923-934.

Aerden, D. G. A. M., 2004. Correlating deformation in Variscan NW-Iberia using porphyroblasts; implications for the Ibero-Armorican Arc. Journal of Structural Geology 26, 177-196.

Beardsmore, T. J., Newbery, S. P., Laing, W. P., 1988. The Maronan supergroup: an inferred early volcanosedimentary rift sequence in the Mount Isa Inlier, and its implications for ensialic rifting in the middle Proterozoic of northwest Queensland. Precambrian Research 40/41, 487-507.

Bell, T. H., 1983. Thrusting and duplex formation at Mount Isa, Queensland, Australia. Nature 304, 493-497.

Bell, T. H., Duncan, A. C., 1978. A rationalized and unified shorthand terminology for lineation and fold axes in tectonites. Tectonophysics 47, T1-T5.

Bell, T. H., Rubenach, M. J., 1983. Sequential porphyroblast growth and crenulation cleavage development during progressive deformation. Tectonophysics 92, 171-194.

Bell, T. H., Johnson, S. E., 1989. Porphyroblast inclusion trails: the key to orogenesis. Journal of Metamorphic Geology 7, 297-310.

Bell, T, H., Hayward, N., 1991. Episodic metamorphic reactions during orogenesis: the control of deformation partitioning on reaction sites and reaction duration. Journal of Metamorphic Geology 9, 619-440.

Bell, T. H., Reinhardt, J., Hammond, R. L., 1992. Multiple foliation development during thrusting and synchronous formation of vertical shear zones. Journal of Structural Geology 14, 791-805.

Bell, T. H., Forde, A., Wang, J., 1995. A new indicator of movement direction during orogenesis: measurement technique and application to the Alps. Terra Nova 7, 500-508.

Bell, T. H., Hickey, K. A., 1998. Multiple deformations with successive subvertical and subhorizontal axial planes in the Mount Isa Region: their impact on geometric development and significance for mineralization and exploration. Economic Geology 93, 1369-1389.

Bell., T. H., Hickey, K. A. and Upton, J. G., 1998. Distinguishing and correlating multiple phases of metamorphism across a multiply region using the axes of spiral, staircase and sigmoidal inclusion trails in garnet. Journal of Metamorphic Geology 16, 767-794.

Bell, T. H., Welch, P. W., 2002. Prolonged Acadian Orogenesis: revalations from foliation intersection axis (FIA) controlled monazite dating of foliations in porphyroblasts and matrix. American Journal of Science 302, 549-581.

Bell, T. H., Ham, A. P., Kim, H. S., 2004. Partitioning of deformation along an orogen and its effects on porphyroblast growth during orogenesis. Journal of Structural Geology 26, 825-845.

Bell, T. H., Kim, H. S., 2004. Preservation of Acadian deformation and metamorphism through intense Alleghanian shearing. Journal of Structural Geology 26, 1591-1613.

Betts, P. G., Ailleres, L., Giles, D., Hough, M., 2000. Deformation history of the Hampden Synform in the Eastern Fold Belt of the Mt Isa terrane. Australian Journal of Earth Sciences 47, 1113-1125.

Blake, D. H., 1987. Geology of the Mount Isa Inlier and environs, Queensland and Northern Territory. Australian Bureau of Mineral Resources, Geology and Geophysics, Bulletin 225, 1-83.

Carter, E. K., Brooks, J. H. and Walker, K. R., 1961. The Precambrian mineral belt of north-western Queensland. Australian Bureau of Mineral Resources, Geology and Geophysics, Bulletin 51.

Cawood, P. A., Dunning, G. R., Lux D. and van Gool, J. A. M., 1994. Timing of peak metamorphism and deformation along the Appalachian margin of Laurentia in Newfoundland: Silurian, not Ordovician. Geology 22, 399-402.

Craw, D., 1985. Structure of schist in the Mt. Aspiring region, northwestern Otago, New Zealand. New Zealand Journal of Geology and Geophysics 28, 55-75.

Daniel, C. G., Spear, F., 1998. 3-Dimensional patterns of garnet nucleation and growth. Geology 26, 503-506.

Davis, B. K., 1995. Regional-scale foliation reactivation and re-use during formation of a macroscopic fold in the Robertson River Metamorphics, north Queensland, Australia. Tectonophysics 242, 293-311.

Derrick, G. M., Wilson, I. H., Hill, R. M., Glikson, A, Y. and Mitchell, J. E., 1977. Geology of the Mary Kathleen 1: 100,000 Sheet area, northwest Queenland. Australia BMR, Geology and Geophysics, Bulletin 193.

Drummond, B. J., Goleby, B. R., Goncharov, A. G., Wyborn, L. A. I., Collins, C. D. N. and MacCready, T., 1998. Crustal-scale structures in the Proterozoic Mount Isa Inlier of North Australia; their seismic response and influence on mineralization. Tectonophysics 288, 43-56.

Florence, F. P., Spear, F. S., and Kohn, M. J., 1993. P-T paths from northwestern New Hampshire: metamorphic evidence for stacking in a thrust/nappe complex. American Journal of Science 293, 939-979.

Giles, D., MacCready, T., 1997. The structural and stratigraphic position of the Soldier Cap Group in the Mount Isa Inlier. In: Ailleres, L., Betts, P. (Eds.), Structural elements of the Eastern Succession – A field guide illustrating the structural geology of the Eastern Mount Isa Terrane, Australia. Australian Crustal Research Centre, Technical Publication 63, 61-73.

Goleby, B. R., MacCready, T., Drummond, B. J., and Goncharov., 1998. The Mount Isa Geodynamic Transect-Crustal Implications. In: Braun, J., Dooley, J., Goleby, B., Van der Hilst, R., Klootwijik, C., (Eds), Structure and Evolution of the Australian continent, Published by American Geophysical Union, Geodynamic 26, 109-117.

Ham, A. P., Bell, T. H., 2004. Recycling of foliations during folding. Journal of Structural Geology 26, 1989-2009.

Hayward, N., 1990. Determination of early fold axis orientation in multiply deformed rocks using porphyroblast inclusion trails. Tectonophysics 179, 353-369.

Holcombe, R. J., Pearson, P. J., Oliver, N. H. S., 1991. Geometry of a Middle Proterozoic extensional decollement in northeastern Australia. Tectonophysics 191, 255-274.

Ikeda, T., Shimobayashi, N., Wallis, S. R. and Tsuchiyama, A., 2002. Crystallographic orientation, chemical composition and three-dimensional geometry of sigmoidal garnet: evidence for rotation. Journal of Structural Geology 24, 1633-1646.

Ilg, B. R., Karlstrom, K, E., 2000. Porphyroblast inclusion trail geometries in the Grand Canyon: evidence for non-rotation and rotation? Journal of Structural Geology 22, 231-243.

Johnson, S. E., 1990a.Lack of porphyroblast rotation in the Otago schists, New Zealand: implications for crenulation cleavage development, folding and deformation partitioning. Journal of Metamorphic Geology 8, 13-30.

Johnson, S. E., 1990b. Deformation history of the Otago schists, New Zealand, from progressively developed porphyroblast-matrix micorstructures: uplift-collapse orogenesis and its implications. Journal of Structural Geology 12, 727-746.

Johnson, S. E., 1999. Porphyroblast microstructures: A review of current and future trends. American Mineralogist 84, 1711-1726.

Kim, H. S., Bell, T. H., *in press*. Combining compositional zoning and foliation intersection axes (FIAs) in garnet to quantitatively determine early P-T-t paths in multiply deformed and metamorphosed schist: north-central Massachusetts, USA. Contributions to Mineralogy and Petrology.

Kretz, R., 1983. Symbols for rock-forming minerals. American Mineralogist 68, 277-279.

Kohn, M. J., Orange, D. L., Spear, F. S., Rumble, D. and Harrison, M. T., 1992. Pressure, temperature and structural evolution of west-central New Hampshire: Hot thrusts over cold basement. Journal of Petrology 33, 521-556.

Loosveld, R and Shreurs, G., 1987. Discovery of thrust klippen, northwest of Mary Kathleen, Mt Isa Inlier, Australia. Australian Journal of Earth Sciences 34, 387-402.

Looseveld, R. J. H., 1989. The synchronism of crustal thickening and high T/low P metamorphism in the Mount Isa Inlier, Australia 1. An example, the central Soldiers Cap belt. Tectonophysics 158, 173-190.

MacCready, T., Goleby, B. R., Goncharov, A., Drummod, B. J., Lister, G. S., 1998. A framework of overprinting orogens based on interpretation of the Mount Isa deep seismic transect. Economic Geology 93, 1422-1434.

Menard, T., and Spear, F. S., 1994. Metamorphic P-T paths for calcic pelitic schists from the Strafford Dome, Vermont, USA. Journal of Metamorphic Geology 12, 811-826.

Mares, V. M., 1998. Structural development of the Soldiers Cap Group in the Eastern Fold Belt of the Mt Isa Inlier: a succession of horizontal and vertical deformation events and large-scale shearing. Australian Journal of Earth Sciences 45, 373-387.

Marshall, J. L., Oliver, N. H. S., 2001. Mechanical controls on fluid flow and brecciation in the regional host rocks for Eastern Fold Belt ironstone Cu-Au deposits, Mt Isa Block. Geological Society of Australia, Specialist Group in Economic Geology “Mineralisation, alteration and magmatism in the Eastern Fold Belt, Mount Isa Block Australia: Geological Review and Field Guide”, Special Publication No 5, 30 -45.

O’ Dea, M. G., Lister, G. S., MacCready, T., Betts, P. G., Oliver, N. H. S., Pound, K. S., Huang, W., Valenta, R. K., 1997a. Geodynamic evolution of the Proterozoic Mount Isa terrane: In Burg, J. P., Ford, M., (Eds.). Orogeny through time. Geological Society of London Special Publication 121, 99-122.

O’ Dea, M. G., Lister, G. S., Betts, P. G., Pound, K. S., 1997b. A shortened intraplate rift system in the Proterozoic Mount Isa terrain, NW Queensland, Australia. Tectonics 16, 425-441.

Oliver, N. H. S., Rubenach, M. J., Valenta, R. K., 1998. Precambrian metamorphism, fluid flow, and metallogeny of Australia. Journal of Australian Geology and Geophysics 17, 31-53.

Page, R. W., Bell, T. H., 1986. Isotopic and structural responses of granite to successive deformation and metamorphism. Journal of Geology 94, 365-379.

Page and MacCready, 1997. Rocks of Mount Isa Group age in the Eastern Fold Belt. AGSO Research Newsletter 26, 16-17.

Page, R. W., Sun, S-S., 1998. Aspects of geochronology and crustal evolution in the Eastern Fold Belt, Mt Isa Inlier. Australian Journal of Earth Sciences 45, 343-361.

Passchier, C. W., Williams, P. R., 1989. Proterozoic extensional deformation in the Mount Isa Inlier: Queensland, Australia. Geological Magazine 126, 43-53.

Passchier, C. W., Trouw, R. A. J., Zwart, H. J., Vissers, R. L. M., 1992. Porphyroblast rotation: eppur si muove? Journal of Metamorphic Geology 10, 283, 294.

Passchier, C. W., Trouw, R. A. J., 1998. Micro-tectonics. Springer-Verlag Berlin, 1-283.

Powell, R., Holland, T., Worley, B., 1998. Calculating phase diagrams involving solid solutions via non-linear equation, with examples using THERMOCALC. Journal of Metamorphic Geology 16, 577-588.

Regnier, J. L., Ring, U., Passchier, C. W., Gessner, K. and Gungor, T., 2003. Contrasting metamorphic evolution of metasedimentary rocks from the Cine and Selimiye nappes in the Anatolide belt, western Turkey. Journal of metamorphic Geology 21, 699-721.

Reinhardt, J., 1992. Low-pressure, high-temperature metamorphism in a compressional tectonic setting: Mary Kathleen Fold Belt, northeastern Australia. Geological Magazine 129, 41-57.

Rosenfeld, J. L., 1968. Garnet rotation due to the major Paleozoic deformation in southeast Vermont. In: Zen, E-AN, White, W. S., Hadley, J. B., 1968. (Eds.), Studies of Appalachian Geology: Northern and Maritime. Interscience publishers, New York 185-202.

Rubenach, M. J., Barker, A. J., 1998. Metamorphic and metasomatic evolution of the Snake Creek Anticline, Eastern Succession, Mt Isa Inlier. Australian Journal of Earth Sciences 45, 363-372.

Rubenach, M. J., Lewthwaite, K. A., 2002. Metasomatic albitites and related biotite-rich schists from a low-pressure polymetamorphic terrane, Snake Creek Anticline, Mount Isa Inlier, north-eastern Australia: microstructures and P-T-d paths. Journal of Metamorphic Geology 20, 191-202.

Spear, F. S., Kohn, M. J., Florence, F. P., and Menard, T., 1991. A model for garnet and plagioclase growth in pelitic schists: implications for thermobarometry and P-T path determinations. Journal of Metamorphic Geology 8, 683-696.

Stallard, A. and Hickey, K., 2002. A comparison of microstructural and chemical patterns in garnet from the Fleur de Lys Supergroup, Newfoundland. Journal of Structural Geology 24, 1109-1123.

Steinhardt, C., 1989. Lack of porphyroblast rotation in noncoaxially deformed schists from Petrel Cove, South Australia, and its implications. Tectonophysics 158, 127-140.

Thompson, P. H., Bard, J. P., 1982. Isograds and mineral assemblages in the eastern axial zone, Montagne Noire (France). Implications for temperature gradients and P-T history. Canadian Journal of Earth Sciences 19, 129-143.

Turnbull, I. M., 1981. Contortions in the schists of the Cromwell district, Central Otago, New Zealand. New Zealand Journal of Geology and Geophysics 24, 65-86.

Vance, D., Mahar, E., 1998. Pressure-temperature paths from P-T pseudosections and zoned garnets: potential, limitations and examples from the Zanskar Himalaya, NW India. Contributions to Mineralogy and Petrology 132, 225-245.

Whitelock, J., 1989. Structural analysis of the synclinal Scott Outlier, Cattle Creek Area, SSW of Mary Kathleen, Mt Isa Inlier. Unpublished Honors thesis, James Cook University, Townsville, Queensland, 1-301.

Williams, P. J., 1998. Metalliferous economic geology of the Mt. Isa Eastern Succession, northwest Queensland. Australian Journal of Earth Sciences 45, 329-341.

Williams, P. F., Jiang, D., 1999. Rotating garnets. Journal of Metamorphic Geology 17, 367-378.

Williams, M. L., Jercinovic, M. J., 2002. Microprobe monazite geochronology: putting absolute time into microstructural analysis. Journal of Structural Geology 24, 1013-1028.

SECTION C

Radical shift in the direction of relative plate motion during Mesoproterozoic orogenesis

Aerially extended, Mesoproterozoic orogenesis accompanying a radical shift in the direction of relative plate motion: seeing through the overprinting effects of penetrative deformation and metamorphism

Abstract

Foliation **I**ntersection/**I**nflection **A**xes within porphyroblast**s** (FIAs) allow the chronological and kinematic linking of deformation episodes with associated metamorphism. Measurement of FIAs in the Eastern Fold Belt of the Mount Isa Inlier has revealed phases of deformation and metamorphism that could not previously be distinguished from one another. Both the 'asymmetry switch' and 'FitPitch' FIA measurement techniques have been applied to key localities of polymetamorphosed and multiply deformed Eastern Fold Belt, and they yielded the same result. These independent techniques have revealed (1) W-E trending structures that formed during N-S bulk shortening (O_1) and N-S oriented structures that formed during W-E bulk shortening (O_2) in the Eastern Fold Belt, (2) the presence of separate periods of metamorphism associated with each direction of bulk shortening, and (3) the crustal scale tectonic processes associated with polymetamorphism. A progressive succession of overprinted FIA trends reveals a clockwise rotation of the principal direction of bulk shortening with time. This requires a radical shift of relative plate movement from N-S to W-E during development of the north Australian craton in the Mesoproterozoic (*ca* 1.60 and 1.50Ga). Middle to upper amphibolite facies metamorphic conditions occurred during O_1 with crustal thickening followed by fast erosion and near-isothermal decompression leading to low-pressure/high-temperature (LP/HT) conditions. This was followed during O_2 by a second period of middle- to upper- amphibolite facies metamorphism. This history appears to correlate better with that observed in the southwest United States, which may have been located against the NE of the Australia at this period in time.

1. Introduction

With progress in the analysis of multiply deformed orogenic belts through numerical simulations of crustal-scale processes (e.g., Schulmann et al., 2002), analogue models (e.g., Harris and Koyi, 2003), computing (Aerden, 2003) and FIA controlled monazite dating (Bell and Welch, 2002), it has become apparent that tectonic processes are far more complicated and lengthy than previously recognized. Most multiply deformed orogenic belts have cyclic and/or polymetamorphic signatures for pro and/or retrograde mineral assemblages that directly link to crustal scale compression and/or decompression phenomena (e.g. Pattison et al., 1999). To resolve these complex histories, detailed microstructural and associated metamorphic analysis is essential as it allows the integration of structural, metamorphic and tectonic processes (e.g., Reinhardt, 1992; Hickey and Bell, 1999; Johnson, 1999; Mathavan and Bowes, 2004).

The Eastern Fold Belt of the Mt Isa Inlier is a multiply deformed polymetamorphosed terrain with extensive intrusive and extrusive complexes that hosts giant structurally controlled Iron Oxide Copper Gold (IOCG) deposits (Fig. 1). It has been argued that the mineralization is controlled by discrete episodes of deformation (e.g., Adshead-Bell, 1998) ranging from *ca.* 1595Ma Osborne Cu-Au (Rubenach et al., 2001) to *ca.* 1505Ma Starra Au-Cu orebodies (Rotherham et al., 1998). Therefore, understanding the regional tectonics and metamorphism is essential for prospect analysis and exploration for more deposits in this region.

The structural framework of the Eastern Fold Belt consists of an intensely developed north-south oriented, subvertical D_2 fabric and associated folds that has obscured and obliterated early D_1 structures. The latter structures are only very locally preserved in low strain zones of D_2. Strain within the inlier, and particularly in the Eastern Fold Belt, is heterogeneously developed from pervasive to semi-pervasive S_2 (D_2) fabric and controlled largely by lithologies ranging from competent to incompetent units. The recognition and geometric interpretation of early D_1 structures is very much dependent on the intensity of D_2 strain zones. These early W-E trending structures have been recognized in some regions (e.g., Loosveld 1989; Mares, 1998; Adshead-Bell, 1998), but in spite of this, their interpretation has been the subject of considerable controversy (e.g., Passchier and Williams, 1989; Bell et al., 1992; Connors and Lister, 1995; O' Dea and Lister, 1995; Giles et al., 1998; Betts et al., 2000).

In this study, **FIAs (F**oliation **I**ntersection/**I**nflection **A**xes preserved within the porphyroblast**s**) have been determined by both the 'asymmetry switch' and 'FitPitch' methods in key areas of the Eastern Fold Belt. They reveal the extensive development of pre-D_2 structures. Both these techniques use inclusion trail patterns within the porphyroblasts as a tool to distinguish primitive microstructures, which can no longer be recognized in the recycled matrix foliation from younger foliations (e.g. Bell et al., 2003; Ham and Bell, 2004; Aerden, 2004). A succession of distinct FIA sets has been obtained in the Eastern Fold Belt that formed contemporaneously with pre-D_2 relic macrostructures. In addition, the succession of FIA sets reveal more deformation events and associated phases of metamorphism than previously recognized. FIA trends have been obtained from the Snake Creek Anticline, Gilded Rose, Tommy Creek Block, White Blow Formation of the Mary Kathleen Fold Belt and southern Selwyn Range (Fig. 1) and can be correlated with the published FIA data in the Eastern Soldiers Cap Group (Mares, 1998) and unpublished FIAs from the Cannington region (H. S. Kim, *unpublished data*) and Gilded Rose areas (Lally, 1997) of the Eastern Fold Belt. The FIA data across the orogen shows remarkably consistent trends and the significance of this data, from more than 2000 oriented thin sections, has been discussed in detail with respect to Mesoproterozoic regional tectonics. These structural overprinting relationships could correlate with low-pressure/high-temperature (LP/HT) metamorphic terrains of southwestern United States (1.7 to 1.6Ga), which were part of Laurentia, where crustal thickening with clockwise P-T path followed by decompression and two near-orthogonal shortening events have recently been recognized (Daniel, 1992; Williams and Karlstrom, 1996; Ilg and Karlstrom, 2000; Karlstrom et al., 2001).

2. Geological setting

The Mt Isa Inlier of NW Queensland is characterized by Mesoproterozoic, multiply-deformed and polymetamorphosed meta-sedimentary rocks and extensive intrusive and extrusive complexes. The inlier is divided into three north-south oriented litho-tectonic belts (Carter et al., 1961). From east to west, these are the Eastern Fold Belt, Kalkadoon-Leichhardt Belt and Western Fold Belt separated by late crustal-scale reverse and or strike slip faults (e.g., Blake, 1987; Betts et al., 2004). The Isan orogenic event (*ca.* 1.6-1.5Ga) was responsible for multiple deformation events and emplacement of Williams and Naraku Batholiths (1550-1500, e.g., Page and Sun, 1998).

Four deformation events have been recognized based on solid outcrop geology and field mapping, i.e., D_1, D_2, $D_{2.5}$ and D_3 during the Isan Orogenesis in the Western and parts of the Eastern Fold Belt (e.g., Bell, 1983; Bell and Hickey, 1998, Adshead-Bell, 1998). D_1 was interpreted to result from north-south shortening, with W-E trending folds preserved locally, whereas D_2 is characterized by east-west shortening and produced upright folds and steep north-south oriented regional foliation that ranges in age from 1575±10Ma to around 1510Ma (e.g., Hand and Rubatto, 2002) suggesting that several similarly oriented foliations are involved. Local, outcrop scale, flat- and steep-structures have been classified as $D_{2.5}$ and D_3, respectively (Bell and Hickey, 1998). However, MacCready et al. (1998) suggested a two-fold tectonic model based on a crustal scale Mt Isa deep seismic section involving D_2 forming by initial west vergent thin-skinned and nappe-style folding followed by thick-skinned and upright folding and faulting. D_1 was interpreted as extensional event (e.g., O' Dea and Lister, 1995; O'Dea et al., 1997; MacCready et al., 1998; Betts et al., 2004). A consensus about the orogenic mechanisms or the number of deformations involved (e.g., Mares, 1998) has never been established regarding pre-D_2 or post D_2 structures in the literature (e.g., Bell et al., 1992; Connors and Lister, 1995; O' Dea and Lister, 1995; MacCready et al., 1998; Adshead-Bell, 1998; Bell and Hickey, 1998).

LP/HT anticlockwise P-T-*t*-*d* paths have been documented in parts of the Eastern Fold Belt with characteristic polymetamorphic mineral assemblages (e.g., Oliver et al., 1991; Reinhardt, 1992; Rubenach and Lewthwaite, 2002). Examples of polymetamorphic assemblages include Crd, And, St, Sill, Bt, Ms (abbreviations after Kretz, 1983) in the Snake Creek Anticline (Rubenach and Lewthwaite, 2002) and Rosebud Syncline of the Mary Kathleen Fold Belt (Reinhardt, 1992). Other metamorphic phases of different generations such as kyanite, sillimanite, andalusite and garnet were also documented (e.g., Rubenach and Lewthwaite, 2002). The occurrence of such complex mineral assemblage implies that the Eastern Fold Belt of the Mt Isa Inlier has undergone discrete phases of metamorphism and associated deformation.

3. Sample description

Sixty-five porphyroblastic samples were collected from the White Blow Formation (samples with prefix WB) of the Mary Kathleen Fold Belt (Fig. 2; Table-1). Most of the samples came from the White Blow schist with a few from interbedded calc-silicate bands. Thirty-seven of these samples contain inclusion trail patterns that allow microstructural analysis by both the 'asymmetry switch' and 'FitPitch' FIA method. Generally, the rocks consist of garnet-biotite-staurolite-muscovite schist with rare andalusite and sillimanite. Accessory minerals include graphite, ilmenite and rarely rutile. Garnet porphyroblasts are generally small (≤2mm), whereas staurolite porphyroblasts typically range from 5mm to 1cm. Inclusion trail patterns within the porphyroblasts range from staircase to slightly sigmoidal shapes and/or preserving differentiated crenulation cleavages (see below).

Forty-four oriented porphyroblastic rocks were collected from the Snake Creek Anticline (samples with prefix SC; Fig. 3; Table-2). The samples mainly came from the eastern and western limbs of the north-south oriented part of the anticline. Twenty-four contain sufficient inclusion trails to use the 'asymmetry switch' method, whereas six were suitable for the 'FitPitch' method. FIAs were mainly obtained from garnet, staurolite, andalusite, chlorite and gedrite porphyroblasts plus and matrix crenulations. No FIAs have been measured from cordierite and kyanite because cordierite in all the analyzed samples has been partially or totally pseudomorphed by muscovite, biotite, quartz and/or albite, whereas kyanite exists as relics or where preserved, contains poor inclusion trail patterns. FIAs have been determined from chloritoid, garnet, staurolite and andalusite porphyroblasts from the Gilded Rose (samples with prefix GR; Table-3) and comparisons have been made with FIAs previously obtained by Lally (1997) and Lewthwaite, (2000). Three out of seven samples from the Tommy Creek Block (samples with prefix TC; Table-3) contain spectacular spiral inclusion trails within garnet porphyroblasts. Garnet ranges in size from ≥2 - ≤ 8mm with distinct inclusion rich cores and inclusion poor rims. This transition is commonly marked by truncation of the inclusion trails in the median region. FIAs have been measured in two rock samples, biotite-staurolite schist from north of Camel Dam, Southern Selwyn Range (samples with prefix SR; Table-3; see also section A of this dissertation).

4. FIA determination

The 'asymmetry switch' method for measuring FIAs is based on the switch in asymmetry of inclusion trail patterns that occurs in porphyroblasts across the FIA trend (Hayward, 1990). The 'FitPitch' method (Aerden, 2003) calculates FIAs based on the intersection of one, two or three best-fit planes from linear structural elements distributed in 3D space from thin sections with different orientations. The principles of both the techniques are discussed below.

4.1. Asymmetry FIA method

Bell et al. (e.g., 1995; 1998; 2003) have described the methodology in detail for measuring FIAs and their implications for tectonic processes, folding and regional deformation partitioning. FIAs are measured with respect to geographic coordinates and the vertical to earth surface and record inflection or intersection lineations defined by foliations preserved within porphyroblasts. A minimum of eight vertical oriented thin sections are required to measure a single FIA within a 10^{o} range one cut every 30^{o} around the compass and two cut 10^{o} apart between the two sections 30^{o} apart where the asymmetry of the inclusion trails switch from 'S' to 'Z' or vice versa (Fig. 4).

4.2. 'FitPitch' FIA technique

The 'FitPitch' technique constructs primitive foliation plane(s) based on the quantitative measurements of pitches of the inclusion trails preserved in the porphyroblasts allowing the FIA to be calculated from their intersections (Aerden, 2003). The technique uses a computer program ‘FitPitch’, which can calculate one, two or three-best fit planes based on unimodal, bimodal and trimodal preferred sets of inclusion trail pitches distributed in 3D space with statistical constraints (Aerden, 2003). The intersection of the two best-fit planes from two distinct group of pitches should, theoretically define the FIA. The technique is quite useful for those inclusion trails showing no asymmetry or for those rocks hosting porphyroblast with straight inclusion trails in it. Extra FIA set(s) can potentially be calculated using ‘FitPitch’ that are not possible through the ‘asymmetry switch’ FIA method (see below).

5. Regional FIA Analysis

5.1. White Blow Formation

Seventy-two FIA measurements were obtained from inclusion trails preserved within garnet and staurolite porphyroblasts and the matrix foliation using the ‘asymmetry switch’ method (Table-1). Figure 5 shows rose plots of total FIA sets and subsets, whereas figure 6 shows FIA orientations separated for garnet versus staurolite porphyroblasts. It is noticeable in figure 6 that the prominent W-E FIAs are hosted within the cores of the porphyroblasts, whereas the prominent N-S FIAs come from porphyroblast rims. Since porphyroblast core growth always predate the rim, the core preserves early formed FIAs. However, porphyroblast growth is episodic and controlled by deformation partitioning (Bell, 1986; Bell et al., 2004); new porphyroblasts generally grow early during successive deformations that accompanied N-S followed by W-E bulk shortening.

The four Modal FIA peaks are oriented WSW-ENE (set 1), WNW-ESE (set 2), NNW-SSE (subset 4a) and SSW-NNE (subset 4b). Sample WB9.1 contains a 135^o trending FIA, which fits in between FIA 2 and FIA 4a with respect to timing of the foliation inside the porphyroblasts and is called FIA set 3. Significantly, the 135^o trending FIA separates the W-E FIAs from the N-S FIAs. Based on the timing and geometry of the inclusion trail patterns from flat to steep events (Fig. 5b) preserved within the porphyroblasts containing multiple FIAs (chapter 2 of this dissertation), it is suggested that the first set in the White Blow Formation developed with a WSW-ENE trend. It was followed by WNW-ESE, NW-SE, NNW-SSE and finally SSW-NNE trends. The first three FIA sets are generally truncated by matrix foliation. Only FIA set 4 is defined by foliations that are continuous with the matrix foliation. The dominance of the W-E and N-S FIA sets suggests orogenesis can be separated into two main periods of orogenesis. FIA sets 1, 2 and 3 resulted from N-S shortening orogenesis 'O_1', FIA subsets 4a and 4b accompanied W-E shortening orogensis 'O_2'. The end product of O_1 was dominantly a subhorizontal foliation that resulted from decompression at the end of O_1 (see below). The last FIA subset 4b trend parallels the present day tectonic grain of the White Blow Formation (*cf.* S_2 stereo plot in Fig. 2, rose plot in Fig. 5).

To test the degree of near-orthogonal horizontal patterns of inclusion trails versus vertical preserved within the porphyroblasts, the pitches of the inclusion trails in vertically oriented set of thin-sections (at least 6 at every 30^o interval) and their trends in the horizontal sections were measured from thirty six samples. Data were divided into two types (after Aerden, 2004). A-type microstructures were assigned to straight or moderately sigmoidal inclusion trails and B-type microstructures were assigned to axial traces of microfolds or different stages of differentiated crenulation cleavage (Fig. 7). A total of 3835 pitches were measured from both A- and B-type microstructures and plotted on rose diagrams. A distinct shallowly oriented modal peak was obtained for A-type and a steep modal peak for B-type microstructures from vertical oriented thin sections (Fig. 8a). Horizontal thin sections yielded dominantly W-E and N-S strikes for inclusion trails within the porphyroblasts (Fig. 8b). This 3D quantitative data is remarkably consistent with the dominant W-E and N-S FIA sets as manifested from the strike orientations of inclusion trails measured from horizontal oriented thin sections. Similarly, flat to steep events preserved as inclusion trails within the porphyroblasts are coherent with the pitches measured from vertical oriented thin sections and to the best-fit planes, which are preferentially located at the periphery and near the center of the stereo plot (Fig 8c).

This 3D pitch data from the thirty six oriented rock sample were put through the 'FitPitch' computer program (Aerden, 2003). Most of the analyzed samples yield similar results to that obtained using the 'asymmetry switch' FIA method (Table-1). There were two significant advantages of 'FitPitch' over the 'asymmetry switch' method. Extra FIA trends were obtained from straight inclusion trails with no asymmetry (e.g., sample WB48, WB161, WB148, WB180). The program calculates apparent FIA plunges. Almost all the apparent FIA plunges lie at less than 40^{o}. This suggests that the FIAs were generally subhorizontal during both the O_1 and O_2 periods of the Isan orogeny (Fig. 8d).

5.2. Snake Creek Anticline

The Snake Creek Anticline is a regional D_2 structure (Rubenach and Lewthwaite, 2002) with a north-south trending fold axis, north of the Saxby Granite (Fig. 3). The anticline hosts the metamorphic assemblage Grt, St, Ky, Fib, And, Crd, Bt, Ms and Qtz.

Most of the cordierite localities lie along to the axis of the Snake Creek Anticline (Fig. 3; Rubenach and Lewthwaite, 2002). Different generations of garnet, staurolite and andalusite have also been recognized (Rubenach and Lewthwaite, 2002).

Forty-nine FIA measurements were obtained from oriented porphyroblastic samples of the Snake Creek Anticline using the 'asymmetric switch' method (Fig. 9a; Table 2). The porphyroblast density in these samples is low compared to samples from the White Blow schist. Andalusite porphyroblasts are abundant in the Snake Creek Anticline, however, they are generally not suitable for FIA analysis because of their size (≥1.5 to ≥4cm) and/or more rarely because of their complex inclusion trail patterns. FIAs were obtained from garnet, staurolite, andalusite, chlorite and gedrite porphyroblasts in descending order of abundance.

Six FIA sets were recognized and the relative timing constraints of successive FIA sets were based on four criteria. (1) multi-FIA analysis preserved within the porphyroblasts (e.g., samples 118, 104), (2) relative successions of prograde porphyroblast growth hosting different orientations or generations of inclusion trails, for example garnet inside staurolite, (3) truncation versus continuous inclusion trail microstructures (e.g., Adshead-Bell and Bell 1999 for description), and (4) FIA trends near-parallel or perpendicular to outcrop foliation. By using these timing criteria, the first formed FIA set developed with a SW-NE (set 0) trend. It was followed by WSW-ENE (set 1), WNW-ESE (set-2), NW-SE (3), SSW-NNE (4) and finally NE-SW (set 5). Significantly, except for the FIA set 0 and 5, the rest of the FIA sets have similar order of the same orientations in samples from the White Blow Formation suggesting a similar regional distribution (e.g., Bell and Kim, 2004). The SW-NE inclusion trails in porphyroblasts belonging to the FIA set 0 are restricted to the core of the porphyroblasts and are not continuous with the matrix. The porphyroblasts belong to this FIA set have either pseudomorphed rims of muscovite or altered reaction rims around garnets (see below). The NE-SW trending FIA set 5 is dominated by porphyroblasts with trails that are always continuous with the matrix. Additionally, most of the matrix crenulation axes are parallel to either FIA set 5 or FIA set 4 (Table-2). In general, the FIA measurements from the Snake Creek Anticline are dominantly N-S (set 4 and 5) as compared to W-E (set 0 to 3) parallel to the N-S trend of the Snake Creek Anticline, which is interpreted as a regional D_2 structure (e.g., Rubenach and Lewthwaite, 2002). FIA sets 0 to 3 formed predominantly during N-S shortening, called orogenic phase 'O_1', whereas FIA sets 4 and 5 formed during mainly W-E shortening, called orogenic phase 'O_2'.

Six samples were suitable for 'FitPitch' FIA analysis. Table-2 shows a comparison of FIAs obtained using both the 'FitPitch' and 'asymmetry switch' methods, whereas figure 9(b,c,d) shows orientation of measured pitches from six samples and the FIA trend and plunge. An example using sample 104 is presented here in detail. This is garnet-biotite schist that hosts multiple FIAs determined by both techniques. The 'asymmetry switch' method gives a garnet core-median FIA at 115^o, where as the rim FIA lies at 005^o. The 'FitPitch' method produced FIAs for the garnet core-median at (117/01) and the rim at (198/12). This suggests two distinct phase of growth of porphyroblasts (Fig. 10; see also Stallard and Hickey, 2002). These compare closely with those obtained independently by the 'asymmetry switch' method.

The relationship of cordierite preserved within andalusite and/or staurolite is noteworthy. No FIA data has been obtained from cordierite as it is always partially or completely pseudomorphed by coarse mica, quartz or albite. However, inclusions preserved inside andalusite and/ or staurolite porphyroblasts are mostly continuous with the matrix foliation and a N-S FIA (related to O_2) has been obtained from these rocks (Fig. 11; e.g., samples SC741, SC29, SC112). Sample SC112 contains pseudomorphed cordierite in the middle of staurolite porphyroblast. In sample-SC113, FIA 0 has obtained from a staurolite core, whereas the median and rim regions are pseudomorphed by coarse muscovite (Fig. 12a). SC490.4 contains relic staurolite at the median and or rim regions of cordierite. Thus, two distinct generations of staurolite were identified; before and after andalusite/cordierite growth. Relic or pseudomorphed staurolite before cordierite formed during O_1 and fresh staurolite after cordierite formed during O_2 (*cf.* Figs. 11a and 12b).

5.3. Gilded Rose

The Gilded Rose area (Fig. 3), north of the Snake Creek Anticline, regionally consists of west-east oriented D_1 structures (e.g., Loosveld, 1989) and contains the metamorphic assemblage Cld, Gt, St, And, Ms, Bt and Qtz. Two samples, GR189 and GR192, collected south of the Gilded Rose and northwest of the Snake Creek Anticline (Fig. 3) contain garnet porphyroblasts with inclusion trails defining W-E FIAs. The garnet preserves Chl, Pl and rare Bt inclusions in the core and median regions. W-E FIA measurements were also obtained from two rock samples in the Gilded Rose area itself. GR482 is a schistose rock contains garnet and chloritoid with sigmoidal inclusion trails (Fig. 13a), andalusite with differentiation crenulations (Fig. 13b), muscovite and biotite in addition to quartz in the matrix. Both garnet and chloritoid preserved W-E FIAs (Table-3). Andalusite often includes garnet and uncommonly chloritoid and this texture relationship suggests that garnet and chloritoid grew before andalusite (Fig. 13c). Sample

G3 contains Grt-St-And. Garnet contains W-E FIAs, whereas no FIAs could be obtained from staurolite and andalusite porphyroblasts because of their poor inclusion trail preservation. However, since both garnet and staurolite are preserved within andalusite, this suggests that andalusite grew late.

Seven FIA measurements were obtained by Lally (1997) from garnet porphyroblasts in Grt-Bt-Ms schist near the Gilded Rose mine. The FIA range in trend between W-E and WNW-ESE (Fig. 9e). He interpreted these FIA trends to a result from early N-S bulk shortening (D_1 of Bell, 1983). W-E trending FIAs were obtained by Lewthwaite (2000) in five samples containing garnet porphyroblasts. No north-south FIA measurements were obtained by any of these authors.

5.4. Tommy Creek Block

Three out of seven rocks yielded a north-northeast FIA trend in garnet porphyroblasts (Fig. 14a). The rest contained too few inclusions to measure. The spiral inclusion trails contain individual segments defining a near-orthogonal pattern and this is obvious from the orientation of 338 measured pitches of the inclusion trails preserved within the porphyroblasts from the differently oriented vertical thin sections (Fig. 14b, c).

Seven north-south FIA measurements were also obtained by Lally (1997), mainly from the southern and central parts of the Tommy Creek Block (Fig. 14a). These FIA trends are consistent with this study. Sample TC508 preserves early W-E FIA (075^{o}) within garnet porphyroblasts. Garnets from this sample preserve relic staurolite as inclusions and are hosted in turn within andalusite. Metamorphically, this texture indicates decompression from staurolite to andalusite through garnet and has important implications for the presence of early higher-pressure metamorphism.

The N-S trending FIAs formed during the W-E shortening period of O_2. Field measurements from the southern Tommy Creek indicate a generally W-E structural trend, whereas the central and northern parts are dominated by N-S structures. Lally (1997) interpreted the W-E structures in the southern part to result from post-D_2 bulk subhorizontal heterogeneous shearing.

5.5. Southern Eastern Fold Belt

Two staurolite-biotite-muscovite schist samples from the southern Sewlyn Range yielded north-northeast FIA trends (Fig. 14d). The inclusion trails within the staurolite porphyroblasts are continuous with the matrix, and the N-NE FIA trend is consistent with the outcrop foliation trend. In addition, all the intersection and mineral lineations measured in the outcrop e.g., L^2_2, L^2_4 and L^2_3, are shallowly plunging to the north-northeast, parallel to the FIA trend (Adshead-Bell, 2000; chapter A of this dissertation).

Nineteen FIA measurements were obtained from garnet and gahnite porphyroblasts from Cannington (Table-3) by H. S. Kim (unpublished data). He recorded sets trending WSW-ENE, NNW-SSE and NNE-SSW (Fig. 14e). The WSW-ENE FIA set predate the NNW-SSE FIA set, and the NNE-SSW set is the youngest (*pers. comm.* H. S. Kim, 2004). This data further constrains the timing of bulk shortening directions as initially N-S followed by W-E to form approximately W-E and N-S trending FIA sets, respectively.

W-E FIAs were also obtained from garnet porphyroblasts north of the Cannington in the Fairmile and Partridge areas (Mares, 1998), where the dominant outcrop foliation is north-northeast (Fig. 14f). The youngest FIA trends measured by Mares (1998) were N-S and NE-SW in agreement with the field measurements of matrix foliation.

6. Discussion and interpretations

6.1. Correlation of FIA trends across the Eastern Fold Belt

Altogether, 179 FIA measurements have been obtained in this study and by previous workers. Figure 15 shows the FIA trends and correlates them across the Eastern Fold Belt. In each case, the dominant W-E FIAs predate the dominant N-S ones. The N-S tectonic grain of the Eastern Fold Belt coincides with the youngest FIA sets 4ab (N-S) and locally FIA set 5 (NW-SE). Porphyroblasts containing these younger FIA sets are generally fresh and the foliations defined by their inclusions are gently dipping and continuous with the steep matrix foliation. This gently dipping foliation is interpreted to be the end product of N-S shortening orogenesis O_1 prior to W-E shortening O_2 (Mares, 1998; see section B of this dissertation). Early W-E followed by N-S FIA sets have also been obtained from the Georgetown inlier, east of the study area (Cihan, 2004). This suggests and extended deformation and associated metamorphism across the north Australian craton (see below).

The three earlier successions of FIA sets (0 to 2) oriented SW-NE, WSW-ENE and WNW-ESE are interpreted to have resulted from changes in the overall N-S directed bulk shortening during O_1. FIA set 3 has a scarce spatial distribution and is interpreted to have resulted from the waning stages of O_1. The dominant O_1 FIA sets WSW-ENE (FIA 1) and WNW-ESE (FIA 2), have been recognized across the Eastern Fold Belt. This suggests regionally extended N-S shortening across the orogen prior to the W-S shortening O_2 that now dominates the matrix. This is supported by several published and unpublished mesosocpic scale examples (e.g., Bell et al., 1992; Giles et al., 1998; Betts et al., 2000), where W-E oriented structures have been recognized in low strain zones associated with O_2. This is supported by a key locality, the Gilded Rose, where there are macroscopic W-E oriented structures with coarsely spaced younger N-S fabrics. Loosveld (1989) interpreted the Gilded Rose structures as related to early D_1 (O_1 of this study).

None of the O_1 related porphyroblasts are continuous with the matrix, except for the Gilded Rose region where O_1 dominates, further supporting their early growth during O_1 tectonism. The consistent FIA trends across the orogen suggests that the porphyroblasts did not rotate during subsequent deformation events (see below). Additionally, pitches of the inclusion trails measured from vertical and horizontal thin sections reveal a distinct near-orthogonal pattern further suggesting that porphyroblasts did not rotate with respect to the regional tectonic grain, in this case N-S, and with respect to geographical coordinates.

6.2. Evidence of early Barrovian-type metamorphism

The Gilded Rose and Snake Creek Anticline areas are distinctly west-east and north-south trending, respectively, in the Eastern Fold Belt of the Mt Isa Inlier. Macrostructural relationship (Loosveld, 1989), detailed FIA analysis and micro-textural evidence reveal that the Gilded Rose area resulted from early north-south bulk shortening and was accompanied by Barrovian-type metamorphism. The mineral assemblages include garnet-chloritoid-staurolite (e.g., samples G3 and G482) with chlorite-biotite-plagioclase inclusions in garnet porphyroblasts (e.g., samples GR192 and GR189). Consequently, O_1 generated amphibolite facies metamorphic conditions. Late andalusite porphyroblast growth around garnet, chloritoid and staurolite reveal a near-isothermal decompression path from this early higher-pressure stage (see also section D of this dissertation). Thus, at the onset of west-east shortening (O_2), the metamorphic conditions were already at low pressure. Continued shortening produced overprinting north-south structures. The transition is readily apparent on the northern hinge of the Snake Creek Anticline (*pers. comm.*, Tim Bell, 2004). Within the Snake Creek Anticline mineral phases, such as cordierite were only found along the axial plane of this regional fold, which is a N-S trending O_2 structure. They were followed by up-pressure mineral phases such as second-generation andalusite, garnet and staurolite (Rubenach and Lewthwaite, 2002). For example, Sample SC112 from the Snake Creek Anticline contains pseudomorphed cordierite and fresh garnet in the staurolite porphyroblast (Fig. 11). Based on textural relationships and timing of porphyroblasts growth, it is suggested that cordierite grew first in this rock followed by garnet and then staurolite. Even though the rock contains pseudomorphed cordierite, which is an indication of LP/HT metamorphic conditions, the garnet porphyroblast shows strong and regular zoning pattern ('bell-shaped' Mn profile from core to rim), suggests increase in metamorphic grade controlled by up-pressure rather than temperature (e.g., Tracy et al., 1976; chapter D of this dissertation). This is consistent with pseudomorphed nature of cordierite in staurolite (e.g., Pattison et al., 1999) and W-E shortening produced N-S FIAs in garnet and staurolite porphyroblasts and steep N-S striking foliation.

If cordierite growth was early in terms of regional metamorphism and tectonics, as argued by Rubenach (*in press*), then this mineral should have formed in the Gilded Rose. However, this is not the case and most of the Crd localities in the Snake Creek Anticline not only follow the axial plane of this regional fold (Rubenach and Lewthwaite, 2002), but also along an albitization front around the Saxby granite (Fig. 3). This albitization front caused the LP/HT conditions that allowed Crd to grow (Mark, 1998;

Mark and Foster, 2000; Pattison et al., 1999). Consequently, between O_1 and O_2 crustal-scale decompression accompanied the transition from N-S to W-E shortening and interrupted the clockwise rotation of the bulk shortening direction (see Bell et al., 2003). This early period of relatively higher-pressure metamorphism, followed by decompression, has not been previously reported from the Eastern Fold Belt of the Mt Isa Inlier.

Theoretical, experimental (e.g., England and Thompson, 1984*ab*) and petrological constraints (e.g., Pattison, 1999) as well as numerical models (e.g., Schulmann et al., 2002) indicate that LP/HT metamorphic conditions appear to require an early high-pressure regime followed by decompression and/or crustal attenuation. In the case of the Eastern Fold Belt of the Mt Isa Inlier, Reinhardt (1992) assumed initial high-pressure metamorphism for D_1 in respond to crustal thickening (O_1 of this study; see also Bell, 1983) up to greenschist facies followed by isostatic rebound that produced LP/HT conditions (near-isothermal decompression). This assumption has not received much attention but is supported by the data described herein, which indicates O_1 was responsible for at least middle-amphibolite facies metamorphism and generated multiple W-E oriented fabrics and was followed by decompression. Hence, a thermally weakened crust existed at the onset of O_2 orogenesis.

6.3 FIA succession vs. porphyroblasts rotation

The succession of FIA sets from early W-E to younger N-S across the Eastern Fold Belt suggests that porphyroblast growth was controlled by deformation partitioning and overprinting of successive near-orthogonal fabric development (e.g., Bell, 1886; Bell and Hayward, 1991) rather than non-coaxial flow (e.g., Williams and Jiang, 1999). The

FIA analysis with its distinct model azimuths with respect to geographical coordinates provides evidence that porphyroblasts retain original foliations, commonly as crenulation, cleavages, with respect to bulk shortening directions and did not rotate during successive deformation events. If rotation of the porphyroblasts had occurred within the matrix during progressive deformation, an enormous spread of FIA trends would have developed. 'FitPitch' analysis from the White Blow Formation and Snake Creek Anticline shows that the FIAs have shallow plunges and occur in four sets. If FIA set 1 was rotated about the axis of FIA set 2, FIA set 3 and FIA subset 4b (Fig. 16; see also Ham and Bell, 2004) an enormous spread of FIA set 1 around the compass would have resulted. Similarly, spreads would have developed in FIA sets 2 and 3. This is not the case and the FIA sets are tightly constrained. Therefore, the porphyroblasts did not rotate during successive deformation events in the study area. They preserve the history of deformation events as a succession of subhorizontal and subvertical foliations.

6.4. Interpretation of the Mt Isa Deep Seismic Section (MacCready et al., 1998)

West-vergent thin- to thick-skinned tectonic style of deformation, based on the W-E oriented Mt Isa Deep Seismic Section (MIDSS), has recently been proposed (MacCready et al., 1998; Goleby et al., 1998) with some field examples (e.g., Betts et al., 2000) for the geodynamic evolution of the Mt Isa Inlier. Their interpretation has been questioned (Sayab, 2004) based on the overprinting of near-orthogonal deformation events recognized from macroscopic to microscopic field relationships in the southern Selwyn Range of the Eastern Fold Belt. Most of the structures in the MIDSS have been interpreted as low angle thrust driven nappes, yet the surface geology is characterized by steep structures. Indeed, the 3D subsurface gravity and magnetic geophysical signatures (*pmd**CRC data; Holden et al., 2000) indicate steep lithological boundaries and structures within the crust, making these interpretations of the seismic section difficult to accept.

6.5. Implications for refining Rodinia

Initially, SWEAT (south-west US – East Antarctica) hypothesis was suggested for Rodinia reconstruction (e.g., Jefferson, 1978; Dalziel, 1991; Hoffman, 1991; Powell et al., 1993). As a part of this reconstruction, the western US was matched with Antarctica, western Canada with Australia and the truncated *ca.* 1.0Ga Grenville orogen of Texas was matched with East Antarctica. Subsequently, a number of piercing points and geologic 'fingerprints' have been described regarding the geological connection between proto-Australia and southwest U.S. (AUSWUS) between 1.8 to 1.0Ga (Fig. 17; Karlstrom et al., 1999). The Yavapai-Mazatzal Provinces (1.8-1.6Ga) in Laurentia are similar to the Arunta-Musgrave blocks of central Australia. Economically significant massive sulfide deposits occur in the Mt Isa and Broken Hill areas of Australia and at Jerome and Bagdad in central Arizona and the Carlin district of Nevada, respectively. Other geologic links have been proposed in a subsequent paper (Karlstrom et al., 2001). A third model, AUSMEX (Australia-Mexico), puts the Australian continent farther south (Wingate et al., 2002) based on paleomagnetic and geochronology data. Debate continues on the relative position of Australian continent with respect to western U.S. in the reconstruction of Rodinia (Karlstrom and Williams, 2002; Meert, 2002). However, both geologic and paleomagnetic data suggest that separation between Laurentia and Australia took place *ca.* 0.8Ga and between Laurentia and Baltica *ca.* 0.6Ga (Karlstrom et al., 2001; Wingate et al., 2002). An attempt is made below to correlate deformation and metamorphism between Australia and the USA, which could provide an additional 'finger print' between the north-Australian craton and the southwestern U. S.

6.5.1. Structural constraints

Based on detailed microstructural analysis, Ilg and Karlstrom (2000) identified two distinct near-orthogonal fabrics preserved within the porphyroblasts in the Mesoproterozoic (*ca.* 1.7-1.6Ga) supracrustal rocks of the Grand Canyon, Arizona using horizontal oriented thin sections. They recognized the regional tectonic grain as a pervasive NE-SW striking subvertical foliation and associated subvertical mineral stretching lineation, which were the product of northwest-southeast shortening (Karlstrom and Bowring, 1993). Most porphyroblast rims preserved this younger NE-SW foliation as inclusion trails continuous with the matrix. However, garnet core and median regions, consistently preserve NW-SE trends. This geometric relationship can potentially be correlated with the White Blow Formation of the Mt Isa Inlier, where dominantly early W-E trends of inclusion trails preserved within the porphyroblasts are overprinted by younger N-S trending inclusion trails in horizontal thin sections. The data is also consistent with the early W-E followed by younger N-S FIAs. This data can be tested further in terms of APWP for refining the Rodinia reconstruction.

6.5.2. Metamorphic constraints

The Mesoproterozoic orogenic belts (*ca.* 1.7-1.6Ga) of the southwestern U.S. is a classic example of large scale LP/HT metamorphism (Karlstrom and Bowring, 1993). Earlier workers (e.g., Grambling 1986; Grambling et al., 1989) argued for an anticlockwise P-T path that they interpreted was synchronous with crustal shortening and post-deformational isobaric cooling. Subsequently, a clockwise path was proposed consisting of early thickening with heating followed by decompression from 6 to 3Kbars for Grand Canyon and Northern New Mexico followed by local thermal pulses (e.g., Daniel, 1992; Williams, 1991; Williams and Karlstrom , 1996).

Based on the metamorphic mineral assemblages and textures presented above, similar P-T conditions have been identified in this study. These are an early higher-pressure event as a result of O_1 crustal thickening followed by decompression and second phase of a prograde path from low pressure to moderate pressure associated with O_2. Thus, there is mounting evidence for similar extensive metamorphism and contractional deformation at ~1.6Ga in Australia and southwestern Laurentia (e.g., Karlstrom and Humphreys, 1998; Karlstrom et al., 2001).

References

Adshead-Bell, N. S., 1998. Evolution of the Starra and Selwyn high-strain zones, Eastern Fold Belt, Mount Isa Inlier: implications for Au-Cu mineralization. Economic Geology 93, 1450-1462.

Adshead-Bell, N. S., 2000. Structural constraints of the ironstone hosted Au-Cu Starra deposit and Selwyn Range Region, Eastern Fold Belt, Mt Isa Inlier. Unpublished Ph. D thesis, James Cook University, Townsville, Queensland, D1-D55.

Adshead-Bell, N. S., Bell, T. H., 1999. The progressive development of a macroscopic upright fold pair during five near-orthogonal foliation-producing events: complex microstructures versus a simple macrostructure. Tectonophysics 306, 121-147.

Aerden, D. G. A. M., 2003. Preferred orientation of planar microstructures determined via statistical best-fit of measured intersection-lines: the 'FitPitch' computer program. Journal of Structural Geology 25, 923-934.

Aerden, D. G. A. M., 2004. Correlating deformation in Variscan NW-Iberia using porphyroblasts; implications for the Ibero-Armorican Arc. Journal of Structural Geology 26, 177-196.

Bell, T. H., 1983. Thrusting and duplex formation at Mount Isa, Queensland, Australia. Nature 304, 493-497.

Bell, T. H., Rubenach, M. J., 1983. Sequential porphyroblast growth and crenulation cleavage development during progressive deformation. Tectonophysics 92, 171-194.

Bell, T. H., 1986. Foliation development and refraction in metamorphic rocks: reactivation of earlier foliation and decrenulation due to shifting pattern of deformation partitioning. Journal of Metamorphic Geology 4, 421-444.

Bell, T. H., Hayward, N., 1991. Episodic metamorphic reactions during orogenesis: the control of deformation partitioning on reaction sites and duration. Journal of Metamorphic Geology 9, 619-640.

Bell, T. H., Reinhardt, J., Hammond, R. L., 1992. Multiple foliation development during thrusting and synchronous formation of vertical shear zones. Journal of Structural Geology 14, 791-805.

Bell, T. H., Forde, A., Wang, J., 1995. A new indicator of movement direction during orogenesis: measurement technique and application to the Alps. Terra Nova 7, 500-508.

Bell., T. H., Hickey, K. A. and Upton, J. G., 1998. Distinguishing and correlating multiple phases of metamorphism across a multiply region using the axes of spiral, staircase and sigmoidal inclusion trails in garnet. Journal of Metamorphic Geology 16, 767-794.

Bell, T. H., Hickey, K. A., 1998. Multiple deformations with successive subvertical and subhorizontal axial planes in the Mount Isa Region: their impact on geometric development and significance for mineralization and exploration. Economic Geology 93, 1369-1389.

Bell, T. H., Welch, P. W., 2002. Prolonged Acadian Orogenesis: revelations from foliation intersection axis (FIA) controlled monazite dating of foliations in porphyroblasts and matrix. American Journal of Science 302, 549-581.

Bell, T. H., Ham, A. P., Hickey, K. A., 2003. Early formed regional antiforms and synforms that fold younger matrix schistosities: their effect on sites of mineral growth. Tectonophysics 367, 253-278.

Bell, T. H., Kim, H. S., 2004. Preservation of Acadian deformation and metamorphism through intense Alleghanian shearing. Journal of Structural Geology 26, 1591-1613.

Bell, T. H., Ham, A. P., Kim, H. S., 2004. Partitioning of deformation along an orogen and its effects on porphyroblast growth during orogenesis. Journal of Structural Geology 26, 825-845.

Betts, P. G., Ailleres, L., Giles, D., Hough, M., 2000. Deformation history of the Hampden Synform in the Eastern Fold Belt of the Mt Isa terrane. Australian Journal of Earth Sciences 47, 1113-1125.

Betts, P. G., Giles, D., Lister, G. S., 2004. Aeromagnetic patterns of half-graben and basin inversion: implications for sediment-hosted massive sulfide Pb-Zn-Ag exploration. Journal of Structural Geology 26, 1137-1156.

Blake, D. H., 1987. Geology of the Mount Isa Inlier and environs, Queensland and Northern Territory. Bureau of Mineral Resources, Geology and Geophysics Bulletin 225, 1-83.

Carter, E. K., Brooks, J. H. and Walker, K. R., 1961. The Precambrian mineral belt of north-western Queensland. BMR, Geology and Geophysics Australia, Bulletin 61.

Cihan, M., 2004. The drawbacks of sectioning rocks relative to fabric orientations in the matrix: A case study from the Robertson River Metamorphics (Northern Queensland, Australia). Journal of Structural Geology 26, 2157-2174.

Connors, K. A., Lister, G. S., 1995. Polyphase deformation in the western Mount Isa Inlier, Australia: episodic or continuous deformation? Journal of Structural Geology 17, 305-328.

Dalziel, I. W. D., 1991. Pacific margins of Laurentia and East Antarctica-Australia as a conjugate rift pair: evidence and implications for an Eocambrian supercontinent. Geology 19, 598-601.

Daniel, C. G., 1992. Metamorphic P-T paths from kyanite-sillimanite-andalusite-bearing rocks in north-central new Mexico. M. S thesis, Albuquerque, University of New Mexico pp97.

England, P. C., Thompson, A. B., 1984a. Pressure-Temperature-Time paths of regional metamorphism I. Heat transfer during the evolution of regions of thickened continental crust. Journal of Petrology 25, 894-928.

England, P. C., Thompson, A. B., 1984b. Pressure-Temperature-Time paths of regional metamorphism II. Their inference and interpretation using mineral assemblages in metamorphic rocks. Journal of Petrology 25, 929-955.

Giles, D., MacCready, T., 1997. The structural and stratigraphic position of the Soldier Cap Group in the Mount Isa Inlier. In: Ailleres, L., Betts, P. (Eds.), Structural elements of the Eastern Succession – A field guide illustrating the structural geology of the Eastern Mount Isa Terrane, Australia. Australian Crustal Research Centre, Technical Publication 63, 61-73.

Giles, D. Ailleres, L., Betts, P., Jeffriess, D., 1998. Geologic traverse of the Camel Dam – Pegmont region, southeast Isa Inlier. Australian Crustal Research Centre, Technical Publication No. 66, 1-29.

Goleby, B. R., MacCready, T., Drummond, B. J., and Goncharov., 1998. The Mount Isa Geodynamic Transect-Crustal Implications. In: Braun, J., Dooley, J., Goleby, B., Van der Hilst, R., Klootwijik, C., (Eds), Structure and Evolution of the Australian continent, American Geophysical Union, Geodynamic 26, 109-117.

Grambling, J. A., 1986. Crustal thickening during Proterozoic metamorphism and deformation in New Mexico. Geology 14, 149-152.

Grambling, J. A., Williams M. L., Smith, R. F., Mawer, C. K. 1989. The role of crustal extension in the metamorphism of Proterozoic rocks in northern New Mexico. Grambling, J. A., Tewksbury, B. J. (editors). Proterozoic geology of the southern Rocky Mountains. Geological Society of America Special Paper 235, 87-110.

Ham, A. P., Bell., T. H., 2004. Recycling of foliations during folding. Journal of Structural Geology 26, 1989-2009.

Hand, M., Rubatto, D., 2002. The scale of the thermal problem in the Mt Isa Inlier. 2002. Preiss,V. P. (Ed). Geoscience 2002: Expanding Horizons. Abstracts of the 16th Australian Geological Convention, Adelaide Convention Centre, Adelaide, SA, Australia 67, 173.

Harris, L. B., Koyi, H. A., 2003. Centrifuge modeling of folding in high-grade rocks during rifting. Journal of Structural Geology 25, 291-305.

Hayward, N., 1990. Determination of early fold axis orientation in multiply deformed rocks using porphyroblast inclusion trails. Tectonophysics 179, 353-369.

Hickey, K. A., Bell., 1999. Behaviour of rigid objects during deformation and metamorphism: a test using schists from Bolton syncline, Connecticut, USA. Journal of Metamorphic Geology 17, 211-228.

Hoffman, P. F., 1991. Did the breakout of Laurentia turn Gondwanaland inside-out? Science 252, 1409-1411.

Holden, D. J., Archibald, N. J., Boschetti, F., Jessell, M. W., 2000. Inferring geological structures using wavelet-based multiscale edge analysis and forward models. Exploration Geophysics 31, 67-71.

Idnurm, M., 2000. Towards a high resolution Late Palaeoproterozoic-earlist Mesoproterozoic apparent polar wander paths for northern Australia. Australian Journal of Earth Sciences 47, 405-429.

Ilg, B. R., Karlstrom, K. E., 2000. Porphyroblast inclusion trail geometries in the Grand Canyon: evidence for non-rotation and rotation? Journal of structural Geology 22, 231-243.

Jefferson, C. W., 1978. Correlation of middle and upper Proterozoic strata between northwestern Canada and central Australia. Geological Society of America, Abstracts 7, A429.
Johnson, S. E., 1999. Porphyroblast microstructures: A review of current and future trends. American mineralogist 84, 1711-1726.

Karlstrom, K. E., Bowring, S. A., 1993. Proterozoic orogenic history in Arizona. In: Van Schmus, W. R., Bickford, M. E. (editors), Transcontinental Proterozoic Provices, Chapter – 4: The Geology of North America Vol, C-2: Precambrian of the Conterminous. U. S. Geological Society of America (DNAG), 188-228.

Karlstrom, K. E., Humphreys, G., 1998. Influence of Proterozoic accretionary boundaries in the tectonic evolution of western North America: interaction of cratonic grain and mantle modification events. Rocky Mt. Geology 33, 161-179.

Karlstrom, K. E., Williams, M. L., McLelland, J., Geissman, J. W., Ahall, K-I., 1999. Refining Rodinina: Geologic evidence for the Australia-Western U.S. connection in the Proterozoic. GSA Today 9(10), 1-7.

Karlstrom, K. E., Ahall, Karl-Inge., Harlan, S. S., Williams, M. L., McLelland, J., Geissman, J. W., 2001. Long-lived (1.8 - 1.0Ga) convergent orogen in southern Laurentia, its extensions to Australia and Baltica, and implications for refining Rodinia. Precambrian Research 111, 5-30.

Karlstrom, K. E., Williams, M., L., 2002. Long-lived (1.8-1.0GA) convergent orogen in southern Laurentia – evaluation of the AUSWUS model for Rodinia. Geological Society of America 2002 Denver Annual Meeting, paper no 245-6.

Kretz, R., 1983. Symbols for rock-forming minerals. American Mineralogist 68, 277-279.

Lally, J. H., 1997. The structural history of the central Eastern Fold Belt, Mount Isa Inlier, Northwest Queensland, Australia. Unpublished Ph.D. thesis, 1-103.

Lewthwaite, K. J., 2000. The structural and metamorphic development of the Soldiers Cap Group SE of Cloncurry: implications for the orogenic development of the Eastern Fold Belt of the Mount Isa Inlier, Australia. Unpublished Ph.D. thesis, James Cook University 1-99.

Loosveld, R. J. H., 1989. The synchronism of crustal thickening and high-T/low-P metamorphism in the Mount Isa Inlier, Australia 1. An example, the central Soldiers Cap belt. Tectonophysics 158, 173-190.

MacCready, T., Goleby, B. R., Goncharov, A., Drummod, B. J., Lister, G. S., 1998. A framework of overprinting orogens based on interpretation of the Mount Isa deep seismic transect. Economic Geology 93, 1422-1434.

Mares, V. M., 1998. Structural development of the Soldiers Cap Group in the Eastern Fold Belt of the Mt Isa Inlier: a succession of horizontal and vertical deformation events and large-scale shearing. Australian Journal of Earth Sciences 45, 373-387.

Mark, G., 1998. Albitite formation by selective pervasive sodic alteration of tonalite plutons in the Cloncurry district, Queensland. Australian Journal of Earth Sciences 45, 765-774.

Mark, G., Foster, D. R. W., 2000. Magmatic-hydrothermal albite-actinolite-apatite-rich rocks from the Cloncurry district, NW Queensland, Australia. Lithos 21, 223-245.

Marshall, J. L., Oliver, N. H. S., 2001. Mechanical controls on fluid flow and brecciation in the regional host rocks for Eastern Fold Belt ironstone Cu-Au deposits, Mt Isa Block. Geological Society of Australia, Specialist Group in Economic Geology "Mineralisation, alteration and magmatism in the Eastern Fold Belt, Mount Isa Block Australia: Geological Review and Field Guide", Special Publication No 5, 30 -45.

Mathavan, V., Bowes, D. R., 2004. Microstructural features of albite porphyroblasts as indicators of sequential Barrovian metamorphic mineral growth in the Caledonides of the SW Scottish Highland. Journal of Metamorphic Geology 22, 639-651.

Meert, J. G., 2002. 2002. Rodinia: problems, issues and acronyms. Geological Society of America 2002 Denver Annual Meeting, paper no 245-1.

O' Dea, M. G., Lister, G. S., 1995. The role of ductility contrast and basement architecture in the structural evolution of the Crystal Creek Block, Mount Isa Inlier, Australian. Journal of Structural Geology 17, 949-960.

O' Dea, M. G., Lister, G. S., MacCready, T., Betts, P. G., Oliver, N. H. S., Pound, K. S., Huang, W., Valenta, R. K., 1997. Geodynamic evolution of the Proterozoic Mount Isa terrane: In Burg, J. P., Ford, M., (Eds.). Orogeny through time. Geological Society of London Special Publication 121, 99-122.

Oliver, N. H. S., Holcombe, R. J., Hill, E. J., Pearson, P. J., 1991. Tectono-metamorphic evolution of the Mary Kathleen Fold Belt, northwest Queensland: A reflection of mantle plume processes? Australian Journal of Earth Sciences 38, 425-455.

Page and MacCready, 1997. Rocks of Mount Isa Group age in the Eastern Fold Belt. AGSO Research Newsletter 26, 16-17.

Page, R. W., Sun, S-S., 1998. Aspects of geochronology and crustal evolution in the Eastern Fold Belt, Mt Isa Inlier. Australian Journal of Earth Sciences 45, 343-361.

Passchier, C. W., Williams, P. R., 1989. Proterozoic extensional deformation in the Mount Isa Inlier: Queensland, Australia. Geological Magazine 126, 43-53.

Passchier, C. W., Trouw, R. A. J., 1998. Micro-tectonics. Springer-Verlag Berlin, 1-283.

Pattison, D. R. M., Spear, F. S., Cheney, J. T., 1999. Polymetamorphic origin of muscovite+cordierite+staurolite+biotite assemblages: implications for the metapelitic petrogenetic grid and for P-T paths. Journal of metamorphic Geology 1999, 685-703.

Powell, C. M., Li, Z. X., McElhiny, M. W., Meert, J. G., Park, J. K., 1993. Paleomagnetic constraints on timing of the Neoproterozoic breakup of Rodinia and Cambrian formation of Gondwana. Geology 21, 889-892.

Reinhardt, J., 1992. Low-pressure, high-temperature metamorphism in a compressional tectonic setting: Mary Kathleen Fold Belt, northeastern Australia. Geological Magazine 129, 41-57.

Rotherham, J. F., Blake, K. L., Carwright, I., Williams, P. J., 1998. Stable isotope evidence for the origin of the Mesoproterozoic Starra Au-Cu deposit, Cloncurry District, northwest Queensland. Economic Geology 93, 1435-1449.

Rubenach, M. J., Lewthwaite, K. A., 2002. Metasomatic albitites and related biotite-rich schists from a low-pressure polymetamorphic terrane, Snake Creek Anticline, Mount Isa Inlier, north-eastern Australia: microstructures and P-T-d paths. Journal of Metamorphic Geology 20, 191-202.

Rubenach, M., Adshead, N., Oliver, N., Tullemans, F., Esser, D., Stein, H., 2001. The Osborne Cu-Au-Deposit: Geochronology, and Genesis of mineralization in relation to host albitites and ironstones. A Hydrothermal Odyssey, 172-173.

Sayab, M., 2004. 3D successions of near-orthogonal progressive bulk inhomogeneous shortening resulting in multiple generations of folds in the Mt Isa Inlier. In McPhie, J., McGoldrick, P. (eds), Dynamic Earth: Past, Present and Future. Abstracts of the 17th Australian Geological Convention, Hobart, Tasmania, Australia 73, 183.

Schulmann, K., Schaltegger U., Jezek, J., Thompson, A. B., Edel J-B., 2002. Rapid burial and exhumation during orogeny: thickening and synconvergent exhumation of thermally weakened and thinned curst (Variscan Orogen in Western Europe). American Journal of Science 302, 856-879.

Stallard, A., Hickey, K., 2002. A comparison of micorstructural and chemical patterns in garnet from the Fleur de Lys Supergroup, Newfoundland. Journal of Structural Geology 24, 1109-1123.

Tanaka,H., Idnurm, M., 1994. Palaeomagnetism of Proterozoic mafic intrusions and host rocks of the Mount Isa Inlier, Australia: Revisited. Precambrian Research 69, 241-258.

Tracy, R. J., Robinson, P., Thompson, A. B., (1976). Garnet composition and zoning in the determination of temperature and pressure of metamorphism, central Massachusetts. American Mineralogist 61, 762-775.

Whitelock, J., 1989. Structural analysis of the synclinal Scott Outlier, Cattle Creek Area, SSW of Mary Kathleen, Mt Isa Inlier. Unpublished Honors thesis, James Cook University, Townsville, Queensland, 1-301.

Williams, M. L., 1991. Heterogeneous deformation in a ductile fold-thrust belt: The Proterozoic structural history of the Tusas Mountains, New Mexico. Geological Society of America Bulletin 103, 171-188.

Williams, M. L., Karlstrom, K. E., 1996. Looping P-T paths and high-T, Low-P middle crustal metamorphism: Proterozoic evolution of the southwestern United States. Geology 24, 1119-1122.

Williams, P. J., 1998. Metalliferous economic geology of the Mt. Isa Eastern Succession, northwest Queensland. Australian Journal of Earth Sciences 45, 329-341.

Williams, P. F., Jiang, D., 1999. Rotating garnets. Journal of Metamorphic Geology 17, 367-378.

Wingate, M. T. D., Pisarevsky, S. A., Evans, D. A. D., 2002. Rodinia connections between Australia and Laurentia: no SWEAT, no AUSWUS? Terra Nova 14, 121-128.

SECTION D

Clockwise P-T path in the Mt Isa Inlier

Decompression through an early clockwise P-T path in the Mt Isa Inlier: implications for early N-S shortening orogenesis

Abstract

Mesoproterozoic terrains of the Australian craton exhibit complex tectonometamorphic histories that are generally considered to result from low-pressure/ high-temperature (LP/HT) metamorphism with an anticlockwise pressure (P) – temperature (T) – deformation (d) path. Yet studies regarding the nature of the P-T history and tectonic regime that led to such a LP/HT signature have been quite limited. A detailed FIA (**F**oliation **I**ntersection/**I**nflection **A**xes preserved in the porphyroblast**s**) analysis combined with textural relationships and P-T pseudosections, using key localities across the Eastern Fold Belt of the Mt Isa Inlier, has resolved the cause of the LP/HT signature. Two periods of porphyroblast growth have been distinguished using a change in FIA trends with time, namely one formed during N-S shortening followed by W-E shortening orogenesis (O_1 and O_2 respectively). Significantly, O_1 porphyroblasts preserving W-E FIAs exhibit mineral textures of Barrovian style, whereas O_2 formed porphyroblasts preserving N-S FIAs are Buchan in style. This supports the emplacement of the Williams/Naraku Batholiths after O_1 around the onset of O_2. Higher-pressure garnet cores, modeled in MnNCKFMASH P-T pseudosections preserve early W-E FIAs and formed during O_1. This was followed by decompression and then low pressure – high temperature (LP/HT) metamorphism when N-S FIAs were preserved within porphyroblasts. This is further supported by the presences of at least two distinctive generations of staurolite and kyanite that grew both before and after andalusite/cordierite. Middle to upper amphibolite facies metamorphic conditions occurred during O_1 with crustal thickening followed by fast erosion and near-isothermal decompression leading to LP/HT conditions. This was followed by O_2 and a second period of middle- to upper-amphibolite facies metamorphism that obliterated and/or obscured the tectonometamorphic signature of primitive O_1 in the matrix of most rocks.

1. Introduction

Rodinian Mesoproterozoic low-pressure/high-temperature (LP/HT) terrains with anticlockwise pressure (P) – temperature (T) – deformation (d) paths are economically very significant. For example, the Mt Isa Inlier (e.g., Loosveld, 1989; Oliver et al., 1991; Reinhardt, 1992; Rubenach, 1992; Rubenach and Lewthwaite, 2002), the Broken Hill Inlier (e.g., Hobbs et al., 1984; Stevens et al., 1988; Daly et al., 1998), and the Arunta Inlier (e.g., Vernon et al., 1990; Collins and Vernon, 1991; Gascombe, 1991; Hand et al.,

1992) in Australia or the basement in the Grand Canyon in Arizona and New Mexico in the southwestern United States (e.g., Grambling, 1986; Grambling et al., 1989; Grambling and Dallmeyer, 1993) or the Yukon in Canada (e.g., Torkelson et al., 2001). Consequently, the tectonic development of such provinces has been a long standing metamorphic petrology question of considerable economic interest (e.g., Loosveld and Etheridge, 1990; Sandiford and Powell, 1991). An added problem in these terrains is that they have undergone long-lived and complex deformation histories (e.g., Page and Bell, 1986; Karlstrom et al., 2001; Williams and Jercinovic, 2002) and associated polymetamorphic high-grade metamorphism (e.g., Williams and Karlstrom, 1996; Rubenach and Lewthwaite, 2002) with extensive intrusive and extrusive igneous activity and regional metasomatic alteration (e.g., Oliver et al., 1998; Williams and Pollard, 2003). Because of the predominant occurrence of Buchan-type or LP/HT minerals in these terrains, anticlockwise paths have been constructed with the assumption that metamorphism starts initially from a LP/HT base. Yet, there are many questions about the nature of the P-T history and tectonic setting that led to such a signature (e.g., Williams and Karlstrom, 1996; Boger and Hansen, 2004).

A major problem in resolving the tectonic development of such terrains is that they newly always contain rocks with a strong schistosity parallel to bedding or compositional layering. It has been recently shown that a lengthy deformation and metamorphic history commonly predates the schistosities that lie parallel to bedding or compositional layering (e.g., Williams, 1994; Ilg and Karlstrom, 2000; Bell et al., 2003; Bell and Kim, 2004). This history can only be resolved by quantitative structural and metamorphic work with porphyroblastic examples of such rocks. Prior to this approach, microstructural relationships (e.g., Johnson and Vernon, 1995), conventional geothermobarometry (e.g., Spear, et al., 1991; Spear, 1993; Florence et al., 1993) and qualitative P-T phase diagrams (e.g., Vance and Mahar, 1998; Zeh et al., 2004) were used but did not discriminate events in rocks where the foliations inside the porphyroblast were truncated by those in the matrix. Combined P-T pseudosections and **FIAs** (**F**oliation **I**ntersection/**I**nflection **A**xes preserved in porphyroblast**s**) provide a technique that separates porphyroblasts of different generations allowing one to characterized multiple periods of deformation and metamorphism that cannot be distinguished by any other means (e.g., Bell and Kim, 2004; Kim and Bell, *in press*).

In this study, FIAs were used to distinguish porphyroblasts of different generations from which the P-T history could be determined. This was done in key localities across the Eastern Fold Belt of the Mt Isa Inlier (Fig. 1). FIAs allow the paths of rocks through P-T pseudosections to be determined and correlated regionally. P-T pseudosections, calculated in the MnNCKFMASH (MnO-Na_2O-K_2O-FeO-MgO-Al_2O_3-SiO_2-H_2O) system, allow the garnet core, median and rim P-T conditions to be calculated. P-T estimates, consistent with textural relationships and field observations, have been obtained different to those previously documented from any part of the Mt Isa Inlier. The combination of new thermodynamic modeling and textural data reported here with re-interpretations of previously published and unpublished data allows a new tectonothermal model to be presented that dramatically extends the deformation history and associated thermal regimes for the Eastern Fold Belt. The model may provide a general explanation for LP/HT terrains characterized by similar tectonometamorphic settings elsewhere.

2. Geological setting

The Mt Isa Inlier of NW Queensland, Australia, is Mesoproterozoic (*ca.* 1.6-1.5Ga; Page and Bell, 1986; Page and Sun, 1998), multiply-deformed and polymetamorphosed terrain with extensive bi-model intrusive and extrusive complexes. The inlier is divided into three major north-south oriented tectono-stratigraphic belts (Carter et al., 1961). From east to west, these are the Eastern Fold Belt, Kalkadoon-Leichhardt Belt and Western Fold Belt separated by late major reverse or strike slip faults (Blake, 1987; Betts et al., 2004). The Isan orogenic event (*ca.* 1.6-1.5Ga) was responsible for multiple deformation events (e.g., Page and Bell, 1986). Emplacement of Williams and Naraku Batholiths occurred around 1550-1500Ma (e.g., Page and Sun, 1998).

Four deformation events have been recognized based on solid outcrop geology and field mapping, i.e., D_1, D_2, $D_{2.5}$ and D_3 during the Isan Orogenesis (Bell, 1983; Bell and Hickey, 1998). D_1 interpreted to result from north-south shortening with west-east trending folds preserved locally, whereas D_2 is characterized by bulk west-east shortening and produced upright folds and steep north-south oriented regional foliation that ranges in age from 1575±10Ma to around 1510Ma (Hand and Rubatto, 2002) suggesting that several similarly oriented foliations are involved. Local outcrop scale flat- and steep-structures have been classified as $D_{2.5}$ and D_3, respectively (Bell and Hickey, 1998).

LP/HT anticlockwise P-T-d paths have been documented in parts of the Eastern Fold Belt with characteristic polymetamorphic mineral assemblages (e.g., Reinhardt, 1992; Rubenach and Lewthwaite, 2002). Examples of polymetamorphic minerals include Crd-St-Bt-Ms (abbreviations after Kretz, 1983) in the Snake Creek Anticline (Rubenach and Lewthwaite, 2002) and Rosebud Syncline of the Mary Kathleen Fold Belt

(Reinhardt, 1992). Other metamorphic phases of different generations such as kyanite, sillimanite, andalusite, and garnet are also present (e.g., Rubenach and Lewthwaite, 2002). The occurrence of such complex mineral paragenesis suggests that the Eastern Fold Belt of the Mt Isa Inlier has undergone more than one discrete phase of metamorphism and deformation.

The Snake Creek Anticline is a regional north-south oriented D_2 structure, north of the Saxby Granite (Fig. 2). The Gilded Rose area, north of the Snake Creek Anticline, is characterized by east-west trending tight to isoclinal folds, of which the Toole Creek Syncline (Fig. 2) is the most pronounced. The area is interpreted to have formed during north-south bulk shortening in D_1 of the Isan orogeny (Loosveld, 1989). Garnet, staurolite, chloritoid and andalusite porphyroblasts have been reported in the Gilded Rose area (Lally, 1997).

The map pattern (Bureau of Mineral Resources, Geology and Geophysics, Australia, 1:100,000 maps, 1983; Loosveld, 1989; Lally, 1997; Rubenach and Barker, 1998) and metamorphic mineral assemblages (Lally, 1997; Rubenach and Lewthwaite, 2002) suggest that the Snake Creek Anticline and Gilded Rose areas are distinct north-south and west- east structural and metamorphic domains in the Eastern Fold Belt, respectively (Fig. 2). If an anticlockwise path is generally accepted for the whole of the Mt Isa Inlier, then these rocks should show mineral textures consistent with this path. However, in this study, new evidence found from the Gilded Rose, Snake Creek Anticline and other parts of the Eastern Fold Belt are inconsistent with the previous interpretations and a new tectonometamorphic evolution has been proposed.

3. Field, micro-structural and textural observations

Two orogenic periods have been recognized in the Eastern Fold Belt based on two near-orthogonal differently directed bulk shortening directions and associated metamorphism (chapters 2 and 3 of this dissertation). The two orogenic periods involved north-south bulk shortening orogenesis (O_1) followed by west-east bulk shortening orogenesis (O_2). In this section, textural evidence is presented that suggests a 'tectonic break' occurred between these two orogenic periods involving crustal scale decompression. Field, microstructural and petrographic observations from the Gilded Rose, Snake Creek Anticline, Tommy Creek Block and southern Selwyn Range (Fig. 1 and 2) are used, as these areas apparently host maximum number of porphyroblast species. Sample numbers with prefix GR stands for (**G**ilded **R**ose), SC (**S**nake **C**reek Anticline), TC (**T**ommy **C**reek Block) and SR (**S**elwyn **R**ange; Fig. 1) and represent specific areas of the Eastern Fold Belt. The microstructures are briefly described in terms of successive foliations and FIAs as they have been defined in detail elsewhere (chapters 2 and 3 of this dissertation). A complete description and methodology for measuring FIAs and their implications for tectonic processes can be found in Bell et al. (e.g., 1998; 2003, 2004).

3.1. Gilded Rose

This area is characterized by west-east trending steeply to moderately dipping macrostructures (Fig. 2; Loosveld, 1989). Garnet, biotite and muscovite porphyroblasts are common, whereas staurolite, chloritoid and andalusite porphyroblasts are uncommon. West-east trending FIAs have been obtained from garnet, chloritoid and andalusite porphyroblasts (Fig. 2; Lally, 1997; chapter 3 of this dissertation). The inclusion trails in garnet and chloritoid porphyroblasts have sigmoidal to spiral patterns and, in most thin sections are truncated by the matrix foliation, particularly in garnet, except for a few rock samples (e.g., GR85; GR390), in which inclusion trails in porphyroblasts are continuous with the matrix foliation.

Sample GR482 contains Cld-Grt-And-Ms-Bt-Qtz (abbreviations after Kretz, 1983). Both garnet and chloritoid are enclosed within andalusite porphyroblasts (Fig. 3ab). The andalusite porphyroblasts overgrew differentiated crenulation cleavages (Fig. 3c) that are continuous with the matrix, whereas the inclusion trails in garnet porphyroblasts are generally truncated. Sample GR3 contains garnet and staurolite porphyroblasts, which commonly lie within large andalusite porphyroblasts (Fig. 3de). The southern part of the Gilded Rose area contains Grt-Bt-Ms schist with abundant garnet porphyroblasts. Sigmoidal or spiral inclusions in garnets are truncated by the matrix foliation (Fig. 3fg). These porphyroblasts contain chlorite-plagioclase and rare biotite inclusions (sample GR192 and GR189; Fig. 3fg). No chlorite occurs in the matrix. It is restricted to garnet cores and/or median zones and can be described by the reaction:

$$\text{Chl+Bt+Pl+Qtz} = \text{Grt+Ms+Qtz}$$

3.2. Snake Creek Anticline

N-S trending FIAs were obtained from most samples containing garnet, staurolite and andalusite porphyroblasts collected from the Snake Creek Anticline. A few samples contain W-E trending FIAs in garnet and staurolite porphyroblasts (Fig. 2; chapter 3 of this dissertation). No FIAs were measurable in cordierite and kyanite porphyroblasts. The cordierite in all the analyzed samples is partially or totally pseudomorphed by quartz, biotite, muscovite and or albite. Kyanite either exists as relics or contains very poorly defined inclusion trails.

At least three generations of staurolite porphyroblasts were found. Sample SC113 (St-Ms-Bt-Qtz schist), collected from the north-western flank of the Snake Creek Anticline, contains staurolite that is about 50% pseudomorphed by muscovite, especially in the median and/or rim region (Fig. 4ab). Where staurolite cores are preserved, the inclusion trails yield a 055^{o} FIA, which correlates with the earliest formed FIA trend in the region (O_1 N-S shortening). Sample SC110 (Grt-St-Ky-Crd-Ged-Qtz-Ab schist) contains staurolite within relic kyanite and relic kyanite plus staurolite in cordierite (Fig.4cde). Even though the matrix of SC110 has been metasomatized (albitized), no albite grains occur within the staurolite, kyanite or garnet porphyroblasts. The significance of this texture is interpreted in section 5.1. Garnet porphyroblasts in this rock have characteristic sigmoidal to spiral shape inclusion trail patterns (Fig. 4f) defining an 025^{o} FIA that has resulted from W-E shortening. The albite grains in the matrix have a sucrose texture and define a weak to moderate foliation (terminology after Twiss and Moores, 1992), suggesting albitization was relatively late in this rock sample. The rock contains late gedrite with albite and quartz inclusions defining a 035^{o} FIA. This correlates with the youngest FIA in the Snake Creek Anticline, because both the albite and quartz inclusion in the gedrite are subparallel and continuous with the matrix. No gedrite has been observed within garnet, cordierite, relic staurolite or kyanite (Fig. 4e). Sample SC490.4 (Crd-St-Bt-Qtz schist) contains relic staurolite in the median and/or rim regions of cordierite (Fig. 4g). Abundant biotite, albite and quartz occur in the matrix of this rock. Figure 5(ab) shows relic staurolite and garnet porphyroblasts within andalusite porphyroblasts (sample SC52.2 – Grt-St-Ky-And-Sill-Bt-Ms schist, sample SC789 St-And-Crd-Bt-Ms schist, provided by Mike Rubenach). In sample SC789, andalusite is rimed by coarse muscovite, whereas relic patches of altered cordierite occurs in the matrix. In some samples, garnet and staurolite porphyroblasts, partially pseudomorphed by muscovite, are preserved within andalusite porphyroblasts (Sample SC-3 provided by Mike Rubenach). Based on these textural relationships, relic staurolite porphyroblasts in all the above mentioned samples from the Snake Creek Anticline are classified as first generation.

Second generation staurolite contains 110^{o} trending FIAs in their core-median regions (e.g., sample SC108 – Grt-St-Bt-Ms-Chl-Qtz schist). The rims of these porphyroblasts are either partially pseudomorphed or occur as remnants. Sample SC112 (Grt-St-Bt-Ms-Crd-Qtz schist), collected from the same location as sample SC113 (~about 10m apart) consists of fresh staurolite with quartz inclusion trails defining a subhorizontal foliation that is continuous with the subvertical matrix foliation (Fig. 5c) and yielded a 015^{o} FIA that formed during W-E shortening (chapter 3 of this dissertation). Staurolite locally contains garnet porphyroblasts with N-S trending FIA and pseudomorphed cordierite (Fig. 5c). Staurolite with these textures and FIA orientations defines a third generation of growth.

Three generations of andalusite porphyroblasts were found. Sample SC103 (And-Grt-Ms-Bt-Qtz schist) contains andalusite porphyroblasts with 115^{o} trending FIA and in all 13 vertical oriented thin sections the inclusion trails are truncated by the matrix foliation (Fig. 5d). No cordierite has been found in these andalusite porphyroblasts. Garnet contains 075^{o} trending FIAs in the same rock. Samples SC27 (And-Crd-Grt-Bt-

Ms-Qtz) and SC104 (And-Crd-Grt-Bt-Ms-Qtz) contain andalusite within pseudomorphed cordierite (Fig.5e). In Sample SC52.2 (Grt-St-And-Ky-Sill-Crd-Ms-Bt-Qtz schist), kyanite and sillimanite are replaced by andalusite (Fig. 5f). Muscovite in this sample occurs as relic patches, especially close to albitized grains. No FIAs were determined for SC52.2 because of the limited number of thin sections available and poor inclusion trail patterns preserved within the porphyroblasts. Second generation andalusite yielded N-S FIAs ((e.g., sample SC741 (And-Crd-Bt-Ms-Qtz), SC26 (And Crd-Grt-Ms-Bt-Qtz) and SC29 (And-Crd-Ms-Bt-Qtz)) defined by inclusion trails that are continuous with the matrix foliations. These porphyroblasts contain pseudomorphed cordierite (Fig. 6a). Third generation andalusite occurs as local overgrowths and contains inclusions that are always parallel and continuous with the matrix foliation (Fig. 6b).

Rubenach and Lewthwaite (2002) found two generations of staurolite. Some preserves bedding S_0 as inclusion trails (fig. 6c in Rubenach and Lewthwaite, 2002). They collected this sample near the cordierite/ablitite locality (their area 4) and they interpreted that staurolite growth occurred prior to syn-S_3 albitization (their D_3 = O_2 of this study, see below), as they had not found any albite within first generation staurolite. They also published a microphotograph (fig. 7 in Rubenach and Lewthwaite, 2002), where andalusite replaces early staurolite. In another example (fig. 6a of Rubenach and Lewthwaite, 2002) they show cordierite hosting S_2, rather than S_1 or S_0, whereas staurolite at the margin of the cordierite contains S_3, which is continuous with the matrix. Cordierite occurs as relict or pseudomorphed by mica. This means that cordierite overgrew S_2 and second generation staurolite overgrew S_3 as interpreted by Rubenach and Lewthwaite (2002). They argued early to syn-D_3 (their D_3= regional D_2 = O_2 of this study) cordierite growth. The staurolite textures reported by Rubenach and Lewthwaite are similar in character to those described in samples SC113, SC110, SC108 (W-E FIA O_1) and SC112 (N-S FIA O_2), discussed above. Furthermore, the cordierite localities are parallel to the axes of the Snake Creek Anticline and albitite vein swarms (Fig. 3; Rubenach and Lewthwaite, 2002). This suggests that the cordierite growth occurred at the onset of west-east shortening (O_2) after north-south (O_1) and this point will be discussed in detail below as it links to decompression phenomena between O_1 and O_2, which have never been previously proposed for any part of the Mt Isa Inlier.

3.3. Tommy Creek Block

Most of the samples from the Tommy Creek Block yield N-S FIA from garnet porphyroblasts (chapter 3 of this dissertation; Lally, 1997). These rocks* are generally Grt-Bt-Ms-Qtz schists except for samples TC508, TC1365and TC1365i (Grt-St-And-Bt-Ms schist). Sample TC508 contains W-E trending FIAs in garnet porphyroblasts. Staurolite remains are enclosed within garnet porphyroblasts and both garnet and staurolite are enclosed within large andalusite porphyroblasts (Fig. 6c). TC1365 and TC1365i contain two generations of garnet and staurolite porphyroblasts. Relic staurolite grains, partially pseudomorphed by coarse muscovite, and relic garnet, with biotite reaction rims, are enclosed in large andalusite porphyroblasts (Fig. 6de). Second generation staurolite and garnet porphyroblasts, with no sings of any reaction rims, contain inclusions trails that are continuous with the matrix foliation (Fig. 7a). N-S FIAs have been obtained from second generation garnet and staurolite porphyroblasts (Fig. 7a; see chapter 3; Lally, 1997).

3.4. Selwyn Region

Because of the limited number of thin sections available, FIAs have only been measured in two rocks (sample SR8.1, SR8.2). Both yield N-S trending FIA within staurolite porphyroblasts. Two distinct generations of garnet porphyroblasts have been observed. First generation garnets have reaction rims of biotite, muscovite or chlorite and rarely cordierite (Fig. 7bc; sample SR14). Second generation garnets have no reaction rims and their inclusions are continuous with the matrix (Fig. 7de; sample SR134B). The textures are similar to those described above.

4. P-T pseudosections

To obtain P-T information, P-T pseudosections, or maps of the stable mineral assemblages in P-T-x space from selected rock samples were constructed using bulk XRF analyses of each sample (Table-1). Calculations were carried out using THERMOCALC-v. 3.21 (Powell and Holland, 1988; Holland and Powell, 1998; Powell et al., 1998). All the P-T pseudosections have been constructed in the chemical system MnO-Na_2O-CaO-K_2O-FeO-MgO-Al_2O_3-SiO_2-H_2O (MnNCKFMASH). The pseudosections were contoured for X_{Fe}, X_{Mn} and X_{Ca} isopleths in garnet with respect to increasing pressure and temperature to provide a means for determining P-T points for the start of garnet growth that can be tested by microprobe point analysis (Microprobe conditions, see Appendix – D). These three compositional isopleths should intersect at a single pressure and temperature for the onset of garnet growth (Vance and Mahar, 1998) and diverge as growth continues due to the fractionation of garnet with respect to evolving bulk rock composition (Evans, 2004). Estimates of the P-T conditions of equilibration between garnet inner-rim and matrix mineral phases were made using average P-T mode in

THERMOCALC-3.21 (Powell and Holland, 1994; Powell et al., 1998). P-T estimates for the median and far median region of the garnets were calculated using the newly developed intersection of isopleths technique that calculates the P-T conditions using the intersection of X_{Mn}, X_{Fe}, X_{Ca} isopleths of garnet porphyroblasts at any point between garnet core and rim (Evans, 2004). The method follows the principles of Rayleigh fractionation equation of mineral growth with effective bulk rock composition.

4.1. Selected samples with FIA present, bulk rock and mineral chemistry

Textural relationships and mineral chemistry shows that the rocks were not affected by albitization (Table-1; see below). Samples GR189, GR192 and GR76 (Grt-Bt-Ms-Qtz schist) from the Gilded Rose area, contain W-E trending FIAs within garnet porphyroblasts. The porphyroblasts range in size from 2-4mm in GR192 and 4-8mm in GR189 and contain abundant plagioclase and chlorite inclusions and rare biotite (Fig. 3fg). Plagioclase is present throughout the garnet cores and in the matrix. However, most plagioclase grains are altered and, therefore, only limited probe data was obtained (Table-2, 3). Chlorite inclusions are only preserved within garnet cores and median zones, and this will be considered in terms of pseudosection topology in the next section. Garnet porphyroblasts in sample GR76 range in size from 1 to 2mm. Even though they are small in size, they have relatively high Ca(wt%) and Mn(wt%) contents in the core (Table – 4). All three samples contain garnet that is zoned in its major element chemistry, especially in Mn, which decreases monotonically from core to rim of garnet porphyroblasts except for very short reversals in the outer rim (Fig. 8, 10, 11; Table 2, 3, 4). Compositional maps for the garnet porphyroblasts under investigation are shown in Figs. 8, 10, 11. Sample SC118 (Grt-And-Ms-Bt-Qtz schist) comes from the northeastern limb of the

Snake Creek Anticline. This sample contains garnet in the matrix as well as tiny garnets (≤1mm) within andalusite porphyroblasts preserving west-east FIAs. This sample was modeled to determine the P-T conditions of the core of the latter tiny garnets (Fig. 12). Table-5 shows representative analyses for garnet and andalusite porphyroblasts.

SC112 (Grt-St-Crd-Ms-Bt-Qtz schist) from the western flank of the Snake Creek Anticline with garnets and staurolite preserved N-S FIAs. Inclusion trails within garnet and staurolite porphyroblasts are continuous with the matrix foliation. Locally, pseudomorphed cordierite and fresh garnets are preserved in staurolite. Garnet ranges in size from 1-3mm, pseudomorphed cordierite (by mica) from 2-3mm and staurolite from 4-9mm. No plagioclase was found in the garnet porphyroblasts. A few plagioclase grains aligned parallel to the matrix foliations were probed (Table-6). The garnet, under investigation, is strongly and regularly zoned (Fig. 13) and, unlike those containing W-E trending FIAs, does not have reversals in the rim. In sample TC186 (Grt-Bt-Ms-Qtz schist), from the Tommy Creek Block, garnet ranges in size from 2-4mm and contains N-S trending FIAs. Scarce and partially altered plagioclase grains are aligned parallel to the matrix foliation (Table-7; Fig. 14).

4.2. Results

Chlorite, plagioclase and biotite inclusions occur in the core and median region of the garnet porphyroblasts in samples GR192 and GRC189. The lack of chlorite in the matrix is predicted by the pseudosections because the X_{Mn}, X_{Fe} and X_{Ca} compositional isopleths for the garnet core intersect uniquely in the Chl-Bt-Pl-Grt stability field (Fig. 8, 10). Garnet inner-rim, matrix plagioclase rim, biotite and muscovite geothermobarometric estimates, using the average P-T feature of THERMOCALC-3.21, lie within the Grt-Pl-Bt field (Fig. 8, 10). Figure 8 and 10 also shows an EDS microprobe traverse on X_{Mn} map from garnet core to rim (see also Tables 2, 3).

In sample GR192, the garnet core is estimated to have grown at 5.6-5.9 kb/526-528 ^{o}C, whereas the inner-rim with matrix phases grew at 6.5±1.1 kb/602±27 ^{o}C. Most of the plagioclase inclusions are altered and biotite inclusions are rare. The P-T estimates between garnet core and rim region were calculated using the intersection isopleths technique (Evans, 2004), which allows for fractionation of the bulk composition (Figs. 8, 9; Evans, 2004). Points '2' and '3' at the median and far median region of the garnet porphyroblast, respectively, have tight compositional (X_{Mn}, X_{Fe} and X_{Ca}) isopleths intersections with respect to effective bulk rock composition (Fig. 9). These two points in the median region give additional P-T estimates and a degree of confidence for the construction of a path between the garnet core and inner-rim region.

For sample GR189, garnet core growth is estimated to have occurred at 4.4-4.6 kb/527-529 ^{o}C, whereas the rim grew at 5.5±1.2 kb/581±26 ^{o}C (Fig. 10). P-T constraints at points '2' and '3' in Fig. 10 were obtained from the median and far-median region of the garnet porphyroblast without using the fractionation technique. This was possible because of the very slight compositional change of the median region (see also Evans, 2004). The core of the GR76 lies close to the garnet-in line at 4.2-4.4 kb/510-513 ^{o}C, whereas rim growth occurred at 4.8-5.2 kb/523-527 ^{o}C (Fig. 11). These are the highest pressure estimates so far reported from any part of the Eastern Fold Belt of the Mt Isa Inlier.

The garnet core in sample SC118 grew at 3.9-4.3 kb/540-544 ^{o}C (Fig. 12) and is preserved within an andalusite porphyroblast. The andalusite-in line in the pseudosection lies below garnet core growth, suggesting that garnet grew at a relatively higher pressure. The garnet core compositional isopleths in samples SC112 intersect at 3.7-3.9 kb/548-550 ^{o}C (Fig. 13). The garnet rim plus matrix mineral phases give 4.8±1.3 kb/592±32 ^{o}C in the Grt-St-Pl-Bt field, in agreement with the textural relationships where garnet is partially preserved within staurolite (Fig. 13). Pseudomorphed cordierite is also preserved within fresh staurolite, which formed relatively higher pressures than cordierite (Fig. 5c; see also Pattison et al., 1999). Such relationships give additional P-T path constraints via the pseudosection topology (Fig. 13). The slope of the Crd and aluminosilicate line is controversial, as some authors suggest it is positive (Dymoke and Sandiford, 1992), whereas others argue that it is low angle negative (Pattison et al., 1999; 2002). However, this does not affect the shape of the path from low pressure to higher pressure as predicted by the pseudosection topology. For sample TC186, the garnet core is calculated at 2.1-2.2 kb/510-515 ^{o}C, whereas the rim plus matrix phases have estimated at 4.8±1.1 kb/600±29 ^{o}C in the Grt-Pl-Bt field (Fig 14).

5. Interpretations

5.1. Textural relationships, timing of porphyroblast growth and reactions

Pattison et al., (1999) argued that the metamorphic mineral assemblage Crd-St-Bt-Ms±And is a product of polymetamorphism and that the textures preserved in such rocks are useful indicators of P-T paths and tectonothermal processes. They suggested that the only way to produce this assemblage that satisfies the timing of mineral growth is to have an earlier higher pressure staurolite-bearing assemblage overprinted by a lower pressure cordierite-bearing ones. Staurolite persists metastably as relics or pseudomorphed by coarse muscovite or as inclusions within andalusite (see also Garcia-Casco and Torres-Roldan, 1996, 1999). A path involving the overprinting of a low pressure cordierite-bearing mineral assemblage by a high pressure staurolite-bearing mineral assemblage could also produce Crd-St-Bt-Ms±And, but the timing of the mineral growth would be the opposite to that observed and cordierite would be partially or totally replaced by mica.

This is shown by the following polymetamorphic reactions. Rocks from the staurolite zone that decompress would pass first through the reaction:

$$Ms+St+Qtz = And+Bt+H_2O \ \ldots\ldots\ldots\ldots\ldots\ (1)$$

yielding andalusite after staurolite, and then pass through the reaction:

$$And+Bt+Qtz+ H_2O=Ms+Crd \ \ldots\ldots\ldots\ldots\ldots\ (2)$$

yielding cordierite after andalusite.

The decompression reaction without cordierite involves:

$$St+Ms+Qtz = Bt+Grt+And+H2O\ldots\ldots\ldots\ (3)$$

Textural relationships indicate, across the Eastern Fold Belt, that medium-pressure assemblages preceded low-pressure metamorphic conditions. Staurolite and garnet are preserved as inclusions within andalusite, in general across the Eastern Fold Belt, and/or kyanite and staurolite in cordierite/andalusite in the Snake Creek Anticline, in particular. The presence of the three aluminosilicates in sample SC52.2 (Fig. 5f) is interpreted to be the consequence of metastable persistence and sequential growth during decompression (see Torres-Roldan, 1981; Garcia-Casco and Torres-Roldan, 1996; Williams and Karlstrom, 1996) rather than an indication of metamorphic conditions close to the triple point (Rubenach and Lewthwaite, 2002).

Sample SC110 can be used to time the albitization with respect to the polymetamorphism. The rock is NaFMASH, geochemical and mass-balance calculations indicate that the formation of albitites (Na^+ gain and K^+/Ca^{2+} loss) required removal of K and addition of Na (e.g., Mark, 1998; Mark and Foster, 2001). Mark (1998) and Mark et al. (2004) argued for a regional Na-Ca input related to the granitiods of the Williams and Naraku Batholiths (*ca*. 1550-1500Ma) in the Eastern Fold Belt. SC110 contains relic kyanite and staurolite preserved within cordierite plus garnet porphyroblasts with a 025^o trending FIA (see also section C of this thesis). Detailed examination of more than 15 oriented thin sections from this sample revealed no albite or gedrite grains in relic kyanite, staurolite or cordierite porphyroblasts (Fig. 4cde). The albite grains have replaced most of the matrix phases and define a moderate to weak foliation. Garnet preserves an 025^o trending FIA with or without albite. Gedrite preserves an 035^o trending FIA with albite. This suggests albitization occurred between development of the 025^o and 035^{o}FIAs in this rock. This textural relationship supports the timing suggested by the north-south oriented albitization front along the axis of the Snake Creek Anticline, north of the Saxby granite (part of the Williams and Naraku Batholiths; Fig. 2) and further supports the Mark (1998) and Mark and Foster (2001) Na-Ca albitization model related to the emplacement of Williams and Naraku Batholiths. However, they proposed several overlapping episodes of Na-Ca metasomatism synchronous with prolonged Williams and Naraku event (*ca*. 1550-1500Ma) during west-east shortening.

At least two separate generations of staurolite have formed with respect to the FIAs and/or staurolite before and after cordierite growth. Two distinct generations of garnet have also been distinguished. These are those with reaction rims or preserved in andalusite and those without reaction rims that host inclusions that are continuous with the matrix. These separate generation of garnet porphyroblasts are further defined by W-E (with or without reaction rims, see below) and N-S FIA trends (see also section C of this thesis). Two distinct generations of andalusite, namely those containing west-east FIAs and/or that have replaced kyanite and those with north-south FIAs preserving inclusion trails that are continuous with the matrix and hosting pseudomorphed cordierite. All these textures indicate near-isothermal decompression from early medium-pressure metamorphism through staurolite to andalusite with or without cordierite production (e.g., Pattison, 1999) related to O_1. Based on these textures, the P-T path for the Snake Creek Anticline, in particular, and for the Eastern Fold Belt, in general, involved early medium-pressure metamorphism in response to crustal thickening, which accounted for the first metamorphic cycle followed by decompression (O_1 – orogenic period). This was followed by a counterclockwise path, from low- to medium-pressure during O_2, with conditions at low-pressure metamorphism during emplacement of the Williams and Naraku Batholiths.

5.2. P-T pseudosections

Samples preserving garnet with W-E FIAs (GR76, GR192, GR189, SC118) have relatively higher-pressure/low-temperature cores than those preserving N-S FIAs (Sample TC186, SC112). Compositional isopleths from garnet cores hosting W-E FIAs intersect in the Chl-Bt-Pl-Grt field, in agreement with the chlorite, plagioclase and rare biotite inclusions observed in samples SC192 and SC189. They formed during N-S shortening and represent part of the early medium-pressure Barrovian clockwise P-T path. Short Mn reversals at the rim of these garnets (GR192, GR189) or local overgrowths (GR76), as indicated by their zoning patterns is considered to be the result of reequilibration during decompression (e.g., Florence et al., 1993).

Garnet in sample SC118 preserved within andalusite formed above the andalusite-in line in the pseudosection, suggesting garnet grew at relatively higher pressure. The garnet porphyroblasts are small (<1mm) and host W-E FIAs, suggesting garnet growth occurred during decompression related to the waning stages of O_1 orogenesis prior to late andalusite growth. Clusters of tiny garnet porphyroblasts preserved within andalusite are a characteristic texture of the Betic Belt, southern Spain, and were produced during decompression (Garacia-Casco and Torres-Roldan, 1996). Garnet cores preserving N-S FIA sets formed under LP/HT conditions during W-E shortening (sample SC112; TC186) and formed part of P-T path proposed for O_2 orogenesis. Thus, sample SC112 preserved pseudomorphed cordierite followed by garnet and staurolite and samples SC26 and SC29 host pseudomorphed cordierite within andalusite followed by garnet and sillimanite in the matrix, typical of Buchan-style metamorphism.

6. Discussion - looping P-T paths and tectonic significance

Standard theoretical and experimental thermal models (e.g., England and Thompson, 1984*ab*), numerical simulations (e.g., Schulmann et al., 2002), and petrological constraints (e.g., Garcia-Casco and Torres-Roldan, 1996; Pattison, 1999) suggest LP/HT metamorphic conditions require an early high-pressure regime followed by decompression and/or crustal attenuation. Pattison et al. (1999) suggested for most of the polymetamorphosed terrains that staurolite (higher pressure) is typically early texturally, and cordierite (low pressure) is late, separated by a significant period of cooling and decompression. In the case of the Eastern Fold Belt of the Mt Isa Inlier, Reinhardt (1992) assumed initial higher-pressure metamorphism for D_1 in response to crustal thickening up to greenschist facies followed by isostatic rebound that produced LP/HT conditions. This assumption received no attention for later workers. This study supports the Reinhardt (1992) hypothesis with data indicating that O_1 was responsible for at least medium-pressure middle-amphibolite facies metamorphism with multiple W-E oriented fabrics followed by decompression. Hence, a thermally weakened crust existed at the onset of O_2. During the second period of metamorphism that accompanied O_2, W-E directed shortening was responsible for recrystallization and/ or obliteration of the early medium-pressure mineral phases formed in the matrix during O_1. Decompression late in O_1 potentially obscured some of the early medium-pressure assemblages as well (e.g., Gracia-Casco and Torres-Roldan, 1999). The extent of replacement and/or obliteration of early medium-pressure mineral assemblages depends on a number of factors such as the relative P-T drop and the magnitude of decompression from one area to another, the bulk composition of the rocks and the H_2O activity (Pattison et al., 1999). At low pressures, cordierite growth would only be expected in rocks with a lower Fe/(Fe+Mg) ratio, that is an Mg-rich composition that could produce cordierite-bearing assemblages. An Fe-rich assemblage develops staurolite, but on decompression never reaches the cordierite stability field, because it too Fe-rich (Pattison et al., 1999). A rock with an appropriate Mg/Fe ratio can produce St+Bt at higher pressure and then And+Bt upon decompression. Further decompression can produced Crd+And+Bt giving rise to Ms+St+And+Crd+Bt assemblages (St will exist as relics).

From field evidence and textural relationships, it is obvious that most cordierite localities occur along the axis of the Snake Creek Anticline, north of the Saxby Granite (see fig. 1 of Rubenach and Lewthwaite). This is interpreted to be the result of the albitization front associated with the Saxby Granite, intruded during O_2, which increases the temperature and decreases the pressure (see Mark, 1998). This interpretation appears to be consistent with areas like the Gilded Rose, Tommy Creek Block and the Selwyn Range where decompression occurred to andalusite with no cordierite. The textures reported in this study indicate a P-T path involving sequential growth during O_1 of staurolite, kyanite and garnet before andalusite, with or without cordierite. In most of the samples from the Snake Creek Anticline, cordierite has been replaced by albite, muscovite, biotite and quartz. This is interpreted to result from the second metamorphic period during O_2 (see also Rubenach and Lewthwaite, 2002).

The evidence for O_1 metamorphism followed by decompression consists of (1) early medium-pressure/low-temperature garnet cores preserving W-E FIAs modeled in MnNCKFMASH pseudosections, (2) chlorite, biotite, and plagioclase inclusions preserved within these medium-pressure core garnets indicating prograde metamorphic conditions (Barrovian-type) suggesting crustal thickening, (3) relic staurolite partially pseudomorphed by muscovite and replaced by late andalusite/cordierite (4) earlier growth of staurolite than cordierite (5) andalusite and relic kyanite within cordierite, (6) relic staurolite (O_1 FIA) before cordierite growth, and pseudomorphed cordierite before fresh staurolite (O_2 FIA) and (7) the presence of pre-D_2 W-E oriented (Bell, 1983; Reinhardt, 1992) relic thrust stacks and associated doubly north-south plunging mineral stretching lineation L^1_1 (Bell et al., 1992), which were responsible for the initial higher pressure metamorphism.

Based on these textural observations and pseudosection results, the P-T path and the timing of the different deformation and metasomatic events in the Eastern Fold Belt, using the topology of Pattison et al., (1999), can be resolved into seven steps (Fig. 15). These are characterized by:

(1) N-S shortening (O_1) resulting in medium-pressure in the kyanite stability field as indicated by relic kyanite + staurolite as inclusions in andalusite and chlorite + biotite + plagioclase inclusions in relatively higher pressure, low temperature garnet cores hosting W-E FIAs,

(2) Near-isothermal decompression from kyanite to andalusite via staurolite with cooling starting at intermediate to low pressure,

(3) Intrusion of the Williams-Naraku granite (1550-1500Ma) with a decrease in pressure and increase in temperature with or without the production of cordierite,

(5) Spatial and temporal association of regional albitization with the Williams and Naraku Batholiths (e.g., Mark, 1998; Rubenach and Lewthwaite, 2002),

(6) W-E shortening (O_2) where cordierite was replaced by andalusite followed by new growth of garnet, staurolite and sillimanite in the matrix (Rubenach and Lewthwaite, 2002),

(7) Post O_2 thermal relaxation as indicated by randomly oriented chlorite in the matrix.

* *Sample AGSO-69200153 (Ky-And-Grt-Ms-Bt schist) is omitted in this study, provided by Australian Geological Survey to Lally (1997), because there is no sample location documented.*

References

Bell, T. H., 1983. Thrusting and duplex formation at Mount Isa, Queensland, Australia. Nature 304, 493-497.

Bell, T. H., Reinhardt, J., Hammond, R. L., 1992. Multiple foliation development during thrusting and synchronous formation of vertical shear zones. Journal of Structural Geology 14, 791-805.

Bell, T. H., Hickey, K. A., 1998. Multiple deformations with successive subvertical and subhorizontal axial planes in the Mount Isa Region: their impact on geometric development and significance for mineralization and exploration. Economic Geology 93, 1369-1389.

Bell., T. H., Hickey, K. A. and Upton, J. G., 1998. Distinguishing and correlating multiple phases of metamorphism across a multiply region using the axes of spiral, staircase and sigmoidal inclusion trails in garnet. Journal of Metamorphic Geology 16, 767-794.

Bell, T. H., Ham, A. P., Hickey, K. A., 2003. Early formed regional antiforms and synforms that fold younger matrix schistosities: their effect on sites of mineral growth. Tectonophysics 367, 253-278.

Bell, T. H., Kim, H. S., 2004. Preservation of Acadian deformation and metamorphism through intense Alleghanian shearing. Journal of Structural Geology 26, 1591-1613.

Bell, T. H., Ham, A. P., Kim, H. S., 2004. Partitioning of deformation along an orogen and its effects on porphyroblast growth during orogenesis. Journal of Structural Geology26, 825-845.

Betts, P. G., Giles, D., Lister, G. S., 2004. Aeromagnetic patterns of half-graben and basin inversion: implications for sediment-hosted massive sulfide Pb-Zn-Ag exploration. Journal of Structural Geology 26, 1137-1156.

Blake, D. H., 1987. Geology of the Mount Isa Inlier and environs, Queensland and Northern Territory. Bureau of Mineral Resources, Geology and Geophysics Bulletin 225, 1-83.

Boger, S. D., Hansen, D., 2004. Metamorphic evolution of the Georgetown Inlier, NE Queensland, Australia; evidence for an accreted Palaeoproterozoic terrane? Journal of Metamorphic Geology 22, 511-527.

Carter, E. K., Brooks, J. H. and Walker, K. R., 1961. The Precambrian mineral belt of north-western Queensland. BMR, Geology and Geophysics Australia, Bulletin 61.

Collins, W. J., Vernon, R. H., 1991. Orogeny associated with anticlockwise, P-T-t paths: evidence form low-P, high-T metamorphic terrains in the Arunta Inlier, central Australia. Geology 19, 835-838.

Daly, S. J., Fanning, C. M., Fairclough, M. C., 1998. Tectonic evolution and exploration potential of the Gawler craton, South Australia. AGSO Journal of Australian Geology and Geophysics 17, 145-168.

Dymoke, P. and Sandiford, M., 1992. Phase relations in Buchan facies series pelitic assemblages: calculations with applications to andalusite-staurolite parageneses in the Mount Lofty Ranges, South Australia. Contributions to Mineralogy and Petrology 110, 121-132.

England, P. C., Thompson, A. B., 1984a. Pressure-Temperature-Time paths of regional metamorphism I. Heat transfer during the evolution of regions of thickened continental crust. Journal of Petrology 25, 894-928.

England, P. C., Thompson, A. B., 1984b. Pressure-Temperature-Time paths of regional metamorphism II. Their inference and interpretation using mineral assemblages in metamorphic rocks. Journal of Petrology 25, 929-955.

Evans, T. P., 2004. A method for calculating effective bulk composition modification due to crystal fractionation in garnet-bearing schist: implications for isopleth thermobarometry. Journal of Metamorphic Geology. Journal of Metamorphic Geology 22, 547-557.

Florence, F. P., Spear, F. S., and Kohn, M. J., 1993. P-T paths from northwestern New Hampshire: metamorphic evidence for stacking in a thrust/nappe complex. American Journal of Science 293, 939-979.

Garcia-Casco, A., Torres-Roldan, R. L., 1996. Disequilibrium induced by fast decompression in St-Bt-Grt-Ky-Sill-And metapelites from the Betic Belt (southern Spain). Journal of Petrology 37, 1207-1239.

Garcia-Casco, A., Torres-Roldan, R. L., 1999. Natural metastable reactions involving garnet, staurolite and cordierite: implications for petrogenetic grids and the extensional collapse of the Betic-Rif Belt. Contributions to Mineralogy Petrology 136, 131-153.

Gascombe, B., 1991. Intense non-coaxial shear and the development of mega-scale sheath folds in the Arunta Block, central Australia. Journal of Structural Geology 13, 299-318.

Grambling, J. A., 1986. Crustal thickening during Proterozoic metamorphism and deformation in New Mexico. Geology 14, 149-152.

Grambling, J. A., and Dallmeyer, R. D., 1993. Tectonic evolution of Proterozoic rocks in the Cimarron Mountains, northern New Mexico, USA: Journal of Metamorphic Geology 11, 739-755.

Grambling, J. A., Williams M. L., Smith, R. F., Mawer, C. K. 1989. The role of crustal extension in the metamorphism of Proterozoic rocks in northern New Mexico. Grambling, J. A., Tewksbury, B. J. (editors). Proterozoic geology of the southern Rocky Mountains. Geological Society of America Special Paper 235, 87-110.

Hand, M., Dirks, P. H. G. M., Powell, R., and Buick, I. S., 1992. How well established is isobaric cooling in Proterozoic orogenic belts? An example from the Arunta inlier, central Australia. Geology 20, 649-652.

Hand, M., Rubatto, D., 2002. The scale of the thermal problem in the Mt Isa Inlier. 2002. Preiss,V. P. (editor). Geoscience 2002: Expanding Horizons. Abstracts of the 16th Australian Geological Convention, Adelaide Convention Centre, Adelaide, SA, Australia 67, 173.

Hobbs, B. E., Archibald, N. J, Etheridge, M. A., Wall, V.J., 1984. Tectonic history of the Broken Hill Block, Australia. In: Kroner, A., Greiling, R. (Eds.), Precambrian Tectonics Illustrated, pp. 353-368.

Holland, T. J. B., Powell, R., 1998. An internally consistent thermodynamic data set of petrological interest. Journal of Metamorphic Geology 16, 309-343.

Holdaway, M. J., 1971. Stability of andalusite and the aluminum silicate phase diagram. American Journal of Science 271, 97-131.

Ilg, B. R., Karlstrom, K. E., 2000. Porphyroblast inclusion trail geometries in the Grand Canyon: evidence for non-rotation and rotation? Journal of structural Geology 22, 231-243.

Johnson, S. E., Vernon, R. H., 1995. Stepping stones and pitfalls in the determination of an anticlockwise P-T-t-deformation path: the low-P, high-T Cooma Complex, Australia. Journal of metamorphic Geology 13, 165-183.

Karlstrom, K. E., Ahall, Karl-Inge., Harlan, S. S., Williams, M. L., McLelland, J., Geissman, J. W., 2001. Long-lived (1.8 - 1.0Ga) convergent orogen in southern Laurentia, its extensions to Australia and Baltica, and implications for refining Rodinia. Precambrian Research 111, 5-30.

Kim, H. S., Bell, T. H., *in press*. Combining compositional zoning and foliation intersection axes (FIAs) in garnet to quantitatively determined early P-T-t paths in multiply deformed and metamorphosed schists: north-central Massachusetts, USA. Contributions to Mineralogy and Petrology.

Kretz, R., 1983. Symbols for rock-forming minerals. American Mineralogist 68, 277-279.

Lally, J. H., 1997. The structural history of the central Eastern Fold Belt, Mount Isa Inlier, Northwest Queensland, Australia. Unpublished Ph.D. thesis, 1-103.

Loosveld, R. J. H., 1989. The synchronism of crustal thickening and high T/low P metamorphism in the Mount Isa Inlier, Australia 1. An example, the central Soldiers Cap belt. Tectonophysics 158, 173-190.

Loosveld, R. J. H., Etheridge, M. A., 1990. A model for low-pressure facies metamorphism during crustal thickening. Journal of metamorphic Geology 8, 257-267.

Mark, G., 1998. Albitite formation by selective pervasive sodic alteration of tonalite plutons in the Cloncurry district, Queensland. Australian Journal of Earth Sciences 45, 765-774.

Mark, G., Foster, D. R. W., 2000. Magmatic-hydrothermal albite-actinolite-apatite-rich rocks from the Cloncurry district, NW Queensland, Australia. Lithos 21, 223-245.

Mark, G., Foster, D. R. W., Pollard, P. J., Williams, P. J., Tolman, J., Darvall, M., Black, K. L., 2004. Stable isotope evidence for magmatic fluid input during large-scale Na-Ca alteration in the Cloncurry Fe oxide Cu-Au district, NW Queensland, Australia. Terra Nova 16, 54-61.

Marshall, J. L., Oliver, N. H. S., 2001. Mechanical controls on fluid flow and brecciation in the regional host rocks for Eastern Fold Belt ironstone Cu-Au deposits, Mt Isa Block. Geological Society of Australia, Specialist Group in Economic Geology “Mineralisation, alteration and magmatism in the Eastern Fold Belt, Mount Isa Block Australia: Geological Review and Field Guide”, Special Publication No 5, 30 -45.

Oliver, N. H. S., Holcombe, R. J., Hill, E. J., Pearson, P. J., 1991. Tectono-metamorphic evolution of the Mary Kathleen Fold Belt, northwest Queensland: A reflection of mantle plume processes? Australian Journal of Earth Sciences 38, 425-455.

Oliver, N. H. S., Rubenach, M. J., Valenta, R. K., 1998. Precambrian metamorphism, fluid flow, and metallogeny of Australia. Journal of Australian Geology and Geophysics 17, 31-53.

Page, R. W., Bell, T. H., 1986. Isotopic and structural responses of granite to successive deformation and metamorphism. Journal of Geology 94, 365-379.

Page and MacCready, 1997. Rocks of Mount Isa Group age in the Eastern Fold Belt. AGSO Research Newsletter 26, 16-17.

Page, R. W., Sun, S-S., 1998. Aspects of geochronology and crustal evolution in the Eastern Fold Belt, Mt Isa Inlier. Australian Journal of Earth Sciences 45, 343-361.

Pattison, D. R. M., 1992. Stability of andalusite and sillimanite and the Al_2SiO_5 triple point: Constraints from the Ballachulish aureole, Scotland. Journal of Geology 100, 423-446.

Pattison, D. R. M., Spear, F. S., Cheney, J. T., 1999. Polymetamorphic origin of muscovite+cordierite+staurolite+biotite assemblages: implications for the metapelitic petrogenetic grid and for P-T paths. Journal of metamorphic Geology 17, 685-703.

Pattison, D. R. M., Spear, F. S., Debuhr, C. L., Cheney, J. T., Guidotti, C. V., 2002. Thermodynamic modeling of the reaction muscovite+cordierite = Al_2SiO_5+biotite+quartz+H_2O: constraints from natural assemblages and implications for the metapelitic petrogenetic grid. Journal of Metamorphic Geology 20, 99-118.

Powell, R., Holland, T. J. B., 1988. An internally consistent thermodynamic dataset with uncertainties and correlations:3. Application methods, worked examples and a computer program. Journal of metamorphic Geology 6, 173-204.

Powell, R., Holland, T., 1994. Optimal geothermometry and geobarometry. American Mineralogist 79, 120-133.

Powell, R., Holland, T., Worley, B., 1998. Calculating phase diagrams involving solid solutions via non-linear equation, with examples using THERMOCALC. Journal of Metamorphic Geology 16, 577-588.

Reinhardt, J., 1992. Low-pressure, high-temperature metamorphism in a compressional tectonic setting: Mary Kathleen Fold Belt, northeastern Australia. Geological Magazine 129, 41-57.

Rubenach, M. J., 1992. Proterozoic low-pressure/high temperature metamorphism and an anticlockwise P-T-t path for the Hazeldene area, Mount Isa Inlier, Queensland, Australia. Journal of Metamorphic Geology 10, 333-346.

Rubenach, M. J., Barker, A. J., 1998. Metamorphic and metasomatic evolution of the Snake Creek Anticline, Eastern Succession, Mt Isa Inlier. Australian Journal of Earth Sciences 45, 363-372.

Rubenach, M. J., Lewthwaite, K. A., 2002. Metasomatic albitites and related biotite-rich schists from a low-pressure polymetamorphic terrane, Snake Creek Anticline, Mount Isa Inlier, north-eastern Australia: microstructures and P-T-d paths. Journal of Metamorphic Geology 20, 191-202.

Sandiford, M., Powell, R., 1991. Some remarks on high-temperature - low-pressure metamorphism in convergent orogens. Journal of metamorphic Geology 9, 333-340.

Schulmann, K., Schaltegger U., Jezek, J., Thompson, A. B., Edel J-B., 2002. Rapid burial and exhumation during orogeny: thickening and synconvergent exhumation of thermally weakened and thinned curst (Variscan Orogen in Western Europe). American Journal of Science 302, 856-879.

Spear, F. S., Kohn, M. J., Florence, F. P., and Menard, T., 1991. A model for garnet and plagioclase growth in pelitic schists: implications for thermobarometry and P-T path determinations. Journal of Metamorphic Geology 8, 683-696.

Spear, F. S., 1993. Metamorphic phase equilibria and Pressure-Temperature-Time Paths. Mineralogical Society of America MONOGRAPH, Washington, D. C. pp, 511-574.

Stevens, B. P. J., Barnes, R. G., Brown, R. E., Stroud, W. J., Willis, I. L., 1988. The Willyama Supergroup in the Broken Hill and Euriowie Blocks, New South Wales. Precambrian Research 40/41, 297-327.

Torkelson, D. J., Mortensen, J. K., Davidson, G. S., Creaser, R. A., Perez, W. A., Abbott, J. G., 2001. Early Mesoproterozoic intrusive breccias in the Yukon, Canada: The role of hydrothermal systems in reconstructions of North America and Australia. Precambrian Research 111, 31-55.

Torres-Roldan, R. L., 1979. The tectonic subdivision of the Betic zone (Betic Cordilleras, Southern Spain): its significance and one possible geotectonic scenario for the westernmost Alpine belt. American Journal of Science 279, 19-51.

Twiss, R. J., Moores, E. M., 1992. Structural Geology. Freeman and Company, pp, 262-281.

Vance, D., Mahar, E., 1998. Pressure-temperature paths from P-T pseudosections and zoned garnets: potential, limitations and examples from the Zanskar Himalaya, NW India. Contributions to Mineralogy and Petrology 132, 225-245.

Vernon, R. H., Clarke, G. L., Collins, W. J., 1990. Local, mid-crustal granulite facies metamorphism and melting: an example in the Mount Stafford area, central Australia. In: Ashworth, J. R., Brown, M. (Eds.), High-temperature Metamorphism and Crustal Anatexis. Unwin Hyman Mineral. Soc. Ser., Lond., pp. 272-319.

Williams, M. L., 1994. Sigmoidal inclusion trails, punctuated fabric development, and interactions between metamorphism and deformation. Journal of Metamorphic Geology 12, 1-21.

Williams, P. J., 1998. Metalliferous economic geology of the Mt. Isa Eastern Succession, northwest Queensland. Australian Journal of Earth Sciences 45, 329-341.

Williams, M. L., Karlstrom, K. E., 1996. Looping P-T paths and high-T, Low-P middle crustal metamorphism: Proterozoic evolution of the southwestern United States. Geology 24, 1119-1122.

Williams, M. L., Jercinovic, M. J., 2002. Microprobe monazite geochronology: putting absolute time into microstrcutral analysis. Journal of Structural Geology 24, 1013-1028.

Williams, P. J., Pollard, P. J., 2003. Australian Proterozoic Iron Oxide-Cu-Au deposits: An overview with new metallogenic and exploration data from the Cloncurry district, northwest Queesnland. Exploration Mining Geology 10, 191-213.

Zeh, A., Klemd, R., Buhlmann, S., Barton, M. J., 2004. Pro- and retrograde P-T evolution of granulites of the Beit Bridge Complex (Limpopo Belt, South Africa): constraints from quantitative phase diagrams and geotectonic implications. Journal of Metamorphic Geology 22, 79-95.

THESIS CONCLUSIONS

Section A

Integrated macro, meso and microstructural analyses of the southern Eastern Fold Belt, Mount Isa Inlier, have revealed that the dominant structures were initially formed as steep pervasive fabric during D_2, which was subsequently rotated to shallow angles due to the effect of subvertical shortening or subhorizontal stretching, D_3 (Sayab, 2004). This observation is strengthened by microstructures that are consistent with the field observations from all three domains with near-orthogonal steep and shallow S_2 and S_3 foliations, respectively. The 3D geophysical data supports a steep crustal signature rather than shallow structures. These results do not support previously suggested non-coaxial west vergent, nappe-style folding in the region.

Section B

3D microstructural analyses of porphyroblast inclusion trails using both the 'asymmetry method' for determining **F**oliation **I**ntersection **A**xes preserved in porphyroblasts (FIAs) and the recently developed 'FitPitch' method, reveal W-E and N-S trending FIA sets in the White Blow Formation of the Mt Isa Inlier. The FIA sets were distinguished based on the relative timing, trend and orientation of inclusion trail patterns. Pitches of the inclusion trails preserved within the porphyroblasts in vertically oriented thin-sections and trends in horizontal sections yield distinct near-orthogonal modal orientations from all the analyzed samples. This indicates that the porphyroblasts host successive fabrics as crenulation foliations and did not rotate with respect to geographical axes. W-E and N-S trending FIAs have been obtained from both garnet and staurolite porphyroblasts hosting differentiated crenulation cleavages. Garnet and staurolite growth during bulk north-south shortening recorded the development of multiple foliations. This period of bulk shortening formed during a period of orogenesis called (O_1). W-E shortening formed N-S striking foliations that preserve a period of orogenesis (O_2), and another succession of metamorphism involving more phases of porphyroblast growth preserving N-S trending FIAs. The porphyroblast inclusion trail patterns preserving W-E trending FIAs provide a window into the lengthy period of earlier deformation and metamorphism that is no longer preserved within the matrix foliations.

Section C

The succession of FIA sets from early W-E to younger N-S across the Eastern Fold Belt suggests that porphyroblast growth was controlled by deformation partitioning and overprinting of successive near-orthogonal fabric development rather than non-coaxial flow. A progressive succession of overprinted FIA trends reveals a clockwise rotation of the principal direction of bulk shortening with time. This requires a radical shift of relative plate movement from N-S to W-E during development of the north Australian craton in the Mesoproterozoic (*ca* 1.60 and 1.50Ga). Middle to upper amphibolite facies metamorphic conditions occurred during O_1 with crustal thickening followed by fast erosion and near-isothermal decompression leading to low-pressure/high-temperature (LP/HT) conditions. This was followed during O_2 by a second period of middle- to upper- amphibolite facies metamorphism. This history appears to correlate better with that observed in the southwest United States, which may have been located against the NE of the Australia at this period in time.

Section D

The principal conclusions of this section are as follows:

(1) N-S shortening (O_1) resulting in medium-pressure in the kyanite stability field as indicated by relic kyanite + staurolite as inclusions in andalusite and chlorite + biotite + plagioclase inclusions in relatively higher pressure, low temperature garnet cores hosting W-E FIAs,

(2) Near-isothermal decompression from kyanite to andalusite via staurolite with cooling starting at intermediate to low pressure,

(3) Intrusion of the Williams-Naraku granite (1550-1500Ma) with a decrease in pressure and increase in temperature with or without the production of cordierite,

(5) Spatial and temporal association of regional albitization with the Williams and Naraku Batholiths,

(6) W-E shortening (O_2) where cordierite was replaced by andalusite followed by new growth of garnet, staurolite and sillimanite in the matrix.

N-S shortening during orogenesis in the Mt Isa Inlier: the preservation of W-E structures and their tectonic and metamorphic significance

Volume II

Thesis submitted by

Mohammad Sayab M. Phil (University of Peshawar, 2001)

in March 2005

for the degree of Doctor of Philosophy

in the School of Earth Sciences

James Cook University of North Queensland

Australia

CONTENTS OF VOLUME II

(Figures, tables and appendices)

Section – A

3D successions of near-orthogonal progressive bulk inhomogeneous shortening resulting in multiple generations of folds in the Mount Isa Inlier

(Figures)

Fig. 1. (a) Outline map of the Mount Isa Inlier showing Western Fold Belt (WFB), Kalkadoon-Leichhardt Belt (KLB) and Eastern Fold Belt (EFB).
(b) Regional geological map of the Eastern Fold Belt showing major lithotectonic units and location of the study area (modified after Blake, 1987; Giles and MacCready, 1997; Williams, 1998; Marshall and Oliver, 2001). Ages after Page and MacCready (1997), Page and Sun (1998).

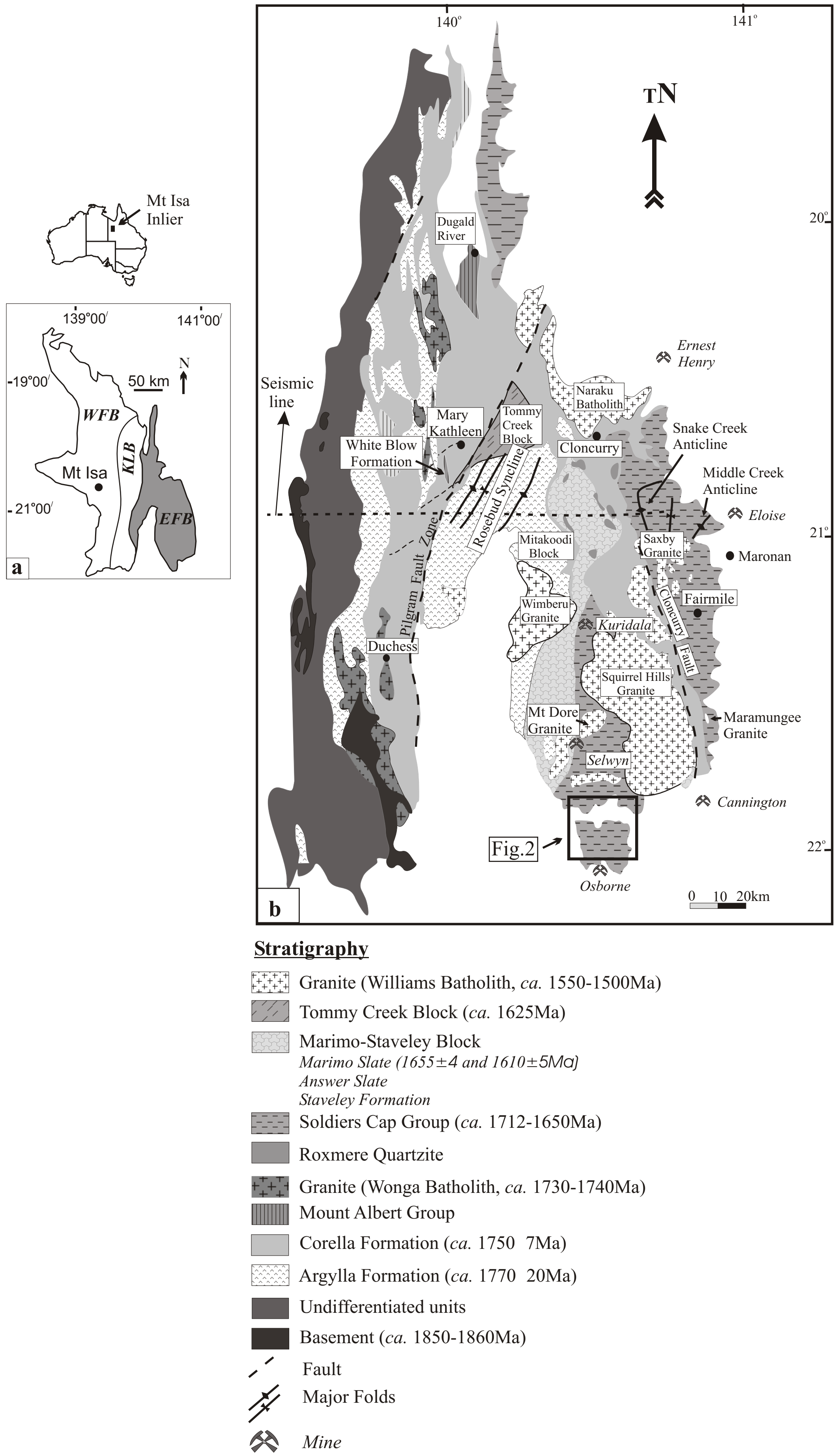
Mt Isa
Inlier
139°00'
141°00'
19°00'
21°00'
50 km
N
WFB
KLB
EFB
Mt Isa
a
140°
141°
20°
21°
22°
TN
Dugald River
Seismic line
Mary Kathleen
Tommy Creek Block
White Blow Formation
Rosebud Syncline
Pilgram Fault Zone
Cloncurry
Naraku Batholith
Ernest Henry
Snake Creek Anticline
Middle Creek Anticline
Eloise
Maronan
Mitakoodi Block
Saxby Granite
Wimberu Granite
Fairmile
Cloncurry Fault
Kuridala
Duchess
Squirrel Hills Granite
Mt Dore Granite
Maramungee Granite
Selwyn
Cannington
Fig.2
Osborne
0 10 20km
b
Stratigraphy
Granite (Williams Batholith, ca. 1550-1500Ma)
Tommy Creek Block (ca. 1625Ma)
Marimo-Staveley Block
Marimo Slate (1655±4 and 1610±5Ma]
Answer Slate
Staveley Formation
Soldiers Cap Group (ca. 1712-1650Ma)
Roxmere Quartzite
Granite (Wonga Batholith, ca. 1730-1740Ma)
Mount Albert Group
Corella Formation (ca. 1750 7Ma)
Argylla Formation (ca. 1770 20Ma)
Undifferentiated units
Basement (ca. 1850-1860Ma)
Fault
Major Folds
Mine

Fig. 1

Fig. 2. (a) Simplified geological map of the southern Eastern Fold Belt, Mt Isa Inlier. Major litholgical units are shown. The area is divided into three domains defined by variations in the lithology, structural intensity and style.
(b) Landsat image of the study area. Bright tones in the Anitra Prospect and Sandy Creek domains are undeformed bodies of granite/pegmatite.
Fig. 2. (b) Landsat imagery courtesy of NASA Goddard Space Flight Center and U.S. Geological Survey.

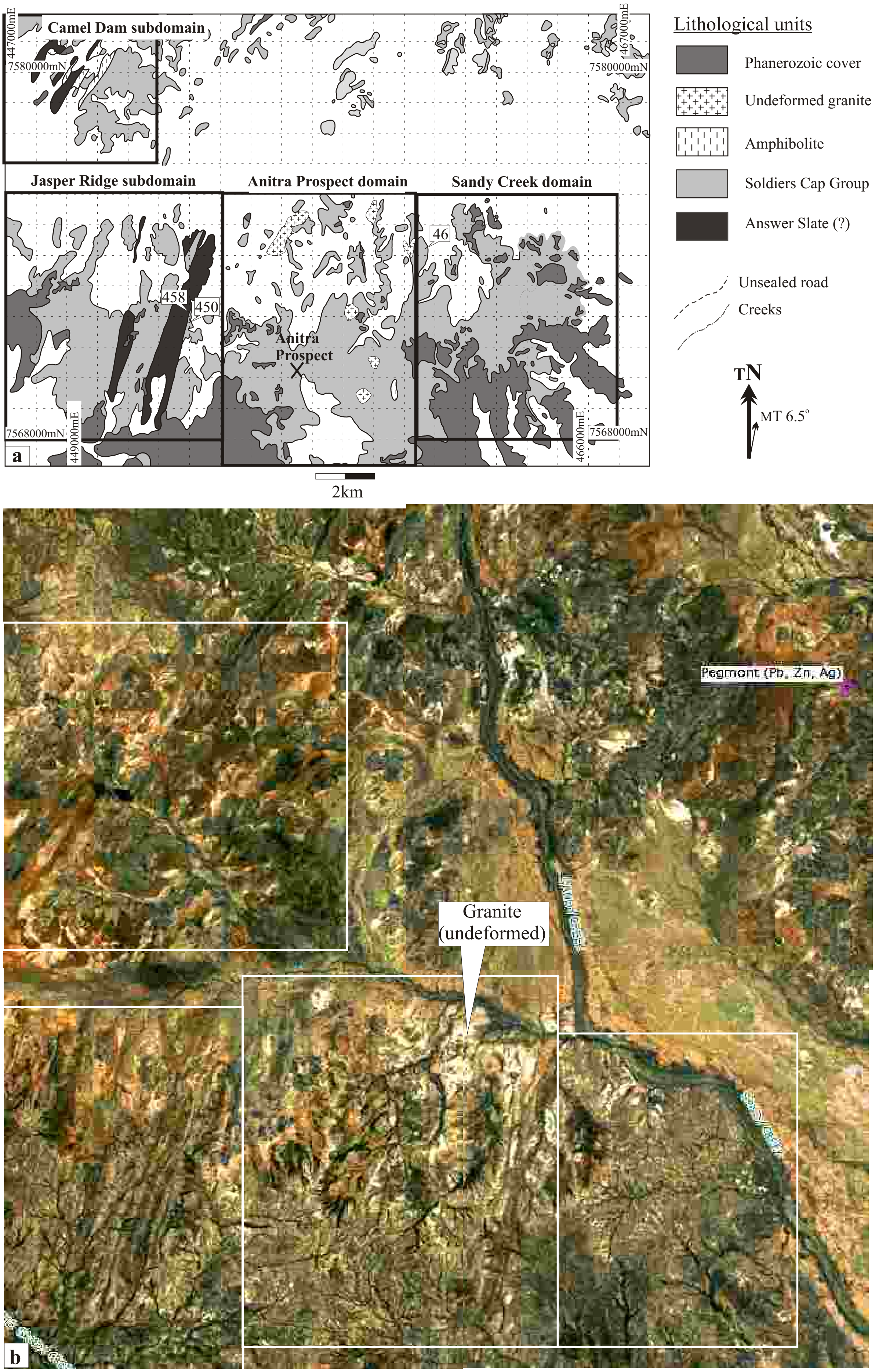

Camel Dam subdomain
Jasper Ridge subdomain
Anitra Prospect domain
Sandy Creek domain
447000mE
467000mE
7580000mN
7580000mN
7568000mN
7568000mN
449000mE
466000mE
458
450
46
Anitra Prospect
a
2km
Lithological units
Phanerozoic cover
Undeformed granite
Amphibolite
Soldiers Cap Group
Answer Slate (?)
Unsealed road
Creeks
TN
MT 6.5°
Granite (undeformed)
Pegmont (Pb, Zn, Ag)
b

Fig. 2

Fig. 3 (a) Lower hemisphere equal-area stereographic plots of poles to foliation planes measured in the field. Note that the steep to shallow orientations of S_2 in the Sandy Creek and Anitra Prospect domain is interpreted due to the effect of later D_3 event. D_3 rotated steep S_2 into moderate and shallow orientations (see text for further discussion).

(b) Lower hemisphere equal-area stereographic plots of lineations measured in the field.

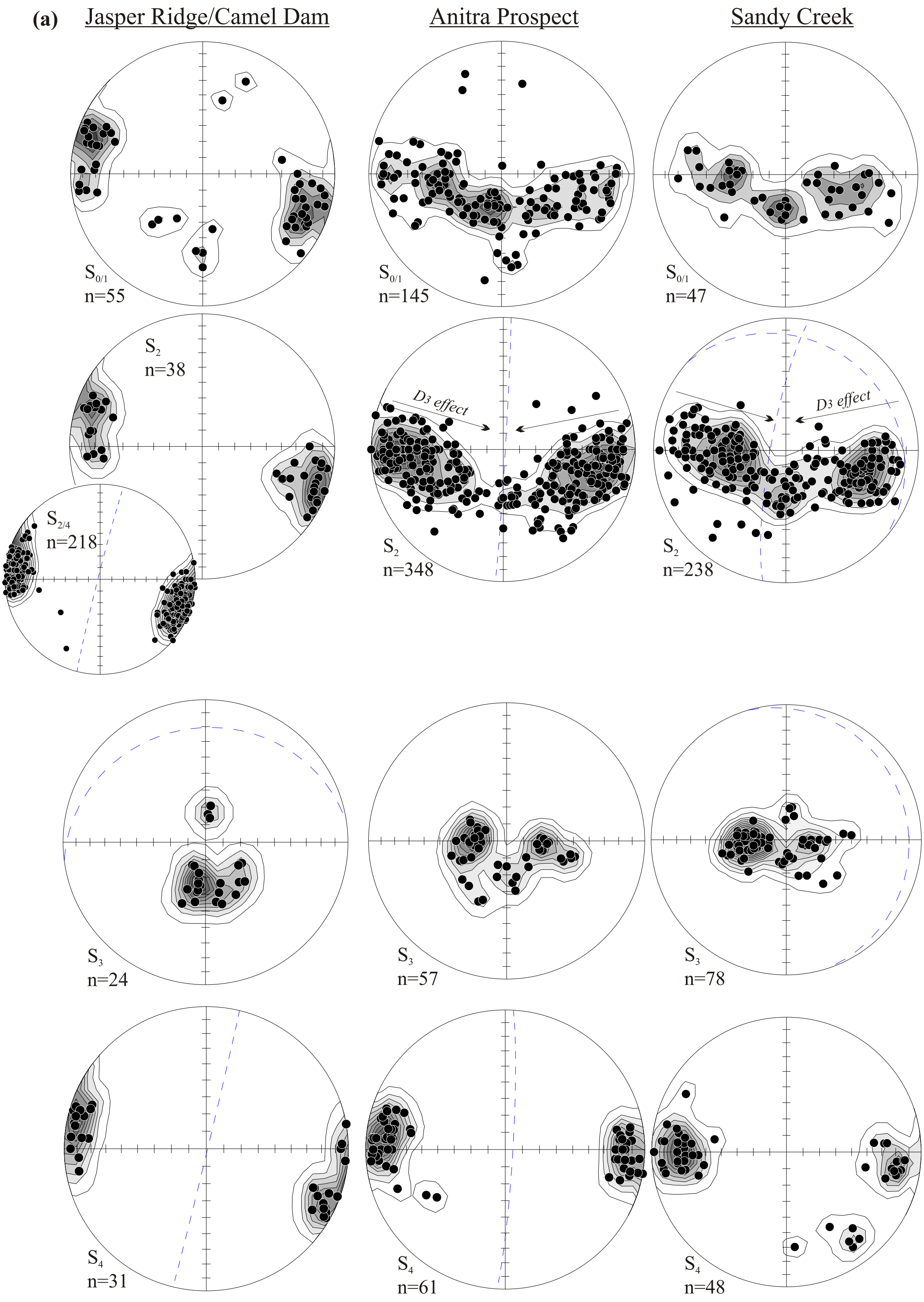

(a)
Jasper Ridge/Camel Dam
Anitra Prospect
Sandy Creek
$S_{0/1}$
n=55
$S_{0/1}$
n=145
$S_{0/1}$
n=47
S_2
n=38
$S_{2/4}$
n=218
D3 effect
S_2
n=348
D3 effect
S_2
n=238
S_3
n=24
S_3
n=57
S_3
n=78
S_4
n=31
S_4
n=61
S_4
n=48

Fig. 3a

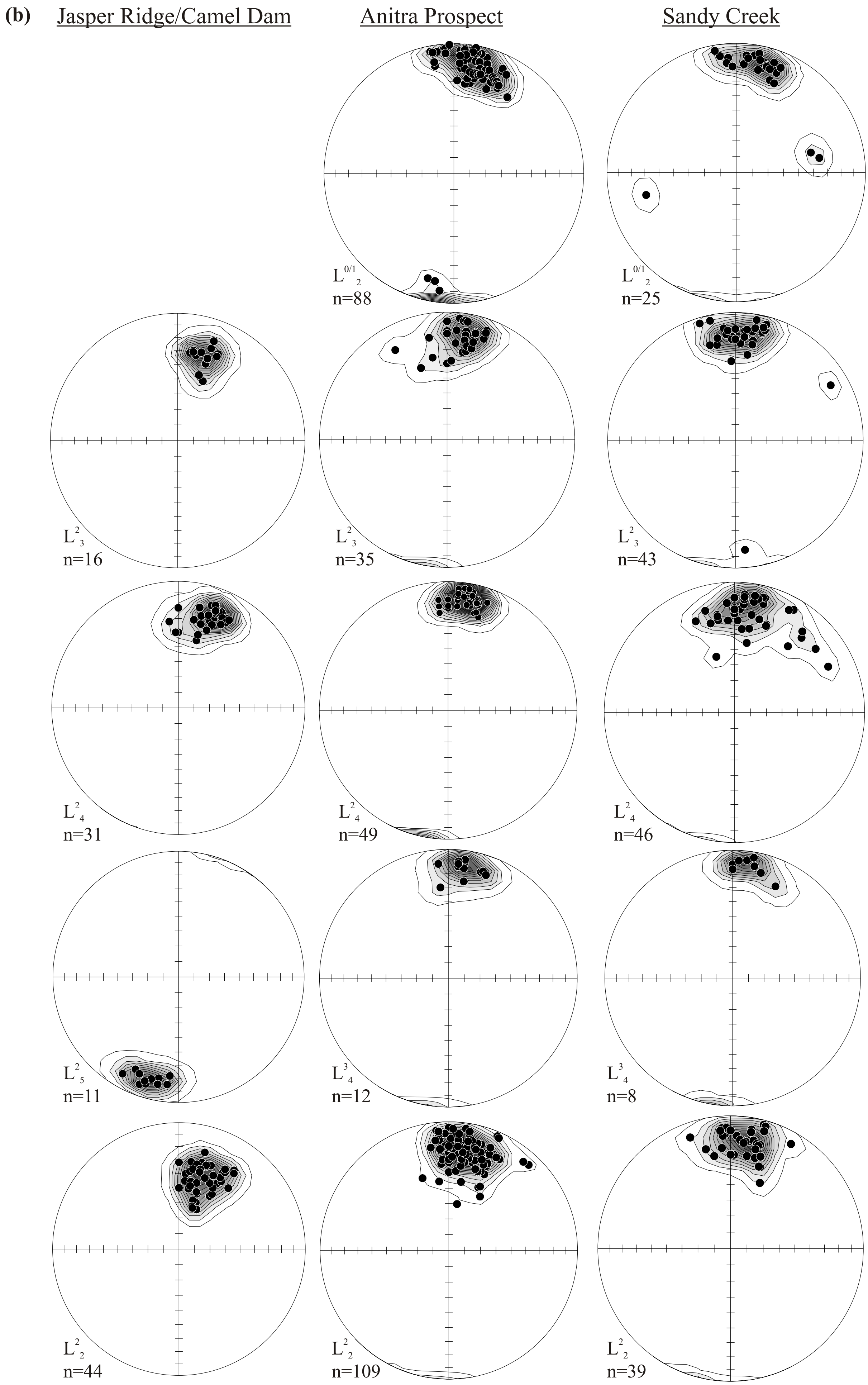
(b)
Jasper Ridge/Camel Dam
Anitra Prospect
Sandy Creek
$L^{0/1}_2$
n=88
$L^{0/1}_2$
n=25
L^2_3
n=16
L^2_3
n=35
L^2_3
n=43
L^2_4
n=31
L^2_4
n=49
L^2_4
n=46
L^2_5
n=11
L^3_4
n=12
L^3_4
n=8
L^2_2
n=44
L^2_2
n=109
L^2_2
n=39

Fig. 3b

Fig. 4. North and south verging mesoscopic F_1 folds.

(a) Photograph and (b) sketch of F_1 fold. The fold shape lies close to the Class 2 similar fold based on the geometry of parallel dip isogons. Low interlimb angle (~50^o) with almost W-E trending fold axis. A downward facing direction is inferred based on variation in grain size, which may represent a part of the Bouma sequence A and B. Single barbed arrow showing north direction, profile view. Photograph taken looking to the west (AMG 453055mE, 7572739mN)

(c) Photograph and (d) sketch showing near Class 1B parallel shape isoclinal recumbent fold with slightly convergent dip isogons. S_0 is defined by medium-grained quartzite. This fold is plunging 06 towards 267^o. Single barbed arrow showing north direction, profile view. Photograph taken looking to the west (AMG 454938mE, 7570775mN).

(e) Photograph and (f) sketch showing almost Class 1B parallel, isoclinal recumbent fold plunging 04 towards 271^o verging to the south. Layer thickness remained constant on one of the measured layers of the fold. This fold is preserved in the hinge of mesoscopic D_2 fold. Possible upward-facing direction has been inferred for this fold based on fining upward grain size variation. Single barbed arrow indicates north direction, profile view. Photograph taken looking to the west (AMG 459426mE, 7574376mN).

(g) Fibrolite, N-S-south trending and shallowly plunging to the north and aligned along L^2_2 mineral lineation. Photograph taken approximately looking to the west (AMG 457700mE, 756893mN). (h) Sillimanite nodules that have replaced K-feldspar. The long axes of the nodules are plunging to the north. Length of the pen is 14cm. Photograph viewing to the east (AMG 457505mE, 7569112mN).

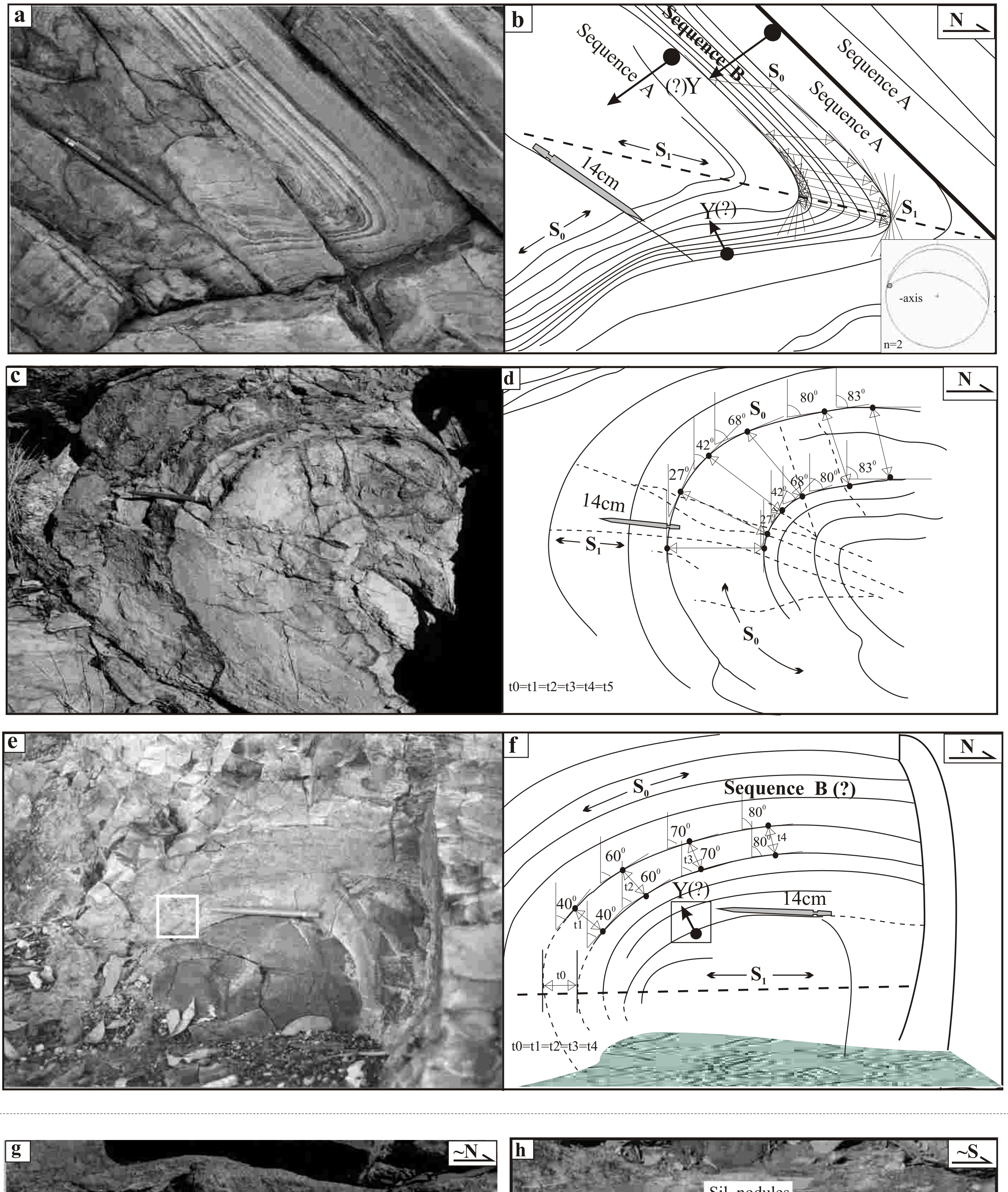

a
b
N
Sequence A
Sequence B
Sequence A
Sequence A
(?)Y
S0
S1
14cm
S0
Y(?)
S1
-axis
n=2
c
d
N
S0
80°
83°
68°
42°
27°
14cm
S1
S0
t0=t1=t2=t3=t4=t5
e
f
N
S0
Sequence B (?)
80°
70°
70°
80°
t4
t3
60°
60°
t2
40°
40°
t1
Y(?)
14cm
S1
t0
t0=t1=t2=t3=t4
g
~N
Sil
Sil
h
~S
Sil nodules

Fig. 4

Fig. 5. (a) Photograph showing upright, isoclinal mesoscopic D_2 fold. Profile view. Photograph taken looking to the north (AMG 460796mE/7571249mN).

(b) Scanned oriented polish block and (c) line drawing of D_2 fold. The shape of the fold varies from Class 1B to Class 1C (layers 11ii and 4ii) and from Class 1C to Class 3 (layers 4i and 11i) similar shape for western limbs on standard layer thickness plot. This variation across the fold is largely due to the fact that the western limb is more strained than the eastern limb. Profile view.

(e) Photograph of upright, tight D_2 fold shallowly plunging to the NNE. The overall shape of the fold is between Class 1C parallel and Class 2 similar fold. Dip isogons constructed in layers 7 and 8. Layer 7 shows weekly convergent isogon pattern, that is, Class 1C, whereas layer 8 shows pattern in between parallel and divergent isogons and lies close to the Class 2 similar fold. The western limb of this fold is overprinted by a pair of D_3 folds, striking west-east with shallow dipping axial plane S_3. Profile view. Photograph taken looking to the south (AMG 465013mE, 7574197mN).

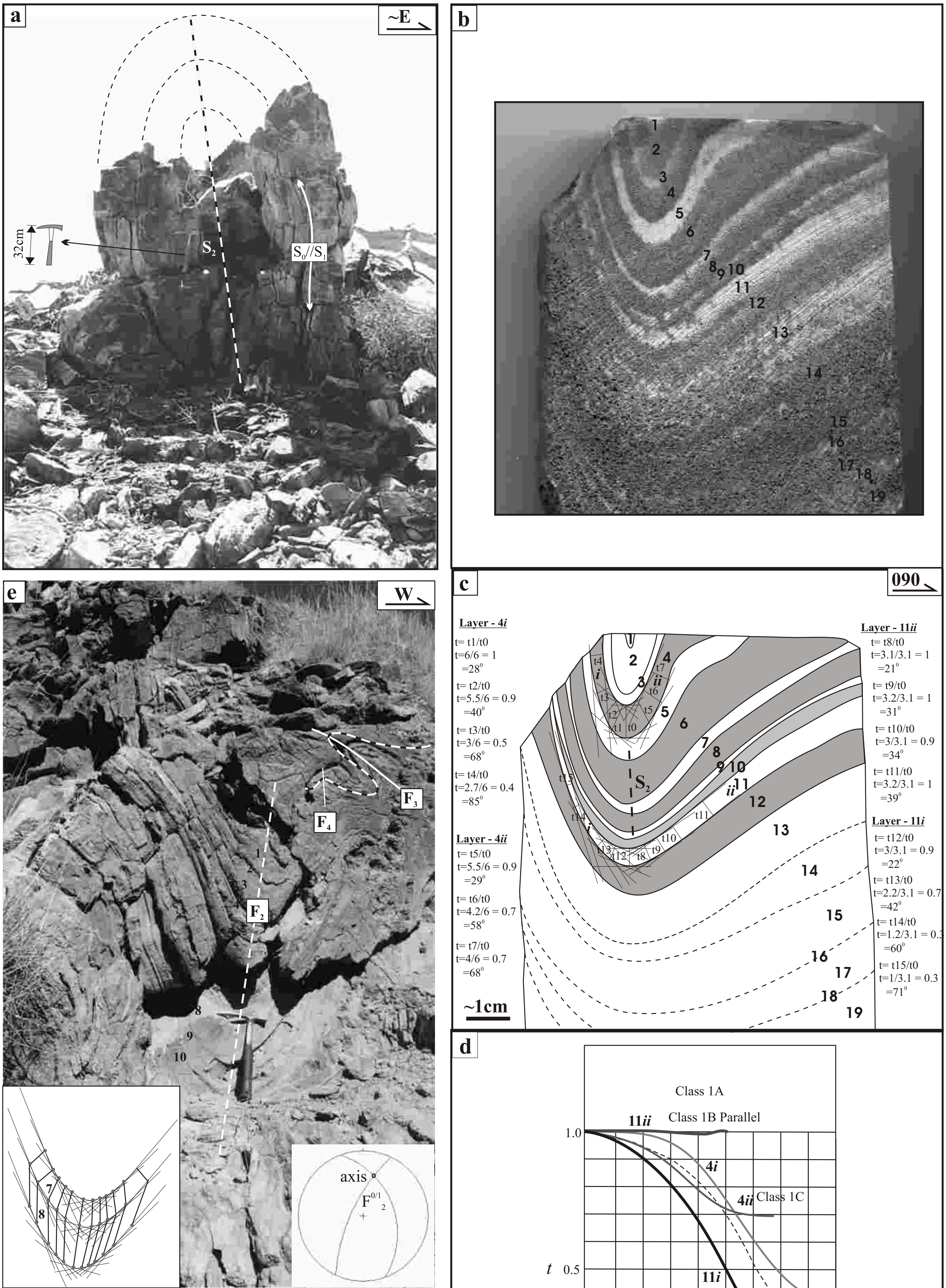

a
~E
32cm
S2
S0//S1
b
1
2
3
4
5
6
7
8
9
10
11
12
13
14
15
16
17
18
19
c
090
Layer - 4i
t= t1/t0
t=6/6 = 1
=28°
t= t2/t0
t=5.5/6 = 0.9
=40°
t= t3/t0
t=3/6 = 0.5
=68°
t= t4/t0
t=2.7/6 = 0.4
=85°
Layer - 4ii
t= t5/t0
t=5.5/6 = 0.9
=29°
t= t6/t0
t=4.2/6 = 0.7
=58°
t= t7/t0
t=4/6 = 0.7
=68°
Layer - 11ii
t= t8/t0
t=3.1/3.1 = 1
=21°
t= t9/t0
t=3.2/3.1 = 1
=31°
t= t10/t0
t=3/3.1 = 0.9
=34°
t= t11/t0
t=3.2/3.1 = 1
=39°
Layer - 11i
t= t12/t0
t=3/3.1 = 0.9
=22°
t= t13/t0
t=2.2/3.1 = 0.7
=42°
t= t14/t0
t=1.2/3.1 = 0.3
=60°
t= t15/t0
t=1/3.1 = 0.3
=71°
S2
~1cm
d
Class 1A
Class 1B Parallel
11ii
4i
4ii
Class 1C
11i
Class 3
Class 2 Similar
t
1.0
0.5
0.0
0
30
60
90
e
W
F3
F4
F2
axis
F2 0/1

Fig. 5

Fig. 6. (a) Field photograph and (b) sketch of inclined, west verging, isoclinal fold composed of thick psammite interbedded with thin pelitic layers. The psammite layers are stretched, especially on the limbs of the folds, forming boudins. Photograph taken looking to the north (AMG 457391mE, 7569706mN).

(c) Field photograph and (b) line diagram of successive near-orthogonal S_2, S_3 and S_4 foliations and respective L^2_3 and L^2_4 intersection lineations in interbedded psammite and psammopelite layers. Thickness of individual layers varies from millimeter to centimeter scale, which is locally transposed during D_2 for this particular outcrop. Two lithological units can be distinguished as psammite (labeled-X) and psammopelite (labeled-Y). The ratio based on true thickness ($\perp$ to layers) of psammite *vs*. psammopelite is almost 1:1. S_2 is subparallel to S_0 and overturned to the west by shallow dipping D_3 folds and S_3 differentiated crenulations. This geometric relationship produced shallowly plunging and north trending L^2_3 intersection lineation. Shear sense on S_3 crenulations is both clockwise and anticlockwise or coaxial. D_4 folds overprinted on S_2 and locally on S_3 produced steep, upright tight to isoclinal F_4 folds and crenulations. Steep S_4 forms L^2_4 intersection lineation with S_2, and L^3_4 where S_4 overprinted on S_3. More clear overprinting relationships can be seen in boxes labeled I and II. Profile view. Photograph looking to the NNW (AMG 457050mE, 7570938mN).

(e) Oriented polished scanned sample and line drawing showing D_3 differentiated crenulations S_3. The intensity of differentiation increases from left to right. Sample no. SR65 (AMG 461393mE, 7573740mN).

(f) Photograph of oriented sample showing pronounced near-orthogonal S_2 and S_3 with L^2_3 intersection lineation, which is shallowly plunging to the north. The asymmetry or vergence on S_3 is top-to-the west. Sample no. SR72.

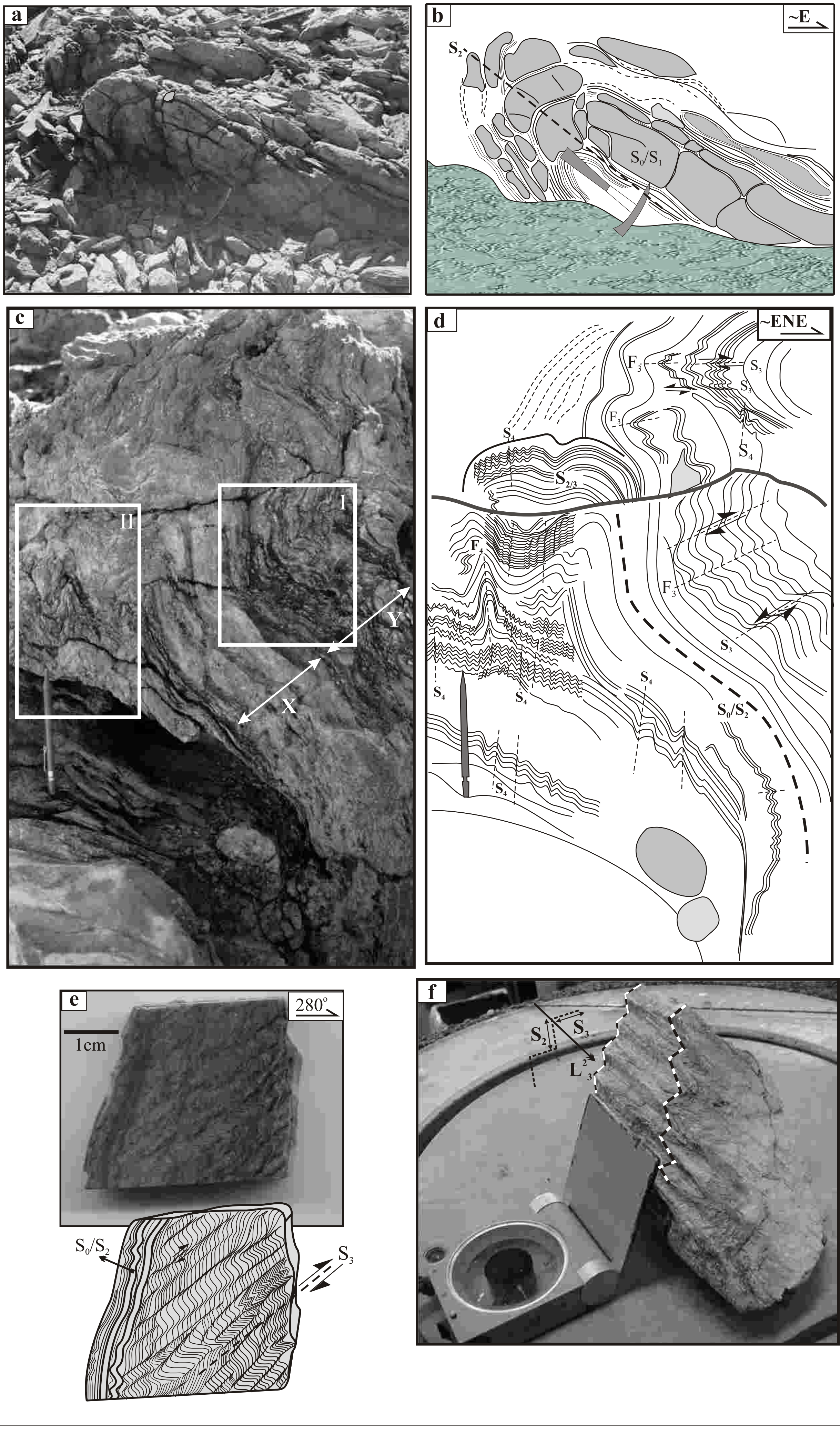
a
b
~E
S2
S0/S1
c
I
II
X
Y
d
~ENE
F3
S3
S4
S2/3
F
S0/S2
e
280°
1cm
S0/S2
S3
f
S2
S3
L23

Fig. 6

Fig. 7. (a) Field photograph and (b) line drawing of recumbent fold (interlimb angle ~52^{o}) with NNE trending subhorizontal fold axis. Shallow dipping spaced S_3 is well-developed as axial plane cleavage. (c) Standard layer thickness variation plot for limbs 6*ii* and 6*i*. The shape of the limbs lie close to the Class 2 similar fold. Note steep S_0/S_2 in the core of the fold. Length of the hammer is 32 cm. Photograph taken looking to the north (AMG 463251mE, 7573311mN).

(d) Photograph and (e) line diagram of tight recumbent (labeled A), and gently inclined (labeled B) folds with subhorizontal north and NNE plunging fold axes, respectively. Both east and west verging folds are present in the outcrop, indicating coaxial deformation during D_3. Profile view. Photograph viewing to the south (AMG 0465616mE, 7573228mN).

(f) Photograph and (g) sketch showing local non-coaxial deformation during D_3 with top-to-the-west shear in the Sandy Creek domain. Shear sense is based on the S_3 differentiation. Top-to-the-west shear sense can also be inferred from localized asymmetric boudin trains. However, boudin faces or flanking structures on inter-boudin zones are not well developed to determine shear senses (e.g., Goscombe et al., 2004).

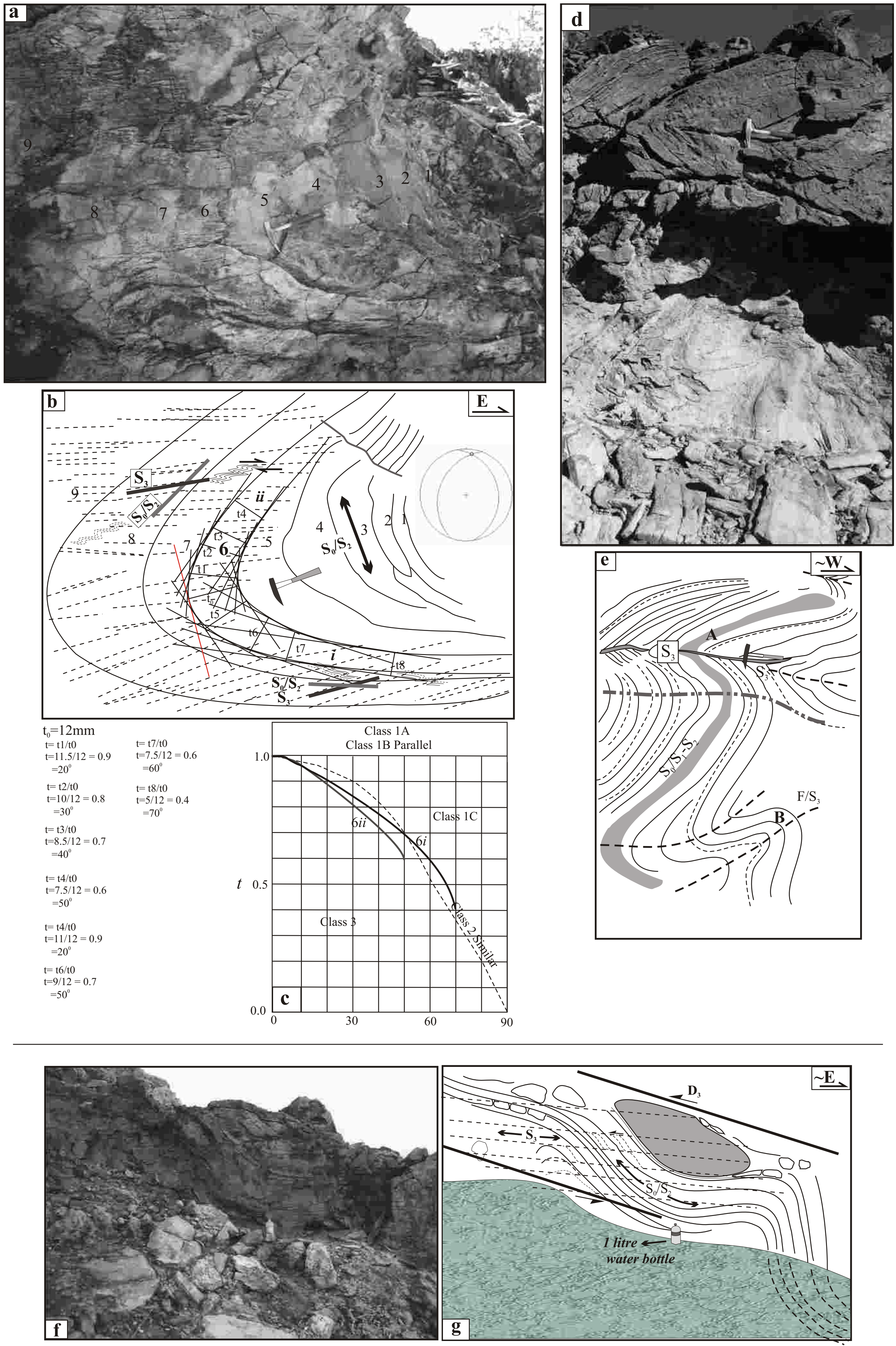

a
9
8
7
6
5
4
3
2
1
d
b
E
S3
S0/S2
9
8
7
6
5
4
3
2
1
ii
i
t1
t2
t3
t4
t5
t6
t7
t8
S0/S2
S3
e
~W
A
S3
S3
S0/S1-S2
F/S3
B
t0=12mm
t= t1/t0
t=11.5/12 = 0.9
=20°
t= t2/t0
t=10/12 = 0.8
=30°
t= t3/t0
t=8.5/12 = 0.7
=40°
t= t4/t0
t=7.5/12 = 0.6
=50°
t= t4/t0
t=11/12 = 0.9
=20°
t= t6/t0
t=9/12 = 0.7
=50°
t= t7/t0
t=7.5/12 = 0.6
=60°
t= t8/t0
t=5/12 = 0.4
=70°
Class 1A
Class 1B Parallel
Class 1C
Class 3
Class 2 Similar
6ii
6i
t
1.0
0.5
0.0
0
30
60
90
c
f
g
~E
D3
S3
S0/S2
1 litre
water bottle

Fig. 7

Fig. 8. Overprinting relationships of L^2_3 and L^2_5 intersection lineations in an outcrop. (a) Photograph and (b) sketch showing pronounced L^2_3 intersection lineation gently plunging to the NNE, whereas L^2_5 is gently to moderately plunging to the SSW. Length of the pencil is 14cm. Photograph looking to the west.
(d) Sketch reproduced from (c) with shallow dipping S_3 forming an intersection with S_2 with top-to-the-east shear and is more intense than S_5. Photograph taken looking to the north. (e) Photograph and (f) sketch of shallow dipping S_5 with top-to-the-west shear sense. Photograph taken approximately looking to the north. (AMG 483436mE, 7594893mN).

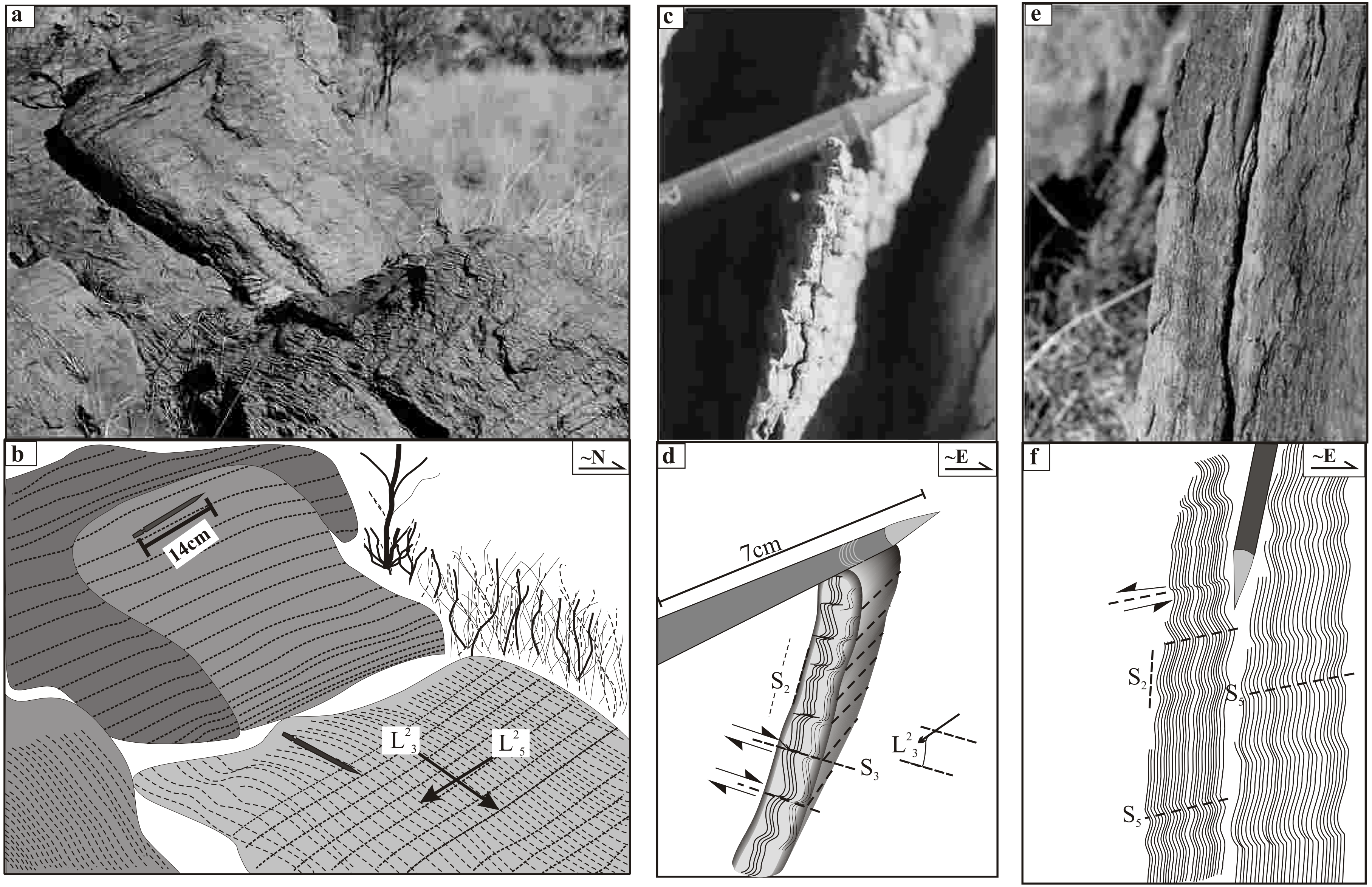

Fig. 8

Fig. 9. (a) Field photograph and (b) line diagram illustrating tight to isoclinal folding of composite $S_{2/3}$ by D_4. Most of the small scale upright, steeply inclined F_4 folds and crenulations have straight parallel limbs and narrow sharp hinges, like chevron folds. These structures are well preserved in competent psammites or interbedded psammopelites. The penetrative intersection lineations L^2_4 or L^3_4 are moderately plunging to the NNE. Length of the pencil is 14cm. Photograph viewing to the north (AMG 458928mE, 7568616mN).

(c) Photograph and (d) sketch of close to tight upright D_4 folds couplet with pronounced L^2_4 intersection lineation, shallowly plunging to the north. Note small scale locally differentiated crenulation cleavages, especially on the limbs of the fold. The shear sense on S_4 on the eastern limb of the antiform is west-side-up, whereas on the western limb it is east-side-up. Length of the pencil is 14cm. Photograph looking to the north (AMG 453516mE, 7570706mN).

(e) Photograph showing overprinting effects of D_4 over S_2 and S_3. The psammopelitic layers were initially folded during D_2 producing S_2 foliation. This is followed by D_3 event with shallow spaced S_3 differentiated cleavage. The S_2 and S_3 were subsequently overprinted by steep S_4 differentiated crenulation cleavage. In this particular outcrop, dominant D_4 shear sense or shear sense on S_4 is west-side-up with local east-side-up cleavages. Right side of the photograph showing S_2 preserved in the low strain zones of D_4, where shallow S_3 can also be observed. However, zones of intense D_4 reactivated S_3 and reused S_2 and is demonstrated in (f).

(f) Sketches showing composite-foliation-forming deformation events after Davis and Forde (1994). S_2 was crenulated by the shallow S_3 foliation. S_2 in the hinge regions of the crenulations remained steep. During D_4 shear and folding, S_2 is subparallel to S_4 in the zones of high shear stain on the limbs. With progressive deformation S_2 is straightened out and re-used by D_4 shear. Dashed arrows indicate reactivation shear on S_3. Progressive D_4 shear rotates S_3 fabric into subparallelism with the composite $S_{2/4}$ foliation (as shown on the right side).

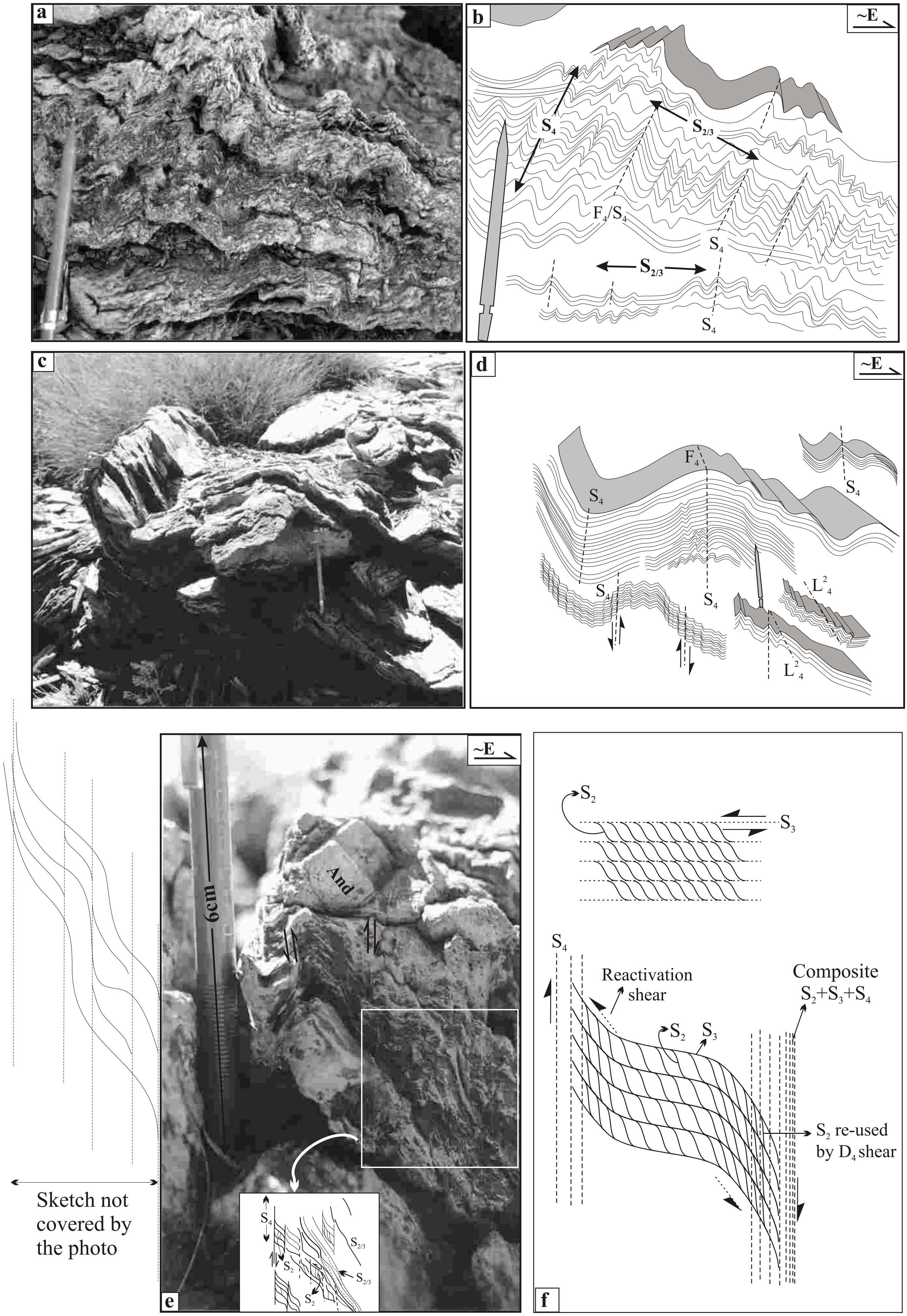

a
b
~E
S_4
$S_{2/3}$
F_4/S_4
S_4
$S_{2/3}$
S_4
c
d
~E
F_4
S_4
S_4
S_4
S_4
L^2_4
L^2_4
~E
6cm
And
S_4
S_2
$S_{2/3}$
$S_{2/3}$
S_2
e
Sketch not covered by the photo
S_2
S_3
S_4
Reactivation shear
S_2
S_3
Composite $S_2+S_3+S_4$
S_2 re-used by D_4 shear
f

Fig. 9

Fig. 10. (a) Bureau of Mineral Resources (BMR, 1984) Selwyn 7054 index base map, 1: 100, 000. (b) Comparing outcrop geology with multiscale edges or worms. Perspective view, the base map is shown as transparent layer with worms. Raw data imported and processed in GOCAD 2.0.7. (c&d) Shows the geometry of worms. The overall dip of worms is steep and indicates steep crustal signature. Note steep worms in the Jasper Ridge/Camel Dam domain and shallow dipping worms in the Sandy Creek domain agree with the surface geology (*cf*. Fig. 2).

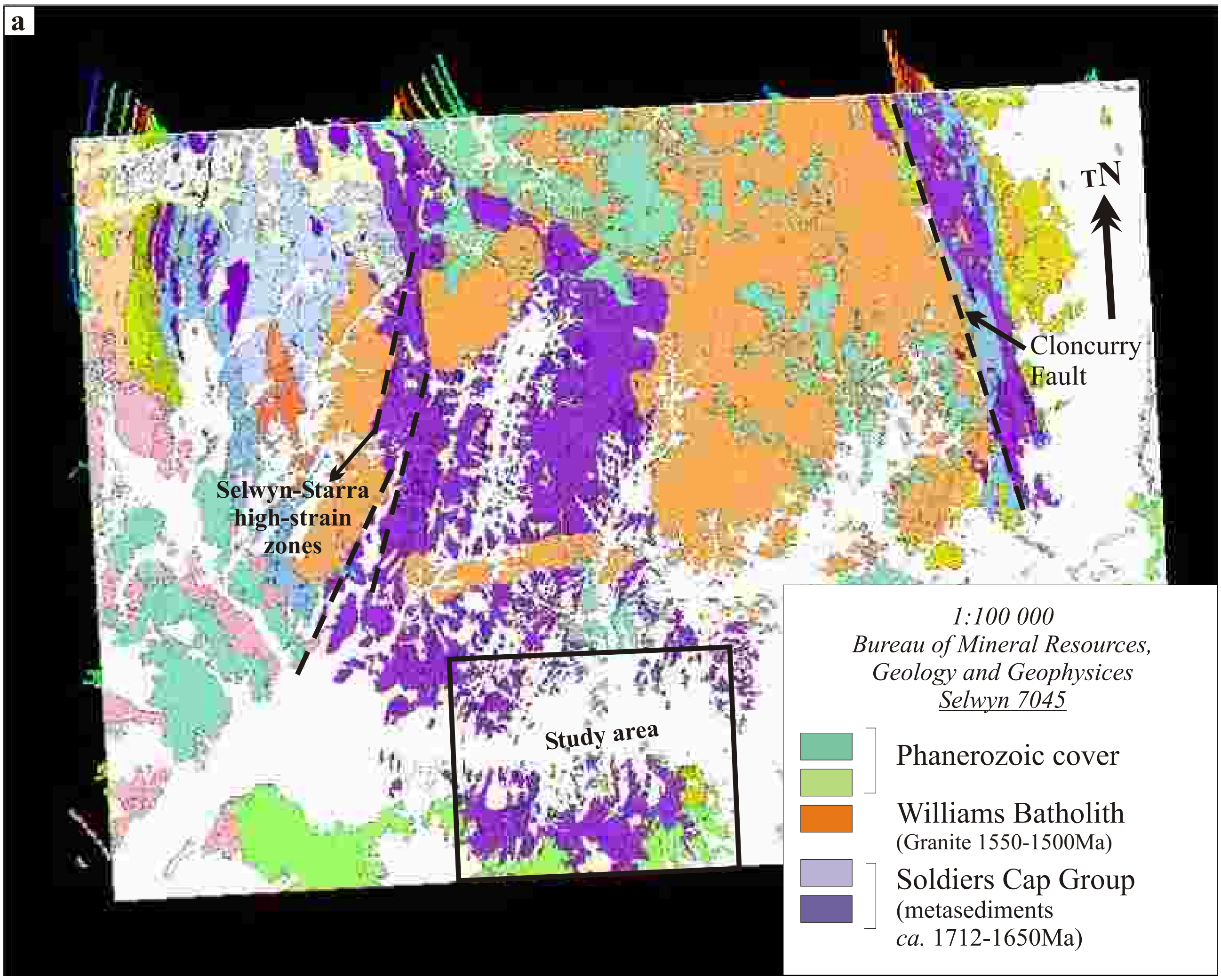

a
TN
Cloncurry
Fault
Selwyn-Starra
high-strain
zones
Study area
1:100 000
Bureau of Mineral Resources,
Geology and Geophysices
Selwyn 7045
Phanerozoic cover
Williams Batholith
(Granite 1550-1500Ma)
Soldiers Cap Group
(metasediments
ca. 1712-1650Ma)

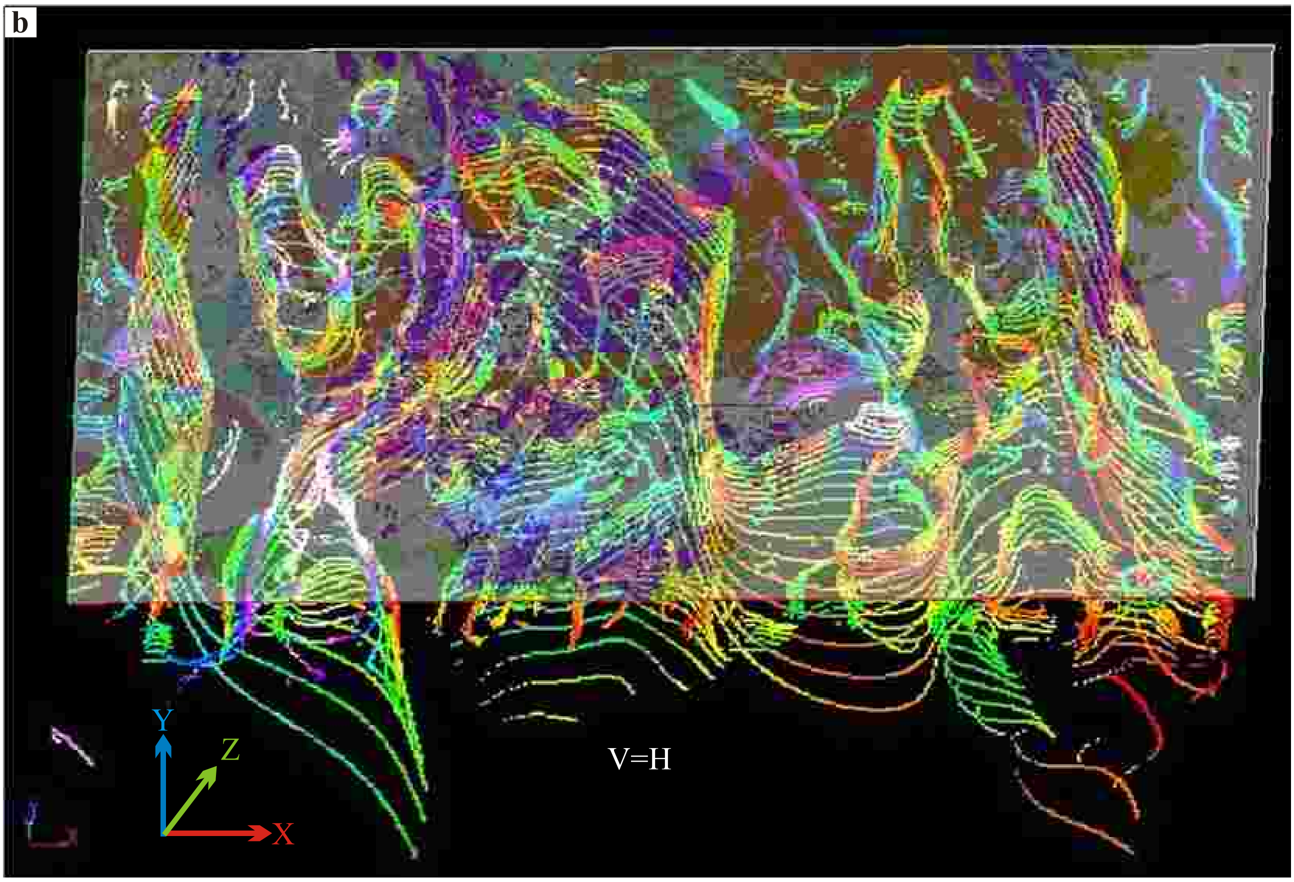

b
Y
Z
X
V=H

Fig. 10a,b

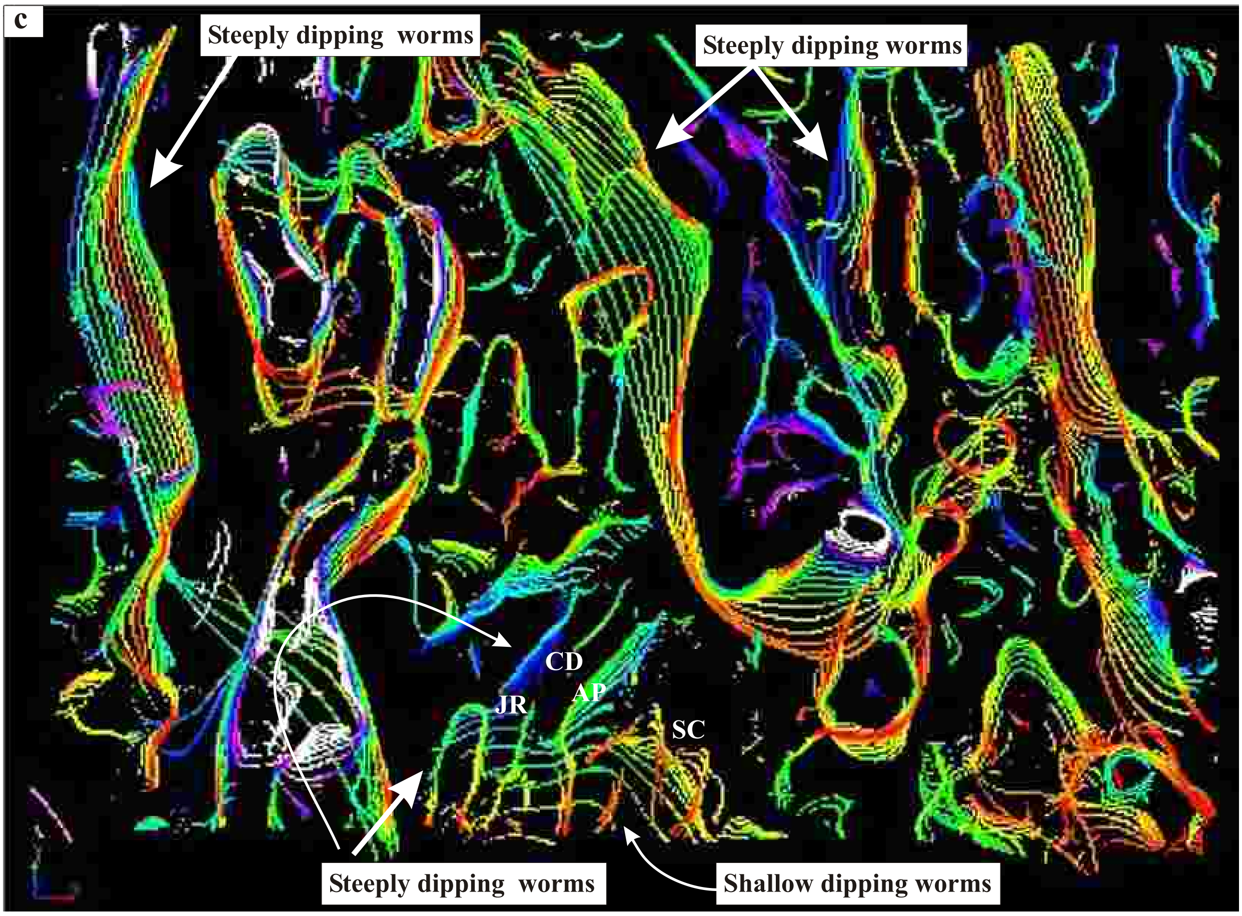
c
Steeply dipping worms
Steeply dipping worms
CD
AP
JR
SC
Steeply dipping worms
Shallow dipping worms

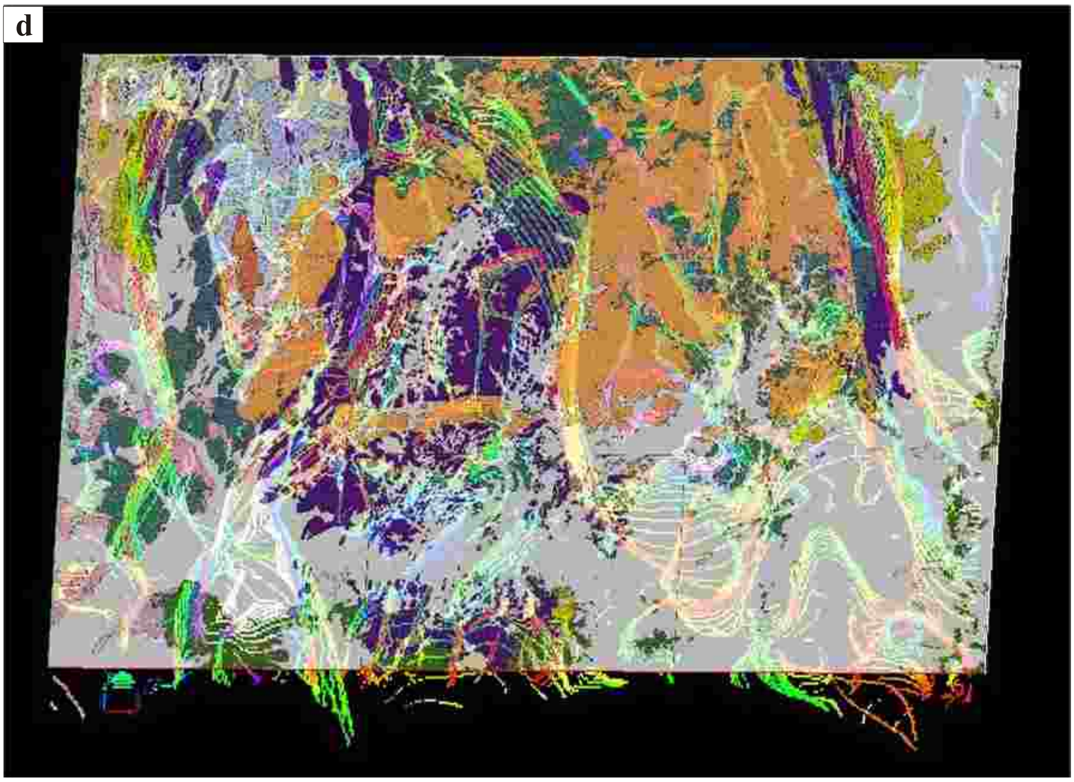
d

Fig. 10c,d

Fig. 11. (a) Sketch showing a P vertical section (parallel, subparallel to $S_{0/1/2}$ and $L^{0/1}{}_2$), an N section (perpendicular to both $S_{0/1/2}$ and $L^{0/1}{}_2$) and an H section (perpendicular to $S_{0/1/2}$ and parallel to $L^{0/1}{}_2$).
(b) Horizontal section showing relic-bedding laminae. Note garnet porphyroblasts with altered medians and rims.

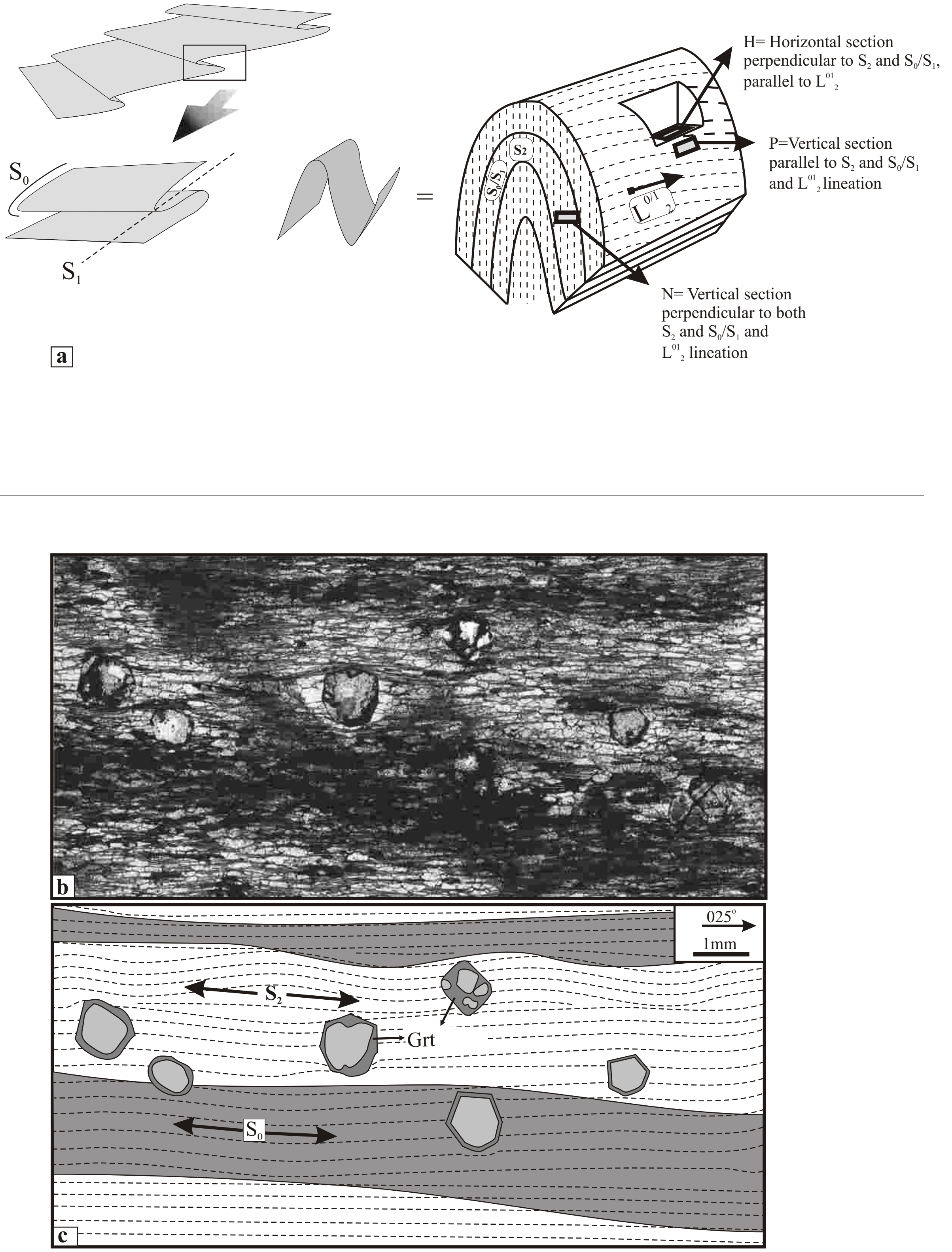

S_0
S_1
a
=
S_2
S_0/S_1
$L^{0/1}_2$
H= Horizontal section perpendicular to S_2 and S_0/S_1, parallel to L^{01}_2
P=Vertical section parallel to S_2 and S_0/S_1 and L^{01}_2 lineation
N= Vertical section perpendicular to both S_2 and S_0/S_1 and L^{01}_2 lineation
b
025°
1mm
S_2
Grt
S_0
c

Fig. 11

Fig. 12. (a,b&c) Photomicrographs showing subvertical S_2 overprinted by subhorizontal S_3 differentiated crenulation cleavage in the matrix. D_3 rotates steep S_2 to moderate dips. However, original subvertical nature of S_2 is locally preserved. Both top-to-the west and top-to-the-east asymmetries are present indicating coaxial deformation during D_3. Shear senses determined along the differentiated cleavage plane (Bell and Johnson, 1992). Samples SR61 (a), SR63 (b) and SR65 (c). Plane polarized light. Vertical thin sections. Single barbed arrow shows strike, bearing and way up.

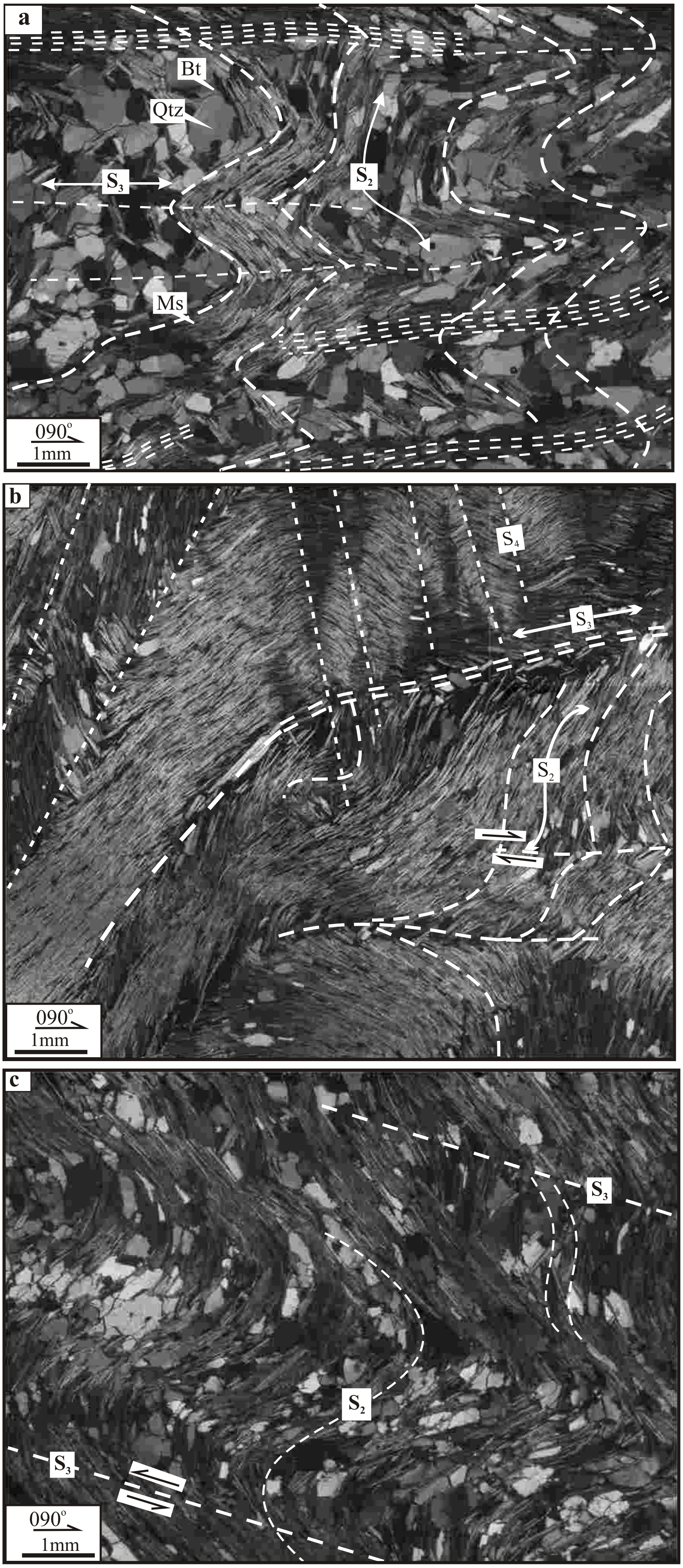

Fig. 12

Fig. 13. (a) Photomicrograph and (b) sketch of penetrative or continuous S_3 in pelite. Heterogonous, weekly developed subvertical S_4 overprints subhorizontal S_3. Note D_3 folded S_0. Sample SR6.1. Cross polarized light. Vertical thin section. Single barbed arrow shows strike, bearing and way up.
(c) Photomicrograph and line diagram of D_4 generated composite foliation $S_{2/4}$. S_2 was initially crenulated by the shallow S_3 foliation and this relationship can be seen in the low strain zones of D_4, for example at the center of the photomicrograph. S_2 in the hinge of S_3 remained steep. With progressive deformation S_2 is straightened out and re-used by D_4 shear and S_3 is reactivated (*cf.* Fig. 9f). Progressive non-coaxial deformation produced a composite $S_{2/3/4}$ foliation. S_5 is spaced, subhorizontal and weakly developed. Sample SR7E, Jasper Ridge subdomain. Cross polarized light. Vertical thin sections. Single barbed arrow shows strike, bearing and way up.

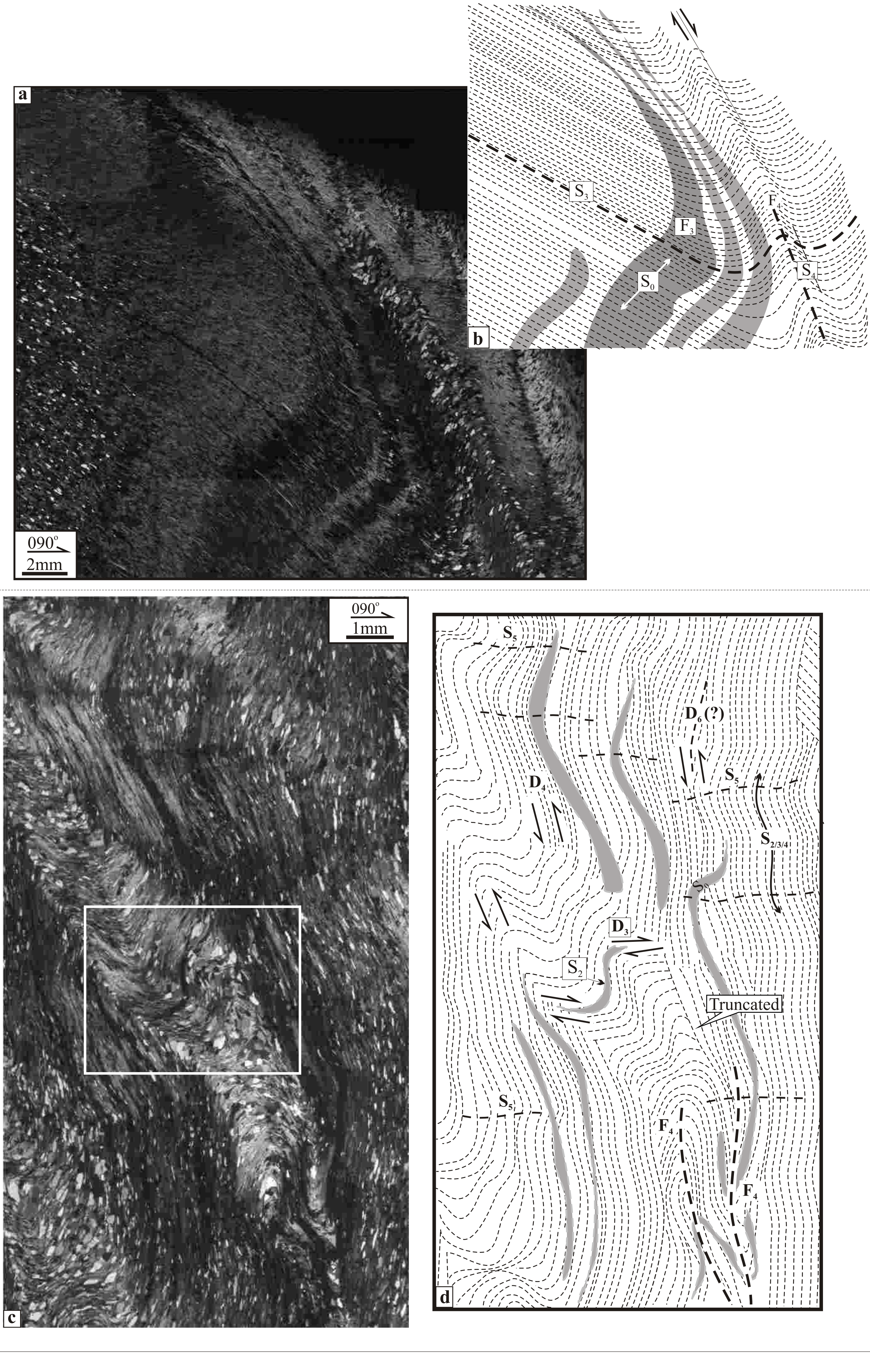
a
090°
2mm
b
S3
F3
S0
F4
S4
c
090°
1mm
d
S5
D6 (?)
D4
S5
S2/3/4
D3
S2
Truncated
S5
F4
F4

Fig. 13

Fig. 14. (a) Photomicrograph showing non-coaxial D_4 generated differentiated crenulation cleavage $S_{4\pm2/3}$ with dominant east-side-up or anticlockwise shear sense. Local clockwise asymmetries are also preserved. Deformation is partitioned into zones of progressive shearing (e.g., labeled X) and zones of progressive shortening (labeled Z). Sample SR7E-b, Jasper Ridge subdomain. Plane polarized light. Vertical thin sections. Single barbed arrow shows strike, bearing and way up.
(b) An example showing development of steep S_2 crenulated by shallow S_3 and subsequently overprinted by D_4. D_4 shear is clockwise and synchronously straightened out and re-used S_2 and reactivated S_3 and S_0. The left side of the photomicrograph is a composite $S_{0/2/3/4}$ foliation (*cf.* with fig. 9e). Sample SR77, Jasper Ridge subdomain. Plane polarized light. Vertical thin sections. Single barbed arrow shows strike, bearing and way up.

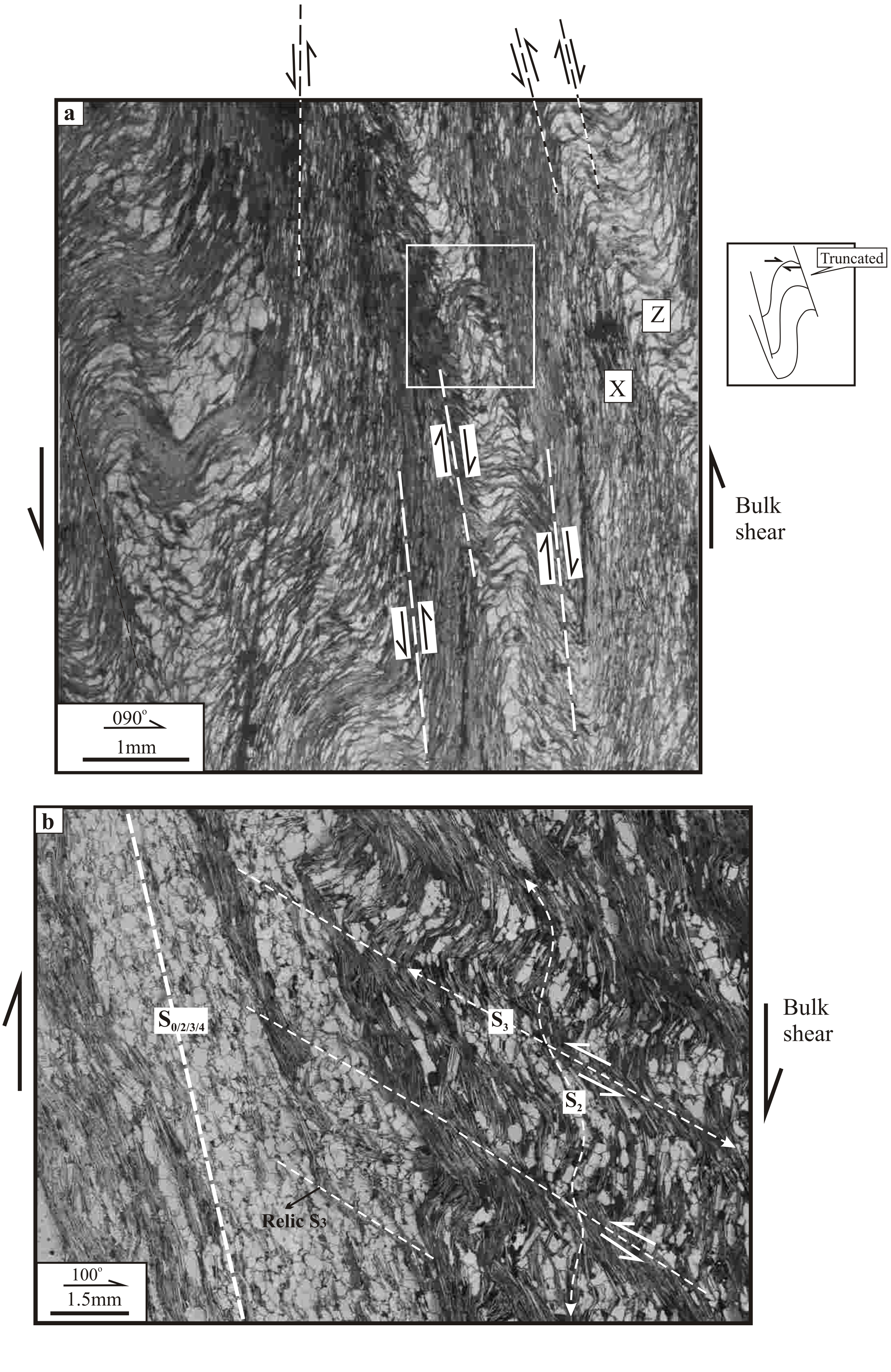
a
Truncated
Z
X
Bulk
shear
090°
1mm
b
S0/2/3/4
S3
S2
Relic S3
Bulk
shear
100°
1.5mm

Fig. 14

Fig. 15. Conceptual model for Jasper Ridge/Camel Dam domain. (a) Regional D_2 fold formed by west-east lateral shortening and generation of a regional S_2 cleavage. (b) The overprinting effects of D_3 on S_2. (c) Penetrative S_4 deformation non-coaxial at thin section to outcrop scale but coaxially developed at the domain scale. During D_4, S_4 differentiated cleavage will reactivate S_3 and S_0, and reuses S_2 as an axial plane foliation. (d) Further deformation destroys remaining hinges and rotates all fabrics into parallelism to form the composite foliation. D_4 reactivation shear becomes progressively less important, and more steeply oriented with increasing rotation of pre-D_4 fabrics into the S_4 shear plane.

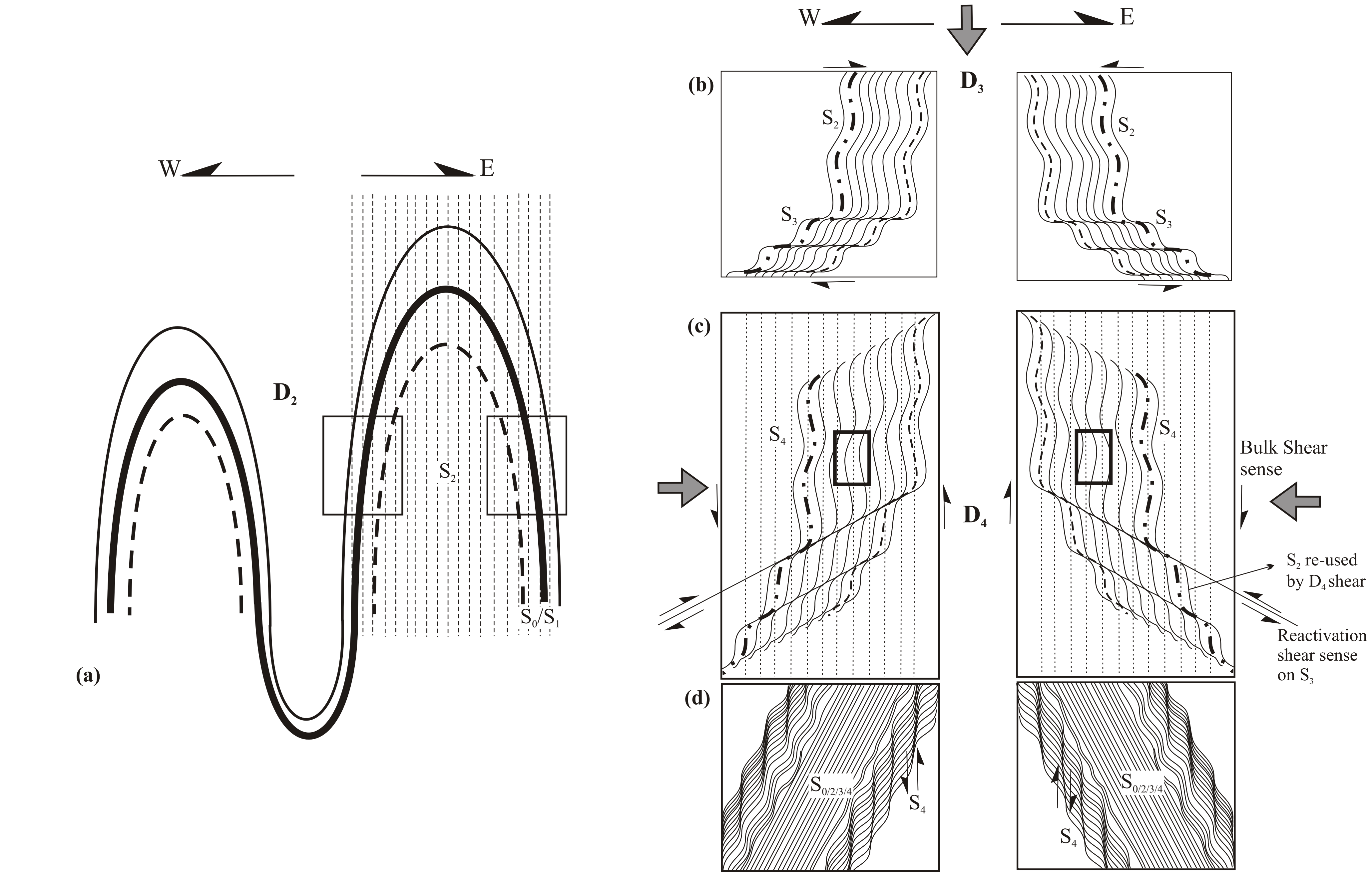

W
E
D2
S2
S0/S1
(a)
(b)
D3
S2
S3
(c)
S4
D4
Bulk Shear sense
S2 re-used by D4 shear
Reactivation shear sense on S3
(d)
S0/2/3/4
S4

Fig. 15

Fig 16. Photomicrographs of staurolite porphyroblasts with inclusion poor (a) to inclusion rich (d) cores with staircase geometry. Porphyroblasts preserve S_2 during D_3 and S_3 during D_4, indicating two stages of porphyroblast growth.
(c&f) Line diagrams of S_2 and S_3 showing the anticlockwise asymmetry of S_2 into S_3. S_3 is horizontal and continuous with steep S_4 with clockwise asymmetry. This anticlockwise from S_2 to S_3 and clockwise from S_3 to S_4 form staircase inclusion trail geometry. Rotation models cannot explain this relationship as shown in (a). Samples SR8.1 (a) and SR8.2 (d) north of the Camel Dam subdomain. Crossed polarized light. Vertical thin sections. Single barbed arrow shows strike, bearing and way up.

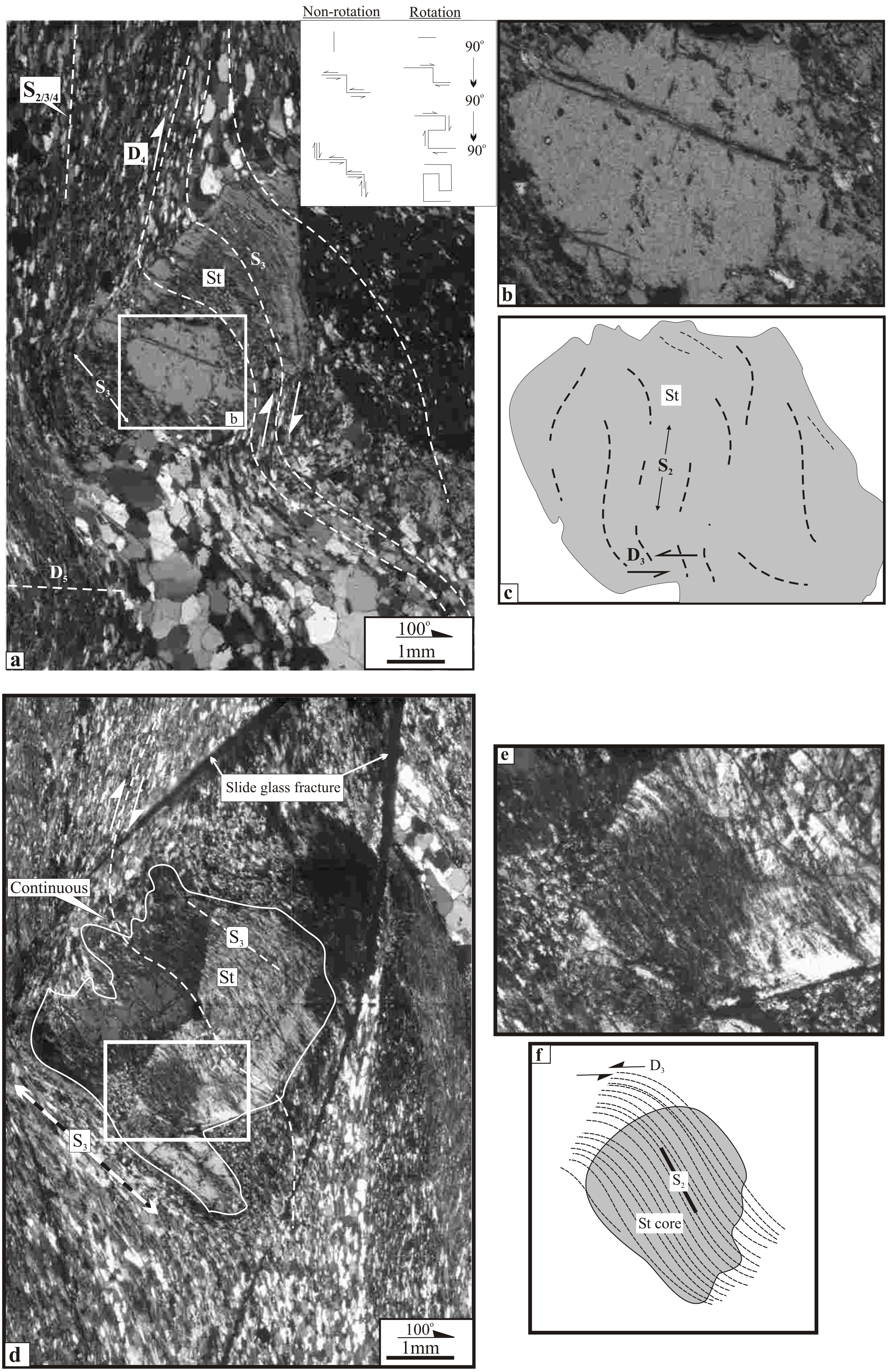
Non-rotation
Rotation
90º
90º
90º
S2/3/4
D4
S3
St
S3
b
D5
100º
1mm
a
b
St
S2
D3
c
Slide glass fracture
Continuous
S3
St
S3
100º
1mm
d
e
f
D3
S2
St core

Fig. 16

Fig. 17. (a) Photomicrograph and (b) line drawing showing andalusite porphyroblast at the upper right corner with inclined S_2 inclusion trails truncated with the matrix. The inclined nature of inclusion trails is possibly due to D_3 effect, which could be reactivated out later during D_4 in the matrix. (c) Sillimanite aligned parallel to S_4. Samples SR7B-f. North of the Jasper Ridge subdomain. Cross polarized light. Vertical thin sections. Single barbed arrow shows strike, bearing and way up.

(d) Andalusite porphyroblast partially pseudomorphed by coarse grained muscovite. Inclusion trail patterns deduced from high magnification. Two generations of Ms can be observed. First-generation Ms parallel to S_3 and second-generation Ms parallel to S_4. Samples SR8c. North of the Camel Dam subdomain. Cross polarized light. Vertical thin section. Single barbed arrow shows strike, bearing and way up.

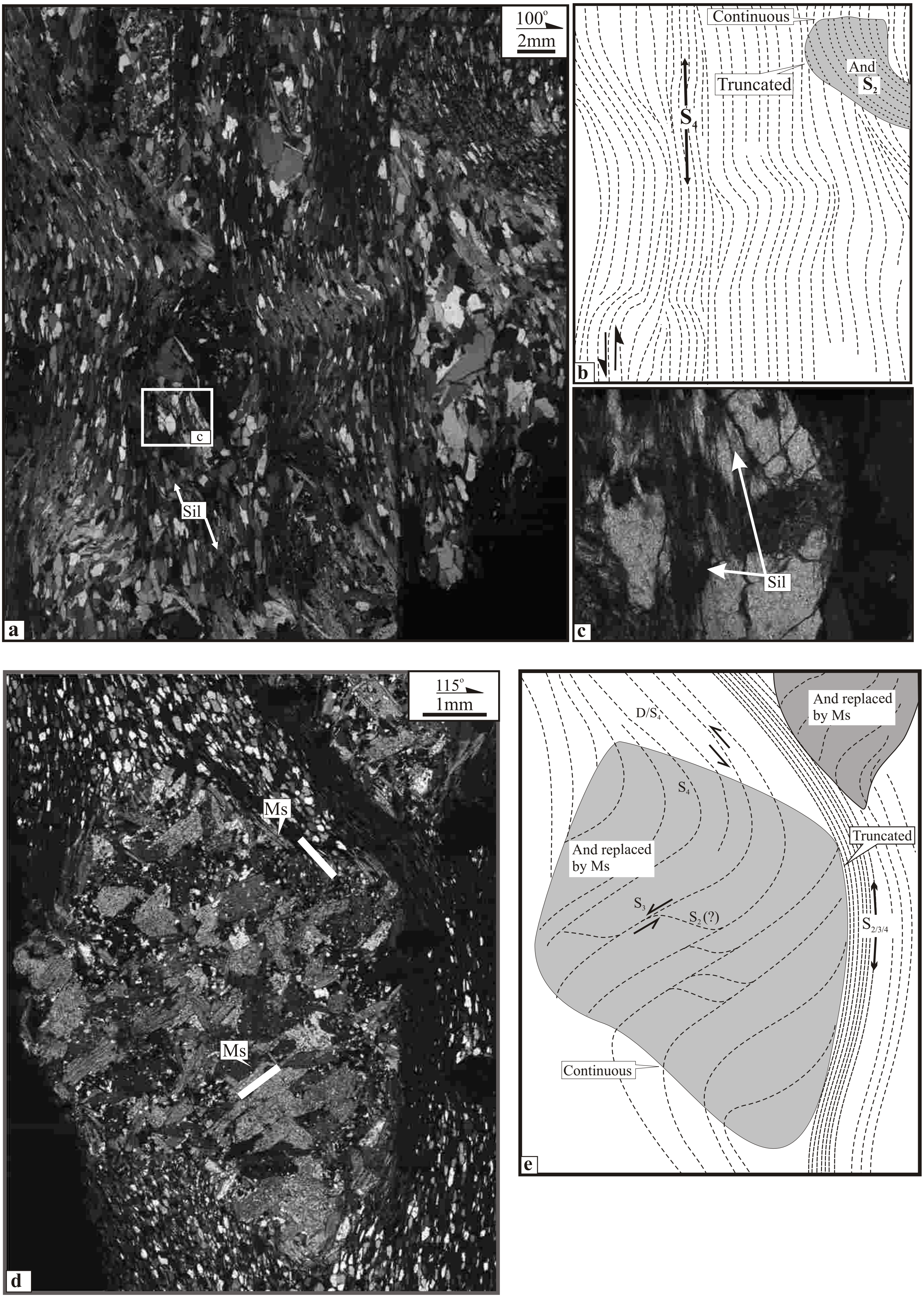

100°
2mm
c
Sil
a
Continuous
Truncated
And
S2
S4
b
Sil
c
115°
1mm
Ms
Ms
d
And replaced by Ms
D/S4
S4
And replaced by Ms
Truncated
S3
S2 (?)
S2/3/4
Continuous
e

Fig. 17

Fig. 18. (a) Shows relic garnet porphyroblasts with altered reaction rims preserved in partially pseudomorphed andalusite porphyroblast. The relic nature and altered reactions rims of garnet porphyroblasts in andalusite indicate low-pressure overprint (in this case And) and that the garnet porphyroblasts were resorbed during decompression (e.g., Garćia-Casco and Torres-Roldán, 1996). Sample SR8A Jasper Ridge subdomian. Plane polarized light. Vertical thin section. Single barbed arrow shows strike, bearing and way up.
(b) Photomicrographs and details shown in (c,d&e). Fibrolite aligned along steep S_2 foliation in the Anitra Prospect domain and subsequently folded by D_3. Samples SR75. Jasper Ridge subdomain. Plane polarized light. Vertical thin sections. Single barbed arrow shows strike, bearing and way up.

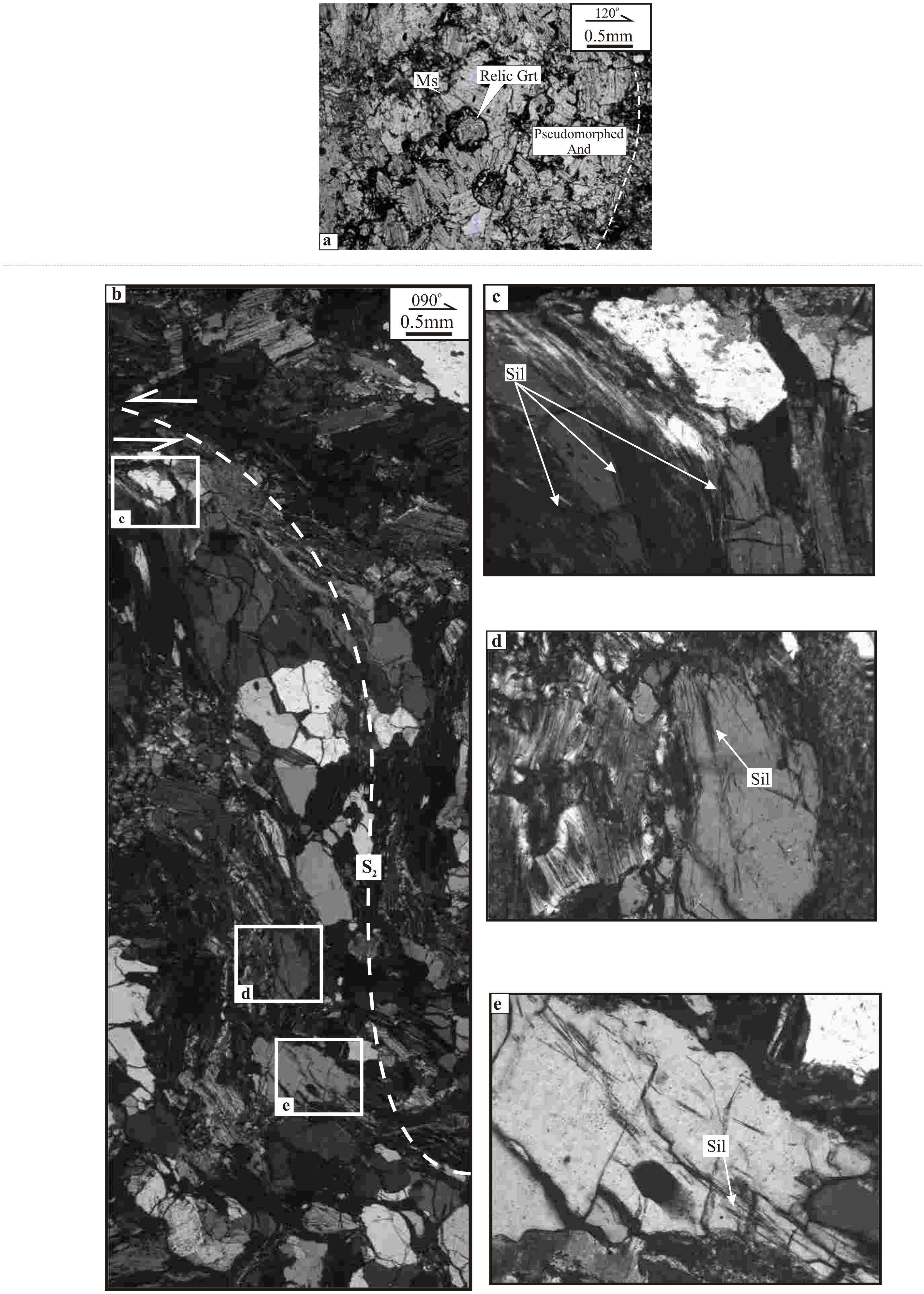
120°
0.5mm
Ms
Relic Grt
Pseudomorphed And
a
b
090°
0.5mm
c
d
e
S2
Sil
Sil
Sil

Fig. 18

Fig. 19. (a) The asymmetry switch method (Hayward, 1990; Bell et al., 1995). If asymmetric microstructures, such as sigmoidal inclusion trails in porphyroblasts, are observed on a fanned array of oriented thin sections maintaining the same viewing direction, then a flip in asymmetry occurs where the axis is crossed. This is the foliation intersection axis or FIA.

(b – f) Asymmetry method to determine the FIA in sample SR8.1. (a&b) Staurolite porphyroblasts with clockwise, sigmoidal shaped inclusion trails – vertical thin sections striking 010^o and 020^o. (d&f) Staurolite porphyroblasts with opposite asymmetries or anticlockwise, sigmoidal or slightly staircase shaped inclusion trails – vertical thin sections striking 030^o and 040^o. FIA at 025^o.

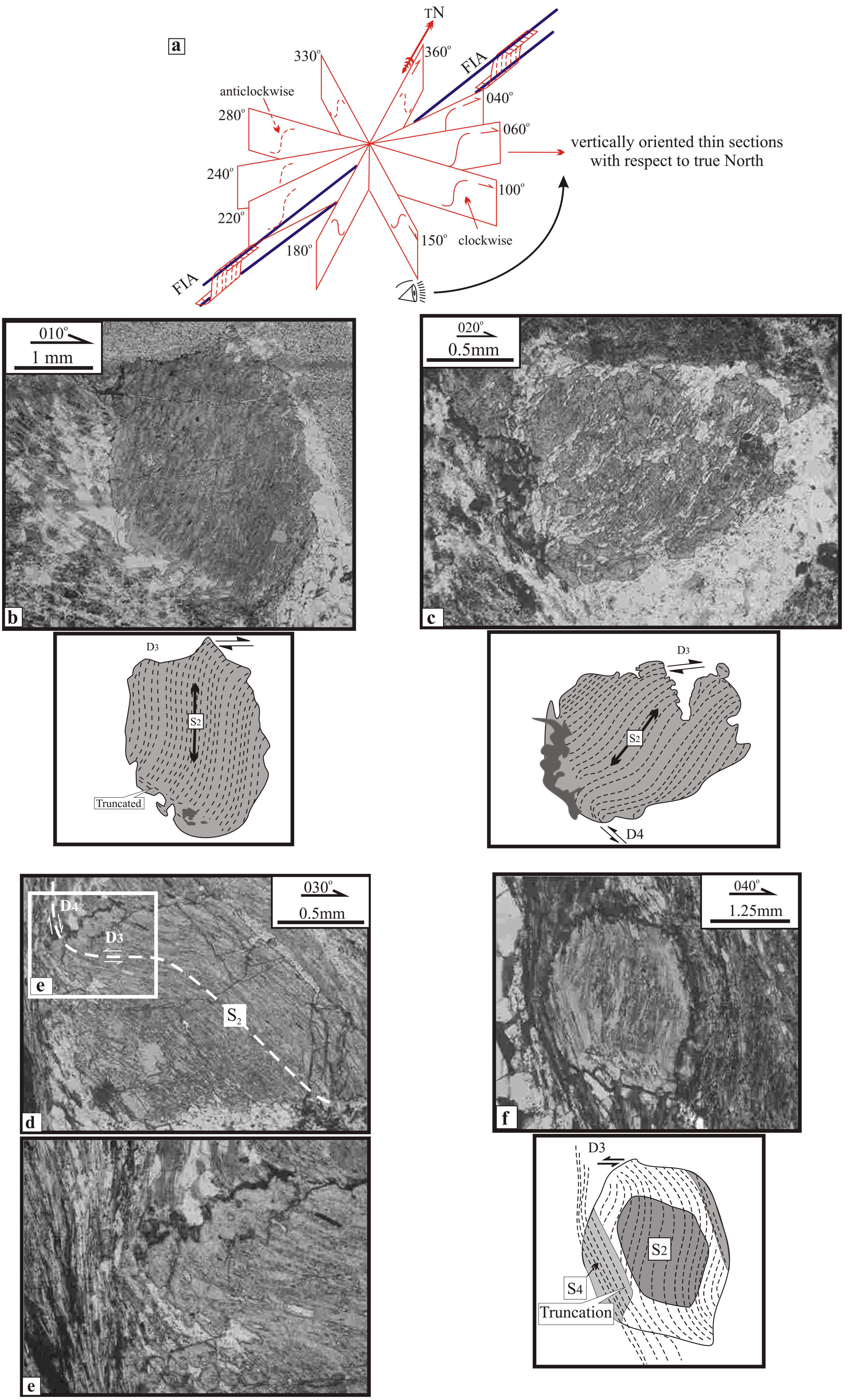
a
TN
330°
360°
FIA
040°
anticlockwise
280°
060°
vertically oriented thin sections
with respect to true North
240°
100°
220°
clockwise
150°
180°
FIA
010°
1 mm
b
020°
0.5mm
c
D3
S2
Truncated
D3
S2
D4
030°
0.5mm
D4
D3
e
S2
d
040°
1.25mm
f
e
D3
S2
S4
Truncation

Fig. 19

Fig. 20. P-T pseudosection in KFMASH (+Ms+Qtz+H_2O) for sample SR8.1. The sample consists of St-Ms-Bt schist and partially pseudomorphed And. Al_2O_3= 10.63, MgO=2.15, MnO=0.00; FeO=5.38, K_2O=2.30 (mol%). The P-T path is based on the appearance and disappearance of D_2 index minerals, as they preserve N-S FIA (see text for discussion). Metamorphic field gradient is shown on the pseudosection. Zone 1 is for Jasper Ridge/Camel Dam domain, whereas zone 2 is for Anita Prospect and Sandy Creek domains.

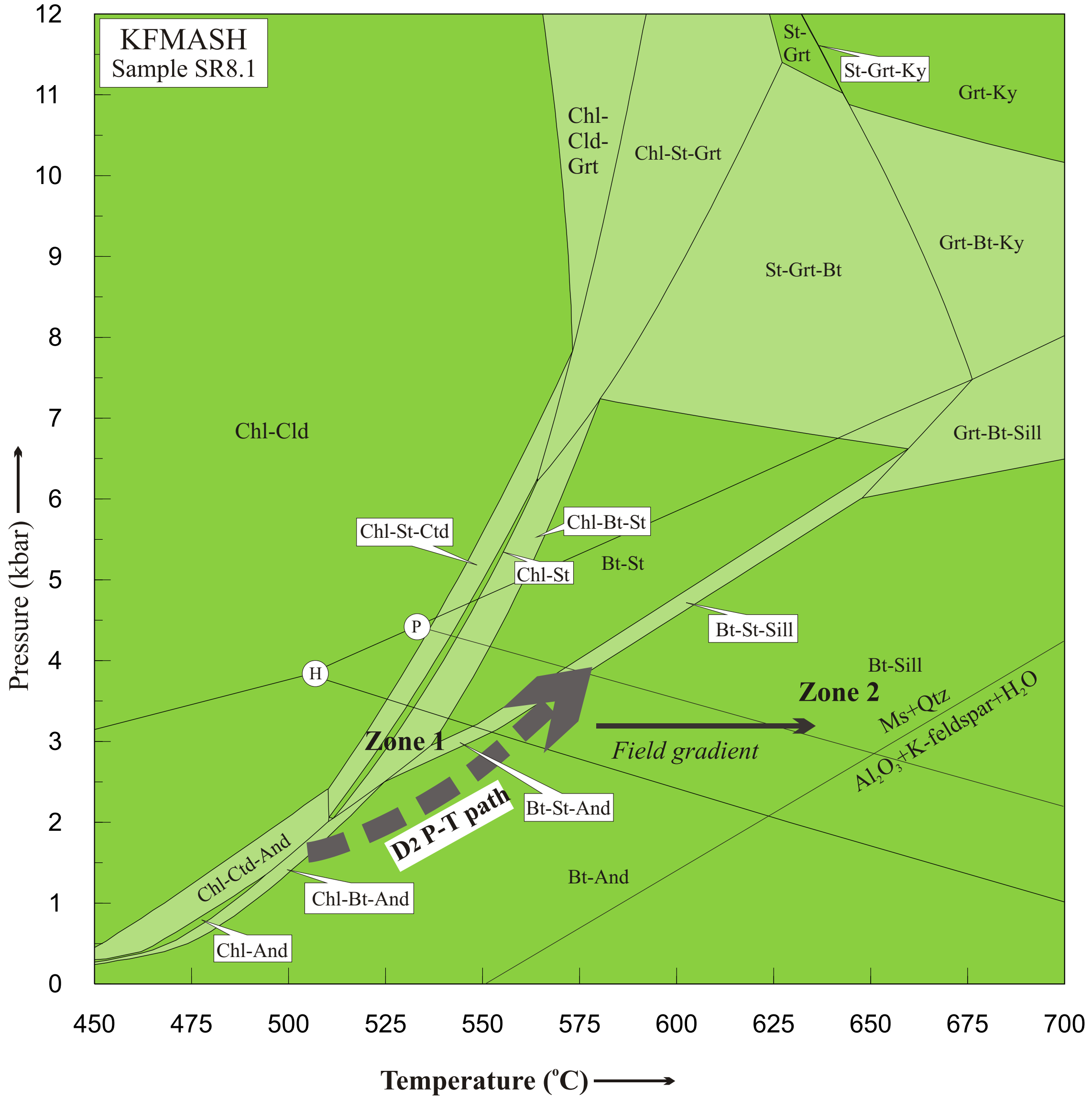
KFMASH
Sample SR8.1
12
11
10
9
8
7
6
5
4
3
2
1
0
Pressure (kbar)
450
475
500
525
550
575
600
625
650
675
700
Temperature (°C)
Chl-Cld
Chl-Cld-Grt
Chl-St-Grt
St-Grt
St-Grt-Ky
Grt-Ky
Grt-Bt-Ky
St-Grt-Bt
Grt-Bt-Sill
Chl-St-Ctd
Chl-Bt-St
Chl-St
Bt-St
Bt-St-Sill
Bt-Sill
P
H
Zone 1
Zone 2
Field gradient
Ms+Qtz
Al2O3+K-feldspar+H2O
Bt-St-And
D2 P-T path
Chl-Ctd-And
Chl-Bt-And
Chl-And
Bt-And

Fig. 20

Fig. 21. (a) Tectonic history for Sandy Creek and Anitra Prospect domains. D_2 crustal shortening by folding and generation of a regional penetrative S_2 cleavage. D_3 heterogeneously developed broadly coaxial subvertical shortening or gravitational collapse. S_3 spaced subhorizontal cleavage related with D_3. From micro- to macroscopic scale S_3 is seen to postdate S_2. D_3 is intensely developed in the Sandy Creek due to high relative abundance of incompetent units or pelites.

(b) Conceptual model after Giles and MacCready (1997) and MacCready et al. (1998) based on the interpretations of Mt Isa deep seismic section. The figure is scanned from Giles and MacCready (1997). A. Extension phase B. Initial thin-skinned shortening and nappe-style folding. C. Continued shortening, thick-skinned deformation and upright folding associated with D_2.

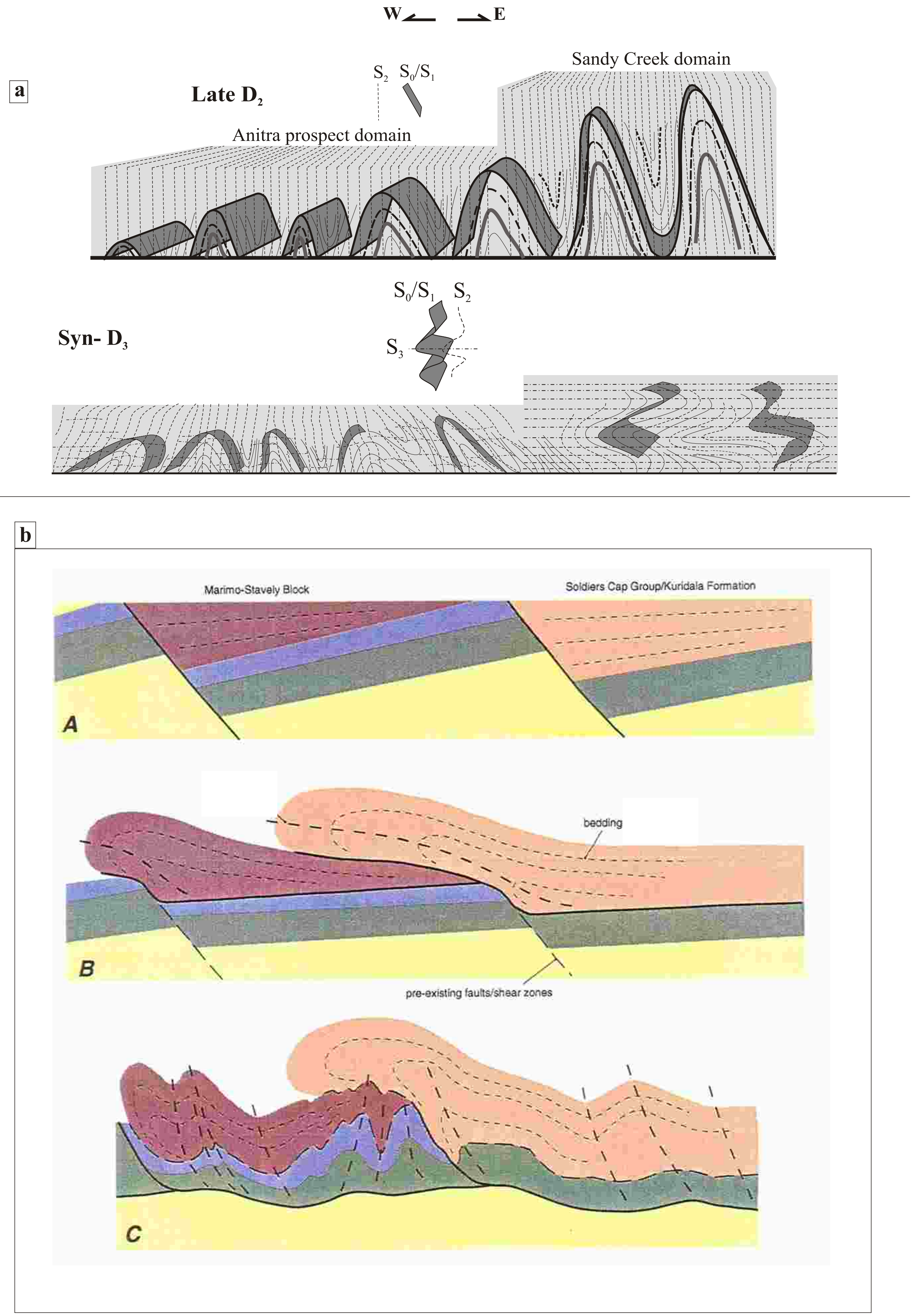

W
E
a
Late D_2
S_2
S_0/S_1
Anitra prospect domain
Sandy Creek domain
Syn- D_3
S_0/S_1
S_2
S_3
b
Marimo-Stavely Block
Soldiers Cap Group/Kuridala Formation
A
bedding
B
pre-existing faults/shear zones
C

Fig. 21

Section – B

Microstructural evidence for N-S shortening in the Mount Isa Inlier: the preservation of early W-E trending foliations in porphyroblasts revealed by independent 3-D measurement techniques

(Figures and Tables)

Fig. 1. (a) Outline map of the Mount Isa Inlier showing Western Fold Belt (WFB), Kalkadoon-Leichhardt Belt (KLB) and Eastern Fold Belt (EFB). (b) Regional geological map of the Eastern Fold Belt showing major lithotectonic units and location of the study area (modified after Blake, 1987; Giles and MacCready, 1997; Williams, 1998; Marshall and Oliver, 2001). Ages after Page and MacCready (1997), Page and Sun (1998).

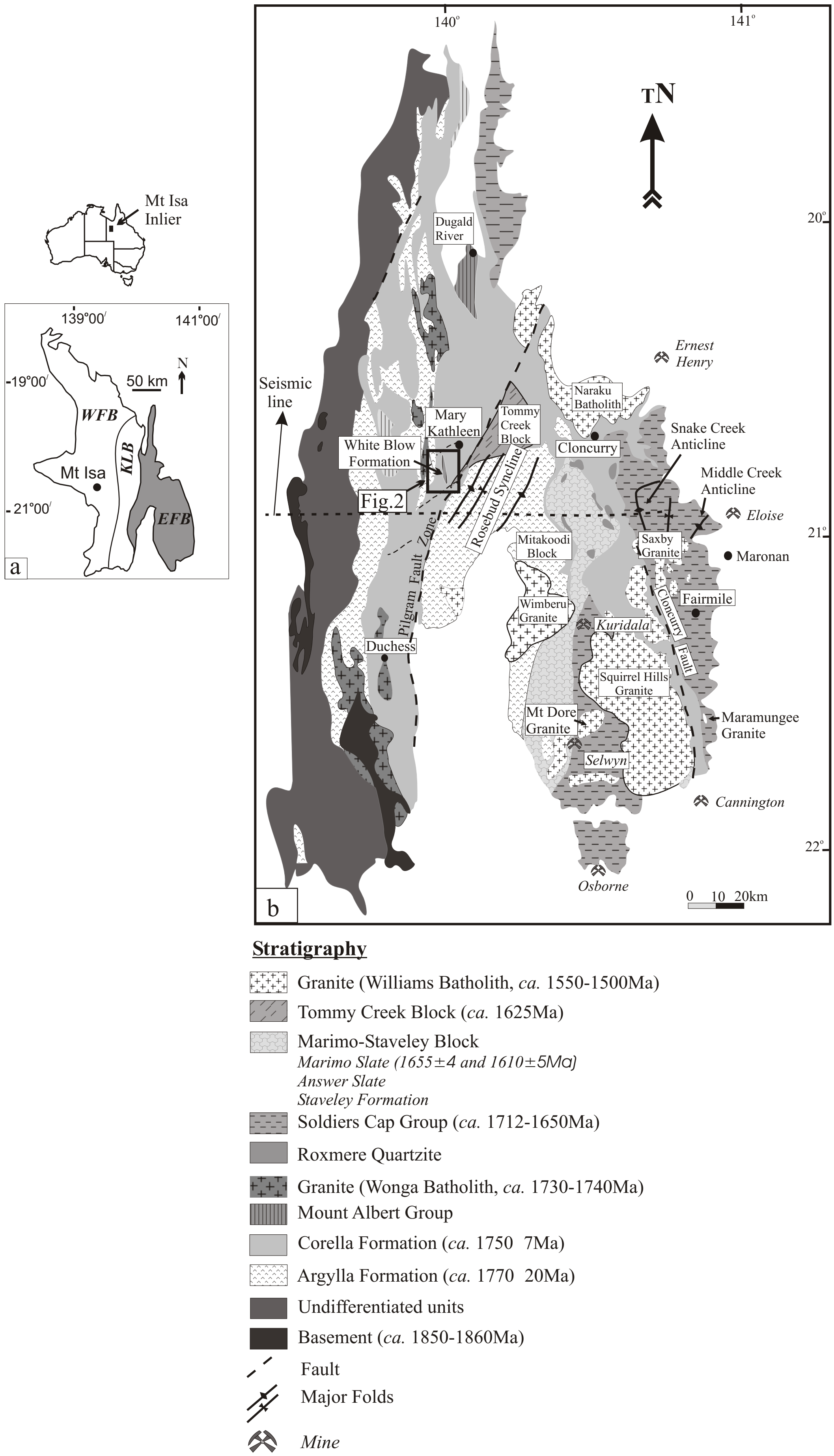
Mt Isa Inlier
139°00′
141°00′
19°00′
21°00′
50 km
N
WFB
KLB
EFB
Mt Isa
a
140°
141°
20°
21°
22°
N
Dugald River
Seismic line
Mary Kathleen
Tommy Creek Block
White Blow Formation
Fig.2
Naraku Batholith
Cloncurry
Ernest Henry
Snake Creek Anticline
Middle Creek Anticline
Eloise
Rosebud Syncline
Pilgram Fault Zone
Mitakoodi Block
Saxby Granite
Maronan
Wimberu Granite
Fairmile
Kuridala
Cloncurry Fault
Duchess
Squirrel Hills Granite
Mt Dore Granite
Maramungee Granite
Selwyn
Cannington
Osborne
0 10 20km
b
Stratigraphy
Granite (Williams Batholith, ca. 1550-1500Ma)
Tommy Creek Block (ca. 1625Ma)
Marimo-Staveley Block
Marimo Slate (1655±4 and 1610±5Ma]
Answer Slate
Staveley Formation
Soldiers Cap Group (ca. 1712-1650Ma)
Roxmere Quartzite
Granite (Wonga Batholith, ca. 1730-1740Ma)
Mount Albert Group
Corella Formation (ca. 1750 7Ma)
Argylla Formation (ca. 1770 20Ma)
Undifferentiated units
Basement (ca. 1850-1860Ma)
Fault
Major Folds
Mine

Fig. 1

Fig. 2. (a) Edge enhanced Landsat band-7 image of the White Blow Formation and adjacent Mary Kathleen Group units. (b) Geological map of the White Blow Formation and adjacent Mary Kathleen Group units (modified from Whitelock, 1989) showing sample locations. Samples with white dots were utilized for 'asymmetry switch' and 'FitPitch' FIA analysis. The prefix WB (stands for White Blow) is removed for each sample (see text for discussion). Grid numbers refer to Australian Map Grid (AMG) zone 54 (c) Lower hemisphere equal-area stereo plots for planar and linear structures in the area.

Fig. 2. (a) Landsat imagery courtesy of NASA Goddard Space Flight Center and U.S. Geological Survey.

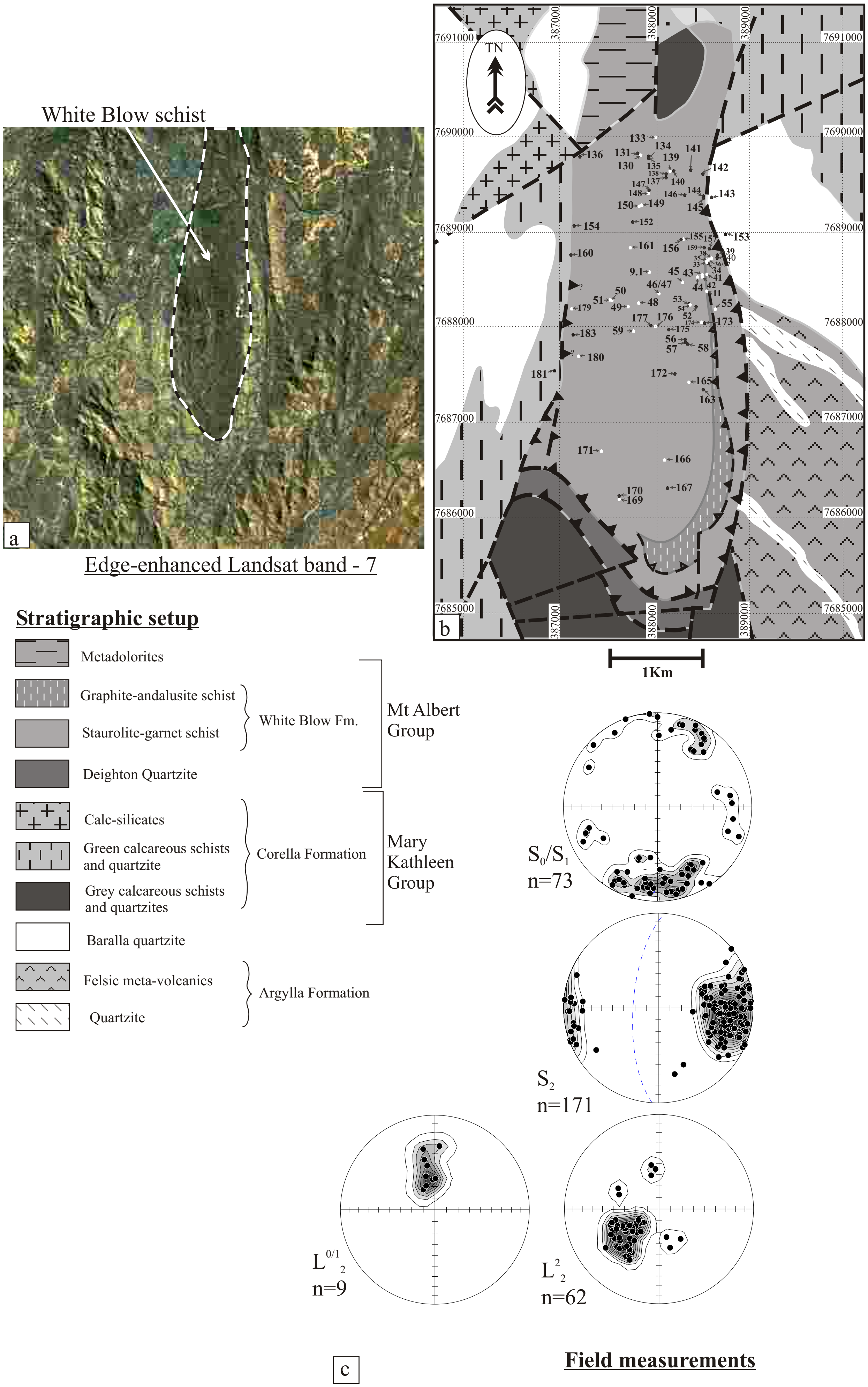
White Blow schist
a
Edge-enhanced Landsat band - 7
TN
b
1Km
Stratigraphic setup
Metadolorites
Graphite-andalusite schist
Staurolite-garnet schist
White Blow Fm.
Deighton Quartzite
Mt Albert Group
Calc-silicates
Green calcareous schists and quartzite
Grey calcareous schists and quartzites
Corella Formation
Mary Kathleen Group
Baralla quartzite
Felsic meta-volcanics
Quartzite
Argylla Formation
S_0/S_1 n=73
S_2 n=171
$L^{0/1}_2$ n=9
L^2_2 n=62
c
Field measurements

Fig. 2

Fig. 3. (a) Spaced S_2 cleavage cross-cutting S_0//S_1 in calc-silicates. The garnets are too small (<1mm) to be visible. Length of the pencil within the photograph is 7cm. (b) Photomicrograph of horizontal oriented thin section showing spaced S_2 cross–cutting S_0//S_1. (c) Typical outcrop exposure of the White Blow schist with a pervasive S_2 schistosity. Photograph taken looking north. (d) Garnet-staurolite schist (same outcrop as Fig. 3c) with steeply southwest plunging L^2_2 biotite mineral lineation. View onto S_2 plane. Length of the pencil within the photograph is 2.5cm. Abbreviations after Kretz (1983).

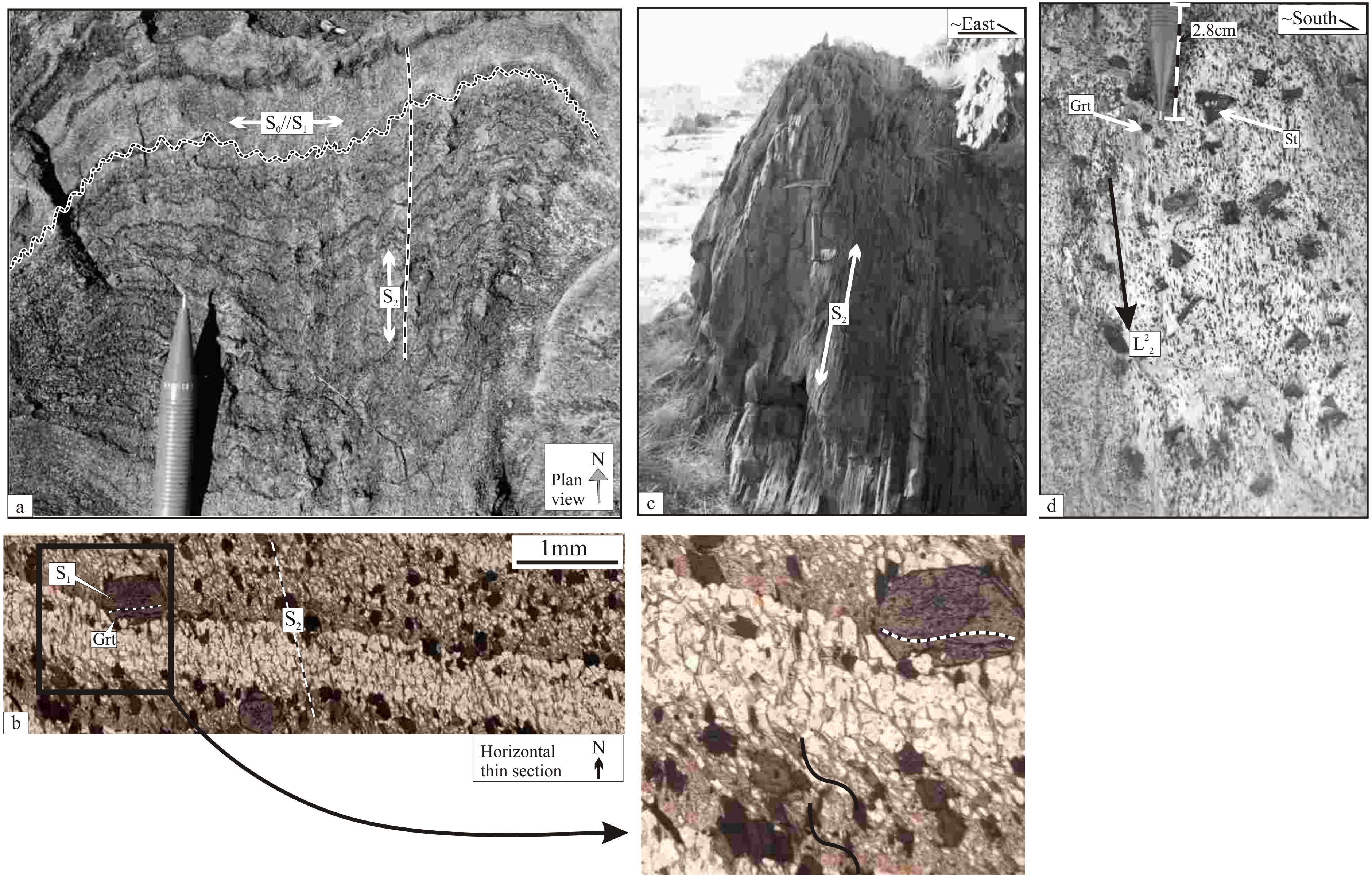

S0//S1
S2
Plan view
N
a
~East
S2
c
~South
2.8cm
Grt
St
L22
d
1mm
S1
Grt
S2
b
Horizontal thin section
N

Fig. 3

Fig. 4. Diagrams showing method developed by Hayward (1990) and Bell et al. (1995) for measuring the trends of foliation intersection/inflection axes (FIA) are measured. (a) Part of an array of vertically oriented thin sections at an acute angle to the fold axis, note switch in the inclusion trail patterns across the axis. If asymmetric microstructures are observed on fanned array of oriented thin section maintaining the same viewing direction, then swap in asymmetry occurs where the axis is crossed. This axis is called as foliation intersection or inflection axis. (b) Schematic sketches of vertically oriented thin sections with sigmoidal inclusion trail geometry. Asymmetry flip occurs from anticlockwise to clockwise. In this case, FIA lies in between these two thin sections at 000^{o}. (c) An example of how FIA and FIA range are determined graphically. The FIA trend (dark line) corresponds to the crossover, or switch in asymmetries. The FIA range (light gray band) is defined by the interval in which both asymmetries are present. (d) Graphical representation of multi-FIAs for garnet core and staurolite rim in single sample (WB149).

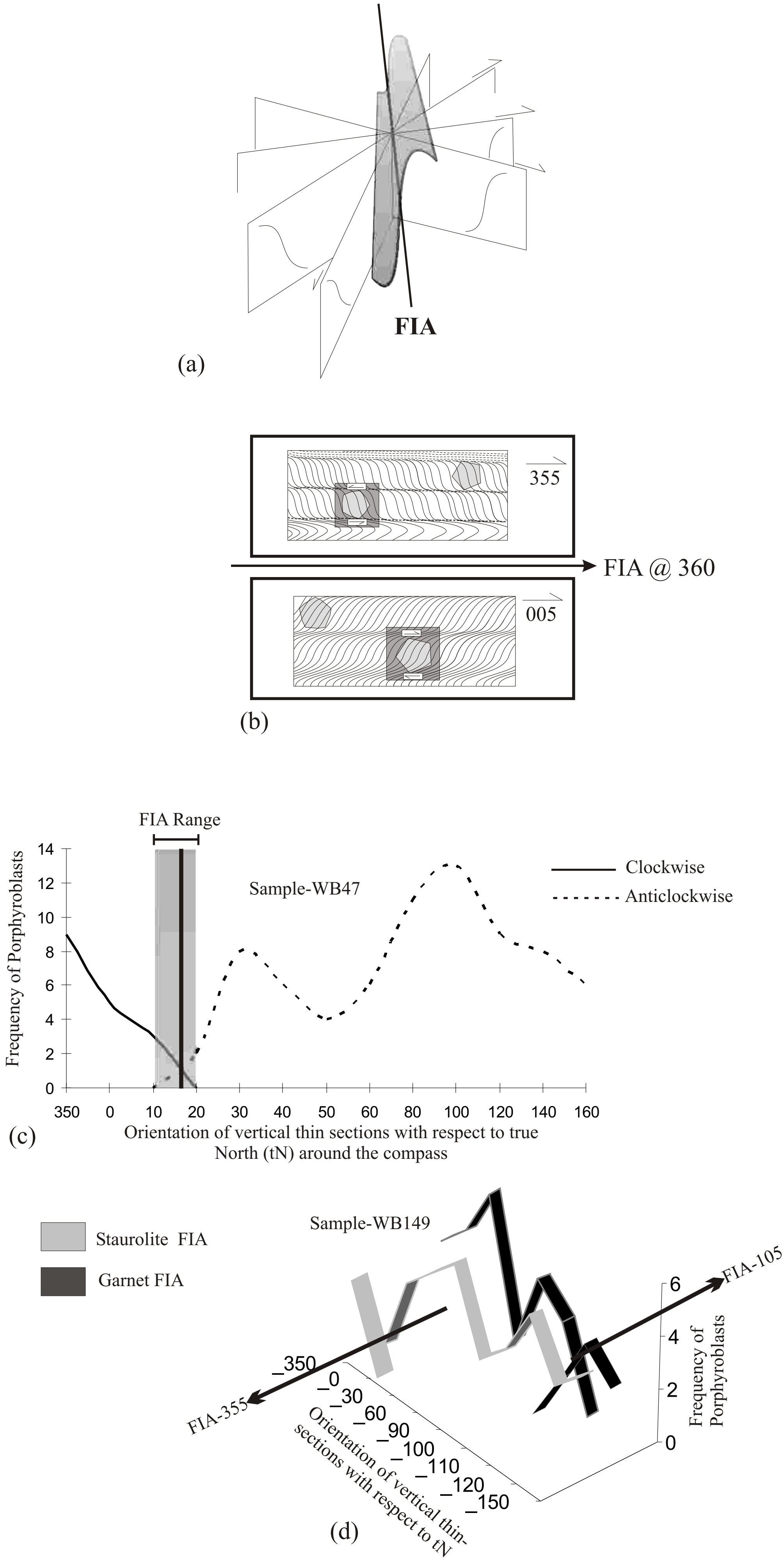
FIA
(a)
355
FIA @ 360
005
(b)
FIA Range
Sample-WB47
Clockwise
Anticlockwise
Frequency of Porphyroblasts
14
12
10
8
6
4
2
0
350
0
10
20
30
40
50
60
80
100
120
140
160
(c)
Orientation of vertical thin sections with respect to true North (tN) around the compass
Staurolite FIA
Garnet FIA
Sample-WB149
FIA-105
FIA-355
6
4
2
0
Frequency of Porphyroblasts
350
0
30
60
90
100
110
120
150
Orientation of vertical thin-sections with respect to tN
(d)

Fig. 4

S. No.	Easting	Northing	FIA trend (true North)				Mtx	FIA 1		FIA 2		FIA 3		FIA 4			FitPitch FIA	
			Grt		*St*													
			Core	*Rim*	*Core*	*Rim*		Grt	St	Grt	St	Grt	St	Grt	St	Mtx		
WB47	388100	7688410		15		15								15	15		13	
WB41	388542	7688637		355	355									355	355		173	
WB38	388604	7688727				5									5		no data	
WB33	388550	7688694		95		10		95							10		98	
WB48	387828	7688263		90	90			90	90								95	9
WB11	388681	7688672	105		105			105	105								112	
WB35	388567	7688718				20									20		25	111
WB149	387854	7689285	105			355	355		105						355	355	293	
WB133	388010	7690005		115	115					115	115						280	
WB176	388003	7688017	115							115							107	
WB171	387434	7686695	115		115					115	115						284	
WB169	387619	7686205	120		120					120	120						288	
WB166	388105	7686616	85	15		15			85					15	15		82	
WB180	387189	7687698	85		85			85	85								85	174
WB179	387118	7688192	100			5			100						5		198	287
WB165	388367	7687426		15		15								15	15		193	
WB155	388294	7688940	150		150									150	150		346	
WB139	388163	7689650			85	120		85			120						81	
WB150	387843	7689284	355		355									355	355		174	
WB161	387739	7688844	85		85	105		85	85		105						82	337
WB148	387934	7689418		0		0								0	0		354	291
WB174	388502	7688059	355											355			351	
WB45	388293	7688477		5		5								5	5		350	
WB49	387712	7688222	85		85			85	85								73	
WB51	387527	7688292	5		100	0			100					5	5		285	
WB50	387537	7688290	105			105		105	105								289	
WB46	388045	7688258	5			5								5	5		352	
WB44	388448	7688532		15		15								15	15		189	
WB42	388600	7688680		5										5			194	
WB36	388570	7688720				105					105						103	
WB9.1	387895	7688562		135		135						135	135				321	
WB37	388600	7688820				355	0								355	0	159	
WB54	388370	7688241		5		20								5	25		192	
WB55	388607	7688217		0		0								0	0		169	
WB59	387772	7687969		95		95		95	95								287	
WB130	387848	7689821	85			85		85	85								80	
WB43	388551	7688563			105	0					105				0		100	354

Table-1. Sample locations with respect to Australian Map Grid (AMG) coordinates, the FIA trend measured in them, FIA sets based on their relative timings and 'FitPitch' FIA trend/plunge (symbols after Kretz, 1983). Mtx: Matrix

Fig. 5. A rose diagram of FIA trend with respect to true North determined from all garnet and staurolite porphyroblasts. Outer plot gives more details of data for FIA trends from garnet and staurolite porphyroblasts. Note that the WSW-ENE and WNW-ESE FIA trends were mainly obtained from the cores of the porphyroblasts, whereas NNW-SSE and SSW-NNE FIA trends are dominantly obtained from the rims of the individual porphyroblasts. Several independent growth phases of porphyroblasts have been identified based on FIAs. (b) 3-D conceptual model showing near-orthogonal multiple deformation history during O_1 and O_2 events of the Isan Orogeny deduced from detailed FIA analysis. Two distinct FIA sets can be recognized during O_1 event or N-S bulk shortening of the Isan Orogeny based not only on the FIA trends but also on the geometry of inclusion trail patterns. O_2 was responsible for W-E shortening, producing N-S FIA trend. Microstructural relationships show that porphyroblasts with N-S FIAs between 350^o-020^o have inclusion trails that are generally continuous with matrix (cf. Figs. 8 & 9).

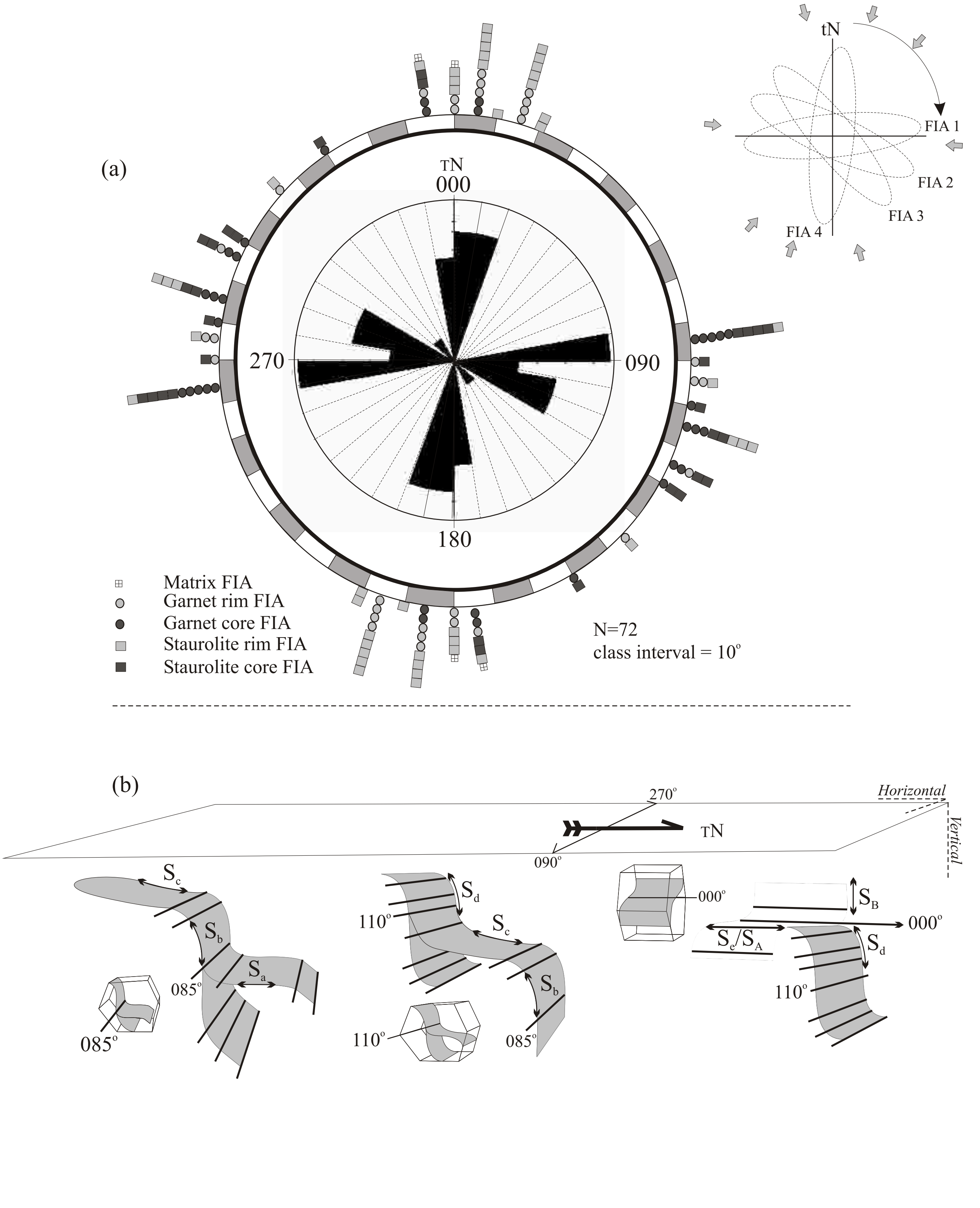
(a)
tN
000
090
180
270
Matrix FIA
Garnet rim FIA
Garnet core FIA
Staurolite rim FIA
Staurolite core FIA
N=72
class interval = 10°
FIA 1
FIA 2
FIA 3
FIA 4
(b)
270°
090°
Horizontal
Vertical
S_c
S_b
S_a
085°
110°
S_d
000°
S_B
S_e/S_A

Fig. 5

Fig. 6. (a & b) Photomicrograph of a staurolite porphyroblast hosting stage 3 differentiated crenulation cleavage in the core. The asymmetry associated with the cleavage is anticlockwise and have 100^{o}FIA trend (set 1). At the rim of the porphyroblast, shallow pitching S_c is overprinted. For 'FitPitch' analysis, the microstructures have been divided into 'A' and 'B' type (see text for discussion).
(c & d) Garnet preserved within staurolite porphyroblast. Both showing differentiated crenulation cleavage patterns. Much of the mica is inferred to have dissolved during porphyroblast growth. Crenulations are curved from sub-horizontal to sub-vertical with anticlockwise asymmetry and interpreted as S_a and S_b, respectively. Vertical thin section with single barbed arrow showing strike, bearing and way up and sample number (in this and subsequent photomicrographs).

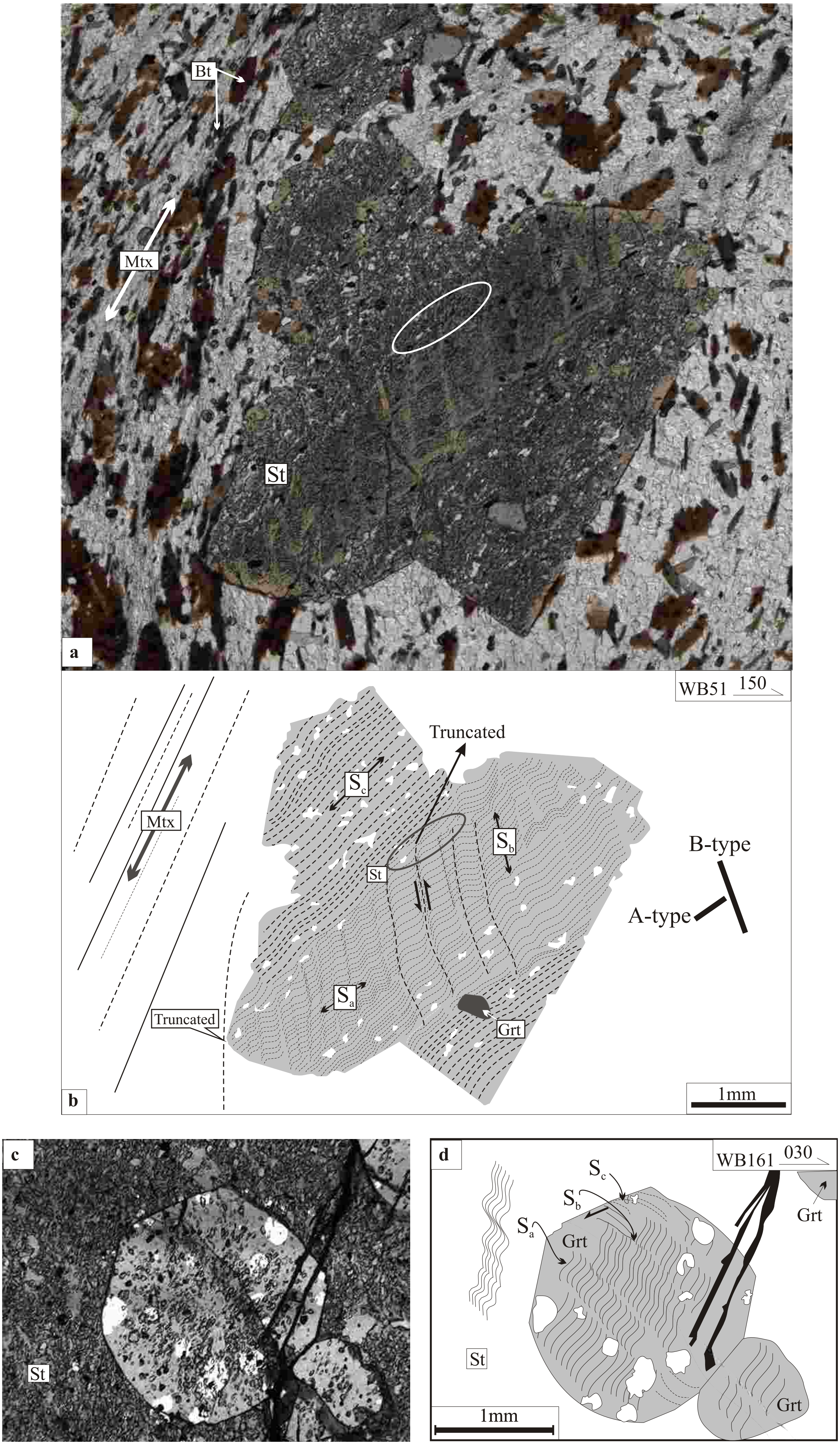

Bt
Mtx
St
a
WB51 150
Truncated
S_c
Mtx
S_b
St
B-type
A-type
S_a
Truncated
Grt
b
1mm
c
St
d
WB161 030
S_c
S_b
S_a
Grt
Grt
St
Grt
1mm

Fig. 6

Table-2. Microprobe analyses for garnet porphyroblast (see Fig. 7).

	core				median				rim		
	ID = 161_1	ID = 161_3	ID = 161_4	ID = 161_5	ID = 161_16	ID = 161_6	ID = 161_7	ID = 161_8	ID=161_18	ID = 161_9	ID=161_10
SiO2	37.96	38.28	38.41	38.01	38.75	38.48	38.76	39.13	39.01	38.57	38.69
Al2O3	21.37	21.48	21.34	20.83	21.14	21.52	21.68	21.65	21.94	21.26	20.85
TiO2	0.23	0.38	0.00	0.03	0.00	0.00	0.13	0.00	0.00	0.11	0.1
FeO	30.37	29.15	30.46	30.54	31.33	31.68	31.85	31.72	32.12	32.45	32.89
MnO	6.19	6.20	5.43	5.63	5.36	4.53	4.13	3.44	3.53	2.66	2.47
MgO	2.21	2.40	1.90	2.55	1.92	1.88	2.38	2.74	2.84	2.21	2.26
CaO	1.72	2.17	1.86	1.85	1.63	2.04	2.15	2.22	1.95	2.06	1.84
Na2O	0.3	0.18	0.00	0.12	0.00	0.00	0.00	0.00	0.00	0.00	0.00
K2O	0.00	0.16	0.00	0.05	0.07	0.00	0.00	0.05	0.05	0.00	0.11
Cl	0.07	0.03	0.10	0.03	0.00	0.09	0.00	0.00	0.00	0.09	0.09
Total	100.42	100.43	99.50	99.64	100.20	100.22	101.08	100.95	101.44	99.41	99.30
Almandine	70.99	68.61	72.99	70.76	74.12	75.01	74.02	73.88	74.26	77.78	78.73
Grossular	5.15	6.54	5.71	5.49	4.94	6.19	6.40	6.62	5.78	6.33	5.64
Pyrope	9.21	10.07	8.12	10.53	8.10	7.94	9.86	11.38	11.70	9.44	9.64
Spessartine	14.65	14.78	13.18	13.21	12.84	10.86	9.72	8.12	8.27	6.46	5.99
Fe/(Fe+Mg)	0.89	0.87	0.90	0.87	0.90	0.90	0.88	0.87	0.86	0.89	0.89

Fig. 7. P-T pseudosection calculated in MnNCKFMASH chemical system based on bulk XRF composition for sample WB161. Compositional contours (isopleths) corresponding to the real composition of garnet core (EDS probe analysis, see also Appendix-B) along with their errors indicated as light shaded thick lines. The isopleths intersect in the Chl-G-Bt-Pl field (abbreviations after Kretz, 1983 except for G=garnet) and yield P-T estimates for the garnet core growth that is, 3.7-4.4Kb/542-547^{o}C. Compositional maps of garnet show regular zoning patterns, where Mn typically decreases from core to rim, with very short reversal at the rim, and Fe is increases from core to rim.

*XRF bulk composition (wt%)**

SiO_2	Al_2O_3	FeO	MnO	MgO	CaO	Na_2O	K_2O
68.9	15.2	6.35	0.12	2.09	0.21	0.50	3.60

** Analysis were normalized to mol.% for calculations*

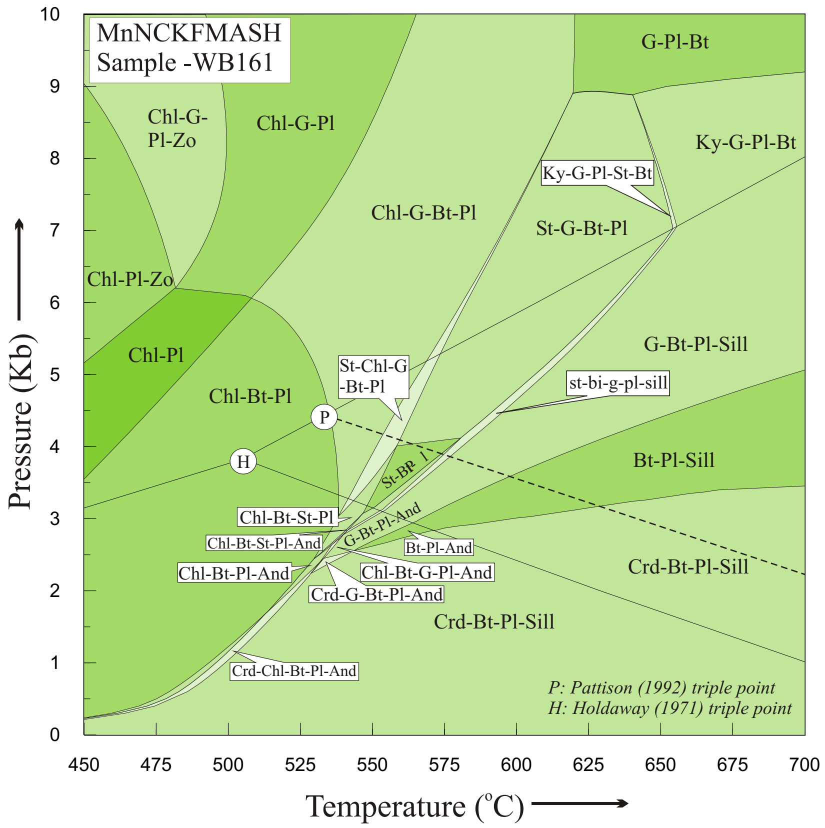

Grt compositional maps

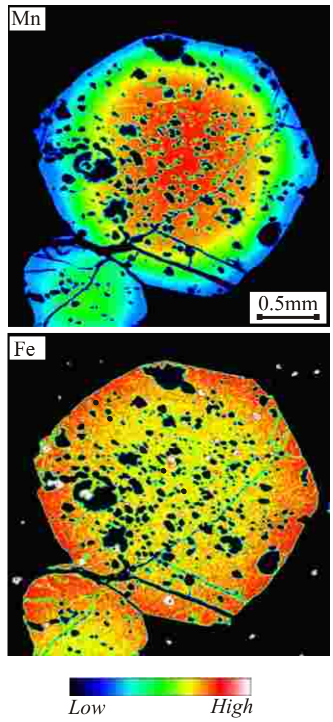

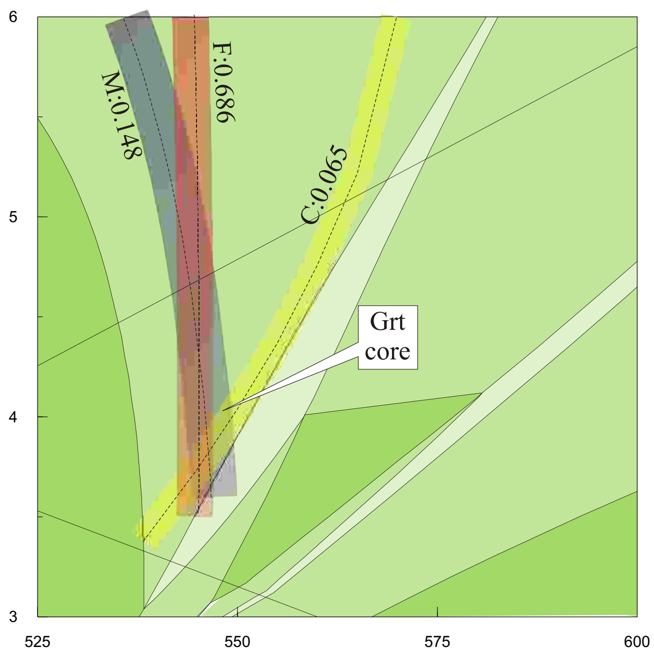

	*Grt core**		
SiO_2	38.28	38.41	38.48
TiO_2	0.38	0.00	0.00
Al_2O_3	21.48	21.34	21.52
FeO	29.15	30.46	31.68
MnO	6.2	5.43	4.53
MgO	2.4	1.9	1.88
CaO	2.17	1.86	2.04
Na_2O	0.18	0.00	0.00
K_2O	0.16	0.00	0.00
Cl	0.03	0.10	0.09
Total	100.43	99.5	100.22

** used in Grt core calculations (e.g., see Vance and Mahar, 1998 and chapter 4 of this dessertation)*

Fig. 7

Fig. 8. An example of subidioblastic staurolite porphyroblast showing sigmoidal inclusion trail geometry. (a) At high magnification, it was observed that the porphyroblast preserved differentiation rather than simple sigmoidal inclusion trail patterns. Anticlockwise asymmetry can be observed along differentiated seams preserved within the porphyroblast. The porphyroblast hosts deformation fabric elements, that is steeply to moderately pitching S_d to shallow pitching S_e/S_A and steeply pitching S_B. (b) S_d is partially truncated with S_e/S_A at the median region, whereas S_B is continuous with the matrix. (c) Garnet porphyroblast preserves straight steep S_B and are continuous with the matrix. (d & e) Garnet porphyroblast preserves simple sigmoidal inclusion trails with an inclusion-rich core and an inclusion-poor rim. Note that the inclusion trails are truncated by the matrix. The porphyroblast shows anticlockwise asymmetry from steep (core) to shallow (rim). However, at high magnification, differentiated crenulations within the steep trails can be inferred. The steep inclusion trails controlling the FIA (115^o) are interpreted as S_d curving to S_e, whereas those in between S_d are interpreted as S_c (see text for further discussion).

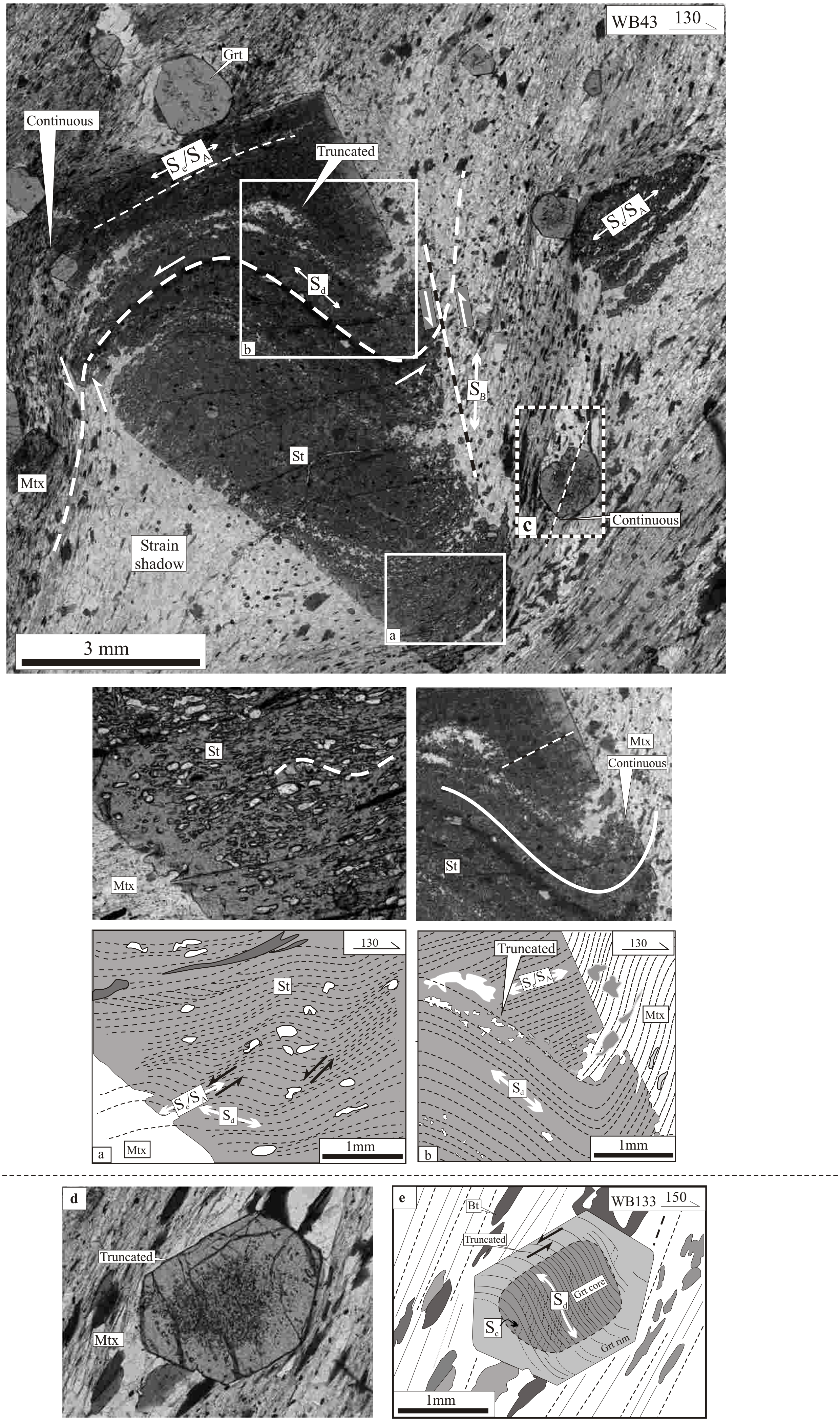

WB43
130
Grt
Continuous
S_e/S_A
Truncated
S_d
S_B
b
Mtx
St
c
Continuous
Strain shadow
a
3 mm
St
Mtx
Mtx
Continuous
St
130
St
S_e/S_A
S_d
a
Mtx
1mm
130
Truncated
S_e/S_A
Mtx
S_d
b
1mm
d
Truncated
Mtx
e
WB133
150
Bt
Truncated
Grt core
S_d
S_c
Grt rim
1mm

Fig. 8

Fig. 9. Excellent examples of continuous and truncated inclusion trail microstructures. 000^o – 020^o FIAs have been obtained from all those garnet and staurolite porphyroblasts, which are continuous with the matrix foliation (as shown in a). However, FIA ranges between 350^o – 000^o are either partially truncated or continuous with the matrix (e.g., as shown in b and c). Porphyroblast preserving FIA set 4 have subhorizontal inclusions and are interpreted as S_e of O_1 or S_A of O_2 followed by steep S_B.

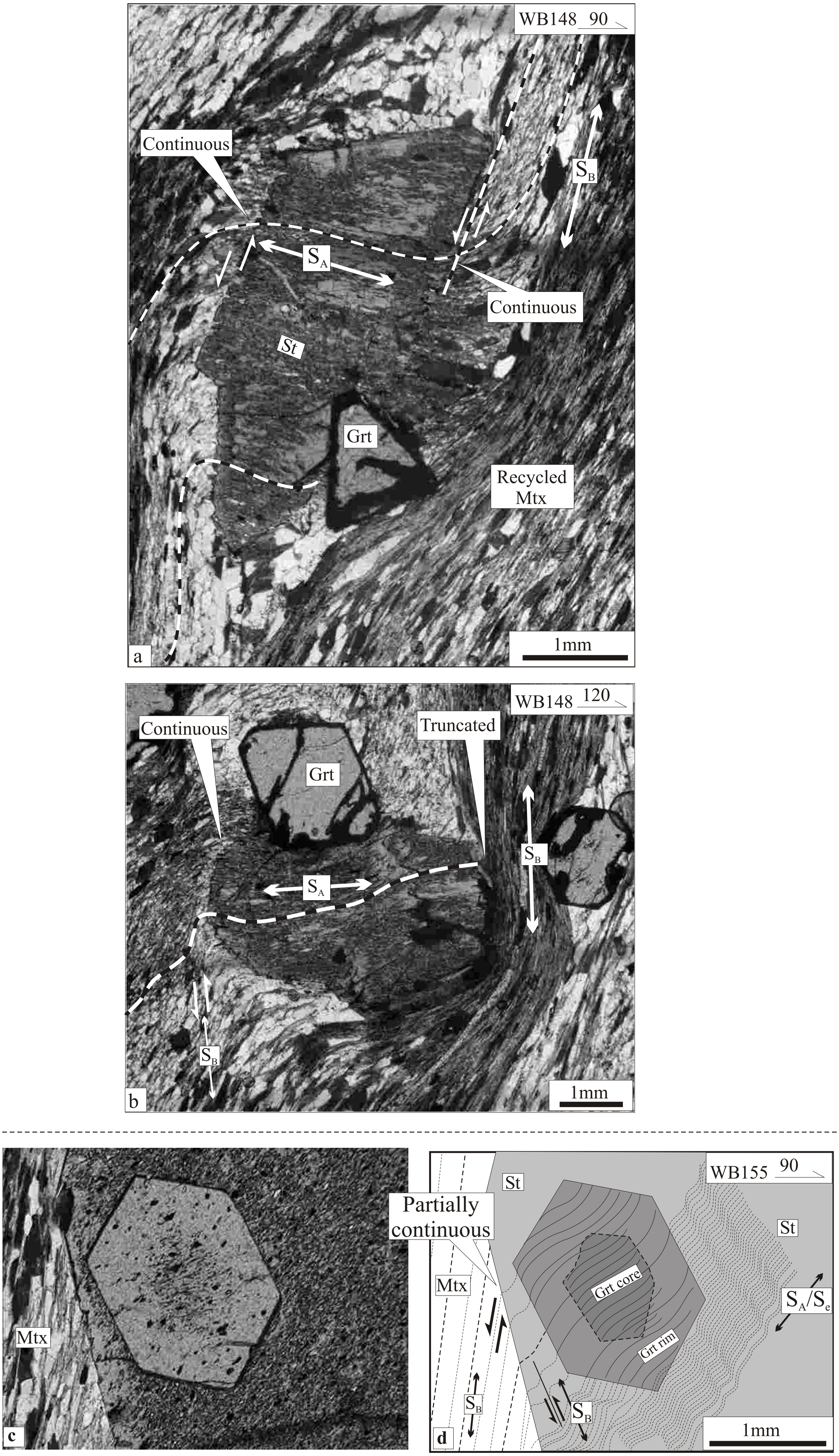

WB148 90
Continuous
S_B
S_A
Continuous
St
Grt
Recycled Mtx
1mm
a
WB148 120
Continuous
Truncated
Grt
S_B
S_A
S_B
1mm
b
Mtx
c
WB155 90
St
Partially continuous
St
Mtx
Grt core
S_A/S_e
Grt rim
S_B
S_B
1mm
d

Fig. 9

Fig. 10. Photomicrograph and associated line diagram of vertical N-S striking thin section showing tight to isoclinal folds with subhorizontal S_c or S_e axial planar trace. The rock sample is from low strain zone of S_2. Inclusion trails preserved within the porphyroblasts show similar kind of geometric relationships, that is, subvertical overprinted by subhorizontal microstructures.

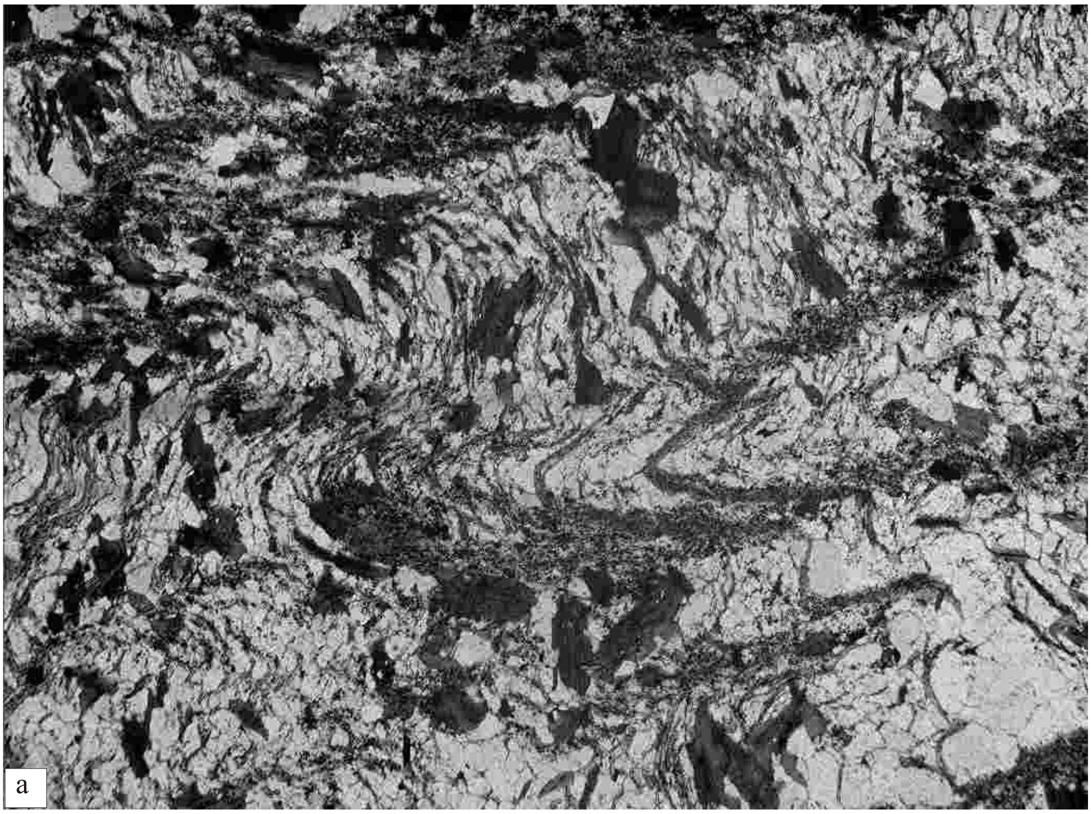

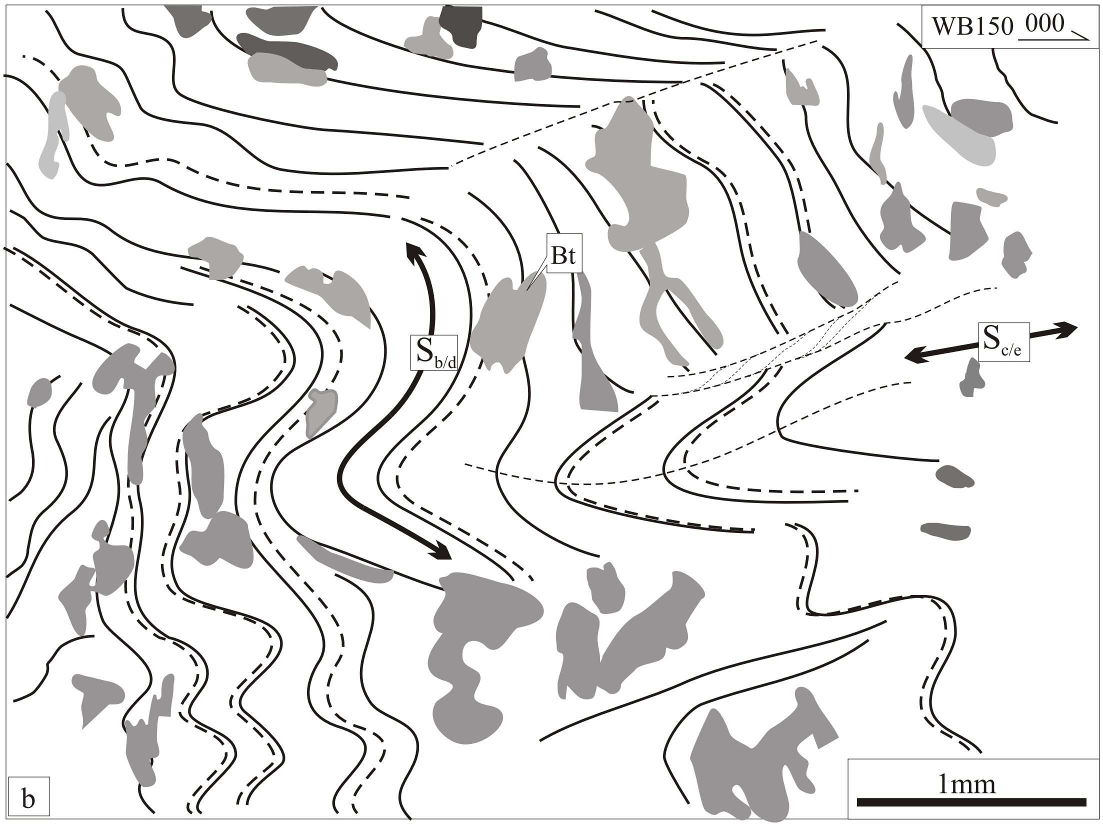

Fig. 10

Fig. 11. Rose diagrams showing pitches of the inclusion trails measured from oriented thin sections. (a) Inclusion trail pitches showing distinct subhorizontal A-type and subvertical B-type modes measured from vertical oriented thin sections. (b) Rose diagrams showing two dominant strike orientations recorded from horizontal oriented thin sections from all the analyzed rocks for 'FitPitch'. Note that the number of W-E striking inclusion trail pitches preserved within the porphyroblasts is dominant than N-S ones (see also Fig. 3b).

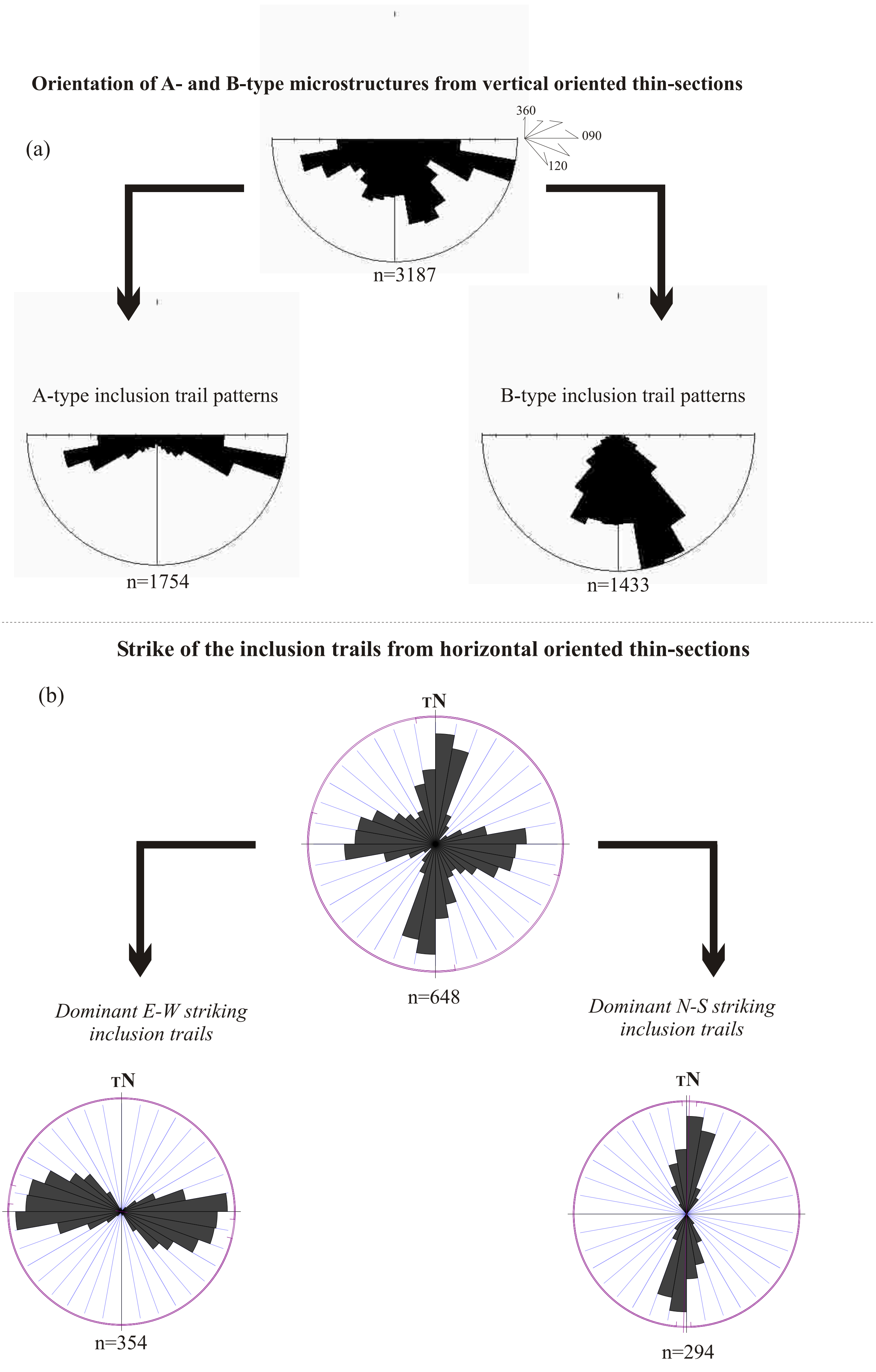
Orientation of A- and B-type microstructures from vertical oriented thin-sections
(a)
360
090
120
n=3187
A-type inclusion trail patterns
n=1754
B-type inclusion trail patterns
n=1433
Strike of the inclusion trails from horizontal oriented thin-sections
(b)
TN
n=648
Dominant E-W striking inclusion trails
TN
n=354
Dominant N-S striking inclusion trails
TN
n=294

Fig. 11

Fig. 12. (a) Lower hemisphere equal-area stereographic plot showing FIA trend and plunge calculated by 'FitPitch'. (b) Poles to the best-fit planes calculated by 'FitPitch'. Note that the poles are preferentially located at the periphery and near center of the stereo plot (see text for further discussion). (c) Graphs showing quantitative 'FitPitch' Rd and Rm values from all the analyzed samples. Two plane Rd/Rm versus three plane Rd/Rm values have been plotted. The selection of two- or three-plane solution is based on the highest Rd and Rm values (Aerden, 2003) and textural relationship. Note that the Rd values are almost equal. However, Rm values are significantly higher and preferred for each and every sample.

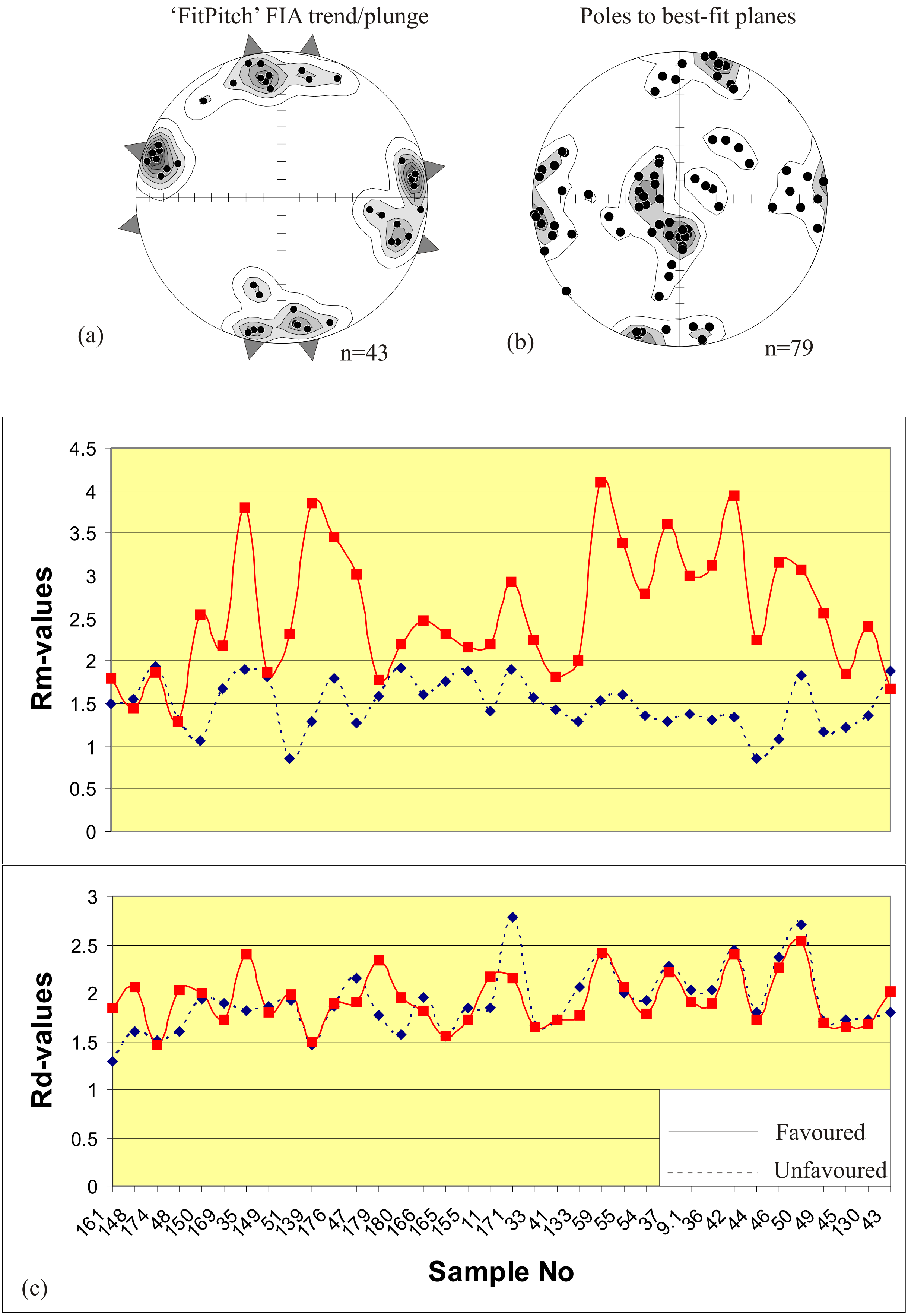

'FitPitch' FIA trend/plunge
Poles to best-fit planes
(a)
n=43
(b)
n=79
Rm-values
Rd-values
Favoured
Unfavoured
Sample No
161 148 174 48 150 169 35 149 51 139 176 47 179 180 166 165 155 11 171 33 41 133 59 55 54 37 9.1 36 42 44 46 50 49 45 130 43
(c)

Fig. 12

Fig. 13. (a) Series of sketches showing an example of how foliation intersection/inflection axes can be determined by ‘asymmetry switch’ and ‘FitPitch’ technique. 095^{o} FIA was assigned using ‘asymmetry switch’ method to this specimen (WB59) as 080^{o} and 090^{o} azimuth thin sections contain porphyroblasts with dominant clockwise whereas, 100^{o} azimuth thin section contains porphyroblasts with dominant anticlockwise asymmetries. ‘FitPitch’ calculates 287/11 degree FIA trend and plunge. If data from two additional thin sections are added e.g., 080^{o} and 100^{o} ‘FitPitch’ FIA would lies very close to the ‘asymmetry switch’ method. (b) Stereographic plot showing two-plane solution with 287/11 FIA trend and plunge for sample WB59 with high Rd and Rm value. The two-plane solution is in excellent agreement with microstructural constraints (see Figure 13a for inclusion trail geometry). Compare data from 060^{o}, 090^{o} and 120^{o} azimuth thin-sections. A flip in the inclusion trails patterns can be observed illustrated in the rose diagrams.

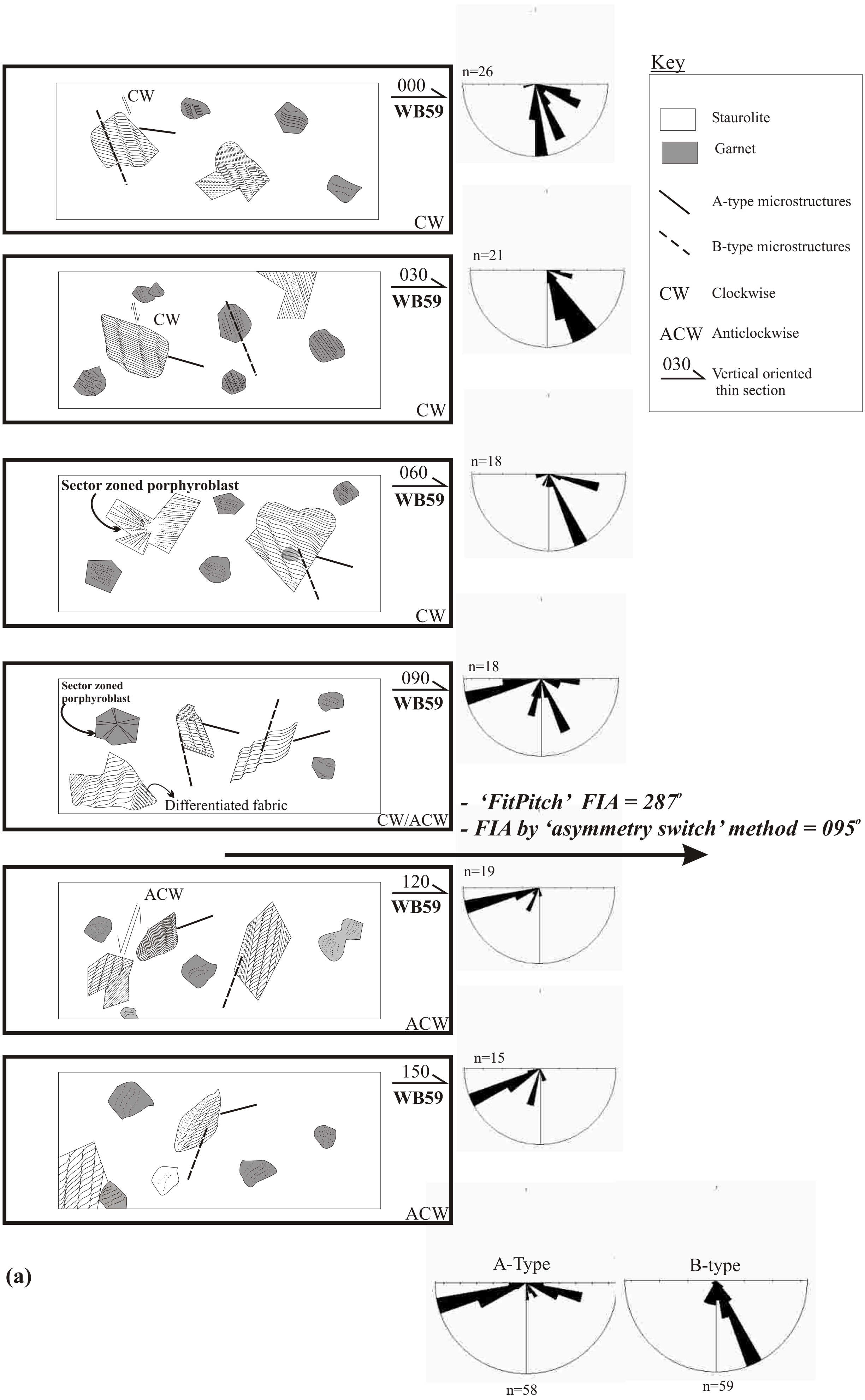

Key
Staurolite
Garnet
A-type microstructures
B-type microstructures
CW Clockwise
ACW Anticlockwise
030 Vertical oriented thin section
000
WB59
CW
n=26
030
WB59
CW
n=21
Sector zoned porphyroblast
060
WB59
CW
n=18
Sector zoned porphyroblast
Differentiated fabric
090
WB59
CW/ACW
n=18
- 'FitPitch' FIA = 287°
- FIA by 'asymmetry switch' method = 095°
ACW
120
WB59
ACW
n=19
150
WB59
ACW
n=15
A-Type
B-type
n=58
n=59
(a)

Fig. 13a

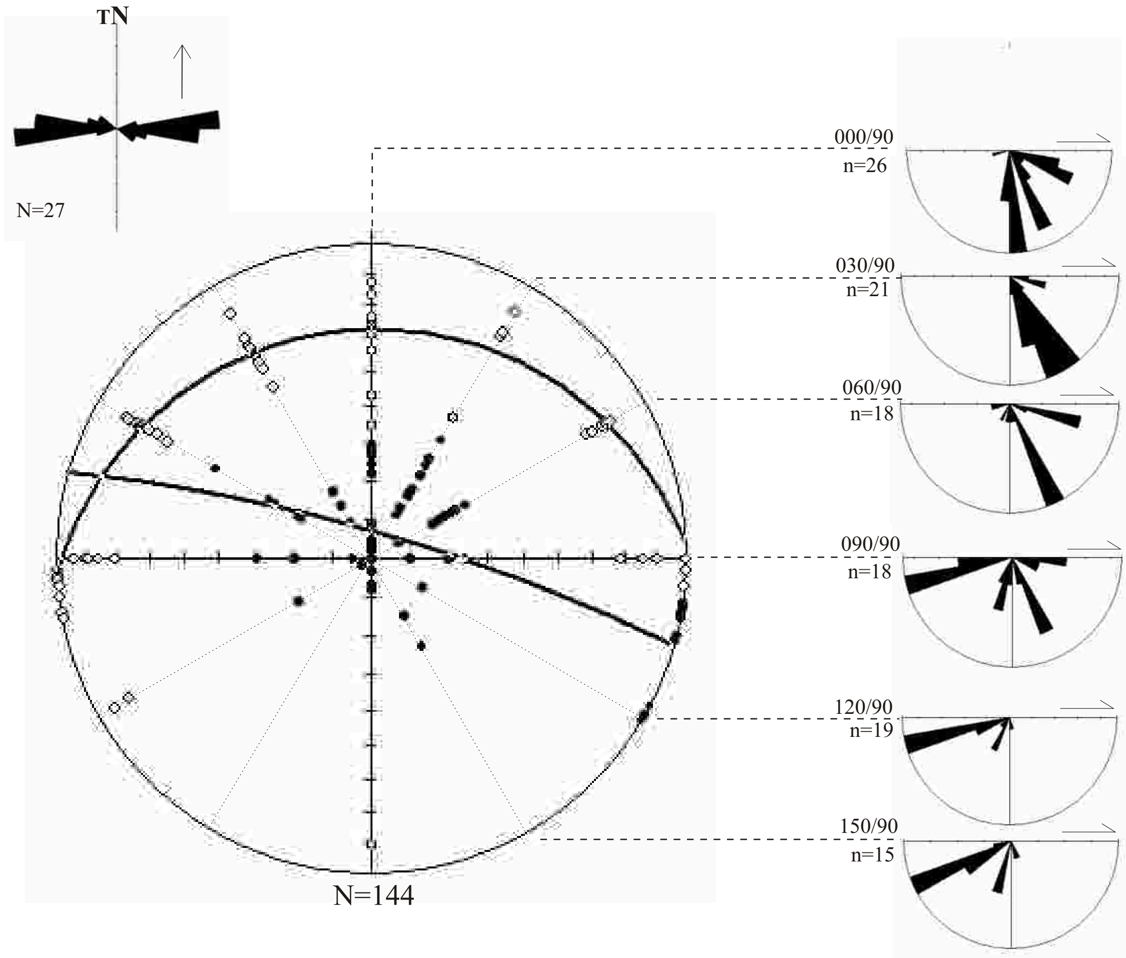

Best Poles	Rd	Rm	FIA
196/07; 177/62	2.516	4.097	287/11 (2-plane solution) - favoured
227/20; 126/04;177/64	2.502	1.531	027/69; 325/22; 035/21 (3-plane solution) - unfavoured

(b)

Fig. 13b

Fig. 14. (a) Sketch showing two slightly differently oriented inclusion trail pitches preserved within the porphyroblasts belonging to one generation in one thin section. Data with varying orientation from different oriented thin sections around the azimuth may fall into the two-plane solution with best statistical constraints for inclusions trails belonging to one deformation. (b) Differentiated B-type microstructures with opposite dips related with one deformation event. Thus, relative timings of porphyroblast growth and microstructural relationship should be born in mind while favoring either unimodal or bimodal best-fit planes.

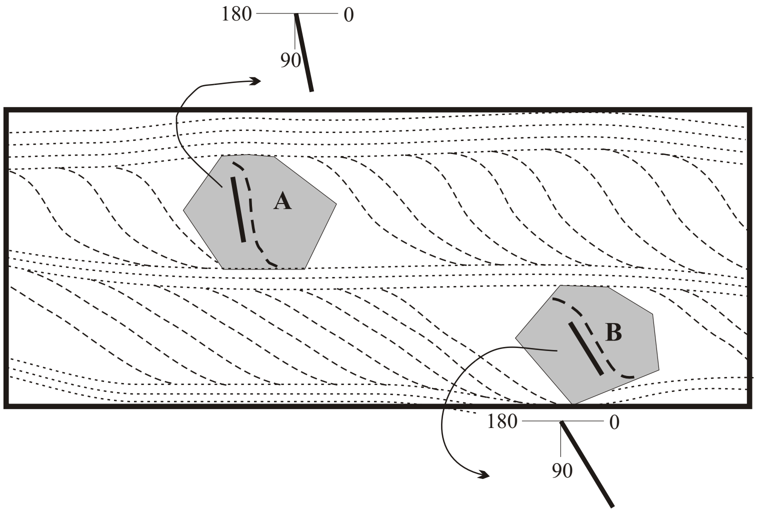

(a)

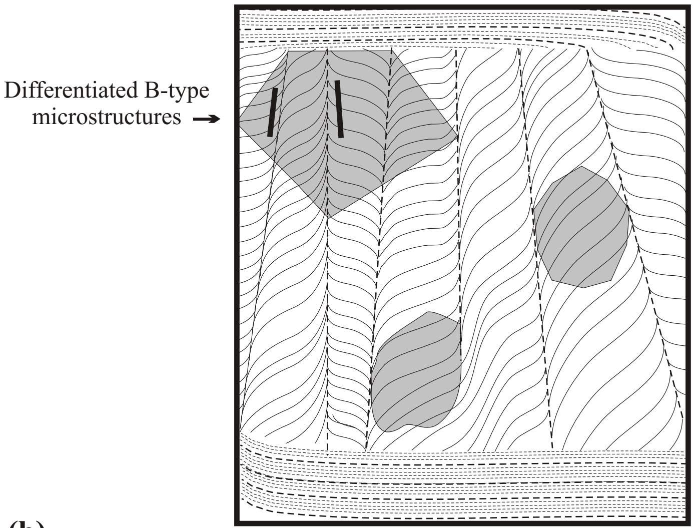

(b)

Fig. 14

Fig. 15. Lower hemisphere equal-area stereo plots with two- and three-plane solutions and associated rose diagrams from vertical oriented thin sections (WB166). The two-plane solution is favored as it is more consistent with the microstructures (see rose diagrams). Note that the 'FitPitch' divided one steep plane into two with high Rd and low Rm values with three FIAs and is not preferred based on textural relationships. The third FIA is an artifact (see also Aerden, 2003).

2-plane solution

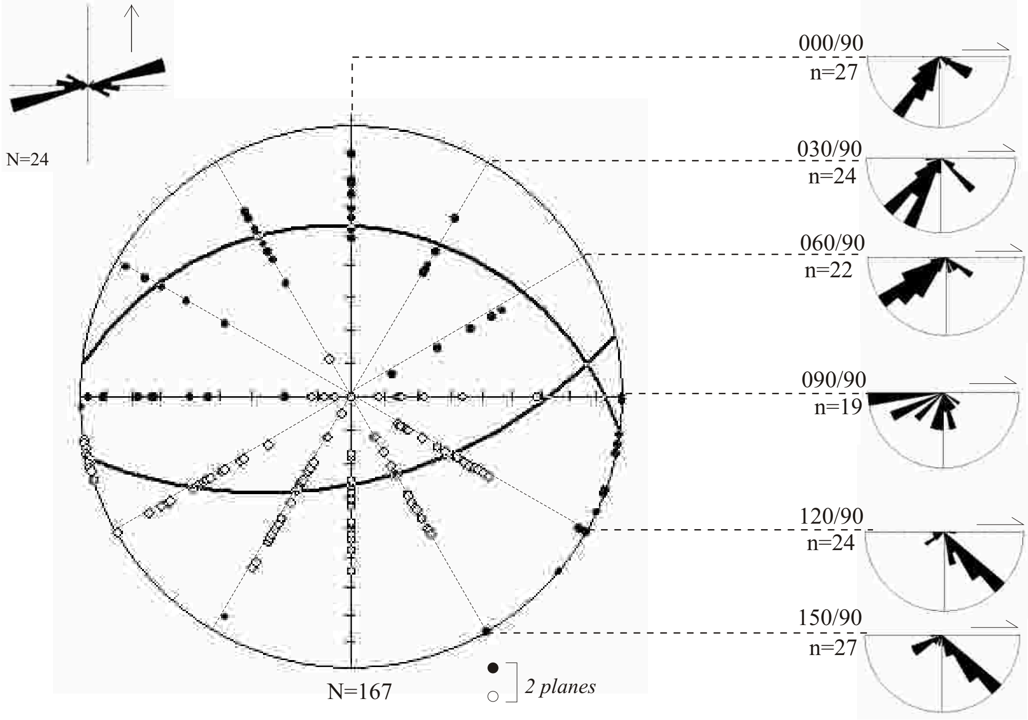

Sample No. WB166

Best Poles	**Rd**	**Rm**	**FIA**
187/53; 347/26	1.813	2.481	82/11 (2-plane solution) - favoured
188/51; 346/34; 336/06	1.917	1.596	84/11; 69/22; 244/17 (3-plane solution) - unfavoured

3-plane solution

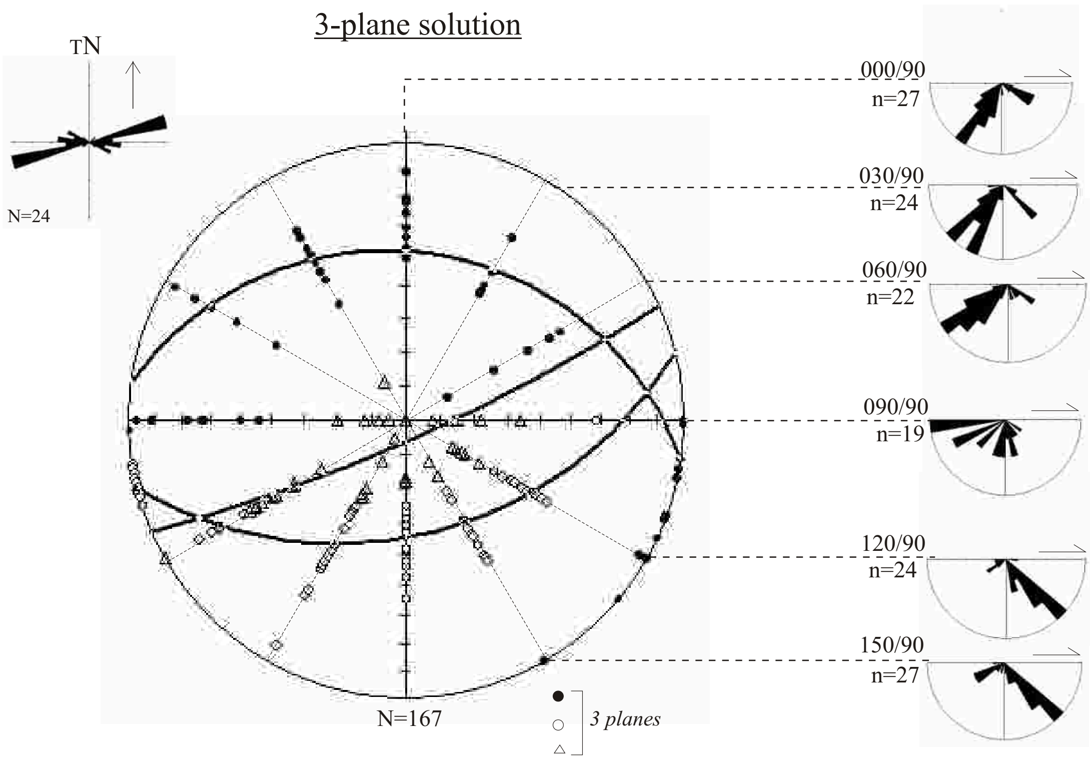

Fig. 15

Fig. 16. Sample WB43. Three-plane solution with steep S_d, shallow S_e and steep S_B with 100/31 and 354/17 FIA trend/plunge, respectively. 166/70 FIA trend/plunge is an artifact as explained in the text in detail. The three-plane solution is in good agreement microstructurally and statistically. This interpretation is also consistent for sample WB148.

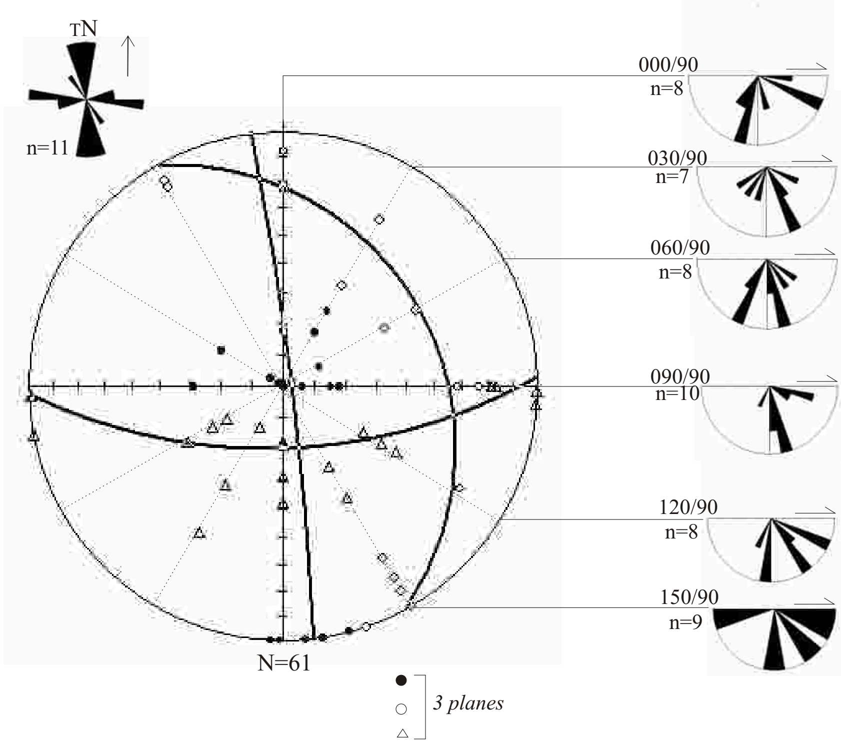

Sample No. WB43

Best Poles	Rd	Rm	FIA
255/29; 356/12	1.697	1.976	105/75 (2-plane solution) - unfavoured
263/02; 241/52; 358/20	2.011	1.711	354/17; 166/70; 100/31 (3-plane solution) - favoured

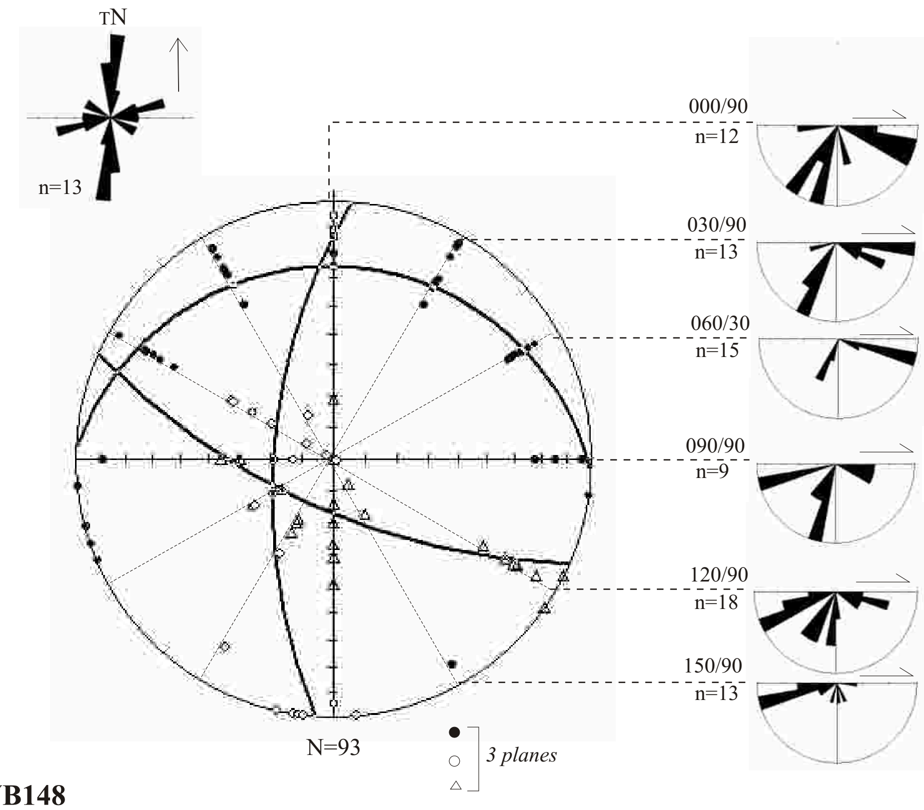

Sample No. WB148

Best Poles	Rd	Rm	FIA
188/70; 081/06	1.602	2.061	349/19 (2-plane solution) - unfavoured
177/64; 094/19; 024/16	2.058	1.448	354/26; 291/11; 248/69 (3-plane solution) - favoured

Fig. 16

Section – C

Aerially extended, Mesoproterozoic orogenesis accompanying a radical shift in the direction of relative plate motion: seeing through the overprinting effects of penetrative deformation and metamorphism

(Figures and Tables)

Fig. 1. (a) Outline map of the Mount Isa Inlier showing Western Fold Belt (WFB), Kalkadoon-Leichhardt Belt (KLB) and Eastern Fold Belt (EFB). (b) Regional geological map of the Eastern Fold Belt showing major lithotectonic units and locations of the study area (modified after Blake, 1987; Giles and MacCready, 1997; Williams, 1998; Marshall and Oliver, 2001). Ages after Page and MacCready (1997), Page and Sun (1998).

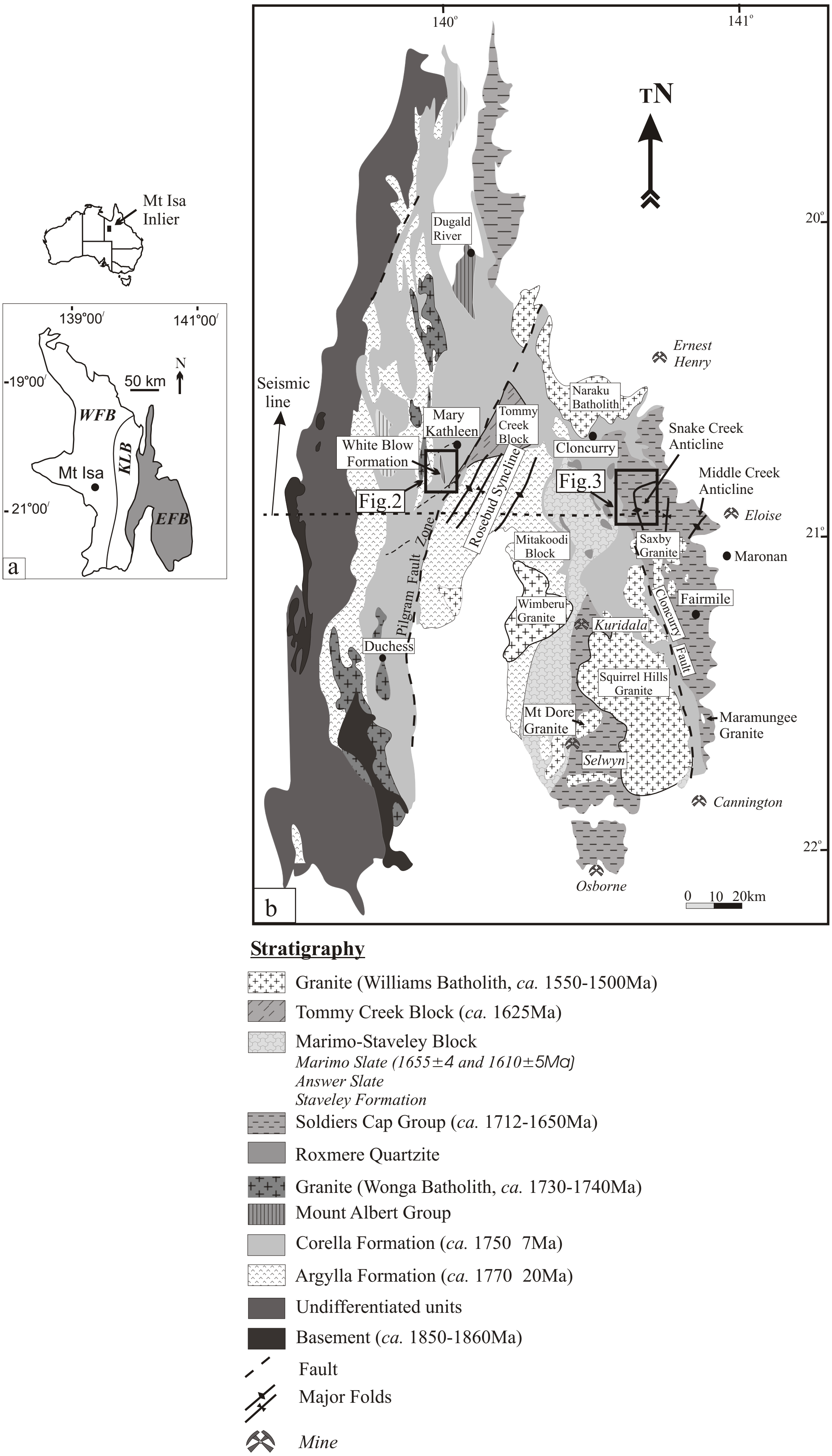
Mt Isa
Inlier
139°00'
141°00'
-19°00'
-21°00'
50 km
N
WFB
KLB
EFB
Mt Isa
a
140°
141°
N
20°
21°
22°
Dugald River
Ernest Henry
Seismic line
Mary Kathleen
Tommy Creek Block
Naraku Batholith
Snake Creek Anticline
White Blow Formation
Cloncurry
Middle Creek Anticline
Fig.3
Fig.2
Eloise
Rosebud Syncline
Pilgram Fault Zone
Mitakoodi Block
Saxby Granite
Maronan
Wimberu Granite
Fairmile
Kuridala
Cloncurry Fault
Duchess
Squirrel Hills Granite
Mt Dore Granite
Maramungee Granite
Selwyn
Cannington
Osborne
0 10 20km
b
Stratigraphy
Granite (Williams Batholith, ca. 1550-1500Ma)
Tommy Creek Block (ca. 1625Ma)
Marimo-Staveley Block
Marimo Slate (1655±4 and 1610±5Ma]
Answer Slate
Staveley Formation
Soldiers Cap Group (ca. 1712-1650Ma)
Roxmere Quartzite
Granite (Wonga Batholith, ca. 1730-1740Ma)
Mount Albert Group
Corella Formation (ca. 1750 7Ma)
Argylla Formation (ca. 1770 20Ma)
Undifferentiated units
Basement (ca. 1850-1860Ma)
Fault
Major Folds
Mine

Fig. 1

Fig. 2. (a) Edge enhanced Landsat band-7 image of the White Blow Formation and adjacent Mary Kathleen Group units. (b) Geological map of the White Blow Formation and adjacent Mary Kathleen Group units (modified from Whitelock, 1989) showing sample locations. Samples with white dots were utilized for 'asymmetry switch' and 'FitPitch' FIA analysis. The prefix WB (stands for White Blow) is removed for each sample (see text for discussion). Grid numbers refer to Australian Map Grid (AMG) zone 54 (c) Lower hemisphere equal-area stereo plots for planar and linear structures in the area.

Fig. 2. (a) Landsat imagery courtesy of NASA Goddard Space Flight Center and U.S. Geological Survey.

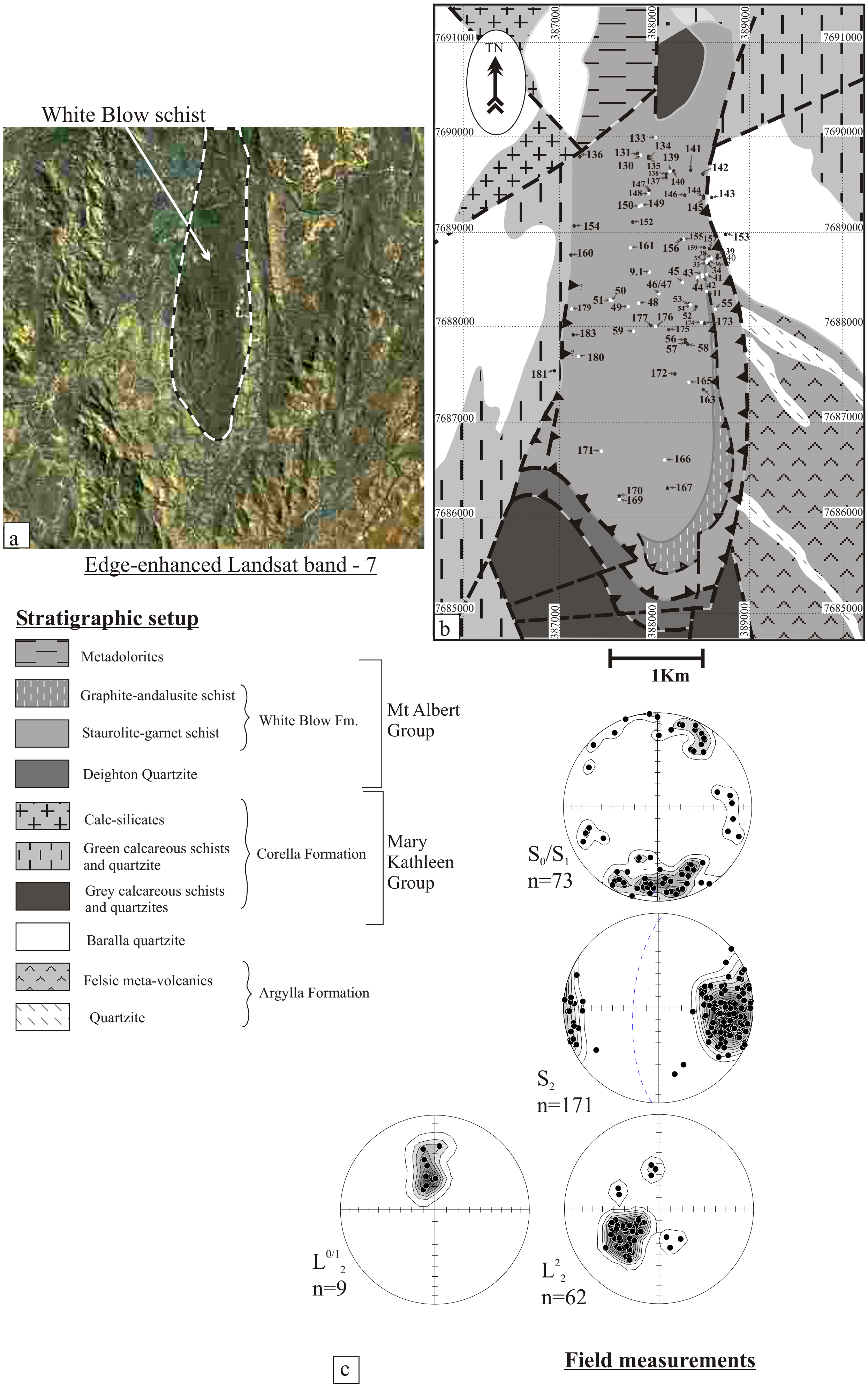

White Blow schist
a
Edge-enhanced Landsat band - 7
b
TN
7691000
7690000
7689000
7688000
7687000
7686000
7685000
387000
388000
389000
1Km
Stratigraphic setup
Metadolorites
Graphite-andalusite schist
Staurolite-garnet schist
White Blow Fm.
Deighton Quartzite
Mt Albert Group
Calc-silicates
Green calcareous schists and quartzite
Grey calcareous schists and quartzites
Corella Formation
Mary Kathleen Group
Baralla quartzite
Felsic meta-volcanics
Quartzite
Argylla Formation
S_0/S_1
n=73
S_2
n=171
$L^{0/1}_2$
n=9
L^2_2
n=62
c
Field measurements

Fig. 2

Fig. 3. (a) Edge enhanced Landsat band-7 image of the Gilded Rose, Snake Creek Anticline (SCA), Saxby Granite (SG) and Cloncurry Fault. (b) Geological map of the Snake Creek Anticline (after Bureau of Mineral Resources, Geology and Geophysics, Australia, 1983; Rubenach and Lewthwaite, 2002) showing sample locations. Lower hemisphere equal-area stereo plot of poles to S_2 showing outcrop measurements recorded during the course of sample collection from the Snake Creek Anticline.

Fig. 3. (a) Landsat imagery courtesy of NASA Goddard Space Flight Center and U.S. Geological Survey.

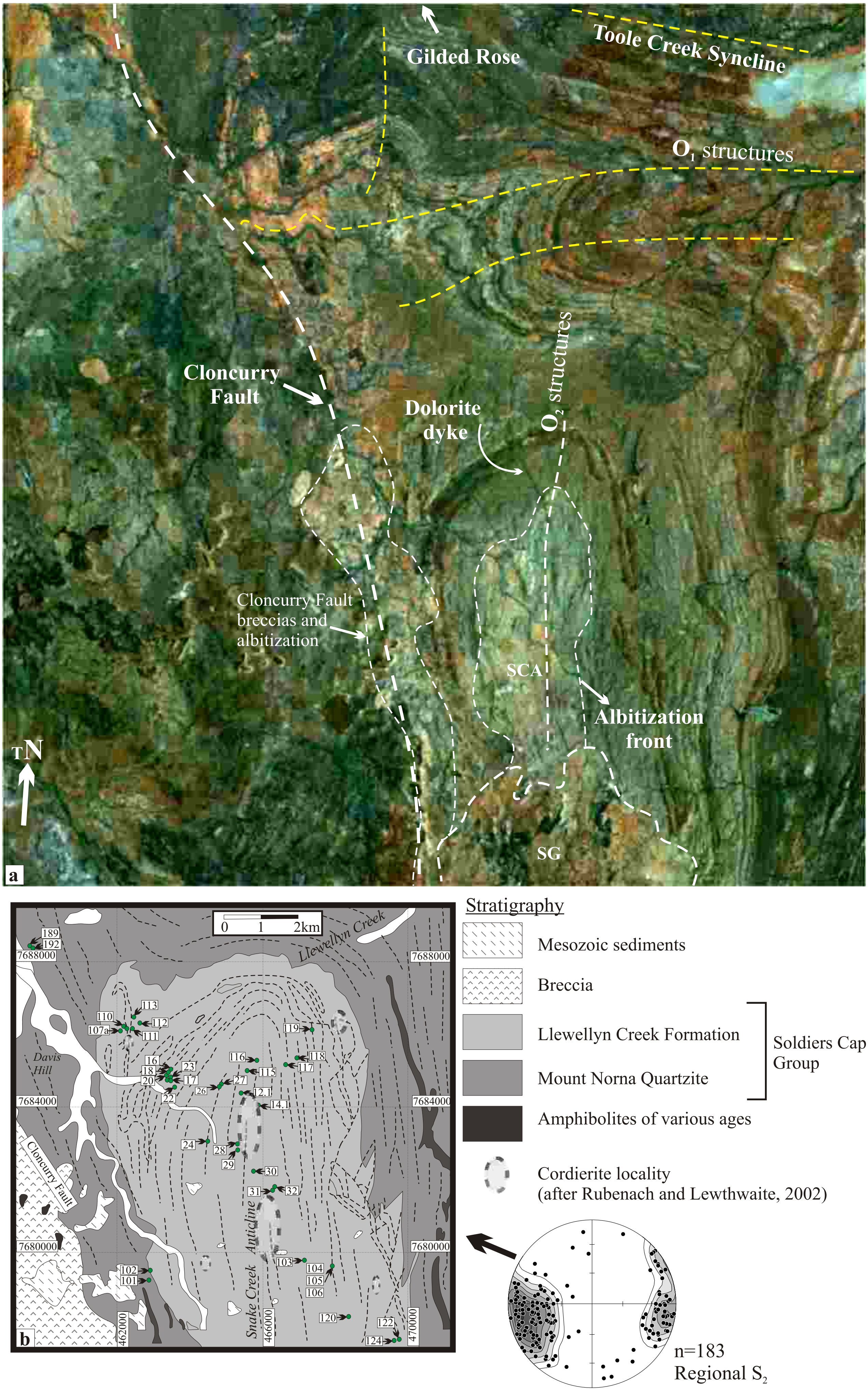

Gilded Rose
Toole Creek Syncline
O_1 structures
Cloncurry Fault
Dolorite dyke
O_2 structures
Cloncurry Fault breccias and albitization
SCA
Albitization front
TN
SG
a
0 1 2km
Llewellyn Creek
189
192
7688000
113
110
112
107a
111
119
Davis Hill
16
23
116
118
18
17
115
117
20
27
22
26
12.1
14.1
7684000
24
28
29
Cloncurry Fault
30
31
32
Anticline
7680000
102
101
103
104
105
106
Snake Creek
120
122
124
462000
466000
470000
b
Stratigraphy
Mesozoic sediments
Breccia
Llewellyn Creek Formation
Mount Norna Quartzite
Soldiers Cap Group
Amphibolites of various ages
Cordierite locality (after Rubenach and Lewthwaite, 2002)
n=183
Regional S_2

Fig. 3

Fig. 4. Technique for determining FIAs. (a) The 'asymmetry switch' method (after Hayward, 1990; Bell and Hayward, 1991). If asymmetric microstructures, such as inclusion trails, are observed on an fanned array of oriented thin sections maintaining the same viewing direction, then a flip in asymmetry occurs where the axis is crossed. This is the foliation inflection/intersection axis or 'FIA'. In this example, the FIA is between 180^o and 220^o sections and is defined by a switch in the asymmetry of simple sigmoidal curvature from clockwise to anticlockwise. (b) Photomicrographs of garnet porphyroblasts taken from six differently striking (360, 030, 060, 090, 120, 150) vertical thin sections of sample GR85 (Gilded Rose, Eastern Fold Belt, Mt Isa). Porphyroblast inclusion trails are sigmoidal or slightly staircase. The crenulation axes or FIA lies at 090^o and is defined by a switch in the asymmetry of inclusion trails curvature from anticlockwise (360^o, 030^o, 060^o) to clockwise (120^o, 150^o) between the 080^o and 100^o sections (not shown). Section 090^o contains both clockwise and anticlockwise inclusion trail asymmetries or millipede (MP) microstructure. Essentially, eight thin sections were used to confine these FIA trends to a 10^o range (see text for further discussion).

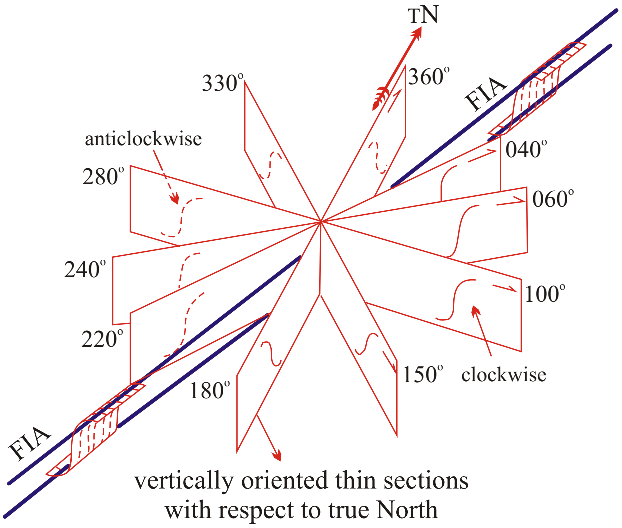
TN
360°
330°
FIA
anticlockwise
040°
280°
060°
240°
100°
220°
150°
clockwise
180°
FIA
vertically oriented thin sections
with respect to true North

(a)

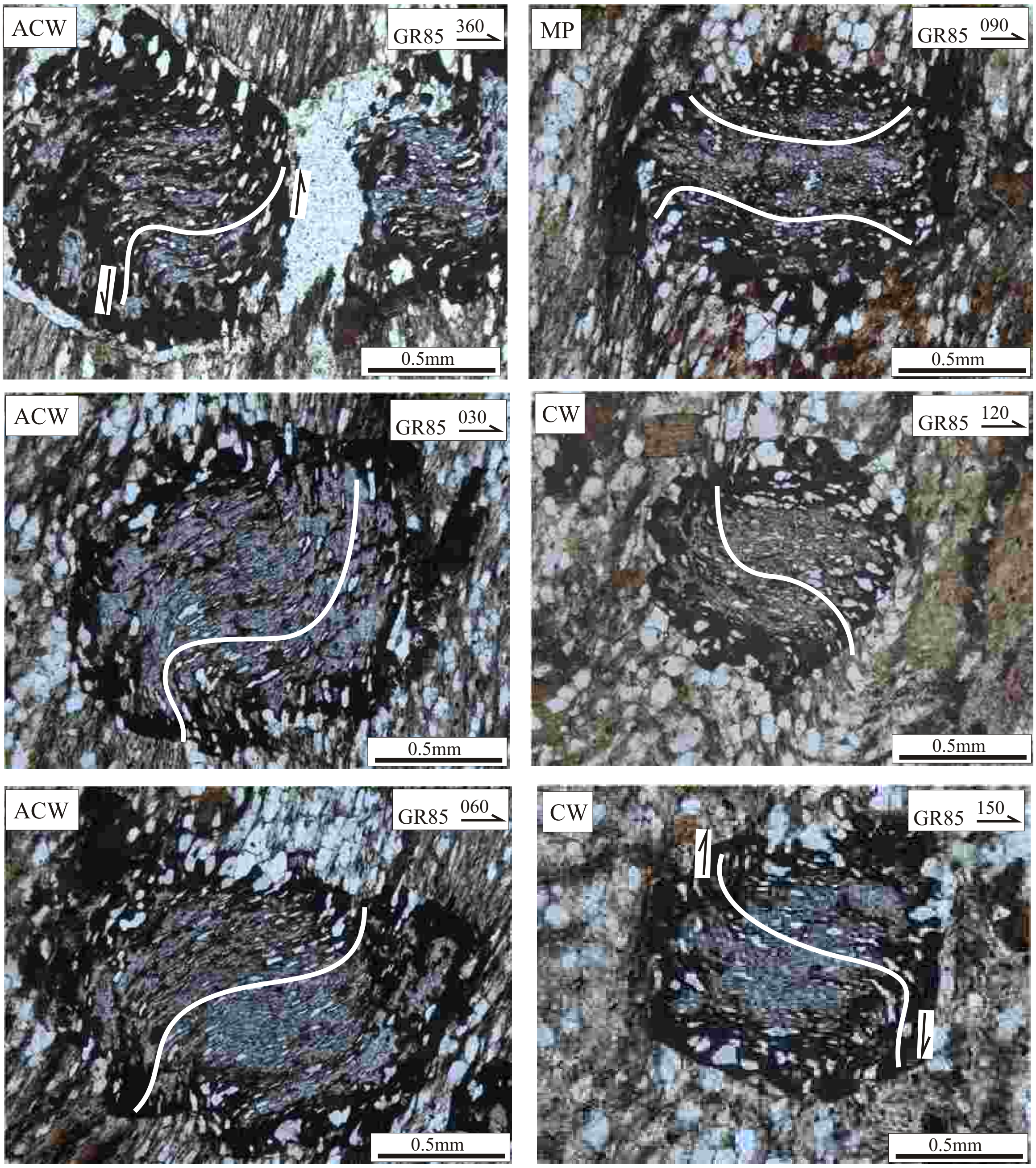
ACW
GR85 360
0.5mm
MP
GR85 090
0.5mm
ACW
GR85 030
0.5mm
CW
GR85 120
0.5mm
ACW
GR85 060
0.5mm
CW
GR85 150
0.5mm

(b)

Fig. 4

S. No.	Easting	Northing	FIA trend (true North)				Mtx	FIA-I		FIA-II		FIA-III		FIA-IV			FitPitch FIA	
			Grt		*St*													
			Core	*Rim*	*Core*	*Rim*		Grt	St	Grt	St	Grt	St	Grt	St	Mtx		
WB47	388100	7688410		15		15								15	15		13	
WB41	388542	7688637		355	355									355	355		173	
WB38	388604	7688727				5									5		no data	
WB33	388550	7688694		95		10		95							10		98	
WB48	387828	7688263		90	90			90	90								95	9
WB11	388681	7688672	105		105			105	105								112	
WB35	388567	7688718				20									20		25	111
WB149	387854	7689285	105			355	355		105						355	355	293	
WB133	388010	7690005		115	115					115	115						280	
WB176	388003	7688017	115							115							107	
WB171	387434	7686695	115		115					115	115						284	
WB169	387619	7686205	120		120					120	120						288	
WB166	388105	7686616	85	15		15			85					15	15		82	
WB180	387189	7687698	85		85			85	85								85	174
WB179	387118	7688192	100			5			100						5		198	287
WB165	388367	7687426		15		15								15	15		193	
WB155	388294	7688940	150		150									150	150		346	
WB139	388163	7689650			85	120		85			120						81	
WB150	387843	7689284	355		355									355	355		174	
WB161	387739	7688844	85		85	105		85	85		105						82	337
WB148	387934	7689418		0		0								0	0		354	291
WB174	388502	7688059	355											355			351	
WB45	388293	7688477		5		5								5	5		350	
WB49	387712	7688222	85		85			85	85								73	
WB51	387527	7688292	5		100	0			100					5	5		285	
WB50	387537	7688290	105			105		105	105								289	
WB46	388045	7688258	5			5								5	5		352	
WB44	388448	7688532		15		15								15	15		189	
WB42	388600	7688680		5										5			194	
WB36	388570	7688720				105					105						103	
WB9.1	387895	7688562		135		135						135	135				321	
WB37	388600	7688820				355	0								355	0	159	
WB54	388370	7688241		5		20								5	25		192	
WB55	388607	7688217		0		0								0	0		169	
WB59	387772	7687969		95		95		95	95								287	
WB130	387848	7689821	85			85		85	85								80	
WB43	388551	7688563			105	0					105				0		100	354

Table-1. Sample locations with respect to Australian Map Grid (AMG) coordinates, the FIA trend measured in them, FIA sets based on their relative timings and 'FitPitch' FIA trend/plunge (symbols after Kretz, 1983) Mtx: Matrix.

Fig. 5. A rose diagram of FIA trend with respect to true North determined from all garnet and staurolite porphyroblasts. Outer plot gives more details of data for FIA trends from garnet and staurolite porphyroblasts. Note that the WSW-ENE and WNW-ESE FIA trends were mainly obtained from the cores of the porphyroblasts, whereas NNW-SSE and SSW-NNE FIA trends are dominantly obtained from the rims of the individual porphyroblasts. Several independent growth phases of porphyroblasts have been identified based on FIAs. (b) 3-D conceptual model showing near-orthogonal multiple deformation history during O_1 and O_2 events of the Isan Orogeny deduced from detailed microstructural FIA analysis. Two distinct FIA sets can be recognized during O_1 event or N-S bulk shortening of the Isan Orogeny based not only on the FIA trends but also on the geometry of inclusion trail patterns. O_2 was responsible for W-E shortening, producing N-S FIA trend.

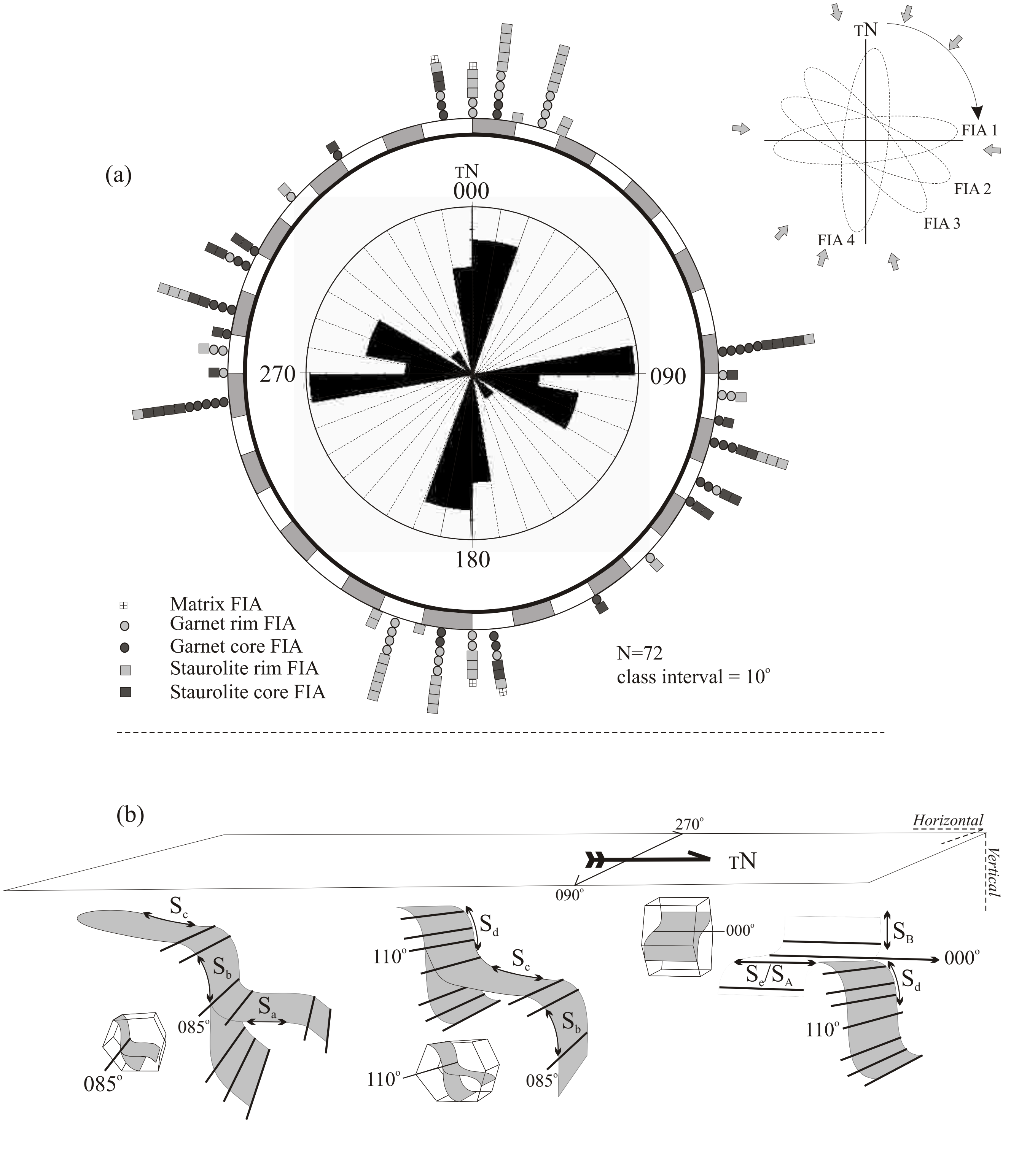
(a)
TN
000
090
180
270
FIA 1
FIA 2
FIA 3
FIA 4
Matrix FIA
Garnet rim FIA
Garnet core FIA
Staurolite rim FIA
Staurolite core FIA
N=72
class interval = 10°
(b)
270°
090°
TN
Horizontal
Vertical
S_c
S_b
S_a
085°
S_d
110°
000°
S_B
S_e/S_A

Fig. 5

Fig. 6. Rose diagram of total FIA distribution trend obtained from garnet porphyroblasts. Note that garnet core FIA trends are dominated by W-E orientations, whereas rim FIA trends are dominated by N-S orientations. The dashed line indicates the position of successive FIA trend sets determined from relative timing criteria (see Table 1 and Fig. 5b). Most of the garnet porphyroblasts are truncated by the matrix except for FIA 4 (specifically FIA ranges from 000-020^{o}). (b) Rose plot of total FIA distribution trend obtained from staurolite porphyroblasts. Four distinct maxima are present, similar to those found in garnet porphyroblasts.

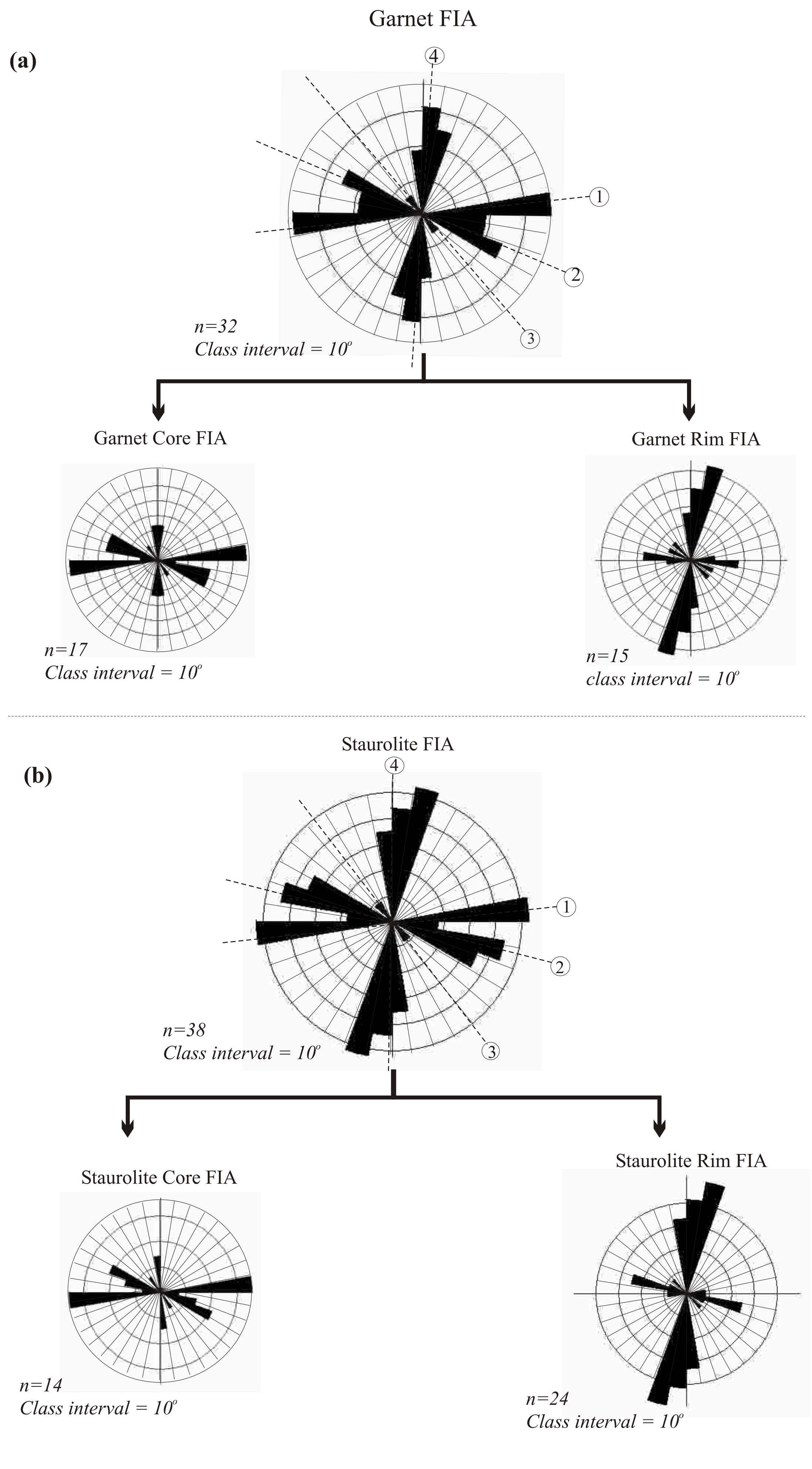
Garnet FIA
(a)
4
1
2
3
n=32
Class interval = 10°
Garnet Core FIA
n=17
Class interval = 10°
Garnet Rim FIA
n=15
class interval = 10°
Staurolite FIA
(b)
4
1
2
3
n=38
Class interval = 10°
Staurolite Core FIA
n=14
Class interval = 10°
Staurolite Rim FIA
n=24
Class interval = 10°

Fig. 6

Fig. 7. Photomicrograph of a staurolite porphyroblast hosting stage 3 differentiated crenulation cleavage in the core. The asymmetry associated with the cleavage is anticlockwise and have 100^{o}FIA trend (set 1). At the rim of the porphyroblast, shallow pitching S_c is overprinted. Note truncation of S_b verses S_c at the median region of the porphyroblast. For 'FitPitch' analysis, the microstructures have been divided into 'A' and 'B' type (see text for discussion). Vertical thin section with single barbed arrow showing strike, bearing and way up (in this and subsequent photomicrographs).

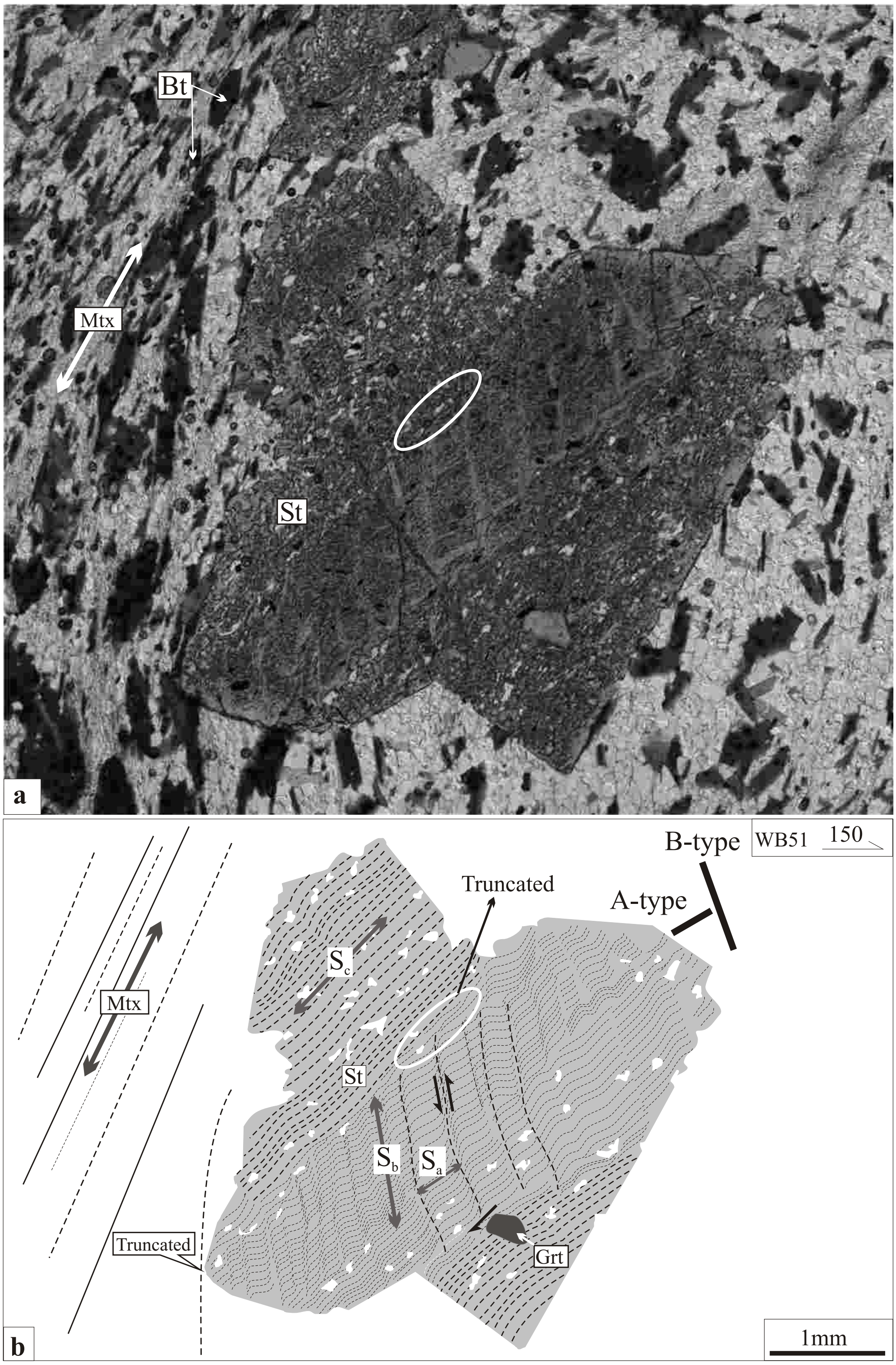
Bt
Mtx
St
a
B-type
WB51
150
Truncated
A-type
Sc
Mtx
St
Sb
Sa
Grt
Truncated
b
1mm

Fig. 7

Fig. 8. Rose diagrams showing pitches of the inclusion trails measured from oriented thin sections. (a) Inclusion trail pitches showing distinct subhorizontal A-type and subvertical B-type modes measured from vertical oriented thin sections. (b) Rose diagrams showing two dominant strike orientations recorded from horizontal oriented thin sections from all the analyzed rocks for 'FitPitch' analysis. Note that the number of W-E striking inclusion trail pitches preserved within the porphyroblasts is dominant than N-S ones. (c) Poles to the best-fit planes calculated by 'FitPitch'. The poles are preferentially located at the periphery and near center of the stereo plot. (d) Lower hemisphere equal-area stereographic plot showing FIA trend and plunge calculated by 'FitPitch'.

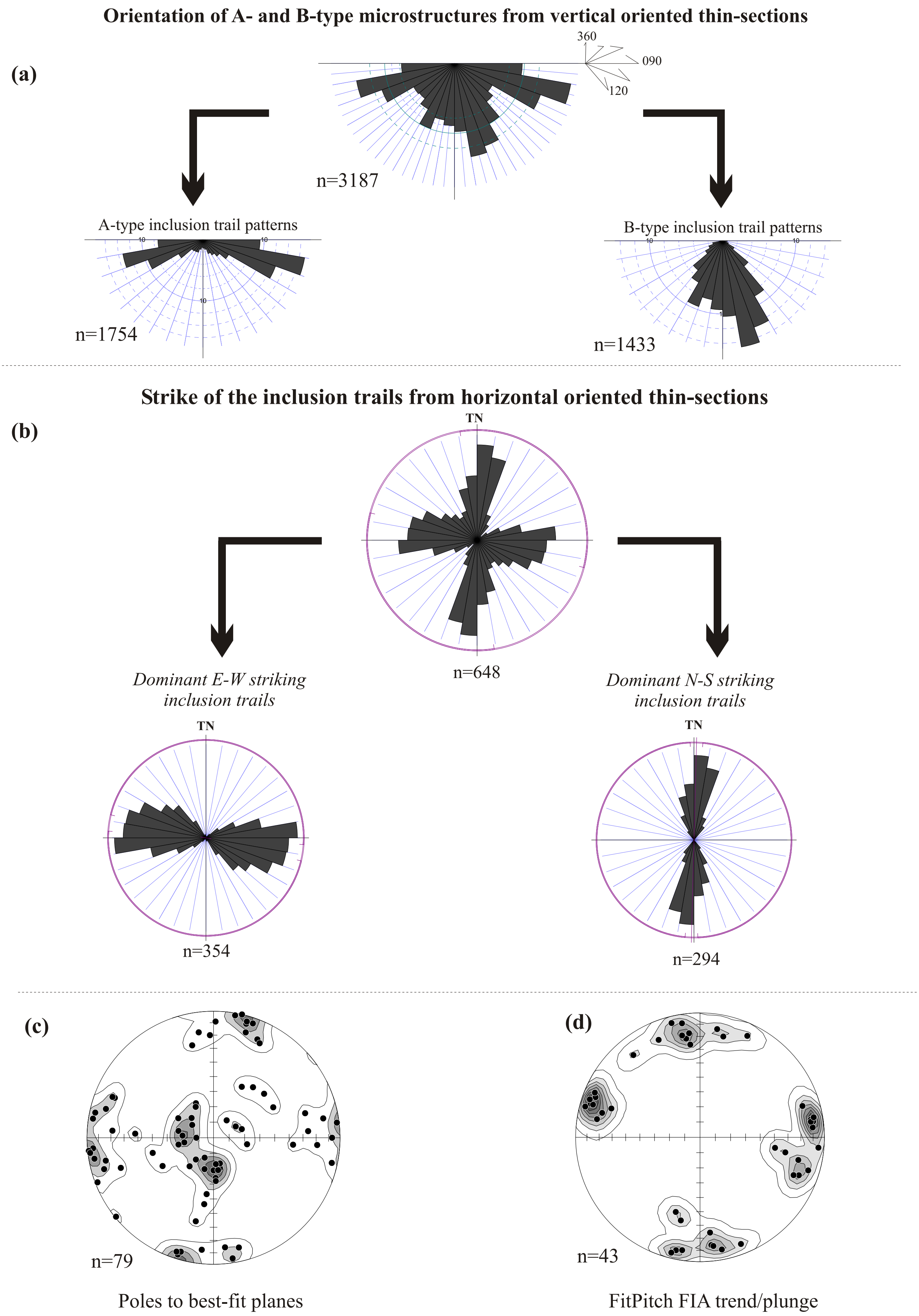

Orientation of A- and B-type microstructures from vertical oriented thin-sections
(a)
360
090
120
n=3187
A-type inclusion trail patterns
n=1754
B-type inclusion trail patterns
n=1433
Strike of the inclusion trails from horizontal oriented thin-sections
(b)
TN
n=648
Dominant E-W striking inclusion trails
TN
n=354
Dominant N-S striking inclusion trails
TN
n=294
(c)
n=79
Poles to best-fit planes
(d)
n=43
FitPitch FIA trend/plunge

Fig. 8

S. No.	Easting	Northing	Grt	St	And	Chl	Ged	Mtx	FitPitch
SC110	462276	7686126	25				35		022/17
GR189	459549	7688387	125						
SC123	469696	7677577	135						
SC112	462566	7686285	15	15		45			187/05
SC118	466906	7685310	80					15	
			25						
SC116	465786	7685237	145					10	
SC108	462054	7686038	110	110					108/10
SC109	462059	7686038	55	25				10	
SC26	464776	7684531	25		15			15	
SC104	467841	7679578	115						117/01
			5		10				198/12
SC117	466603	7685129	80						
			5					5	
SC106	467850	7679578	55					55	052/03
SC119	467303	7686071	40	40					209/03
SC27	464819	7684572	60					65	
SC15	463393	7684918	55					55	
SC25	464464	7683019	60					5	
SC113	462417	7686409		55				55	
SC29	465284	7682762	35		35				
SC103	467098	7679722	75		115			20	
SC30	465704	7682194						5	
SC107a	462150	7686038	65						
SC122	469696	7677577	355						
SC23	463402	7684776						5	
SC741					35			35	

Table-2. Sample locations (AMG), FIA trends measured in porphyroblasts and matrix and 'FitPitch' FIA trend/plunge from the Snake Creek Anticline. (Symbols after Kretz, 1983). Mtx: matrix

Fig. 9. (a) FIA trends for successive FIA sets in the Snake Creek Anticline. FIA sets get progressively younger with increase in the set number. Note that FIA set 4 (N-S) dominates in terms of FIA measurements and trend parallel along the axis of the anticline (see Fig. 3). (b) Pitch angles from vertical and horizontal oriented thin sections from 6 samples. Note that NNE-SSW trending pitches, preserved in the porphyroblasts, from horizontal oriented thin sections dominate and parallel to the regional trend of the Snake Creek Anticline and FIA set 4. (c) Lower hemisphere equal-area stereo plot showing poles to the best-fit planes. (d) Shows points after intersection of best-fit planes calculated for individual samples or 'FitPitch FIAs'. (e) FIA trend from Gilded Rose area, north of the Snake Creek Anticline, including FIA measurements of Lally (1997) and Lewthwaite (2000).

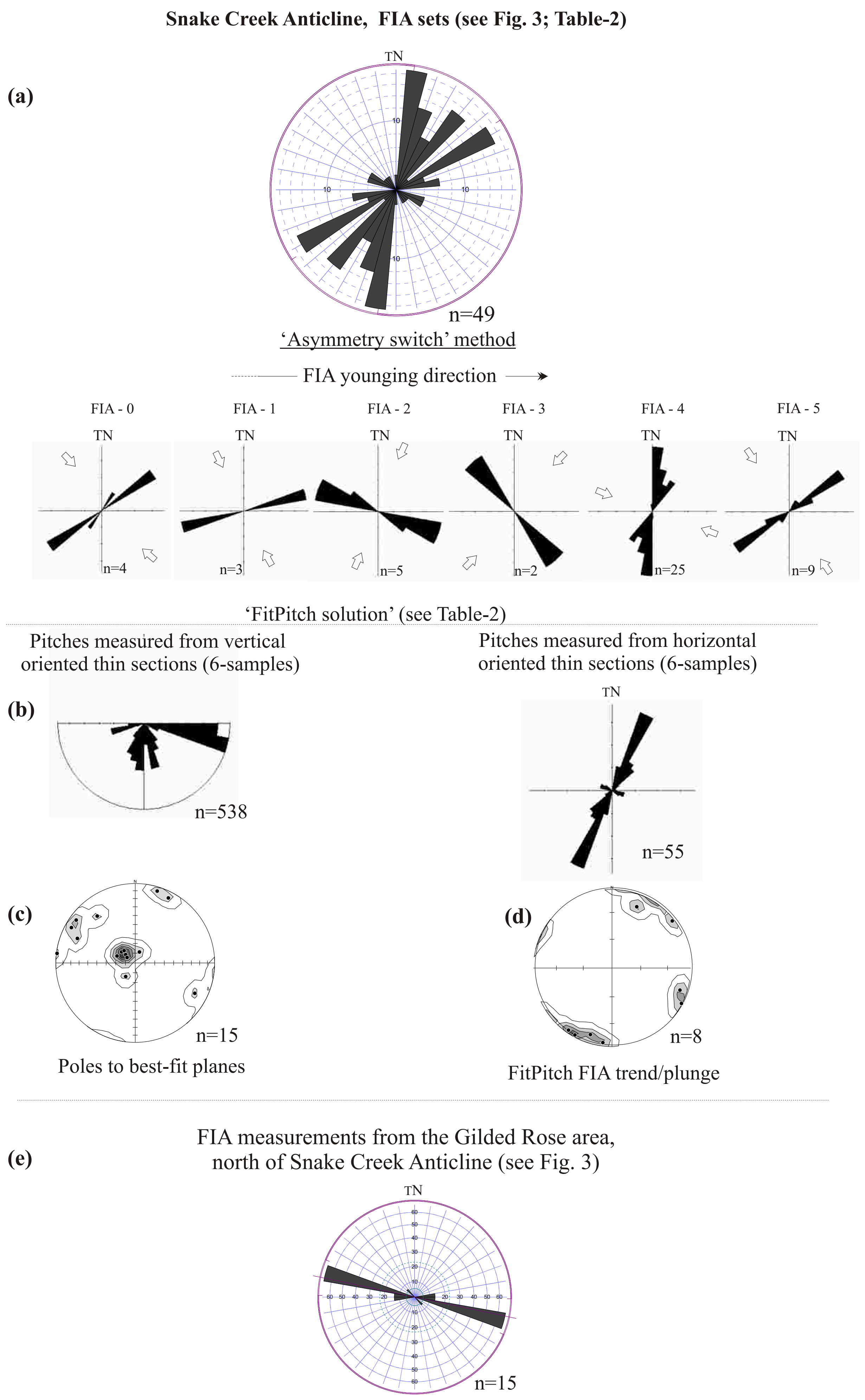
Snake Creek Anticline, FIA sets (see Fig. 3; Table-2)
(a)
TN
n=49
'Asymmetry switch' method
FIA younging direction
FIA - 0
FIA - 1
FIA - 2
FIA - 3
FIA - 4
FIA - 5
TN
n=4
n=3
n=5
n=2
n=25
n=9
'FitPitch solution' (see Table-2)
Pitches measured from vertical oriented thin sections (6-samples)
Pitches measured from horizontal oriented thin sections (6-samples)
(b)
n=538
TN
n=55
(c)
n=15
Poles to best-fit planes
(d)
n=8
FitPitch FIA trend/plunge
(e)
FIA measurements from the Gilded Rose area, north of Snake Creek Anticline (see Fig. 3)
TN
n=15

Fig. 9

S. No.	Easting	Northing	Grt	St	And	Chl	Ged	Mtx	FitPitch
SC110	462276	7686126	25				35		022/17
GR189	459549	7688387	125						
SC123	469696	7677577	135						
SC112	462566	7686285	15	15		45			187/05
SC118	466906	7685310	80					15	
			25						
SC116	465786	7685237	145					10	
SC108	462054	7686038	110	110					108/10
SC109	462059	7686038	55	25				10	
SC26	464776	7684531	25		15			15	
SC104	467841	7679578	115						117/01
			5		10				198/12
SC117	466603	7685129	80						
			5					5	
SC106	467850	7679578	55					55	052/03
SC119	467303	7686071	40	40					209/03
SC27	464819	7684572	60					65	
SC15	463393	7684918	55					55	
SC25	464464	7683019	60					5	
SC113	462417	7686409		55				55	
SC29	465284	7682762	35		35				
SC103	467098	7679722	75		115			20	
SC30	465704	7682194						5	
SC107a	462150	7686038	65						
SC122	469696	7677577	355						
SC23	463402	7684776						5	
SC741					35			35	

Table-2. Sample locations (AMG), FIA trends measured in porphyroblasts and matrix and 'FitPitch' FIA trend/plunge from the Snake Creek Anticline. (Symbols after Kretz, 1983). Mtx: matrix

Fig. 10. 'FitPitch' results for sample SC104 and best-fit solutions with two (garnet core+median inclusion trails) and three planes (garnet core+median+rim inclusion trails). The intersection of two best-fit planes produced WNW FIA trend with shallow plunge. (b) 'FitPitch' three-plane solution including porphyroblasts rim measurements. In this case, the median+rim best-fit plane intersection is shallowly plunging to the south. Note that the intersection of two steep best-fit planes generates steeply plunging FIA, which is interpreted to an artifact.

Garnet core + median inclusion trails ‘FitPitch’ analysis

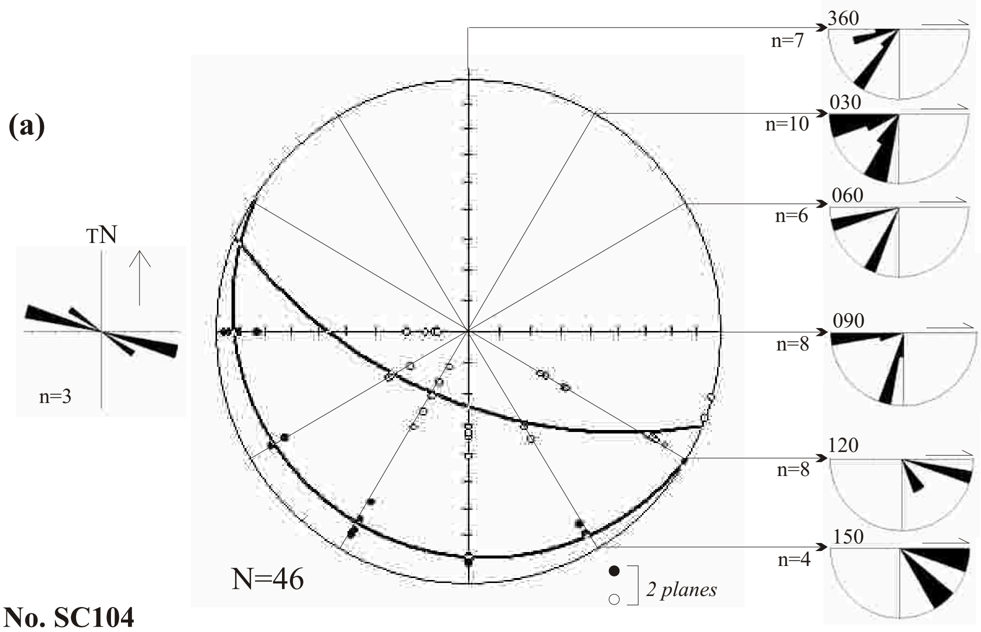

Sample No. SC104

Best Poles	Rd	Rm	FIA
032/77; 022/23	2.913	3.024	291/03 (2-plane solution) - favoured
018/77; 073/10; 005/18	3.733	1.908	165/11; 274/03; 198/72 (3-plane solution) - unfavoured

Garnet core + median + rim inclusion trails ‘FitPitch’ analysis

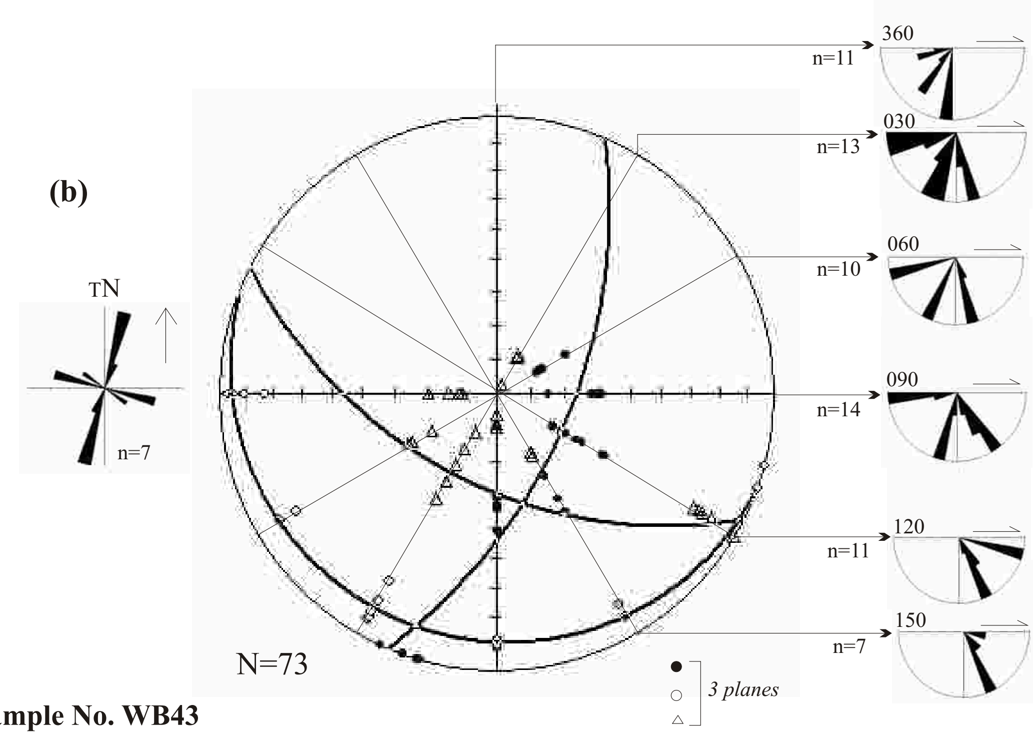

Sample No. WB43

Best Poles	Rd	Rm	FIA
293/22; 021/78; 027/09	2.548	1.565	198/12; 139/66; 117/01 (3-plane solution) - favoured

Fig. 10

Fig. 11. (a) Shows photomicrograph of staurolite porphyroblast, which contains inclusions trails of quartz and are continuous with the steep matrix foliation. Relic cordierite pseudomorphed by coarse muscovite and biotite occurs in the middle of the staurolite porphyroblast. The pseudomorphed nature of cordierite is due to higher pressure overprint (in this case St; Pattison et al., 1999) and formed during W-E shortening O_2 (sample SC112). (b) Zoned garnet porphyroblast from the same sample (SC112) preserving N-S FIA. Based on textural relationships and timing of porphyroblasts growth, it is suggested that cordierite grew first in this rock followed by garnet and then staurolite. Even though the rock contains pseudomorphed cordierite, the garnet porphyroblast shows strong and regular zoning pattern ('bell-shaped' Mn profile from core to rim), suggests increase in metamorphic grade controlled by pressure rather than temperature (e.g., Tracy et al., 1976). This is consistent with 1) pseudomorphed nature of cordierite in staurolite (e.g., Pattison et al., 1999), 2) W-E shortening produced N-S FIAs in porphyroblasts and steep N-S striking foliation. (c) Fresh andalusite preserved partially pseudomorphed cordierite. Note that the inclusion trails in andalusite porphyroblast are continuous with the matrix and interpreted to be related with O_2 metamorphic phase (see text for further discussion).

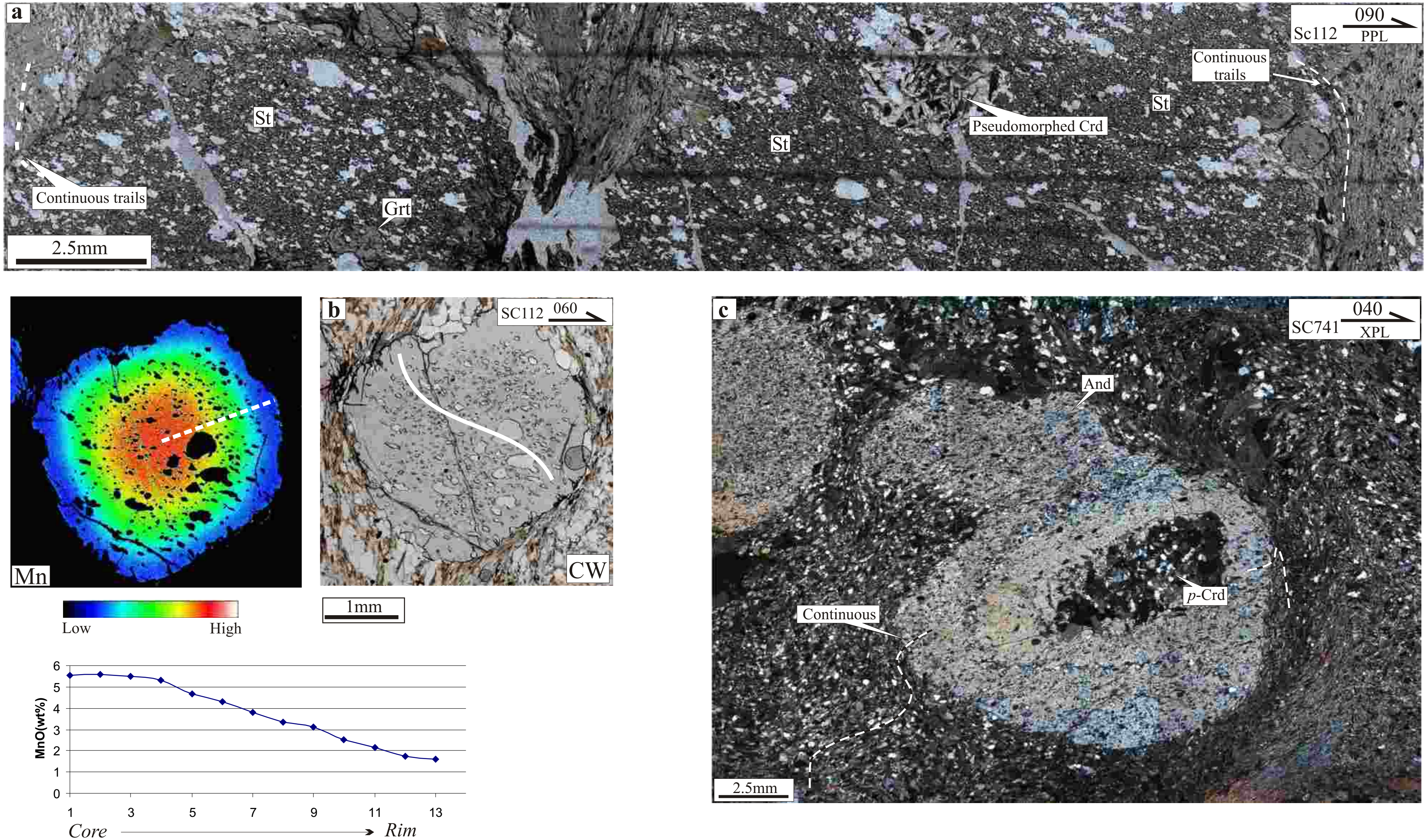
a
Sc112
090
PPL
Continuous trails
St
St
Pseudomorphed Crd
St
Continuous trails
Grt
2.5mm
Mn
Low
High
b
SC112
060
CW
1mm
c
SC741
040
XPL
And
p-Crd
Continuous
2.5mm
MnO(wt%)
Core
Rim

Fig. 11

Fig. 12. (a) Photomicrograph of relic staurolite porphyroblast partially pseudomorphed by coarse muscovite at median and rim, interpreted to formed during O_1 (sample SC113). (b) Typical decompression texture showing relic staurolite at the median and rim regions of fresh cordierite (*cf.* Fig. 11a). In this case the staurolite is interpreted to be earlier and cordierite late (Sample SC490.4). Cordierite is surrounded by late biotite growth (see also Pattison et al., 1999). (c) Staurolite porphyroblast shows partial pseudomorphed texture and marked by transition from fresh to relic character.

.

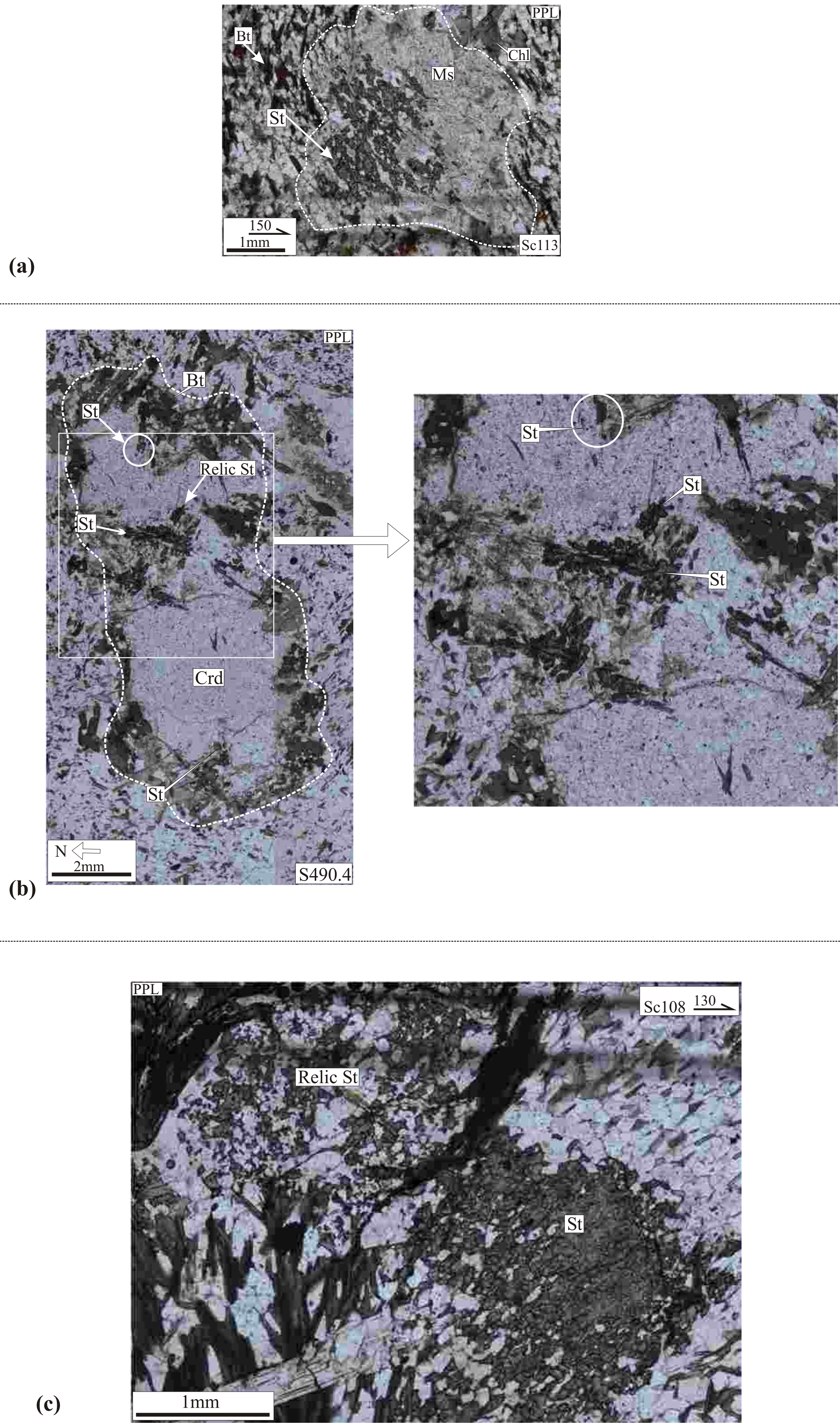
PPL
Bt
Chl
Ms
St
150
1mm
Sc113
(a)
PPL
Bt
St
Relic St
St
Crd
St
N
2mm
S490.4
St
St
St
(b)
PPL
Sc108
130
Relic St
St
1mm
(c)

Fig. 12

Fig. 13. (a) Chloritoid porphyroblast with sigmoidal inclusion trail pattern. Note that the tiny garnet near the rim region of the porphyroblast. (b) Andalusite porphyroblast with differentiated crenulation seams, which are continuous with the matrix, indicate that the porphyroblast growth occurred late in the deformation history and did not rotate (*cf.* figs. 7.4 and 7.5 of Passchier and Trouw, 1998). Tiny garnets preserved within andalusite porphyroblast. (c) Chloritoid and garnet within andalusite porphyroblast.

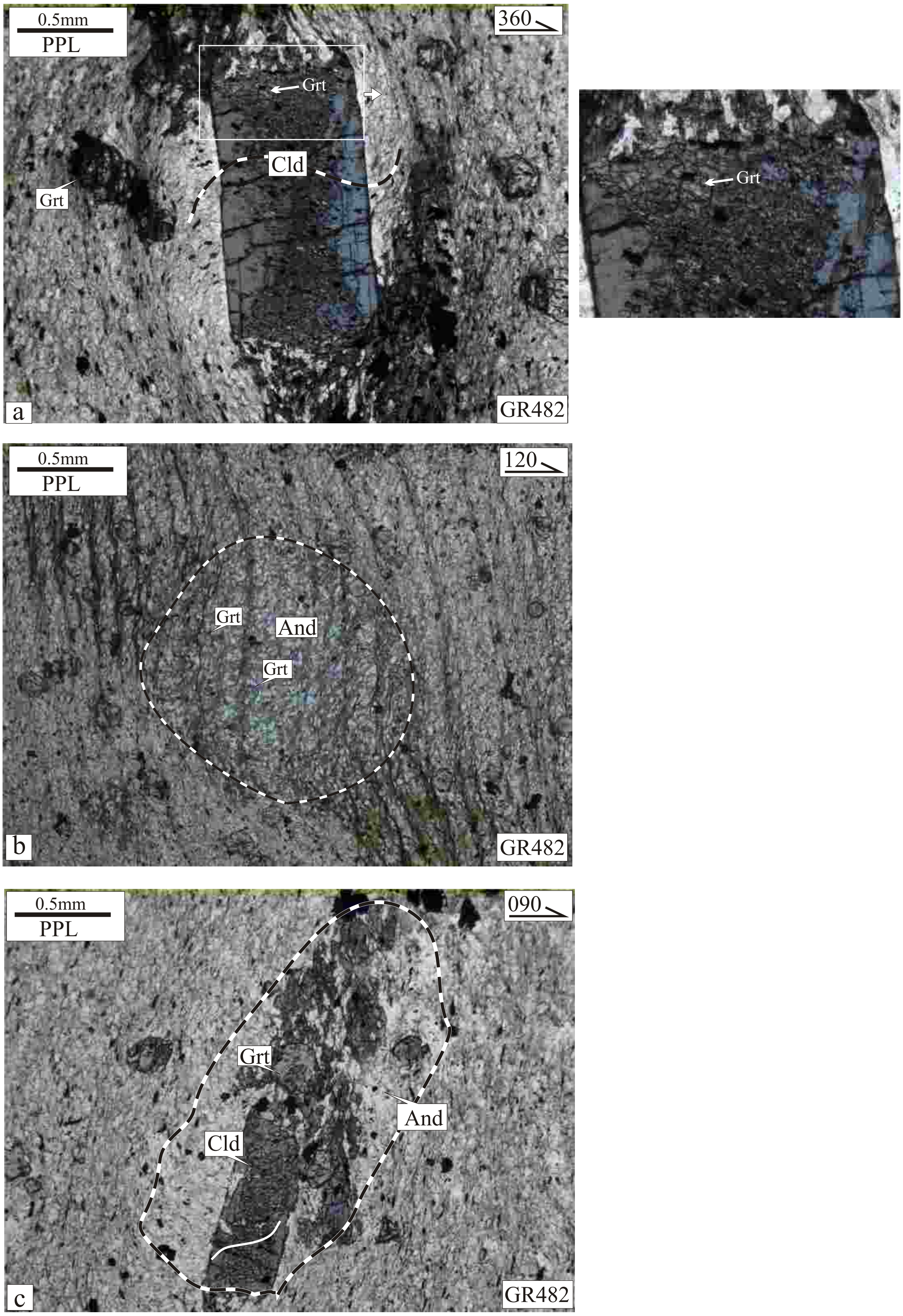
0.5mm
PPL
360
Grt
Cld
Grt
a
GR482
Grt
0.5mm
PPL
120
Grt
And
Grt
b
GR482
0.5mm
PPL
090
Grt
And
Cld
c
GR482

Fig. 13

Fig. 14. (a) Shows the FIA trends preserved in garnet porphyroblasts on equal area rose diagram around the Tommy Creek Block. (b) Orientation of pitches measured from 3 samples from the Tommy Creek Block on a total of 18 vertical oriented thin sections with variable strike across the compass. (c) An example showing how different segments of inclusion trails preserved within the garnet porphyroblasts were measured. Note steep compositional gradient (MnO wt% probe analysis from near core to rim), marked by truncation of inclusion trails at the median region of garnet porphyroblast, either represent a hiatus in garnet growth or change in garnet-forming reactions (see also Stallard and Hickey, 2002).
Rose diagrams showing trends of successive FIAs from (d) southern Selwyn Range, (e) Cannington and (f) Fairmile/Partridge areas (see text for discussion and references).

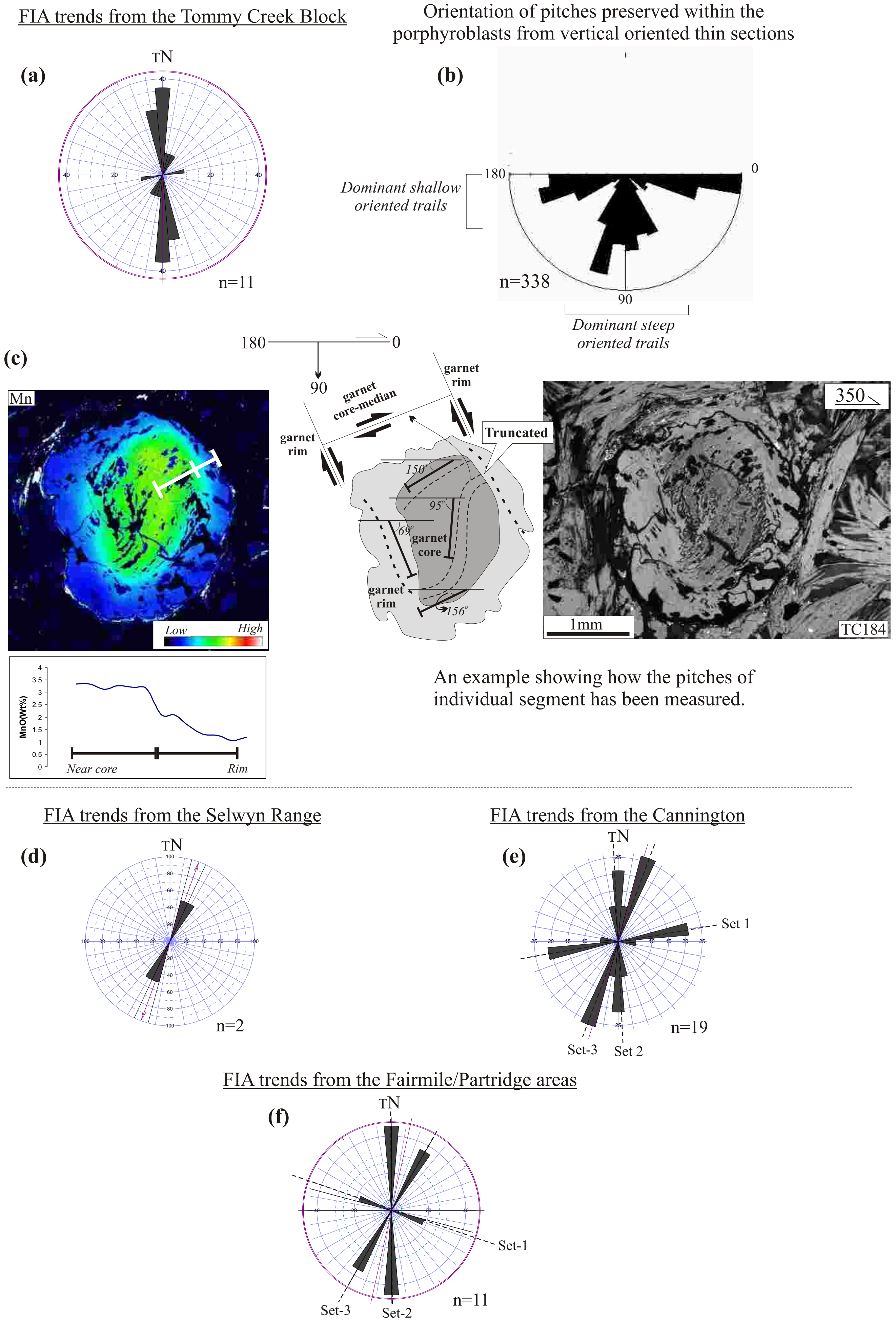

FIA trends from the Tommy Creek Block
(a)
TN
40
20
n=11
Orientation of pitches preserved within the porphyroblasts from vertical oriented thin sections
(b)
180
0
90
Dominant shallow oriented trails
Dominant steep oriented trails
n=338
(c)
Mn
Low
High
MnO(Wt%)
Near core
Rim
180
0
90
garnet core-median
garnet rim
garnet rim
Truncated
150°
95°
69°
garnet core
garnet rim
156°
350
1mm
TC184
An example showing how the pitches of individual segment has been measured.
FIA trends from the Selwyn Range
(d)
TN
n=2
FIA trends from the Cannington
(e)
TN
Set 1
Set-3
Set 2
n=19
FIA trends from the Fairmile/Partridge areas
(f)
TN
Set-1
Set-3
Set-2
n=11

Fig. 14

Fig. 15. Equal area rose diagrams of FIA trends for successive FIA sets and their correlation across the Eastern Fold Belt. In each case, dominant W-E FIAs are primitive as compared to dominant N-S ones.

Regional FIA correlation, Mt Isa Inlier

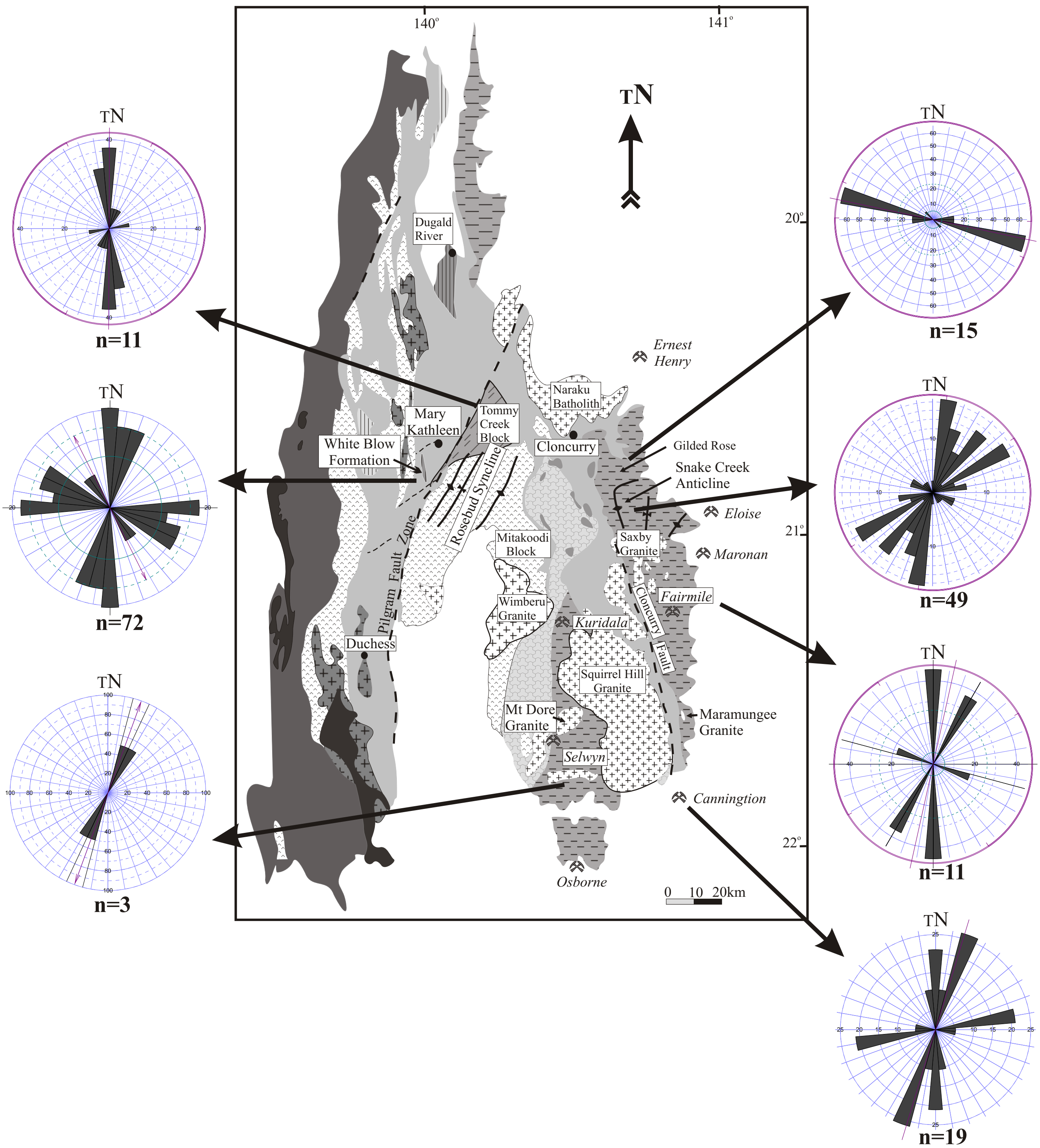

Fig. 15

Fig. 16. (a) Stereo plot showing the effects of rotating FIA set 1 around the mean trend of the next FIA in the succession. Effects of rotating FIA set 1 around the mean trend of FIA set 2 by 100^o, recorded by FIA set 2, spreads FIA set 1 trends over at least 45^o. Effects of further rotating FIA set 1 around FIA 3 spreads FIA set 1 trend over at least 75^o. Effects of rotating FIA set 1 around FIA set 4b produced spread of FIA set 1 over at least 160^o. (b) Effects of rotating FIA set 2 about FIA sets 3 and 4b.

(a)

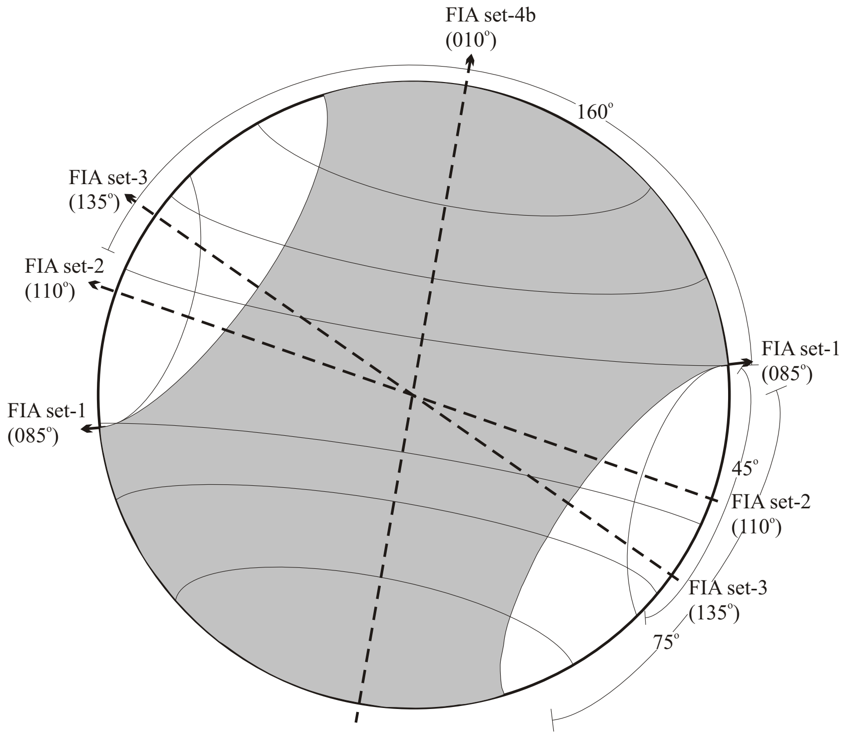
FIA set-4b
(010°)
160°
FIA set-3
(135°)
FIA set-2
(110°)
FIA set-1
(085°)
FIA set-1
(085°)
45°
FIA set-2
(110°)
FIA set-3
(135°)
75°

(b)

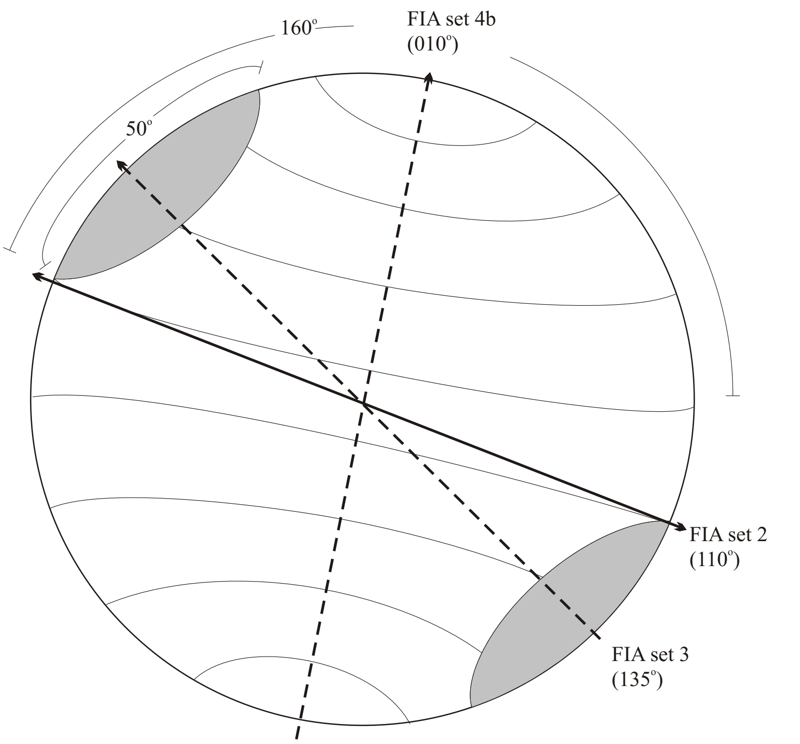
160°
FIA set 4b
(010°)
50°
FIA set 2
(110°)
FIA set 3
(135°)

Fig. 16

Fig. 17. SWEAT (*S*outh-*W*est US – *E*ast *Ant*arctica), AUSWUS (*Aus*tralia – *W*estern *US*) and AUSMEX (*Aus*tralia – *Mex*ico) reconstructions for supercontinent Rodinia. A: Australia, L: Laurentia, An: Antarctica.
SWEAT (e.g., Hoffman, 1991; Powell et al., 1993) and AUSWUS (e.g., Karlstrom et al., 2001) hypothesis are based on matching geological and tectonic features and age provinces across the Rodinia supercontinent, whereas, AUSMEX reconstruct Rodinia based on geochronological and paleomagnetic data (e.g., Wingate, 2002).

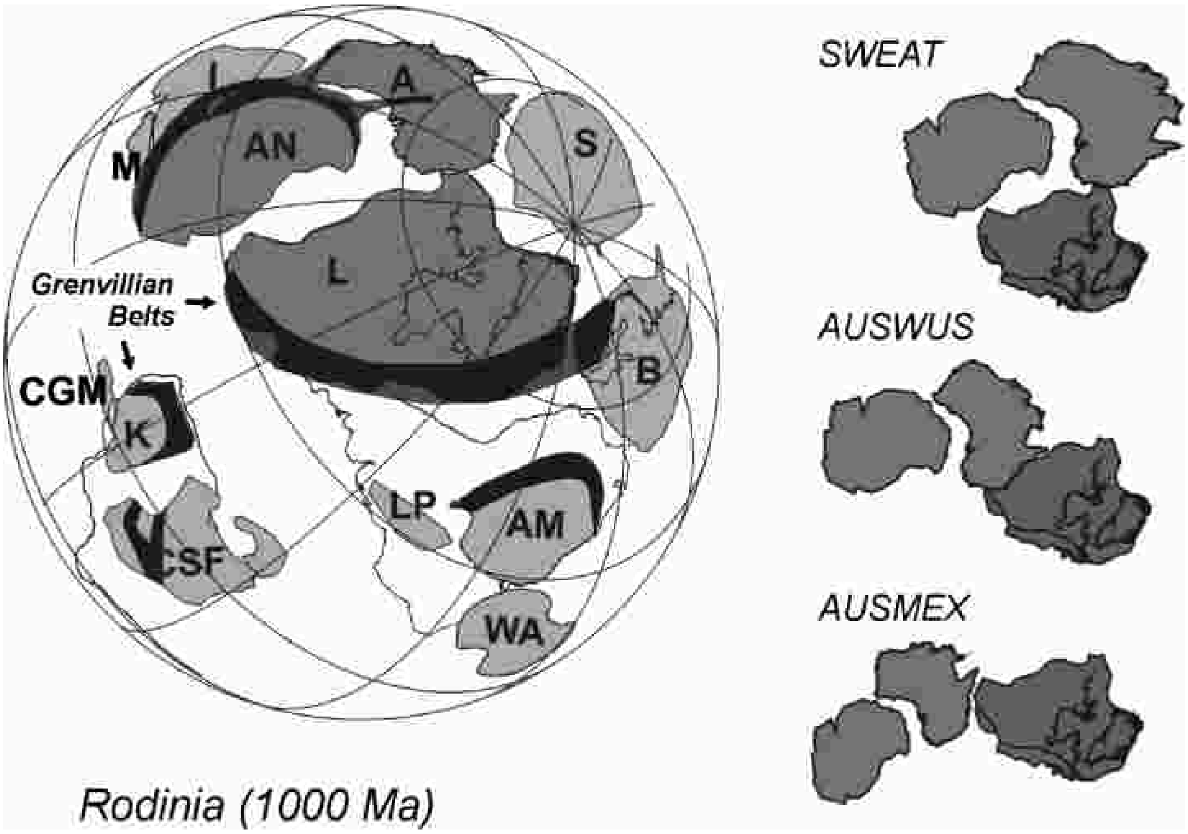

SWEAT
AUSWUS
AUSMEX
A
AN
M
S
L
Grenvillian
Belts
CGM
K
B
LP
AM
CSF
WA
Rodinia (1000 Ma)

Fig. 17

Section – D

Decompression through an early clockwise P-T path in the Mt Isa Inlier: implications for early N-S shortening orogenesis

(Figures and Tables)

Fig. 1. (a) Outline map of the Mount Isa Inlier showing Western Fold Belt (WFB), Kalkadoon-Leichhardt Belt (KLB) and Eastern Fold Belt (EFB). (b) Regional geological map of the Eastern Fold Belt showing major lithotectonic units and locations of the study area (modified after Blake, 1987; Giles and MacCready, 1997; Williams, 1998; Marshall and Oliver, 2001). Ages after Page and MacCready (1997), Page and Sun (1998).

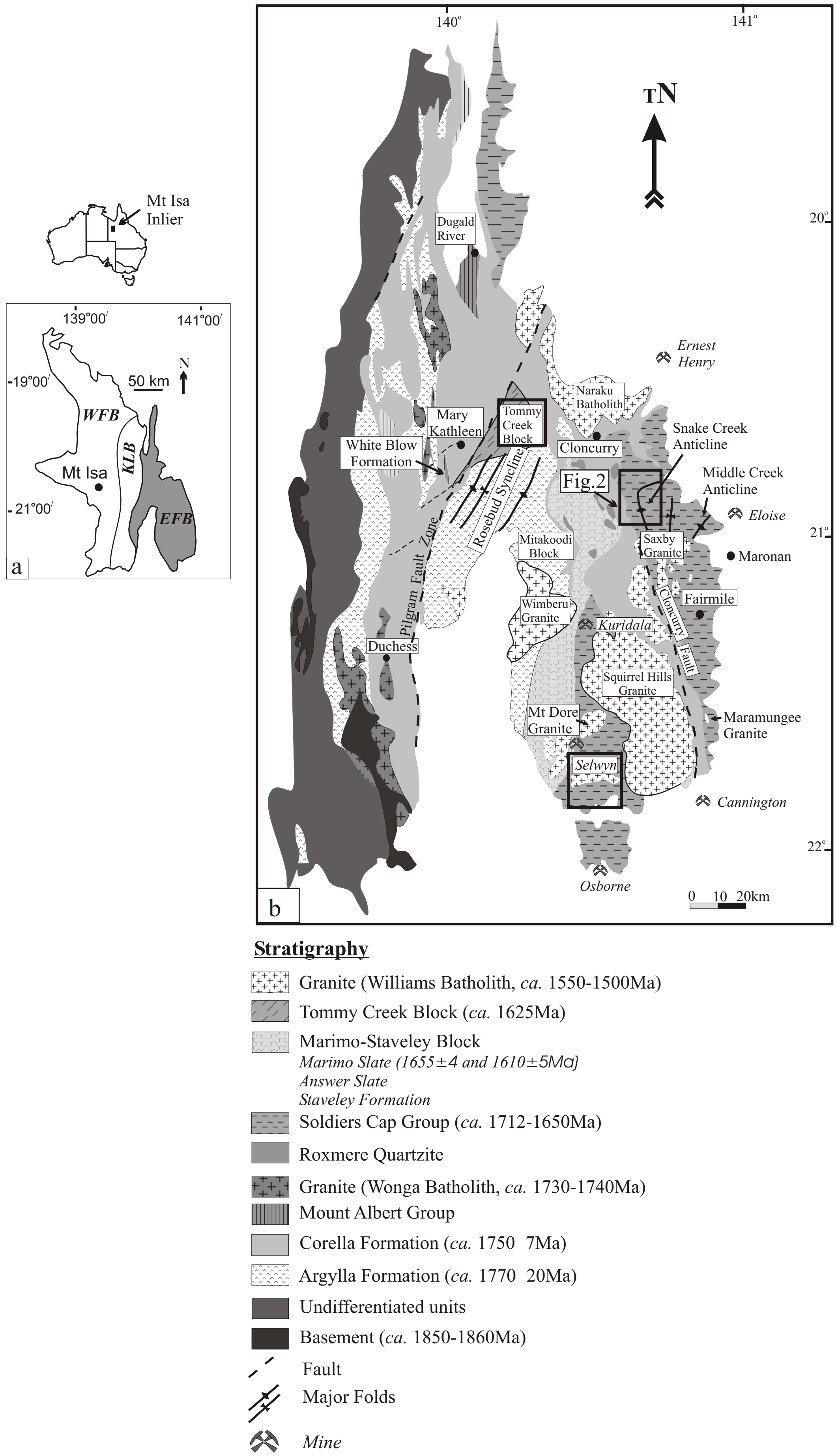

Mt Isa
Inlier
139°00'
141°00'
19°00'
21°00'
50 km
N
WFB
KLB
EFB
Mt Isa
a
140°
141°
20°
21°
22°
N
Dugald
River
Ernest
Henry
Naraku
Batholith
Tommy
Creek
Block
Mary
Kathleen
White Blow
Formation
Cloncurry
Snake Creek
Anticline
Middle Creek
Anticline
Fig.2
Eloise
Rosebud Syncline
Pilgram Fault Zone
Mitakoodi
Block
Saxby
Granite
Maronan
Wimberu
Granite
Fairmile
Kuridala
Cloncurry
Fault
Duchess
Squirrel Hills
Granite
Mt Dore
Granite
Maramungee
Granite
Selwyn
Cannington
Osborne
0 10 20km
b
Stratigraphy
Granite (Williams Batholith, ca. 1550-1500Ma)
Tommy Creek Block (ca. 1625Ma)
Marimo-Staveley Block
Marimo Slate (1655±4 and 1610±5Ma)
Answer Slate
Staveley Formation
Soldiers Cap Group (ca. 1712-1650Ma)
Roxmere Quartzite
Granite (Wonga Batholith, ca. 1730-1740Ma)
Mount Albert Group
Corella Formation (ca. 1750 7Ma)
Argylla Formation (ca. 1770 20Ma)
Undifferentiated units
Basement (ca. 1850-1860Ma)
Fault
Major Folds
Mine

Fig. 1

Fig. 2. Edge enhanced Landsat band-7 image showing Snake Creek Anticline (SCA), Saxby Granite (SG; northern part of the Williams Batholiths), Gilded Rose and Cloncurry Fault. The albitization front occurs along the axes of the Snake Creek Anticline, north of the Saxby Granite, where most of the cordierite has been found (*cf.* fig.1 of Rubenach and Lewthwaite, 2002). No cordierite occurs in the Gilded Rose area. W-E FIA trends obtained from the Gilded Rose whereas dominant N-S and NE-SW FIAs obtained from the Snake Creek Anticline.
Landsat imagery courtesy of NASA Goddard Space Flight Center and U.S. Geological Survey.

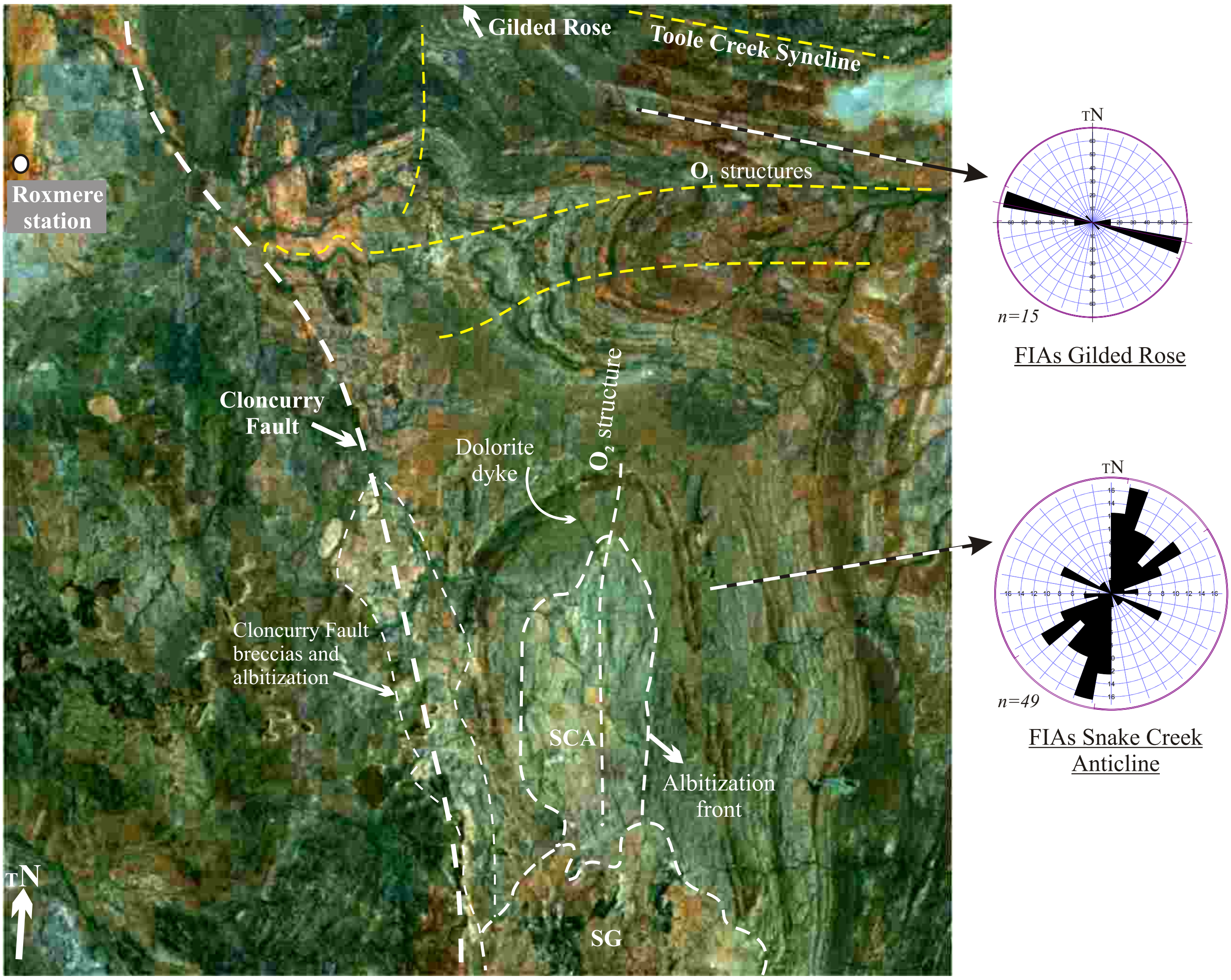

Gilded Rose
Toole Creek Syncline
O_1 structures
Roxmere station
Cloncurry Fault
Dolorite dyke
O_2 structure
Cloncurry Fault breccias and albitization
SCA
Albitization front
SG
TN
TN
n=15
FIAs Gilded Rose
TN
n=49
FIAs Snake Creek Anticline

Fig. 2

Fig. 3. (ab&c) Photomicrographs showing garnet and chloritoid porphyroblasts enclosed within andalusite (sample GR482 from Gilded Rose). Chloritoid contains garnet as inclusions in 'a'. Andalusite hosts crenulations, which are continuous with the matrix foliation in 'b' and 'c'. (d&e) Garnet and staurolite porphyroblasts enclosed within andalusite (sample GR3). (f&g) Garnets from sample GR192 (from southern Gilded Rose) contains spiral inclusion trails that are truncated with the matrix foliation. The garnet porphyroblasts contain chlorite, altered plagioclase and rare biotite inclusions. No chlorite is present in the matrix.
Plane polarized light (PPL). Vertical thin sections. Single barbed arrow shows strike, bearing and way up (in this and subsequent photomicrographs). Abbreviations are after Kretz (1983).

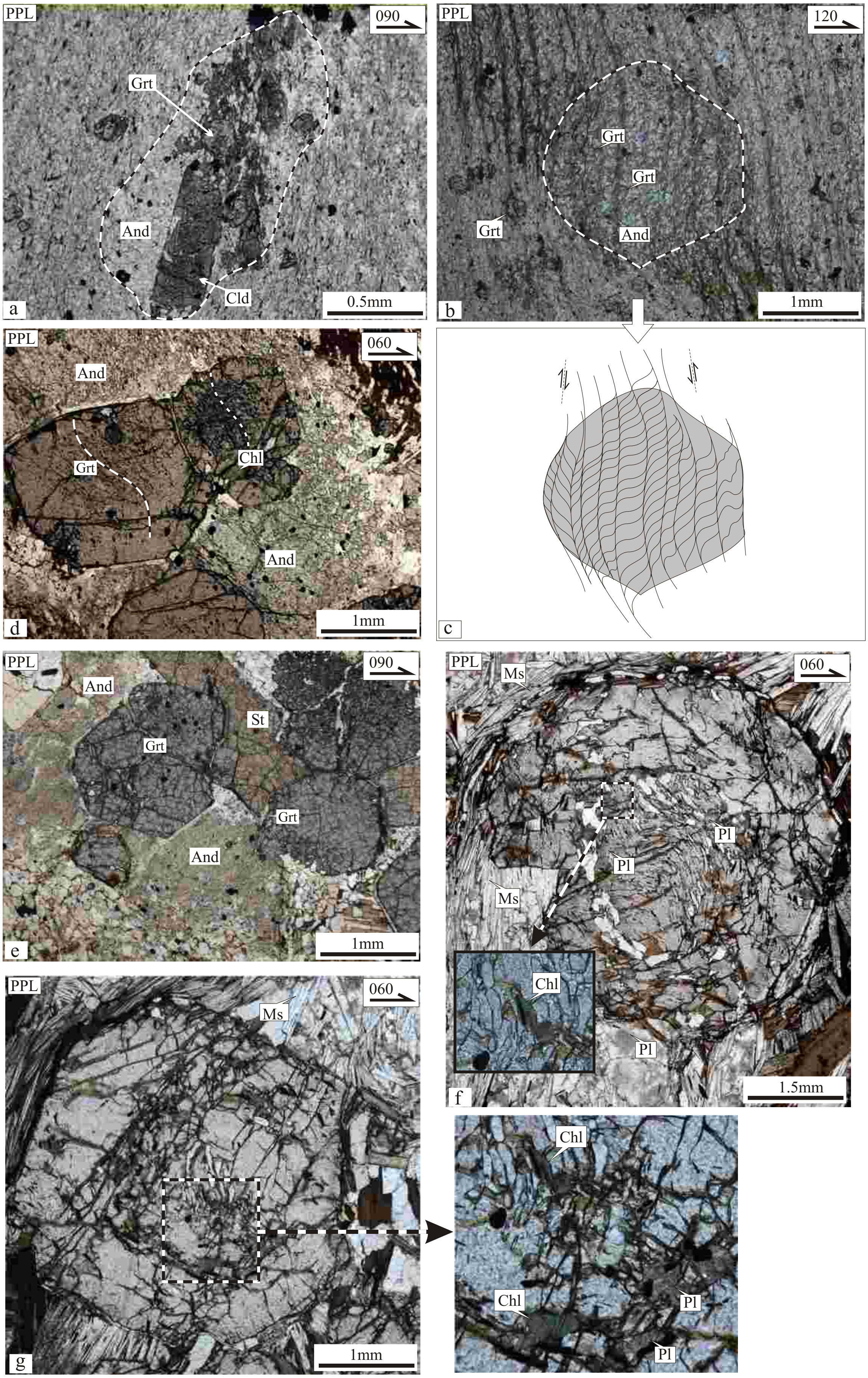

PPL
090
Grt
And
Cld
0.5mm
a
PPL
120
Grt
Grt
Grt
And
1mm
b
PPL
060
And
Grt
Chl
And
1mm
d
c
PPL
090
And
St
Grt
Grt
And
1mm
e
PPL
060
Ms
Pl
Pl
Ms
Chl
Pl
1.5mm
f
PPL
060
Ms
1mm
g
Chl
Chl
Pl
Pl

Fig. 3

Fig. 4. (a&b) Photomicrographs of relic staurolite porphyroblasts partially pseudomorphed by coarse muscovite at median and rim regions, interpreted to formed during O_1 (sample SC113 from the Snake Creek Anticline; see text for discussion). (cd&e) Photomicrographs of relic staurolite and kyanite porphyroblasts preserved within cordierite indicate near-isothermal decompression. The relic nature of St and Ky is due to lower-pressure overprint. Some of the relatively large cordierites show characteristic lamellar or concentric twining (e.g., the one shown in'd'). Matrix is albitized as indicated by albite grains with sucrosic texture. No albite grains have been observed within relic kyanite, staurolite and/or in cordierite indicate late albitization input into this rock (sample SC110 from the Snake Creek Anticline). (f) Garnet porphyroblast from sample SC110 contains sigmoidal inclusion trail pattern. 025^{o} FIA is obtained from such type of garnet porphyroblasts. (g) Relic staurolite preserved within cordierite porphyroblast (sample SC490.4 from the Snake Creek Anticline).

Single barbed arrow shows strike, bearing and way up. Plane polarized light (PPL) and cross polarized light (XPL). Abbreviations are after Kretz (1983).

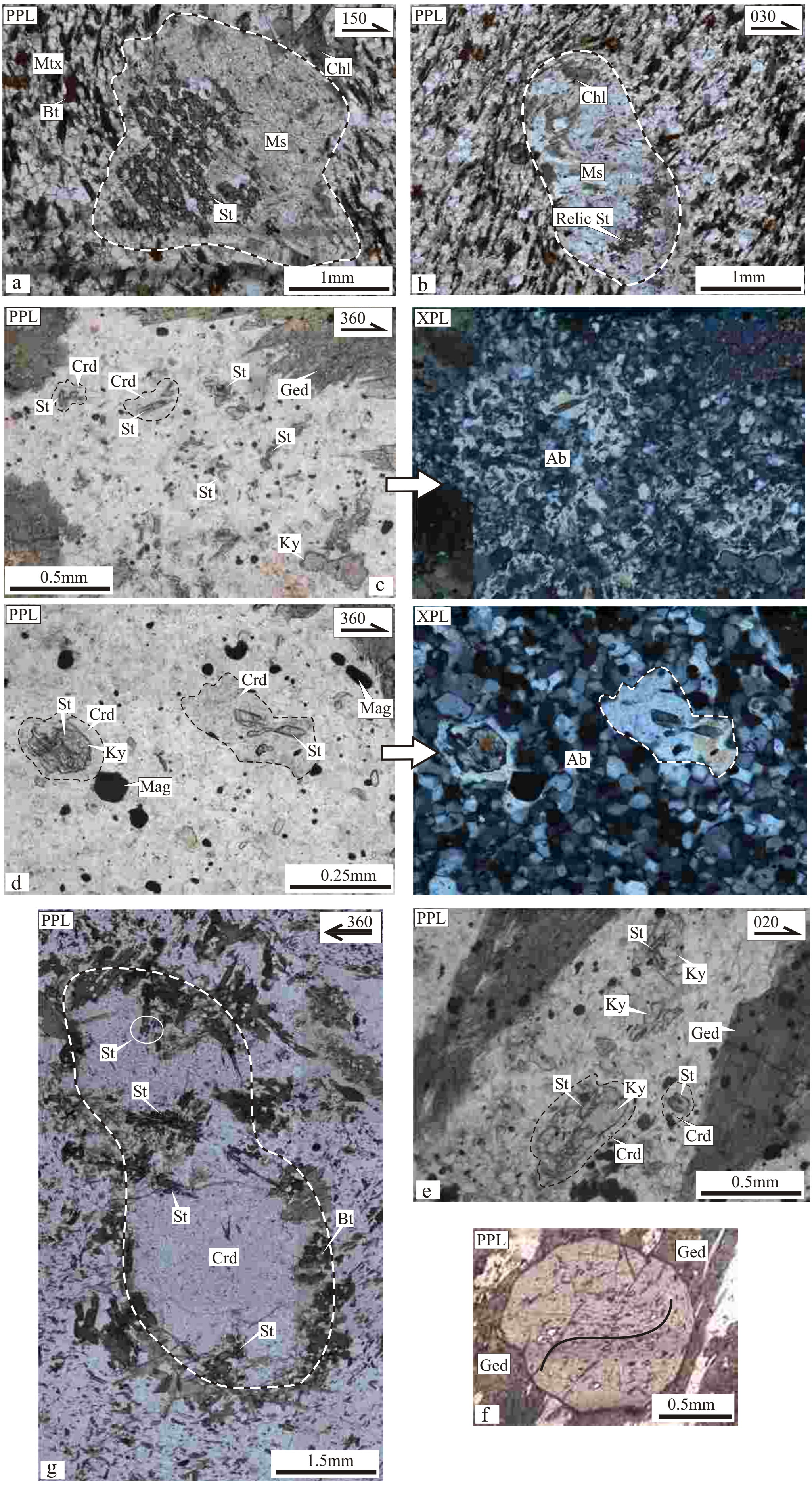

PPL
150
Mtx
Bt
Chl
Ms
St
1mm
a
PPL
030
Chl
Ms
Relic St
1mm
b
PPL
360
Crd
Crd
St
St
St
Ged
St
St
Ky
0.5mm
c
XPL
Ab
PPL
360
Crd
St
Crd
Ky
Mag
St
Mag
0.25mm
d
XPL
Ab
PPL
360
St
St
St
Bt
Crd
St
1.5mm
g
PPL
020
St
Ky
Ky
Ged
St
Ky
St
Crd
Crd
0.5mm
e
PPL
Ged
Ged
0.5mm
f

Fig. 4

Fig. 5. (a&b) Showing partial pseudomorphing of staurolite by andalusite (samples SC52.2 and SC789 from the Snake Creek Anticline). Note garnet porphyroblasts in andalusite with altered reaction rims (sample SC52.2). (c) Shows fresh staurolite, which contains inclusions trails of quartz and are continuous with the steep matrix foliation. Relic cordierite pseudomorphed by coarse muscovite and biotite occurs in the middle of the staurolite porphyroblast. The pseudomorphed nature of Crd is due to higher pressure overprint (in this case St) and formed during W-E shortening O_2 (sample SC112 from the Snake Creek Anticline). (d) Andalusite porphyroblasts with inclusions truncated with matrix and interpreted to formed at the end of O_1 before cordierite (sample SC103 from the Snake Creek Anticline). (e) Andalusite porphyroblast replaced by pseudomorphed (coarse muscovite) cordierite related to O_1 (SC104). (f) Kyanite prism showing direct replacement by andalusite with or without sillimanite (SC52.2). The photomicrograph also shows relic staurolite (of O_1) replaced by andalusite.

Plane polarized light (PPL) and cross polarized light (XPL).

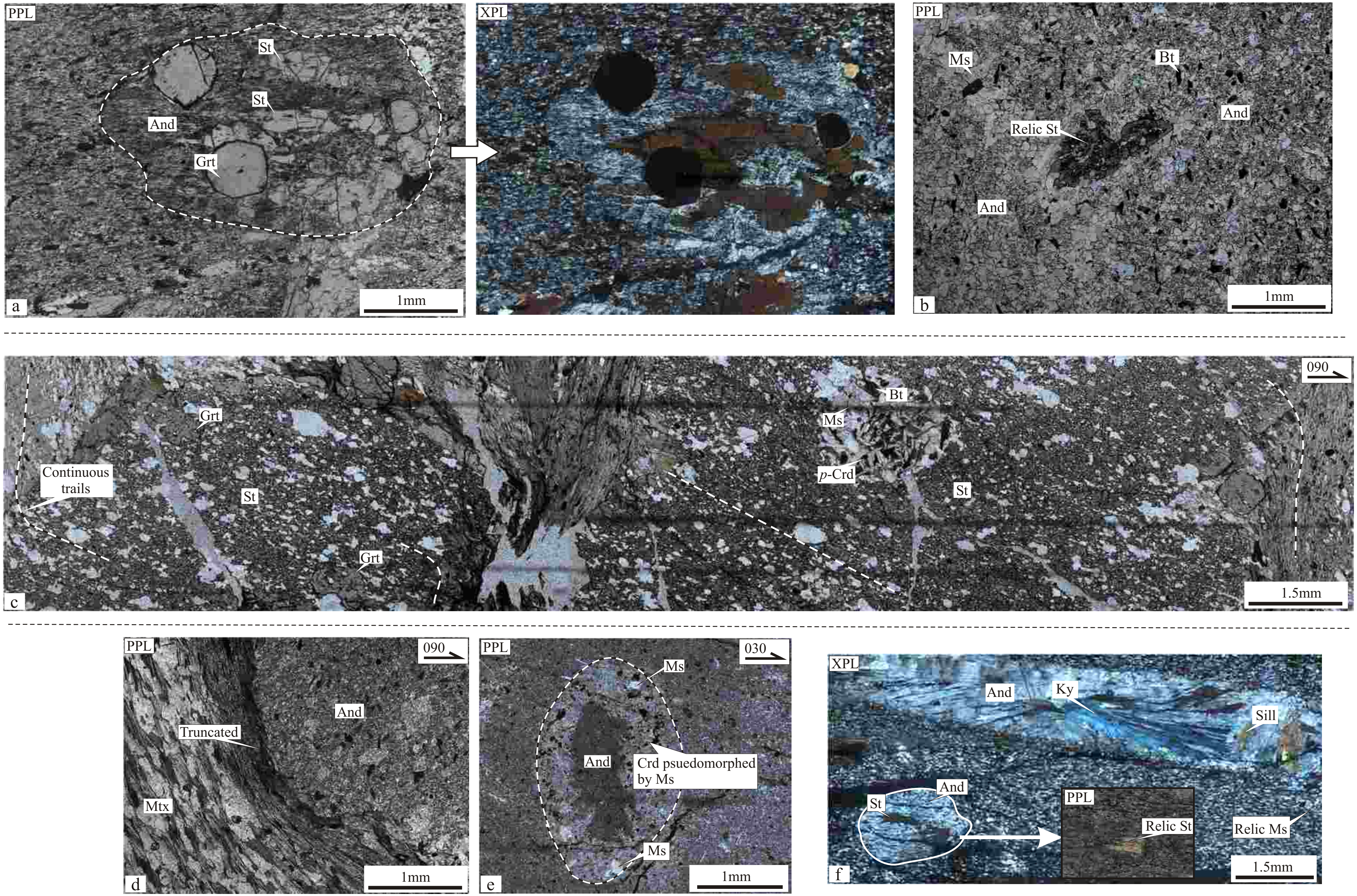
PPL
St
St
And
Grt
1mm
a
XPL
PPL
Ms
Bt
And
Relic St
And
1mm
b
090
Bt
Grt
Ms
Continuous trails
p-Crd
St
St
Grt
1.5mm
c
PPL
090
And
Truncated
Mtx
1mm
d
PPL
030
Ms
And
Crd psuedomorphed by Ms
Ms
1mm
e
XPL
And
Ky
Sill
And
St
PPL
Relic St
Relic Ms
1.5mm
f

Fig. 5

Fig. 6. (a) Fresh andalusite preserved partially pseudomorphed cordierite in the core. Note that the inclusion trails in andalusite porphyroblast are continuous with the matrix and interpreted to be related with O_2 metamorphic phase (see text for further discussion). (b) Showing local overgrowths of andalusite preserving steep foliations, which are parallel and continuous with the matrix. (c) Sample TC508 (from Tommy Creek Block; collected by Lally, 1997) with W-E FIA preserved within garnet porphyroblasts (determined in this study). Garnet preserved relic staurolite and both staurolite and garnet porphyroblasts are preserved within large andalusite (extends past the photomicrograph). (d) Garnet porphyroblast, where the rim replaced by biotite, preserved within large andalusite porphyroblast (sample TC1365 from Tommy Creek Block). (e) Showing staurolite grain partially pseudomorphed by coarse muscovite.
Plane polarized light (PPL) and cross polarized light (XPL).

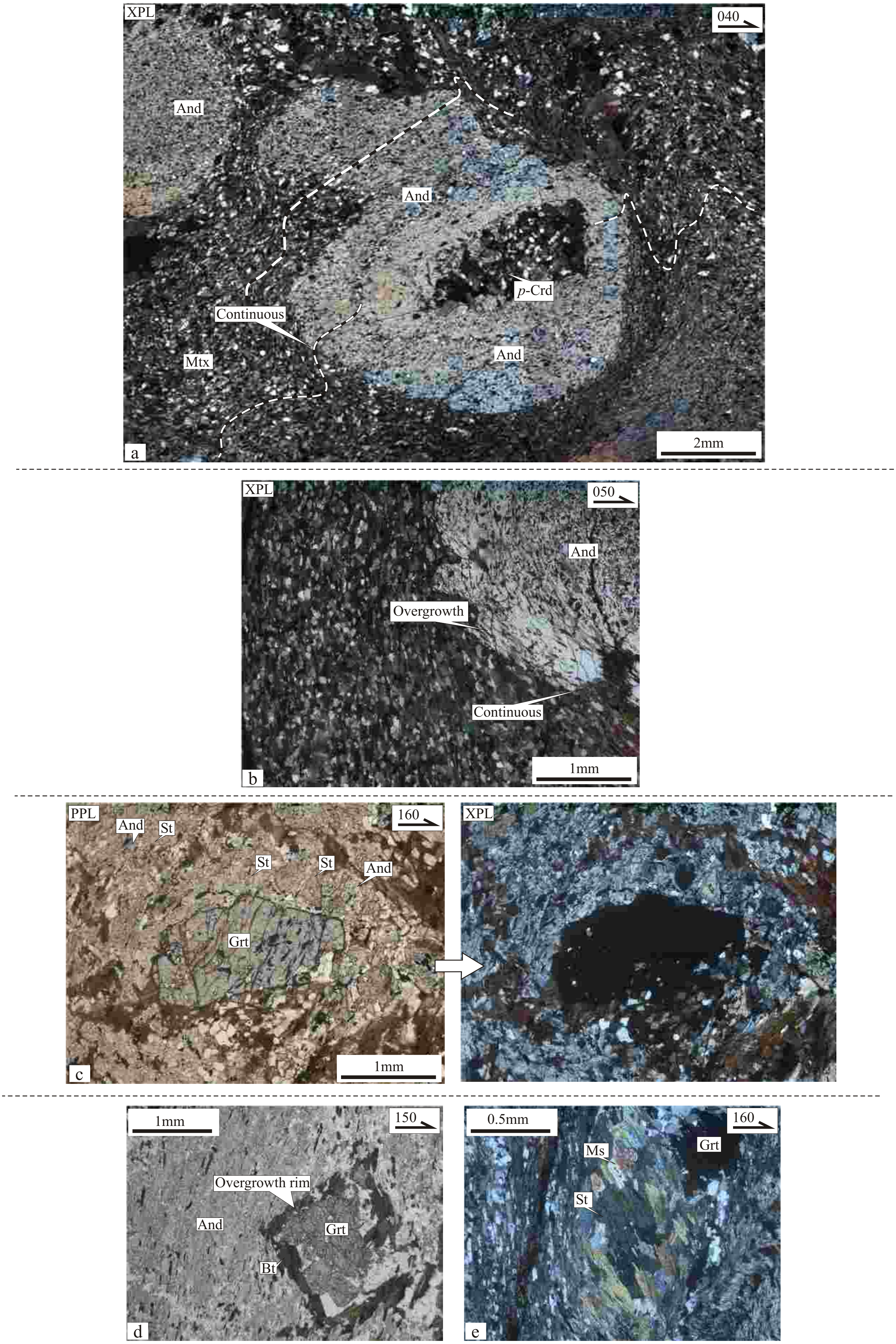
XPL
040
And
And
p-Crd
Continuous
Mtx
And
2mm
a
XPL
050
And
Overgrowth
Continuous
1mm
b
PPL
160
And
St
St
St
And
Grt
1mm
c
XPL
1mm
150
Overgrowth rim
And
Grt
Bt
d
0.5mm
160
Ms
Grt
St
e

Fig. 6

Fig. 7. (a) Garnet and staurolite porphyroblasts preserving inclusion trails continuous with the matrix and that have N-S FIA preserved in them (sample TC1365 from Tommy Creek Block). (b) Garnet with reaction rim of biotite and cordierite from the Selwyn Range. The matrix is dominated by muscovite (sample SR14). (c) Garnet partially pseudomorphed by chlorite and biotite (SR14). (d&e) Showing garnet porphyroblast with inclusions continuous with the matrix without reaction rims and interpreted to related with O_2 from the Selwyn Range (sample SR134B).

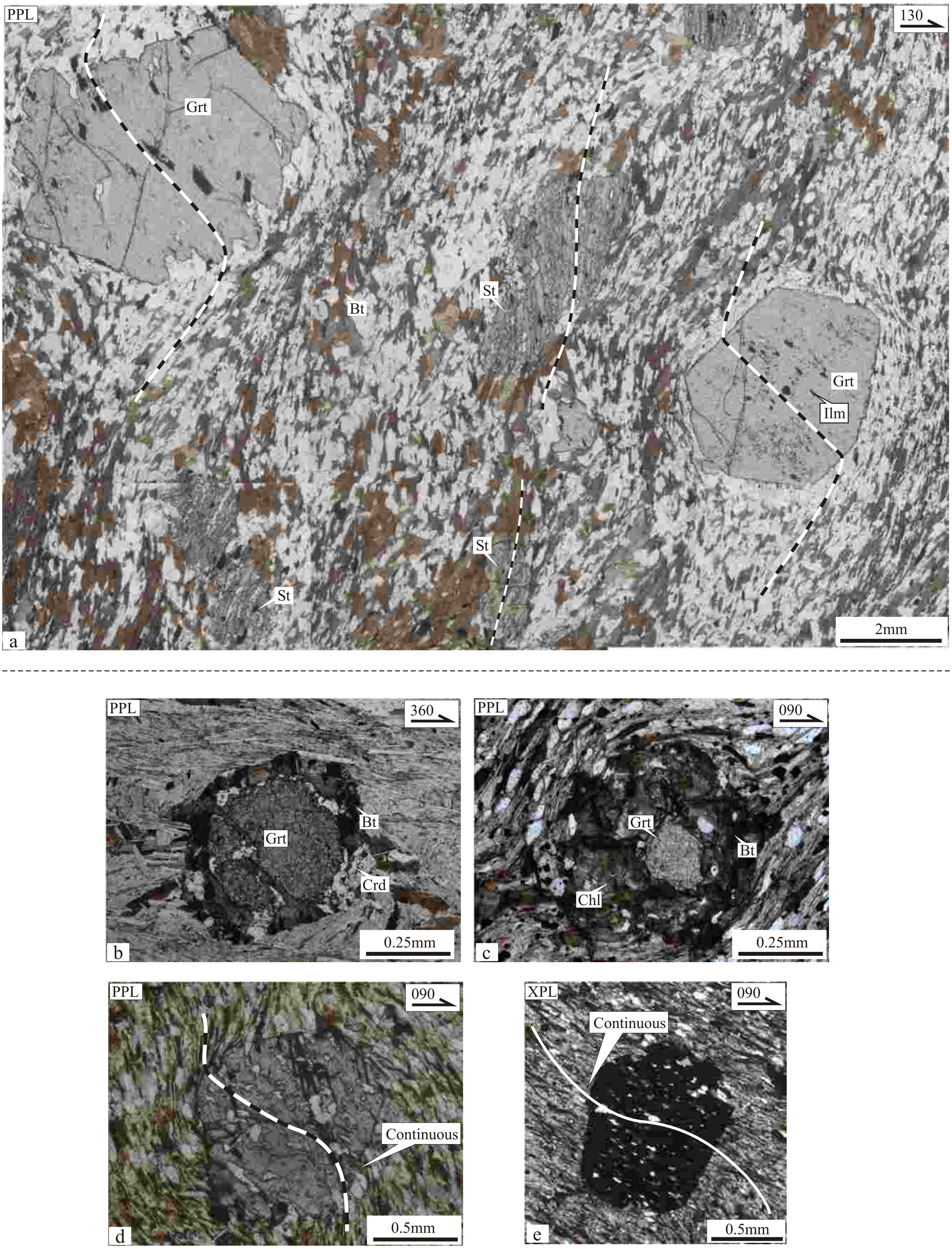
PPL
130
Grt
Bt
St
Grt
Ilm
St
St
2mm
a
PPL
360
Grt
Bt
Crd
0.25mm
b
PPL
090
Grt
Bt
Chl
0.25mm
c
PPL
090
Continuous
0.5mm
d
XPL
090
Continuous
0.5mm
e

Fig. 7

Table-1. Major element compositions (wt%) of selected samples for MnNCKFMASH pseudosection calculations*.

Sample	GR189	GR192	GR76	SC112	SC118	TC186	Average Pelite**
SiO_2	58.2	53.5	63.3	62.8	62.4	48.00	59.77
Al_2O_3	21.4	24.4	18.8	19.8	17.9	20.4	16.57
FeO	7.20	7.87	6.18	6.22	7.14	15.57	5.88
MnO	0.07	0.14	0.10	0.10	0.12	0.39	0.07
MgO	1.36	1.22	1.16	1.65	1.82	1.44	2.62
CaO	0.67	1.09	0.20	0.18	0.17	0.65	2.17
Na_2O	0.83	2.01	0.32	1.44	0.41	0.17	1.73
K_2O	5.75	5.05	4.48	4.01	4.34	5.22	3.53

** Normalized for psedosection calculations (mol%; see Appendix D MnNCKFMASH data file).*

***Average pelite composition from Symmes and Ferry (1991).*

TiO_2 in all samples is less than 1.0wt%

Fig. 8. P-T pseudosection calculated in MnNCKFMASH based on bulk XRF composition for sample GR192, which is from the south of the Gilded Rose. (a) The pseudosection is contoured with respect to garnet composition isopleths Mn, Ca and Fe with increasing pressure and temperature. (b) Compositional contours corresponding to the real composition (microprobe) of garnet core along with their errors indicated as light shaded thick lines. Garnet rim plus matrix phases were calculated using average P-T mode in THERMOCALC-3.21 (sigfit = 0.9). The median region P-T path and estimates were calculated by using fractionation method of garnet porphyroblast with respect to evolving bulk rock composition (Evans, 2004). Micoprobe EDS spot traverse is shown on X-ray compositional (Mn) garnet map from core to rim (Table 1 for representative analysis; see Fig. 3f).

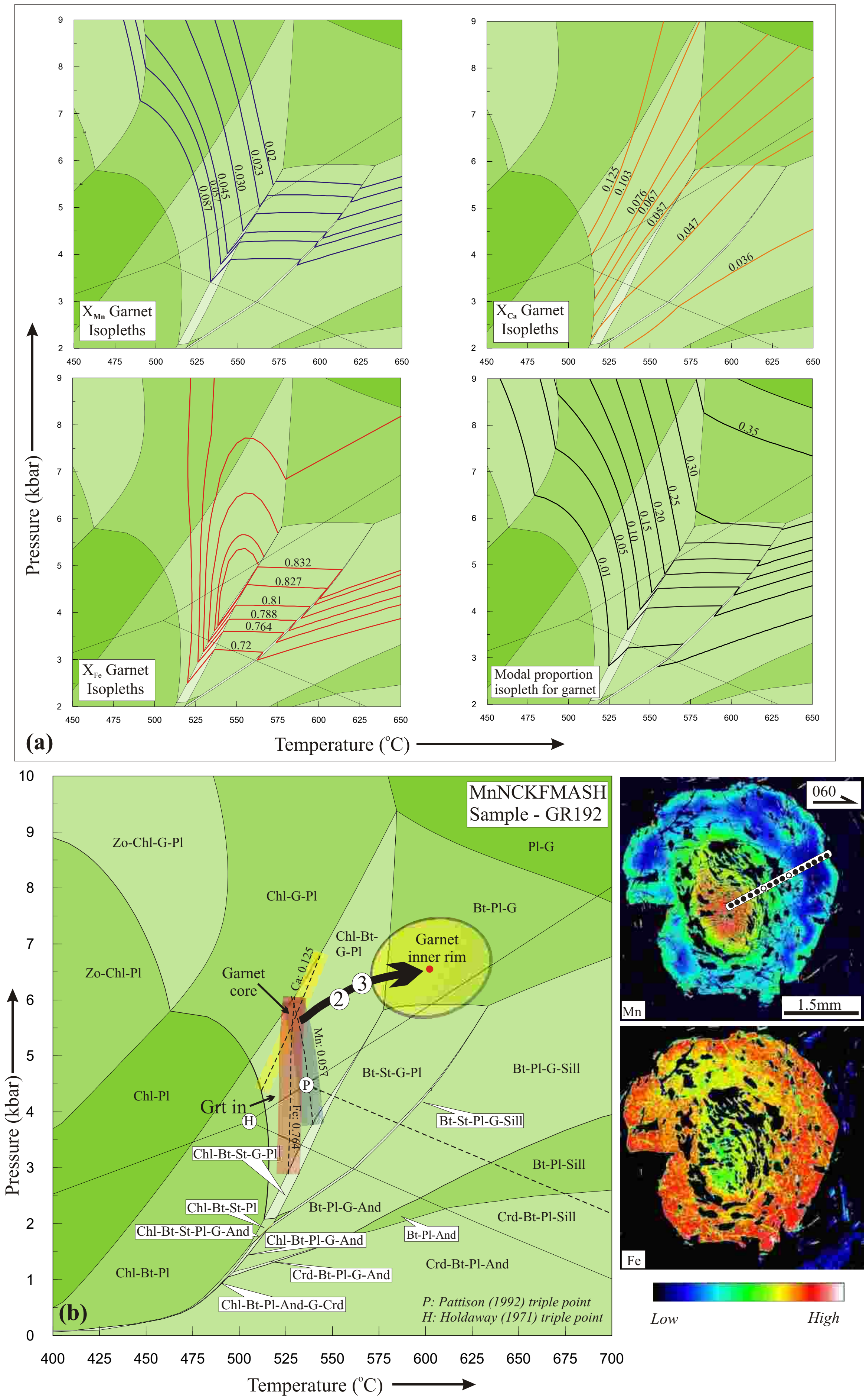

XMn Garnet Isopleths
XCa Garnet Isopleths
XFe Garnet Isopleths
Modal proportion isopleth for garnet
Pressure (kbar)
Temperature (°C)
(a)
MnNCKFMASH
Sample - GR192
Zo-Chl-G-Pl
Chl-G-Pl
Pl-G
Bt-Pl-G
Chl-Bt-G-Pl
Garnet inner rim
Zo-Chl-Pl
Garnet core
Chl-Pl
Grt in
Bt-St-G-Pl
Bt-Pl-G-Sill
Bt-St-Pl-G-Sill
Bt-Pl-Sill
Chl-Bt-St-G-Pl
Chl-Bt-St-Pl
Chl-Bt-St-Pl-G-And
Chl-Bt-Pl-G-And
Bt-Pl-G-And
Bt-Pl-And
Crd-Bt-Pl-Sill
Crd-Bt-Pl-G-And
Crd-Bt-Pl-And
Chl-Bt-Pl
Chl-Bt-Pl-And-G-Crd
P: Pattison (1992) triple point
H: Holdaway (1971) triple point
(b)
Ca: 0.125
Mn: 0.057
Fe: 0.764
060
1.5mm
Mn
Fe
Low
High

Fig. 8

Fig. 9. P-T conditions determined by using fractionation method of garnet growth with effective bulk rock compositions (see Evans, 2004). Compositional isopleths are plotted based on real microprobe garnet analysis from median and far-median region. See Fig. 8 for individual EPMA points on X-ray Mn map. EDS spots, calculated for fractionation technique are shown as white circles.

Fractionation of bulk rock with respect to garnet composition
and P-T conditions at medium and far-medium
region for sample GR192 (see Evans, 2004)

Effective bulk composition at GR192_Gt-6 (mol%)

Al_2O_3	CaO	MgO	FeO	K_2O	Na_2O	MnO
16.96	1.22	2.10	6.03	3.99	2.42	0.05

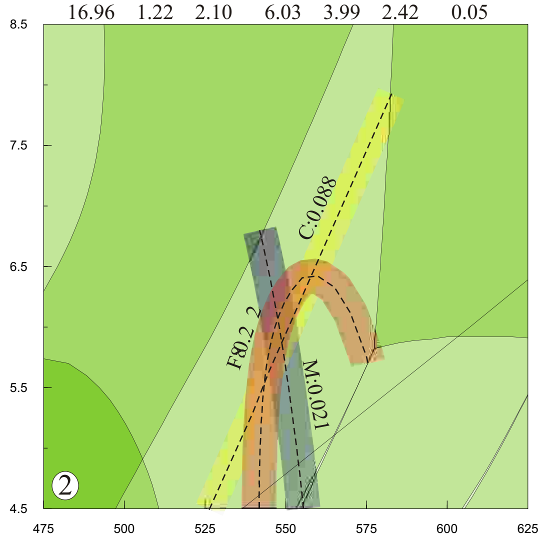

Effective bulk composition at GR192_Gt-9 (mol%)

Al_2O_3	CaO	MgO	FeO	K_2O	Na_2O	MnO
16.88	1.17	2.07	5.47	4.03	2.44	0.04

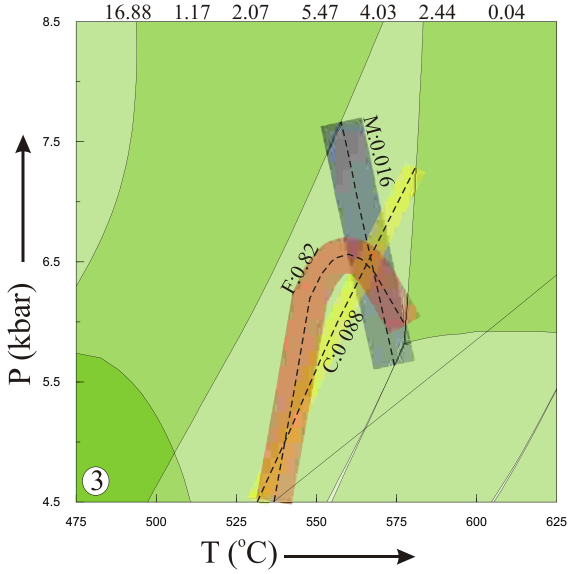

Fig. 9

Fig. 10. P-T pseudosection calculated in MnNCKFMASH based on bulk XRF composition for sample GR189 (south of the Gilded Rose). (a) The pseudosection is contoured with respect to garnet composition isopleths Mn, Ca and Fe with increasing pressure and temperature. (b) Compositional contours corresponding to the real composition of garnet core along with their errors indicated as light shaded thick lines. Garnet rim plus matrix phases were calculated using average P-T mode in THERMOCALC-3.21 (sigfit = 0.59). Points 2 and 3 were calculated without fractionation technique of garnet growth with respect to effective bulk rock due to near-homogenous composition of major elements (Mn, Fe, Ca) from core to near-median zones of garnet porphyroblast.

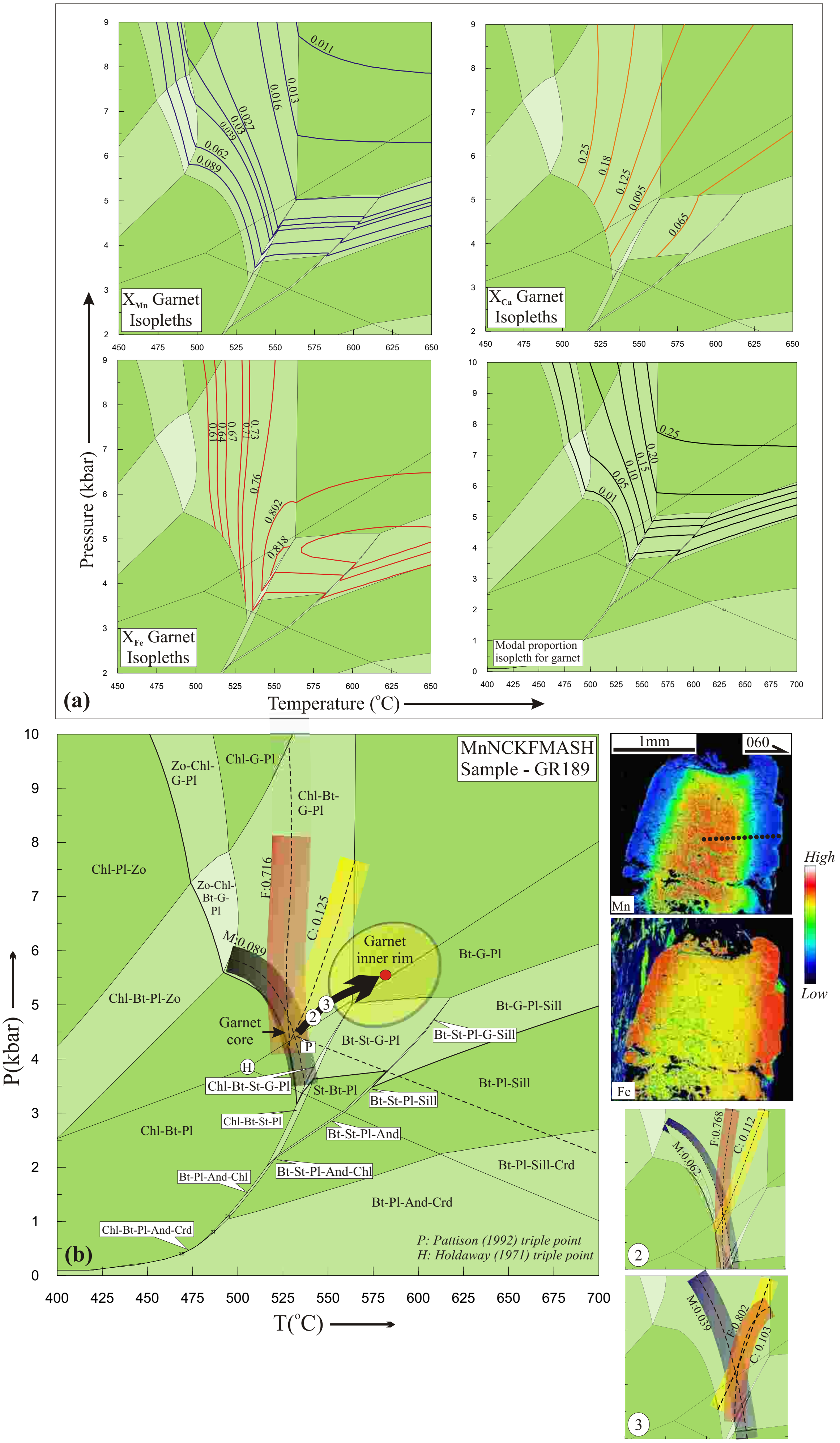

X_Mn Garnet Isopleths
X_Ca Garnet Isopleths
X_Fe Garnet Isopleths
Modal proportion isopleth for garnet
Pressure (kbar)
Temperature (°C)
(a)
MnNCKFMASH Sample - GR189
Chl-Pl-Zo
Zo-Chl-G-Pl
Chl-G-Pl
Chl-Bt-G-Pl
Zo-Chl-Bt-G-Pl
Chl-Bt-Pl-Zo
Bt-G-Pl
Bt-G-Pl-Sill
Bt-St-Pl-G-Sill
Bt-St-G-Pl
Garnet inner rim
Garnet core
Chl-Bt-St-G-Pl
St-Bt-Pl
Bt-St-Pl-Sill
Bt-Pl-Sill
Chl-Bt-St-Pl
Chl-Bt-Pl
Bt-St-Pl-And
Bt-Pl-And-Chl
Bt-St-Pl-And-Chl
Bt-Pl-Sill-Crd
Bt-Pl-And-Crd
Chl-Bt-Pl-And-Crd
P: Pattison (1992) triple point
H: Holdaway (1971) triple point
(b)
P(kbar)
T(°C)
1mm
060
Mn
Fe
High
Low

Fig. 10

Fig. 11. P-T pseudosection calculated in MnNCKFMASH based on bulk XRF composition for sample GR76 from Gilded Rose. (a) Compositional contours corresponding to the real composition of garnet core along with their errors indicated as light shaded thick lines. (b) Points 2, 3 and 4 were calculated without fractionation technique from median to inner-rim because of near-homogenous Ca content (see WDS Ca map). Note the distinct overgrowth at the rim region of the porphyroblast.

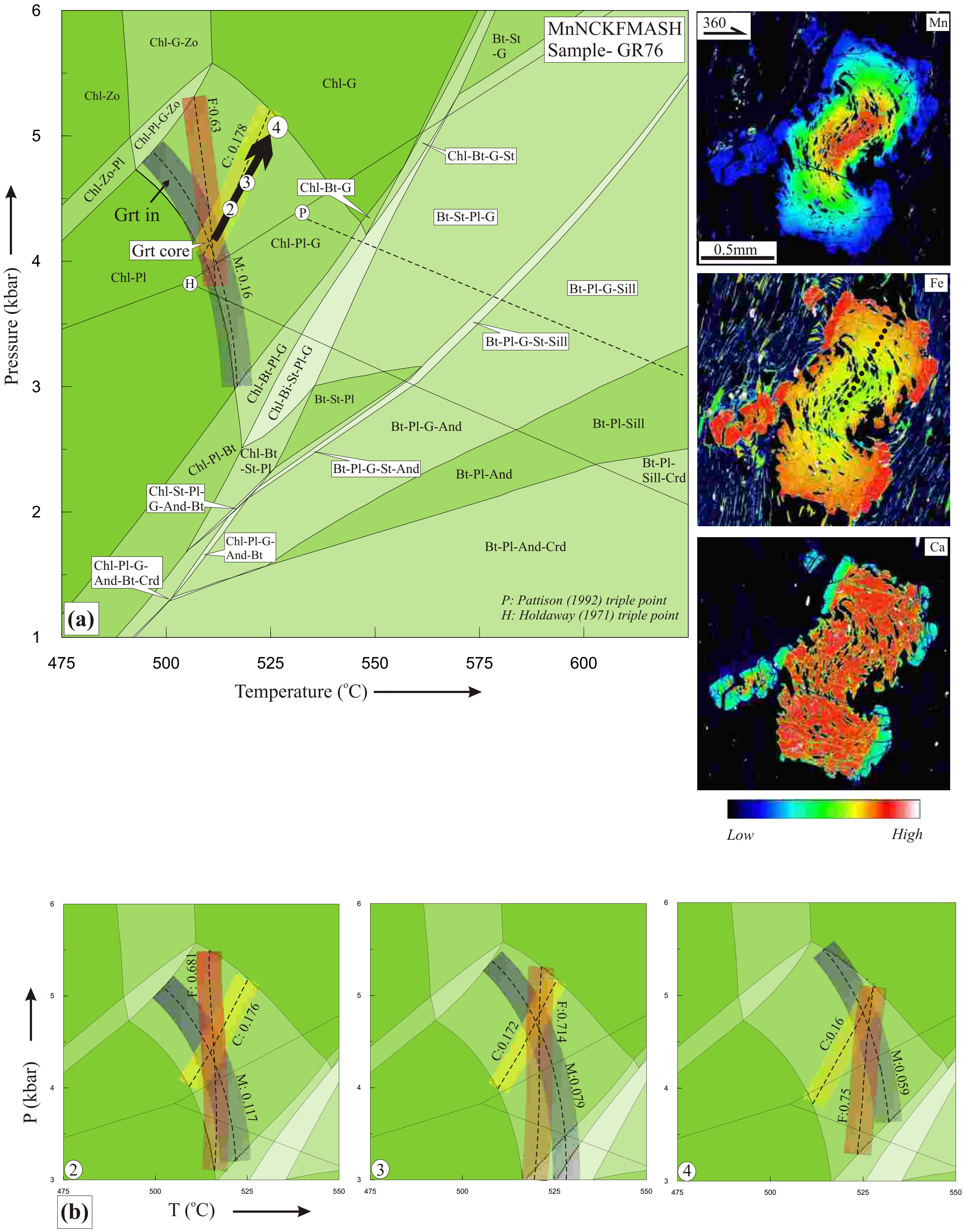

MnNCKFMASH
Sample- GR76
Chl-G-Zo
Chl-Zo
Chl-G
Bt-St
-G
Chl-Pl-G-Zo
Chl-Zo-Pl
F:0.63
C: 0.178
Grt in
Grt core
Chl-Bt-G-St
Chl-Bt-G
Bt-St-Pl-G
Chl-Pl-G
M: 0.16
Chl-Pl
Bt-Pl-G-Sill
Bt-Pl-G-St-Sill
Chl-Bt-Pl-G
Chl-Bi-St-Pl-G
Bt-St-Pl
Bt-Pl-G-And
Bt-Pl-Sill
Chl-Pl-Bt
Chl-Bt
-St-Pl
Bt-Pl-G-St-And
Bt-Pl-And
Bt-Pl-
Sill-Crd
Chl-St-Pl-
G-And-Bt
Chl-Pl-G-
And-Bt
Bt-Pl-And-Crd
Chl-Pl-G-
And-Bt-Crd
P: Pattison (1992) triple point
H: Holdaway (1971) triple point
(a)
Pressure (kbar)
Temperature (°C)
360
Mn
0.5mm
Fe
Ca
Low
High
F: 0.681
C: 0.176
M: 0.117
C:0.172
F:0.714
M:0.079
C:0.16
F:0.75
M:0.059
(b)
P (kbar)
T (°C)

Fig. 11

Fig. 12. P-T pseudosection calculated in MnNCKFMASH based on bulk XRF composition for sample SC118 from the Snake Creek Anticline. Core of the tiny garnet (≤1mm) preserved within the andalusite is modeled with respect to compositional isopleths from microprobe analysis. Andalusite-in line in the system is below the garnet core growth suggesting garnet grew at relatively higher pressure than andalusite.

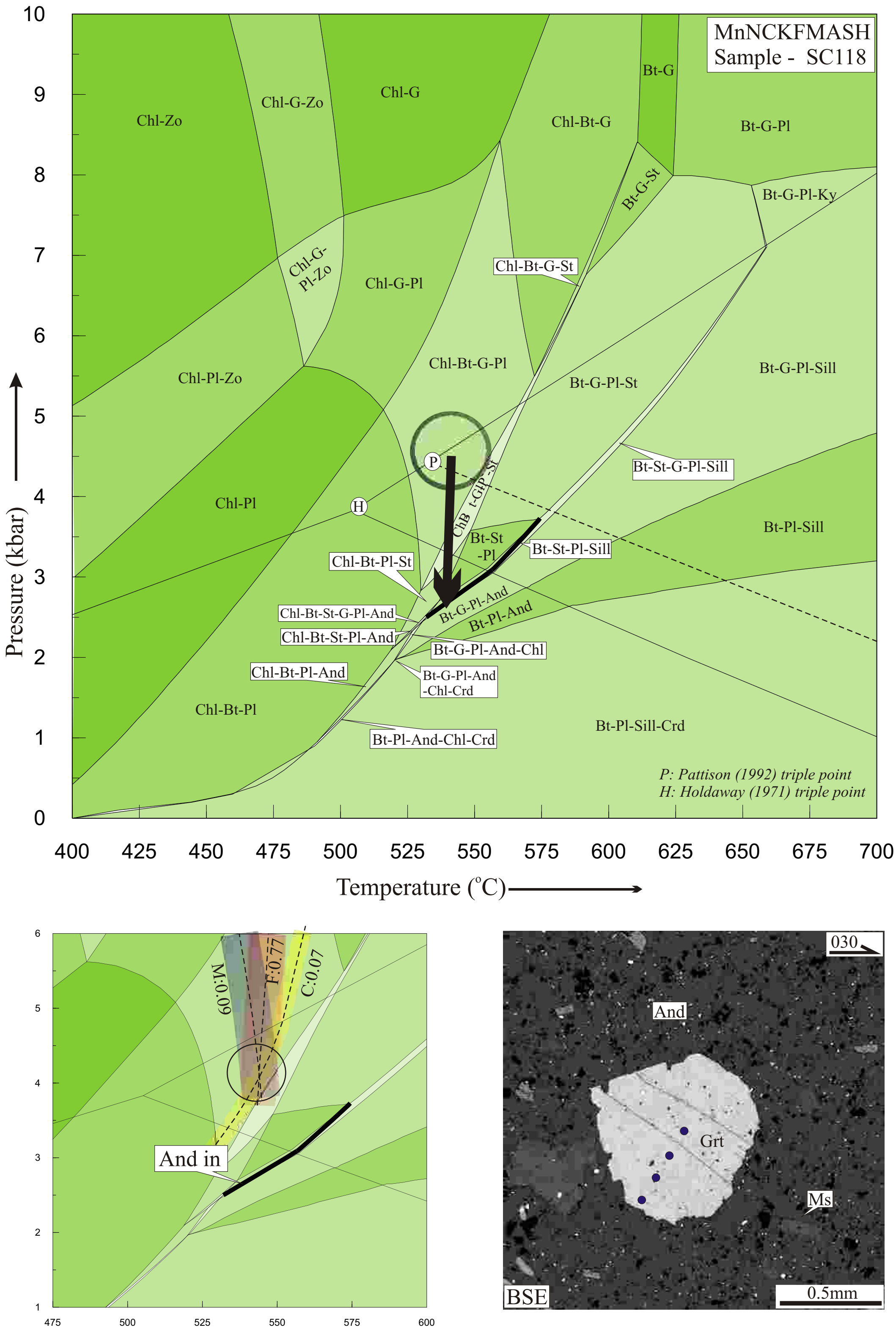

MnNCKFMASH
Sample - SC118
Chl-Zo
Chl-G-Zo
Chl-G
Bt-G
Chl-Bt-G
Bt-G-Pl
Bt-G-St
Bt-G-Pl-Ky
Chl-G-Pl-Zo
Chl-G-Pl
Chl-Bt-G-St
Chl-Pl-Zo
Chl-Bt-G-Pl
Bt-G-Pl-St
Bt-G-Pl-Sill
Bt-St-G-Pl-Sill
Chl-Pl
Bt-Pl-Sill
Bt-St-Pl
Bt-St-Pl-Sill
Chl-Bt-Pl-St
Chl-Bt-St-G-Pl-And
Chl-Bt-St-Pl-And
Bt-G-Pl-And
Bt-Pl-And
Bt-G-Pl-And-Chl
Chl-Bt-Pl-And
Bt-G-Pl-And-Chl-Crd
Chl-Bt-Pl
Bt-Pl-Sill-Crd
Bt-Pl-And-Chl-Crd
P: Pattison (1992) triple point
H: Holdaway (1971) triple point
Pressure (kbar)
Temperature (°C)
M:0.09
F:0.77
C:0.07
And in
030
And
Grt
Ms
BSE
0.5mm

Fig. 12

Fig. 13. P-T pseudosection calculated in MnNCKFMASH based on bulk XRF composition for sample SC112 from the Snake Creek Anticline. (a) The pseudosection is contoured with respect to garnet composition isopleths Mn, Ca and Fe with increasing pressure and temperature. (b) Compositional contours corresponding to the real composition (probe) of garnet core along with their errors indicated as light shaded thick lines. Garnet rim plus matrix phases were calculated using average P-T mode in THERMOCALC-3.21 (sigfit = 1.0) and lies within St-Bt-G-Pl field, in agreement with textural relationships where staurolite and rare plagioclase found in the matrix.

Dashed line represents path from Crd to Grt core. This is based on the textural relationships (see Fig. 5c; and text for further discussion), where pseudomorphed cordierite and Grt are preserved within fresh staurolite porphyroblast. The pseudomorphed nature of Crd is due to higher-pressure overprint (St).

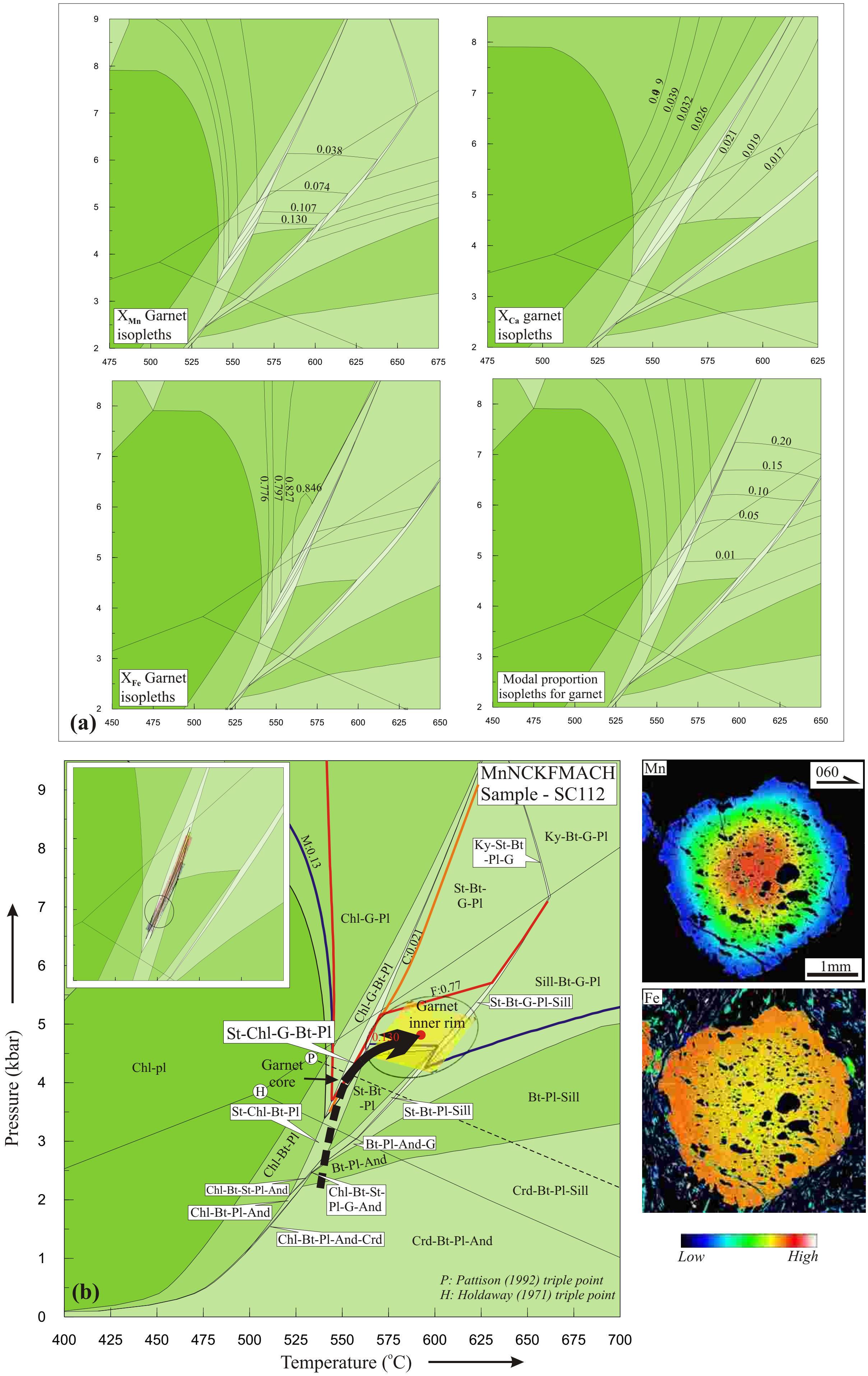

X_Mn Garnet isopleths
X_Ca garnet isopleths
X_Fe Garnet isopleths
Modal proportion isopleths for garnet
(a)
(b)
MnNCKFMACH
Sample - SC112
Pressure (kbar)
Temperature (°C)
Chl-pl
Chl-G-Pl
St-Chl-G-Bt-Pl
Garnet core
Garnet inner rim
Ky-St-Bt-Pl-G
Ky-Bt-G-Pl
St-Bt-G-Pl
Sill-Bt-G-Pl
St-Bt-G-Pl-Sill
Bt-Pl-Sill
St-Bt-Pl-Sill
Bt-Pl-And-G
Bt-Pl-And
St-Chl-Bt-Pl
Chl-Bt-Pl
Chl-Bt-St-Pl-And
Chl-Bt-Pl-And
Chl-Bt-St-Pl-G-And
Chl-Bt-Pl-And-Crd
Crd-Bt-Pl-And
Crd-Bt-Pl-Sill
P: Pattison (1992) triple point
H: Holdaway (1971) triple point
Mn
Fe
060
1mm
Low
High

Fig. 13

Fig. 14. P-T pseudosection calculated in MnNCKFMASH based on bulk XRF composition for sample TC186 from the Tommy Creek Block. (a) compositional contours corresponding to the real composition of garnet core along with their errors indicated as light shaded thick lines. Garnet rim plus matrix phases were calculated using average P-T mode in THERMOCALC-3.21 (sigfit = 0.7). The near-median region (point Gt_3) P-T estimates were calculated using the fractionation method of garnet with effective bulk rock composition (Evans, 2004). However, no P-T path calculations were done beyond this point, as Fe and Mn are almost parallel with increasing pressure and temperature from real garnet analysis. (b) The pseudosection is contoured with respect to garnet composition isopleths Mn, Ca and Fe with increasing pressure and temperature.

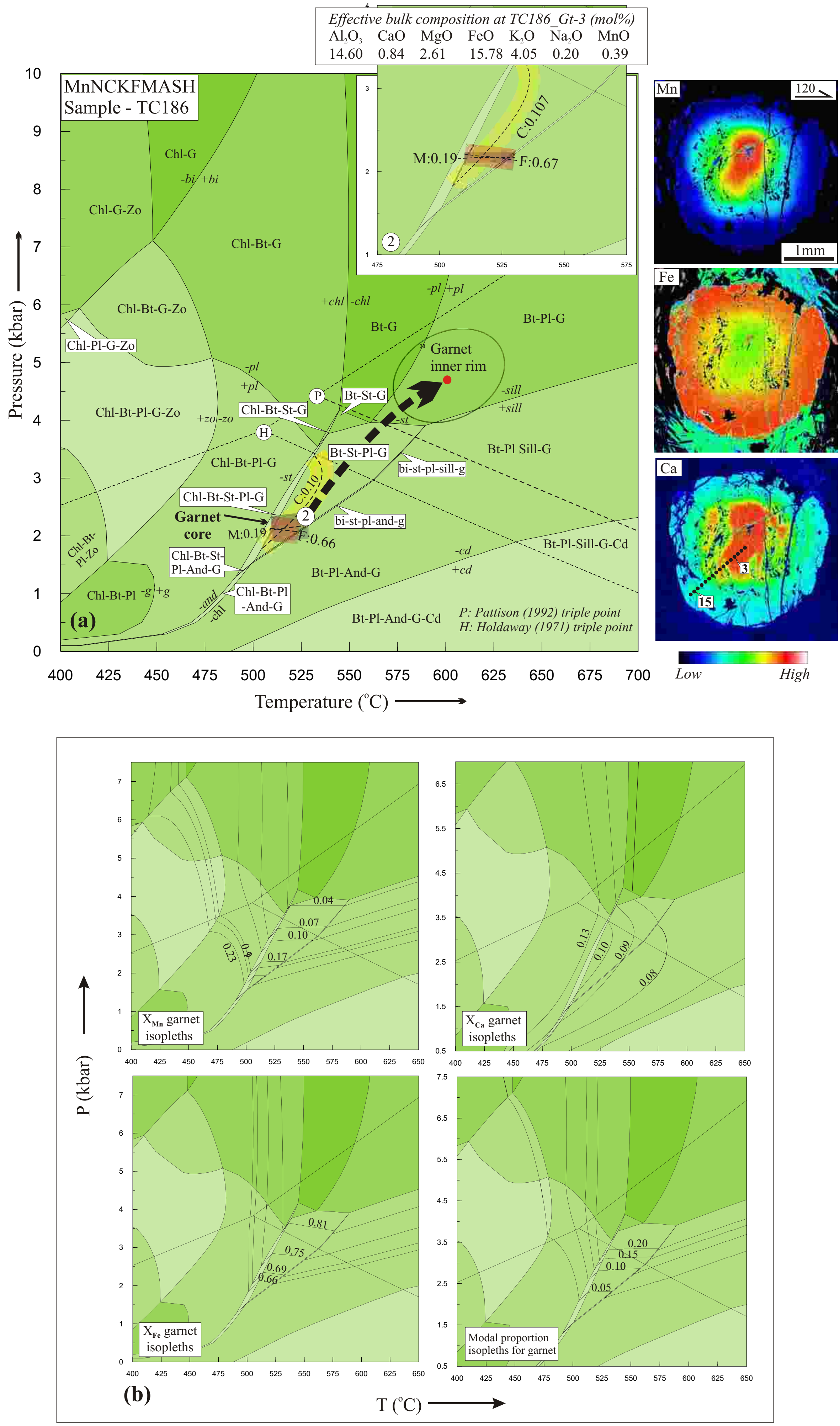

Effective bulk composition at TC186_Gt-3 (mol%)
Al2O3 CaO MgO FeO K2O Na2O MnO
14.60 0.84 2.61 15.78 4.05 0.20 0.39
MnNCKFMASH
Sample - TC186
Chl-G
Chl-G-Zo
Chl-Bt-G
Chl-Bt-G-Zo
Chl-Pl-G-Zo
Chl-Bt-Pl-G-Zo
Chl-Bt-Pl-G
Chl-Bt-St-G
Chl-Bt-St-Pl-G
Chl-Bt-St-Pl-And-G
Chl-Bt-Pl-And-G
Chl-Bt-Pl-Zo
Chl-Bt-Pl
Bt-G
Bt-St-G
Bt-St-Pl-G
Bt-Pl-G
Bt-Pl Sill-G
Bt-Pl-Sill-G-Cd
Bt-Pl-And-G
Bt-Pl-And-G-Cd
bi-st-pl-sill-g
bi-st-pl-and-g
Garnet inner rim
Garnet core
M:0.19
F:0.66
F:0.67
C:0.10
C:0.107
P: Pattison (1992) triple point
H: Holdaway (1971) triple point
(a)
Pressure (kbar)
Temperature (°C)
Mn
Fe
Ca
1mm
Low
High
X_Mn garnet isopleths
X_Ca garnet isopleths
X_Fe garnet isopleths
Modal proportion isopleths for garnet
P (kbar)
T (°C)
(b)

Fig. 14

Fig. 15. (a) P-T paths for orogenesis I and orogenesis II (topology after Pattison et al., 1999). (a) N-S shortening (O_1) (see also Bell et al., 1991; Reinhardt, 1992) was responsible for early medium-pressure clockwise metamorphism followed by isostatic rebound and or decompression leading to low-pressure overprint. However, this low-pressure overprint varies across the inlier with or without the production of cordierite growth related with the emplacement of Williams and Naraku Batholiths at 1550-1500 (see text for further discussion). (b) E-W shortening (O_2) was started initially from low-pressure because of the O_1 decompression metamorphism and or the emplacement of Williams and Naraku event. However, the shape of the anticlockwise P-T path (O_2) slightly varies across the inlier (e.g., Reinhardt, 1992; Rubenach and Lewthwaite, 2002).

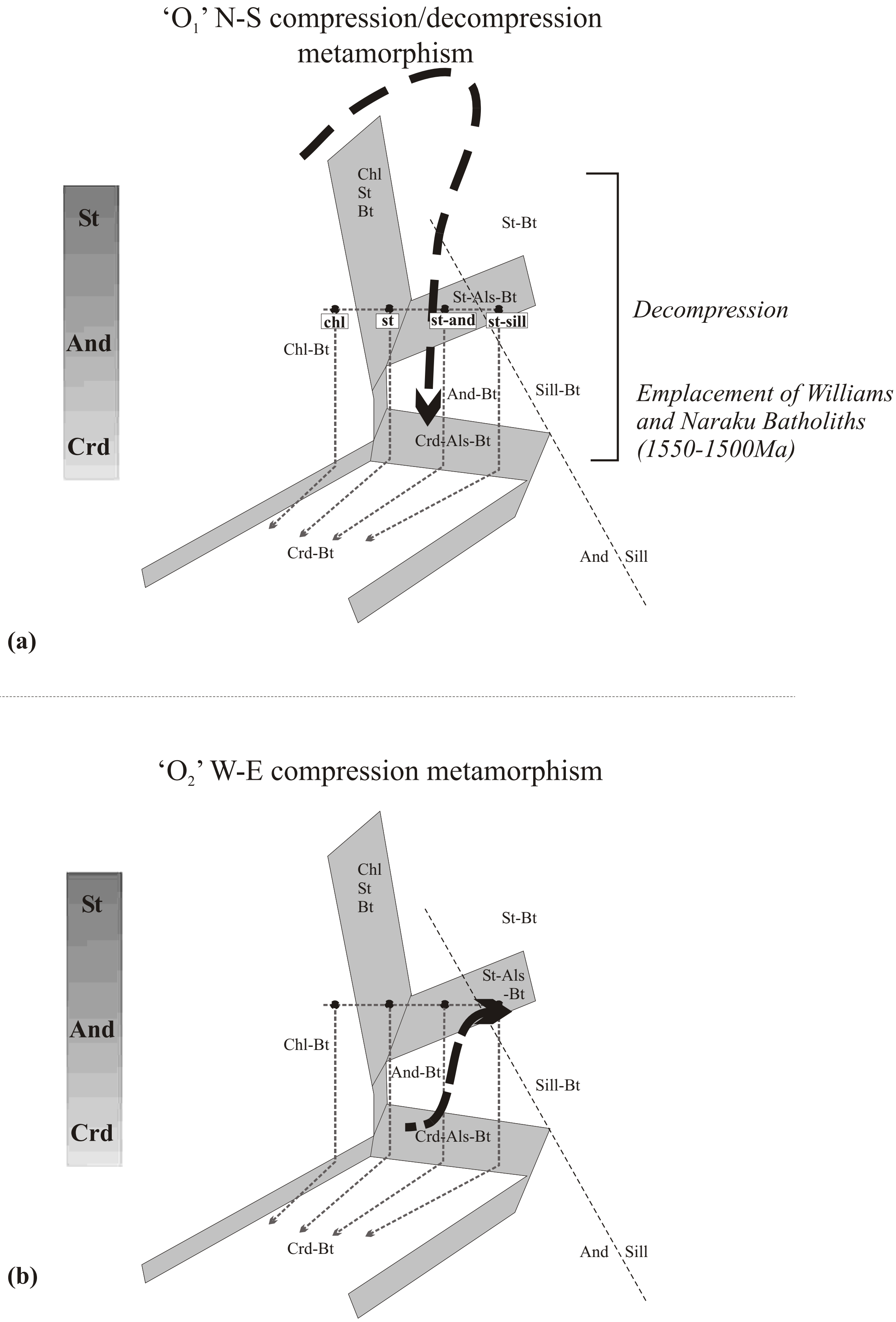

'O_1' N-S compression/decompression metamorphism
St
And
Crd
Chl
St
Bt
St-Bt
St-Als-Bt
chl
st
st-and
st-sill
Chl-Bt
And-Bt
Sill-Bt
Crd-Als-Bt
Crd-Bt
And
Sill
Decompression
Emplacement of Williams and Naraku Batholiths (1550-1500Ma)
(a)
'O_2' W-E compression metamorphism
St
And
Crd
Chl
St
Bt
St-Bt
St-Als -Bt
Chl-Bt
And-Bt
Sill-Bt
Crd-Als-Bt
Crd-Bt
And
Sill
(b)

Fig. 15